Université catholique de Louvain
Faculté des sciences

Louvain Institute of Biomolecular Science and Technology

Functional consequences of *Peroxiredoxin-5* gene inactivation in the mouse

Thèse présentée par Vasiliki Argyropoulou en vue de l'obtention du grade de docteur en sciences

Promoteur	Pr. Bernard Knoops
Membres du jury	Pr. René Rezsohazy
	Pr. François Huaux
	Pr. Thierry Arnould
	Dr. Marcus Conrad
Président du jury	Pr. Patrice Soumillion

Juillet 2019

Acknowledgments

Starting writing this thesis, my mind is going back in the first day I came to Belgium in order to start this amazing trip in science (and not only). It was the evening of 23th September 2013, when I arrived in the North carrying 2 suitcases, 1 handbag and my laptop. Winter was coming…. While I arrived in Louvain-la-Neuve that night, the students' guindailles had already started, reminding me the carnival of Patras. I was a bit shocked, tired, anxious and stressed for the new start, but on the same time excited and motivated to live and work in this place. Next morning, I visited the new lab. Julie Goemaere welcomed me and she drove me to Bernard Knoops' office, to meet him. After a very nice talk with el patron, Julie was in charge to show me everything in the lab, to introduce me to the all the colleagues and explain me my new project. I have to confess that that day was so confusing to me. At the end, I was not able to remember all the names and the faces, the different projects, the different rooms in the lab. One week later, I have been used in the new life in Belgium and I was preparing myself for the second challenge: the FRIA….!!! Despite of the first time was not successful for me, I achieved to obtain the FRIA with the second try, so I was able to continue my journey. AMCB became my second home, my colleagues became my second family, my supervisor became my second father and Belgium became my second country.

I would like to thank first personally el patron Bernard Knoops. In his lab I was able to evolve as a scientist, to open my horizons with new techniques, new experiments and new chances. Bernard is the most kind and happy person I have ever met in my life. He was always next to me through these years, helping me in the beginning to find an apartment, to do my inscription in the UCL, giving me advices for the experiments, correcting my reports, posters and this manuscript, proposing to attend meetings and conferences, and of course providing to all of us the pain au chocolat and the croissants every week in the lab meetings… We had many great times with all the team in parallel of the science, in the BBQs, recreative days of LIBST, Christmas dinners, horse-riding, football matches, Greek dances, origami training and skiing. Thank you Bernard for everything you gave to me all these years.

Of course, I want to thank all the members of my jury, Patrice, René, François, Thierry and Marcus for the nice discussion, their comments and

their propositions during my private defense and all the time they spent to read my manuscript.

I cannot forget all the people where next to me in the lab during these years. Geoffroy with his smile and a new joke every single day. His help to teach me French as soon as possible, giving me a very precious book of the French gros mots. He was also supporting my tries in the cooking, asking me to cook for him delicious Greek plates. My good friend Markos with his Irish gentleness and accent, helping me to speak better English and showing me the secrets of the Western blotting. Oksana with her kind but also strong character, showing me how to deal with the difficult situations. Sarah with her great ideas in the lab and the teaching of the origami science. André (or Tin-Tin) with his all the help in so many experiments, ready to explain me all the techniques and the little secrets of them.

My favorite Marina (or Colonelle or Doityourself girl) who is always next to me to share the morning coffee, desserts, chocolates, fries, pizzas and chips. She is always finding solutions in different problems, like how to break in your own car using a tennis ball and a lighter, while you have locked your keys inside it. A really good friend to discuss your problems and organize BBQs, drinks and recreative days for the Institute. Julien (or Zouzouni) with his sarcasm and the targeted comments in each conversation. A good partner for parties and beer games by time to time.

It would be pity to not mention my 3 brilliant master students, Charlotte, Morgane and Laurence. I was glad to meet all of them and collaborate during their master thesis. Their contribution in this manuscript was really precious and I want to thank them and wish them good luck for their future in science.

I would like to thank all the other people from AMCB that we share a lot of things in the lab during my thesis. Françoise for her advices, her efficient organization of the lab and the animal facility and of course being member of my accompanying committee. Patrick for his questions in the seminars and the delicious honey he produces. Thanks to Maryse for her hilarious laugh, to Charlotte for her delays in the appointments, to Laura for her good mood every day, to Benoit for giving nice nicknames to all of us and playing fantastic music, to Benjamin for always laughing, Bertrand for his timidity, Cedric for his Nutella. Of course I would like to thank Marie-Therese for her kindness and all her help in the experiments we shared and Coralie for her help with the mice. Daniel for his nice compliments every morning in the cafeteria.

Veronique for all the stories that was telling us during lunch every day. Cyril (or Kyrilos) who brought another atmosphere in the lab the last year, always happy and motivated to participate in different activities.

AMCB lists is continuing with all the people from the 0 floor. René, Isabelle, André, Marie-Anne, Philippe, Raphael, Matthew, Noémie, Magali, Damien, Laure, Amandine, Tamara, Manu, Caroline. I am glad to meet all of them, spending beautiful moments in the lab (and not only!).

I also have to thank all the people we collaborated during this project. Julie Goemaere and Fadel Tissir for the Prdx5 KO model generation. Olivier Schackman and Philippe Gailly for their help with the behavioral tests in mice. Yves Guiot, Etienne Marbaix, Christine Galant, Nicolas van Baren and Alessandra Camponi for the tumor analysis of the mice. Pierre Morsomme and Hervé Degand for the proteomic analysis and all the time we spent together analyzing the data.

Of course I cannot forget the most important people in my life. Family and friends. The people were next to me all these years, even if they were thousands of kilometres far away. My dad Alexandros, my mom Chrisanthi, my little brother Nikos, my grandparents Giannis and Kali, my uncle Paris. My family supported my decision to move in Belgium and follow my dream. Even if they miss me every single day... Thank you a lot for all the things you have done for me.

I thank also my good friends which are also supported me and we shared so many beautiful moments. My childhood friend Katerina and her husband Nick for all the time we spent together in Netherlands and Belgium. My good friend Marie-Claire that she is next to me from the 1st day I arrived in Belgium and she became a sister to me. She helped me a lot in the bad moments, always with a smile and a joke about me to say. Rania, Antonia and my cousin Vaso, for all the crazy things we did together the 1st year in Belgium. Katerina, Zoe and Martha, my new sisters in the crimes!! I really loved all the nights staying the 4 of us in my apartment, eating pizza and watching GNTM!!

The long list of people I want to mention is nearly finished with Theodoros. A very special person to me, who had been my partner for over 10 years, I thank him for all his support during all my studies until recently…

I am obliged to stop here, otherwise nobody will continue reading the next pages of this thesis.

Thank everybody again for one more time (so many thanks in a few pages!) and enjoy my manuscript.

Contents

Summary

Peroxiredoxins (Prdxs) are a superfamily of peroxidases widely distributed among prokaryotes and eukaryotes. Prdx5 is the last isoform identified and characterized among the six mammalian Prdxs. Prdx5 is ubiquitously expressed in tissues and its role as cytoprotective antioxidant enzyme as well as modulator of redox signaling have been largely reported in vitro. The goal of this work was to study in vivo Prdx5 functions through the generation of transgenic mice in which Prdx5 gene was disrupted using gene trapping strategy. Prdx5 knockout (*Prdx5*$^{-/-}$) mice are viable and fertile. Compared to wild-type (*Prdx5*$^{+/+}$) animals, *Prdx5*$^{-/-}$ mice do not present any growth differences during the first months and histological analyses did not show clear abnormalities. A microarray analysis revealed that isoforms of CYP450 genes are significantly upregulated in *Prdx5*$^{-/-}$ mice. A significant higher protein carbonylation was measured in brain as well as a higher lipid peroxidation in muscle of *Prdx5*$^{-/-}$ mice. Because Prdx5 gene has been shown to be upregulated in mouse macrophages upon pro-inflammatory stimulation and because high levels of ROS/RNS are produced during inflammation, the vulnerability of *Prdx5*$^{-/-}$ mice to lipopolysaccharide (LPS) in vivo was examined. Our results show that *Prdx5*$^{-/-}$ mice mortality is significantly higher after intraperitoneal injection of 20 mg/kg of LPS compared to the *Prdx5*$^{+/+}$. A proteomic analysis of proteins extracted from

primary culture of *Prdx5*$^{-/-}$ and *Prdx5*$^{+/+}$ phagocytes, exposed for 24 hours to 1 µg/ml LPS revealed that proteins related to inflammation, cancer, apoptosis and redox state regulation were altered in the *Prdx5*$^{-/-}$ phagocytes. Also, 41 % of old *Prdx5*$^{-/-}$ mice (between 12 and 30 month-old) developed significantly more tumors compared to 16% of *Prdx5*$^{+/+}$ animals, suggesting that Prdx5 protein is involved in tumor suppression in vivo. Most of the tumors have been histologically analyzed and characterized as lymphoma and hepatocarcinoma. Moreover, the Akt/PTEN signaling pathway in *Prdx5*$^{-/-}$ MEF cells was investigated by exposing the cells to increasing concentrations of H_2O_2, LPS, *t*BHP and SIN-1. Our results showed that phosphorylation of Akt is higher in *Prdx5*$^{-/-}$ cells exposed to H_2O_2. It appeared also that the Akt/PTEN pathway is affected in some *Prdx5*$^{-/-}$ tumors. Finally, the consequences of Prdx5 gene inactivation was examined in the central nervous system especially with regard to the recently discovered homozygous non-sense mutation in human Prdx5 linked to brain atrophy, mental retardation and epilepsy. *Prdx5*$^{-/-}$ mice present significantly less motor coordination and a tendency of higher anxiety. Additionally, absence of Prdx5 is linked to glial cell proliferation in hippocampus, suggesting a role in neuroinflammation. Altogether, our results suggest that Prdx5 may play important roles in inflammation and in tumor suppression.

Abbreviations

4-HNE	4-hydroxy-2-nonenal	**HIF**	Hypoxia-inducible factors
8-OH-dG	8-hydroxy-2-deoxyguanosine	**HMGB1**	High mobility group box 1 protein
AβO	Amyloid-beta oligomers	**HNO_2**	Nitrous acid
AFM	Atomic force microscopy	**HOCl**	Hypochlorous acid
AhpC	Alkyl hydroperoxide reductase	**HUCB**	Human umbilical cord blood cells
ALD	Alcohol liver disease	**IAP1**	Inhibitor of apoptosis protein 1
ALS	Amyotrophic lateral sclerosis	**IFN-γ**	Interferon gamma
AP-1	Activator protein 1	**Il-x**	Interleukin x
aP2	Adipocyte protein 2	**Ilf3**	Interleukin enhancer-binding factor 3
APP	Amyloid precursor protein	**ION**	Ionomycin
ATP	Adenosine triphosphate	**IP3R**	Inositol trisphosphate receptor
BHT	Butylated hydroxytoluene	**Jak**	Janus kinases
BMM	Bone marrow-derived macrophages	**JNK**	c-Jun N-terminal kinases
C/EBPa	CCAAT/enhancer-binding protein alpha	**Keap1**	Kelch-like ECH-associated protein 1
CAT	Catalase	**LDH**	Lactate dehydrogenase
CCD	Childhood cortical dysplasia	**LIG**	Ligustilide
CcO	Cytochrome c oxidase	**LMM**	Low-molecular-mass
CD82	Cluster of differentiation 82	**LOOH**	Lipid hydroperoxide
CNS	Central nervous system	**LPS**	Lipopolysaccharide
CREB	cAMP response element-binding protein	**MAPK**	Mitogen-activated protein kinases
DAMP	Damage-associated molecular pattern	**MDA**	Malondialdehyde

DJ-1	Protein deglycase 1	**MMP9**	Matrix metallopeptidase 9
DNPH	2,4-dinitrophenylhydrazine	**MNG**	Multinodular goiters
DPPC	Dipalmitoyl phosphatidyl-choline	**MPD**	Myeloperoxidase
DRG	Dorsal root ganglia	**MPP+**	1-methyl-4-phenylpyridimium ion
Drp1	Dynamin-related protein 1	**MTS**	Mitochondrial targeting sequence
EGF	Epidermal growth factor	**MyD88**	Myeloid differentiation primary response 88
EMT	Epithelial-to-mesenchymal transition	**NADPH**	Nicotinamide adenine dinucleotide phosphate
ER	Endoplasmic reticulum	**NF-κB**	Nuclear factor-kappa B
Erk	Extracellular signal-regulated kinase	**$NO^{\bullet}$**	Nitric oxide
Ets	E26 transformation-specific	**NO^{-}_{2}**	Nitrite ion
$FADH_2$	Flavin adenine dinucleotide	**NO^{-}_{3}**	Nitrate ion
$FMNH_2$	Flavin mononucleotide	**NOX**	NADPH oxidase
Fox3	Forkhead box P3	**Nrf**	Nuclear respiratory factor
GATA1	GATA-binding factor 1	**$O^{\bullet -}_{2}$**	Superoxide radical
GDE2	Glycerophosphodiester phosphodiesterase 2	**$^{1}O_2$**	Singlet oxygen
GDF-9	Growth differentiation factor-9	**$OH^{\bullet}$**	Hydroxyl radical
GLUT4	Glucose transporter type 4	**$ONOO^{\bullet}$**	Peroxynitrite
GMP	Guanosine monophosphate	**p53**	Tumor protein 53
GPI	Glycosylphosphatidylinositol	**PAMP**	Pathogen-associated molecular pattern
GSH	Glutathione	**PDK3**	Pyruvate dehydrogenase

			lipoamide kinase isozyme 3
Gpx	Glutathione peroxidase	**PD-L1**	Programmed death ligand 1
GR	Glutathione reductase	**PI3K**	Phosphoinositide 3-kinase
Grx	Glutaredoxin	**PK**	Pyruvate kinase
GSSG	Oxidized glutathione	**PLA_2**	Phospholipase A_2 activity
gt	Gene trap	**PMA**	Phorbol myristate acetate
GTP	Guanosine-5'-triphosphate	**PPARγ**	Peroxisome proliferator-activated receptor gamma
H_2O_2	Hydrogen peroxide	**Prdx**	Peroxiredoxin
PTEN	Phosphatase and TENsin homolog	**SOD**	Superoxide dismutase
PTP	Protein tyrosine phosphatase	**SP1**	Specificity protein 1
PTS1	Peroxisomal targeting sequence 1	**Srx**	Sulfiredoxin
PUFA	Polyunsaturated fatty acids	**Stat**	Signal transducer and activator of transcription proteins
Ras	Rat sarcoma	**Tak1**	Mitogen-activated protein kinase kinase kinase 7
RBH	Rhodamine B hydrazide	**TBA**	Thiobarbituric acid
RNS	Reactive nitrogen species	**TBH**	t-butylhydroperoxide
ROOH	Alkyl peroxide	**TLR2/4**	Toll-like receptor 2/4
ROS	Reactive oxygen species	**TNF-α**	Tumor necrosis factor alpha
R-S-N=O	Nitrosothiol	**TP53**	Tumor protein 53
R-SOH	Sulfenic acid	**Trx**	Thioredoxin
$R\text{-}SO_2H$	Sulfinic acid	**TrxR**	Thioredoxin reductase

R-SO_3H	Sulfonic acid	**TSA**	Thiol-specific antioxidant
RSV	Respiratory syncytial virus	**VEGF**	Vascular endothelial growth factor
SAH	Subarachnoid hemorrhage	**Wnt**	Wingless-related integration site
sGC	Soluble guanylyl cyclase	**πGST**	π isoform of glutathione S-transferase
SLC2A3	Solute Carrier Family 2 Member 3		

PART I: Introduction

1. The Redox World

1.1. Aerobic metabolism and free radicals

The introduction of the oxygen into the primordial anoxic atmosphere was performed with the photosynthesis of the first cyanobacteria. Continuously, dioxygen reduction to ozone (O_3) created a protective layer for organisms from the ultraviolet radiation of the sun, so these organisms could set up on the land. The introduction of the oxygen into the metabolism and ultimately reduction in water is remarkable because it led to energy gains for cells through aerobic metabolism. However, the reduction of oxygen with various molecular systems of the cells is not always perfect and leads to the generation of reactive oxygen/nitrogen species (ROS/RNS) among which we find free radicals. ROS/RNS are a central point of study in biochemistry of oxidative stress [1]–[4].

The term free radical is defined as each atom or molecule bearing one or more unconnected electrons (the electron that occupies itself an atomic or molecular orbital and denoted by a dot as an exponent on the right side of its chemical formula). There are many molecules, among them the simple atomic molecule hydrogen, which are known to have a single electron. A free radical is formed by a non-radical that (a) loses an electron, (b) receives an electron, or (c) undergoes homolytic fission of a covalent bond [1], [3].

Most of the free radicals are derived from the partial reduction of oxygen and nitrogen, therefore the term reactive oxygen and nitrogen species (ROS and RNS) is used (Fig.1). In particular, the progressive reduction of molecular oxygen after receiving an electron at a time leads to the formation of the superoxide anion radical ($O_2^{\bullet -}$), the hydrogen peroxide (H_2O_2) and the hydroxyl radical ($OH^{\bullet}$). Although ROS and RNS are mainly produced in cells as a result of specific reactions, they could be generated by extracellular factors, such as the radiation, pollutants, smoke, ozone and xenobiotics [1], [3], [5].

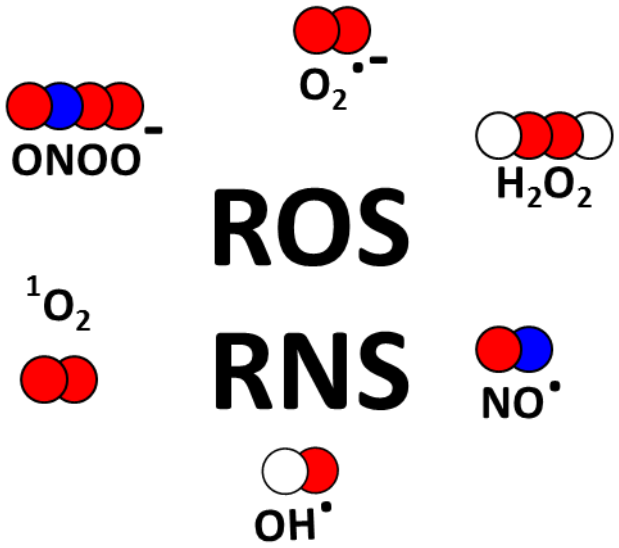

Figure 1. Reactive oxygen (ROS) and nitrogen (RNS) species in living organisms. $O_2^{\bullet -}$: superoxide anion radical; H_2O_2: hydrogen peroxide; $OH^{\bullet}$: hydroxyl radical; $^1O_2$: singlet oxygen; $NO^{\bullet}$: nitric oxide; $ONOO^-$: peroxynitrite. The oxygen is represented with red ball, the hydrogen with white and the nitrogen with blue ball.

Table 1. Main ROS and RNS and their characteristics. [331]

Name	Formula	Characteristics
Hyperoxide/ superoxide	$^{\bullet}O_2^-$	Highly unstable, signaling function, synaptic plasticity
Hydrogen peroxide	H_2O_2	Cell toxicity, signaling function, generation of other ROS
Hydroxyl radical	$^{\bullet}OH$	Free radical, highly unstable, very reactive agent
Alkoxyl radical	$RO^{\bullet}$	Free radical, reaction product of lipids
Peroxyl radical	$ROO^{\bullet}$	Free radical, reaction product of lipids
Hypochlorite anion	OCl^-	Reactive oxygen species, reactive chlorine species, enzymatically generated by myeloperoxidase
Singlet oxygen	$^1O_2$	Induced/excited oxygen molecule, radical and nonradical form
Ozone	O_3	Environmental toxin
Nitric oxide	$^{\bullet}NO$	Environmental toxin, endogenous signal molecule
Peroxynitrite	$ONOO^-$	Highly reactive reaction intermediate of $^{\bullet}O_2$ and $^{\bullet}NO$
Nitrogen dioxide	$^{\bullet}NO_2$	Highly reactive radical, environmental toxin
Nitrogen oxides	NO_x	Environmental toxins, including NO and $^{\bullet}NO_2$, derived from the combustion process

Abbreviations: RNS, reactive nitrogen species; ROS, reactive oxygen species.

1.2. Reactive oxygen species

The free radicals of oxygen are notably produced in cells during the electron transport in the inner mitochondrial membrane, where the failure of the cytochrome oxidases to reduce O_2 to H_2O leads to the formation of the superoxide radical ($O_2^{\bullet-}$) [1]. Other proteins, enzymes and different molecules, like NADPH oxidases, xanthine oxidase, cytochrome P450 oxidases and haem proteins, glyceraldehyde, $FMNH_2$, $FADH_2$, adrenalin, noradrenalin and thiol compounds produce also $O_2^{\bullet-}$ [6]. The $O_2^{\bullet-}$ is a free radical but it cannot react directly with the different biomolecules in the cells. Its lifespan is really short in a cell. However, it is a precursor of more reactive oxygen molecules, such as hydrogen peroxide (H_2O_2) and hydroxyl radical ($OH^{\bullet}$) [7], and it can combine to $^{\bullet}NO$ to form very reactive $ONOO^-$ [8].

Hydrogen peroxide (H_2O_2) is a non-radical molecule that is able to attack the main biomolecules of the cells, like the lipids, the DNA and the proteins, but also to inactivate different enzymes, like phosphatases and caspases. It is a middle product between the $O_2^{\bullet-}$ and water (H_2O) during antioxidant enzyme reactions in cells (see section 2.1). Several other enzymes were also shown to contribute to the formation of H_2O_2, such as xanthine, urate, glucose and lysyl oxidases. It is a weak one-electron oxidant agent, and this fact allows it

to play a role in signal transduction [1], [7], [9], [10] (see below the section *Redox signaling*).

The hydroxyl radical ($OH^{\bullet}$) is a very reactive ROS in cells, generated by H_2O_2 through reaction with transition metals or by its UV-induced homolytic fission of the O-O bond. Ozone and peroxynitrite are also able to produce $OH^{\bullet}$. The $OH^{\bullet}$ is the most reactive free oxygen radical and is an extremely powerful oxidizing agent that reacts almost instantaneously with any type of biomolecules being near its site of formation [1].

1.3. Fenton and Haber-Weiss reactions

The Fenton reaction was first proposed in 1876. Through this reaction, the generation of hydroxyl radical and other oxygen-radical species from hydrogen peroxide is possible in cells, with the implication of a transition metal, usually iron [1], [3], [9].

Table 2. Oxidation (Fenton reaction) and reduction of Fe in cells.

$Fe^{2+} + H_2O_2 \rightarrow Fe^{3+} + OH^{\bullet} + OH^-$	(1) (Fenton reaction)
$Fe^{3+} + H_2O_2 \rightarrow Fe^{2+} + HOO^{\bullet} + H^+$	(2)
$2\ H_2O_2 \rightarrow OH^{\bullet} + HOO^{\bullet} + OH^- + H^+$	(3)

Iron(II) (Fe^{2+}) is oxidized by H_2O_2 to iron(III) (Fe^{3+}), forming a hydroxyl radical ($HO^{\bullet}$) and a hydroxide ion (OH^-) in the process (Reaction 1, called also as Fenton reaction). Fe^{3+} is then reduced back to Fe^{2+} by another molecule of H_2O_2, forming a hydroperoxyl radical ($HOO^{\bullet}$) and a proton (H^+) (Reaction 2). The net effect is a disproportionation of H_2O_2 to create two different oxygen-radical species, with water ($H^+ + OH^-$) as a byproduct (Reaction 3).

Table 3. Fenton and Haber-Weiss reaction

$Fe^{2+} + H_2O_2 \rightarrow Fe^{3+} + OH^{\bullet} + OH^-$	(1) (Fenton reaction)
$Fe^{3+} + O_2^{\bullet-} \rightarrow Fe^{2+} + O_2$	(4)
$H_2O_2 + O_2^{\bullet-} \rightarrow OH^{\bullet} + OH^- + O_2$	(5) (Haber-Weiss reaction)

The Haber–Weiss reaction generates $OH^{\bullet}$ from H_2O_2 and $O_2^{\bullet-}$ (Reaction 5). This reaction can occur in cells and is therefore a possible source for oxidative stress. The reaction is very slow, but it is catalyzed also by iron. Iron(II) (Fe^{2+}) is oxidized by H_2O_2 to iron(III) (Fe^{3+}), forming a hydroxyl radical ($HO^{\bullet}$) and a hydroxide ion (OH^-) in the process (Reaction 1). Fe^{3+} is then reduced back to Fe^{2+} by superoxide radical ($O_2^{\bullet-}$), forming an oxygen molecule (O_2) (Reaction 4). The net effect is a hydrogen peroxide reacting with a superoxide radical to form hydroxyl radical, with oxygen and hydroxide ion (OH^-) as byproducts (Reaction 5).

1.4. Reactive nitrogen species

As mentioned before, among reactive nitrogen species (RNS) there are also free radicals that are produced in the cells, mainly through nitric oxidase synthases (NOS) that generate the radical nitric oxide ($^{\bullet}NO$) from L-arginine [1], [11], [12]. $^{\bullet}NO$ has a fundamental role in cell signaling and immune responses [11]–[15]. $^{\bullet}NO$ activates pathways controlling gene expression, through the conversion of GTP to cGMP, inhibits the cytochrome c oxidase activity in mitochondria and causes posttranslational modifications, as S-nitrosylation, S-glutathionylation and tyrosine nitration [12]. $^{\bullet}NO$ reacts with $O_2^{\bullet-}$ to form peroxynitrite ($ONOO^-$) or with $OH^{\bullet}$ to form HNO_2. In general, because of these reactions, the $^{\bullet}NO$ acts more as a free radical scavenger in the cells, becoming a powerful inhibitor of lipid peroxidation [16], [17].

The peroxynitrite ($ONOO^-$) is a non-radical RNS, which can react with lipids, DNA and proteins, causing damages to cells. The most known damage in proteins caused by $ONOO^-$ is the conversion of tyrosine to 3-nitrotyrosine which is used as a biomarker of nitrooxidative stress [18], [19]. The nitration of the tyrosine often leads to enzyme inactivation [12], [20]. It was shown that S-nitrosylation of Prdx2 can inactivate the enzyme by inhibiting its peroxynitrite reductase activity and increase the tyrosine protein nitration caused by the $ONOO^-$ [20]. On the other hand, it is reported that tyrosine

nitration of plant Prdx2 in an non-catalytic residue, can increase Prdx2 peroxidase activity and protect the enzyme from overoxidation, proposing another mechanism of modulation for Prdx enzymes [21].

1.5. Oxidative stress damage

Oxidative stress, an imbalance between the production of ROS/RNS and the ability of a cell to detoxify them, is responsible for causing a variety of damages in the cells, causing changes in macromolecules (Fig.2). One of the important components of the cell are nucleic acids (DNA and RNA), which can undergo oxidative changes in their bases (e.g. addition of $OH^{\bullet}$, deamination, removal of H) and ribose, leading to fragmentation and nicks, mutations, deletions or translocations or DNA-protein cross-links [1], [5], [22]–[25]. The most known DNA damage is the formation of the oxidized derivative of deoxyguanosine, the 8-hydroxy-2-deoxyguanosine (8-OH-dG), that is widely used as a biomarker for DNA oxidation [5], [26]. The 8-OH-dG formation in transcription factor binding sites can cause the change of

expression of many genes and can lead to disease development and carcinogenesis [5].

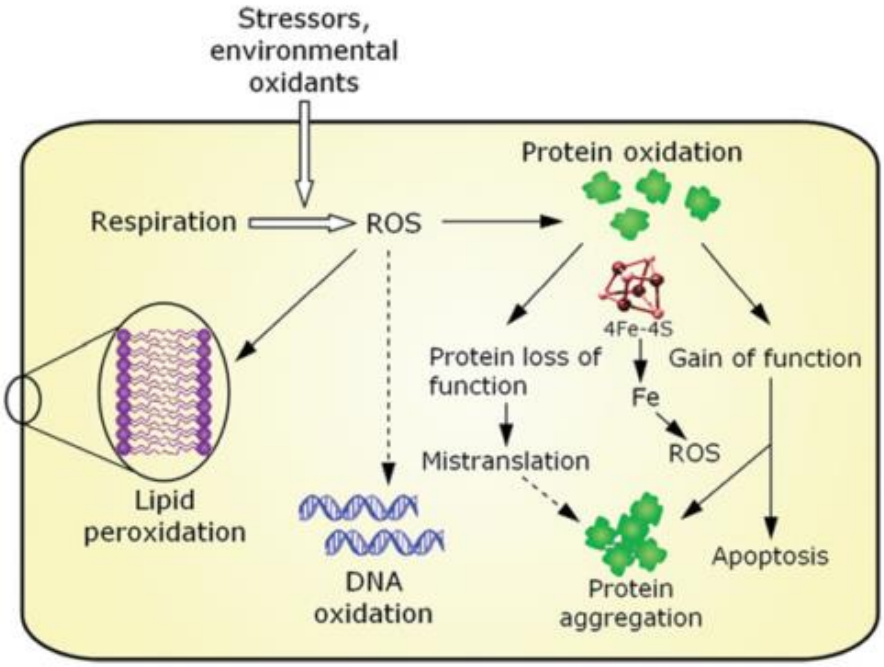

Figure 2. Oxidative stress damage in the main biomolecules of cells. ROS and RNS cause damages to nucleic acids, lipids and proteins. [25]

Additionally, cellular lipid components are among the most important targets of ROS/RNS [1], [3]. Lipid peroxidation, especially in polyunsaturated fatty acids (PUFAs), involves two stages. The initiation stage, which begins when a highly reactive ROS molecule (e.g., $OH^{\bullet}$) cleaves a hydrogen atom from a methylene (CH_2) group. This intersection leads to the creation of a carbon-centered radical ($L^{\bullet}$) with an unconnected electron, which usually undergoes

an intramolecular rearrangement and converts to a conjugated diene. In the propagation step, the carbon radical is linked to an O_2 molecule and produces a peroxyl radical ($LOO^{\bullet}$). The free peroxyl radical is very reactive and can extract a hydrogen atom from a neighboring PUFA molecule, converting it to the corresponding hydroperoxide (LOOH) [3], [25]. The most known products of lipid peroxidation are the malondialdehyde (MDA) and the 4-Hydroxy-2-nonenal (4-HNE). They are used as a biomarker of lipid peroxidation and can be quantitated in cell extracts [5], [27]. MDA inactivates many proteins by forming protein cross-linkage, while 4-HNE causes depletion of intracellular GSH, activates epidermal growth factor receptor and induces fibronectin production [5]. The LOOH levels can be also measured by direct reaction of LOOH with thiobarbituric acid (TBA) [27].

Finally, oxidative damage in proteins is common, such as the formation of superoxides in the peptide chain or the amino acid side groups, oxidation of -SH groups, protein carbonyl formation and deamination, which result in changes in structure and function of proteins [1], [25], [28], [29]. Addition of $OH^{\bullet}$ in proteins leads to $OH^{\bullet}$-dependent abstraction of a hydrogen atom from the α-carbon of amino acids and the protein polypeptide backbone, and also from the aliphatic side chains of hydrophobic amino acid residues. This corresponds to the initial stage of the attack and the formation of a carbon-centered radical ($R^{\bullet}$), which, in the presence of oxygen, is rapidly converted

to the peroxyl radical ($ROO^{\bullet}$). The $ROO^{\bullet}$ reacts with the $HO_2^{\bullet}$ to form alkyl peroxide (ROOH) [28]. ROS/RNS can also cause the cleavage of peptide bonds, nitration and chlorination [28], [29]. Protein carbonylation in amino acids residues (such as serine, lysine, arginine, threonine, proline, histidine and cysteine) is a well-established marker of protein damage caused by oxidative stress, through the reaction of the carbonyls with the 2,4-dinitrophenylhydrazine (DNPH) or the rhodamine B hydrazide (RBH) [30], [31].

1.6. Redox Signaling

With the term redox signaling, we refer to a cellular response to an oxidant or to an alteration in redox status of a cellular component, which can lead to a variety of downstream effects on cell functions. Usually the molecules that could serve as messengers in the redox signaling are oxidants themselves, such as H_2O_2 and $^{\bullet}NO$, or organic peroxides [5], [7], [9], [10], [13], [32], [33].

As it was mentioned previously, H_2O_2 is a ROS that can oxidize a wide range of molecules. However, H_2O_2 reacts with a few cellular biomolecules, and is more prone to react with thiols. Many regulatory proteins, including protein tyrosine phosphatases (PTPs), phosphatases, kinases and transcription factors, contain critical cysteine residues that can be oxidized by H_2O_2,

causing a change of their biological activity [34]–[36]. H_2O_2 can react very fast with cysteine- or selenocysteine-dependent antioxidant enzymes, such as Prdxs and Gpxs. When facing high concentrations of H_2O_2, these enzymes can be over- or hyperoxidized and inactivated. Moreover, a cascade of molecular events follows. Prdx inactivation through over- or hyperoxidation and accumulation of H_2O_2 have led to the floodgate theory (see below). Alternatively, several Prdxs can be also inactivated by phosphorylation and this can lead again to H_2O_2 accumulation [35] (Fig.3).

These mechanisms make H_2O_2 an ideal molecule to transmit signals by oxidizing thiol proteins [13], [35]. However, the rate constants of reactions of the H_2O_2 with regulatory thiol proteins is much lower than the rate constants of reactions of the H_2O_2 with the antioxidant enzymes. The consequence is that signaling molecules cannot compete with known protein antioxidant systems that remove H_2O_2. It was shown also that different H_2O_2

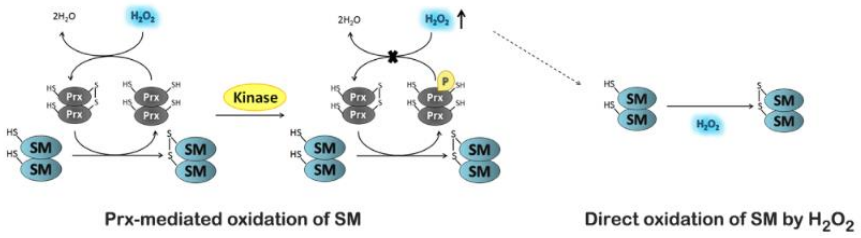

Figure 3. Localized increase of H_2O_2 levels mediated through inhibition of peroxiredoxin activity by phosphorylation. Peroxiredoxins (Prdxs) transmit the signal to a signaling molecule (SM). A kinase phosphorylates the peroxiredoxin that leads to its inactivation and H_2O_2 accumulation around membranes. This promotes the direct oxidation of SM by the H_2O_2. [35]

concentrations could lead to different responses of signaling pathways, impairing or enhancing it, such the Akt signaling pathway [37].

H_2O_2 regulates different transcription factors, which are mostly involved in the regulation of cell damage response, cell proliferation, differentiation and apoptosis in different ways. Transcription factor deregulation can lead to different pathophysiological situations such as tumorigenesis [35]. More specifically, H_2O_2 regulates several transcription factors at the transcriptional (AP-1, TP53, HIF-1α) [38]–[41], post-transcriptional (TP53) [42], [43] and translational levels (Nrf2, SP1) [44]–[48]. On the other hand, H_2O_2 is also able to modulate the degradation of key modulators of transcription factor function, such as the E3 ubiquitin ligase complex, in the case of NRF2 and TP53 transcription factors [49]–[54] or to cause post-translational modifications of the transcription factors that increase or decrease their association with the E3 ubiquitin ligase complex [55]–[58]. It has been shown also that H_2O_2 can control the cytoplasm-nuclear trafficking of transcription factors by activation mediated either by post-translational modification in the transcription factor [59], [60], either by association/dissociation from partners [61], [62], or through release from membrane by proteolytic processing [63], [64]. Finally, transcription factors can sense directly H_2O_2, and change their conformation and their affinity for DNA. This modulation of DNA binding could be done by oxidation or reduction of the transcription

factor [65]–[69], by post-translational modifications [70]–[72], by binding to a co-activator [73], by release from an inhibitor [74], [75] or by affecting the chromatin state [76].

•NO is also involved in redox signaling, participating in different signaling pathways [12]. In the case of the classical signaling, •NO forms a complex with soluble guanylyl cyclase (sGC), causing a conformational change of this enzyme and increasing its activity in the conversion of GTP to cGMP [15]. The generation of the cGMP triggers pathways related to gene expression, by activating cGMP-dependent protein kinases [77]. Additionally, •NO competes with O_2 for binding to cytochrome c oxidases (CcO), the terminal enzyme of the mitochondrial electron transport chain, which catalyzes the oxidation of cytochrome c and the reduction of O_2 to water. This competition suggests that •NO can act as a physiological regulator of the O_2 sensitivity of respiration in tissues, by inhibiting cytochrome oxidase [78]–[80]. Finally, •NO participates in non-classical signaling pathways, mainly by causing post-translational modifications of target proteins, in their cysteine and tyrosine residues [12]. The most known post-translational modifications are S-nitrosylation, S-glutathionylation, and tyrosine nitration. S-nitrosylation is a reversible post-translational modification that refers to the incorporation of a nitroso group to a cysteine thiol, forming a nitrosothiol (R–S–N=O) [81], [82]. S-glutathionylation (or S-thiolation) is the binding of a low-molecular-

mass (LMM) thiol, usually GSH, to a protein via formation of a mixed disulfide bridge between a cysteine residue and the LMM thiol [83], [84]. The tyrosine nitration involves the incorporation of a nitro group ($-NO_2$) to the phenolic ring of tyrosine residues to form a 3-nitrotyrosine residue [18], [19].

2. Redox enzymes

Aerobic organisms have developed enough defensive mechanisms to survive severe oxidative stress conditions. It is important that they maintain intracellular concentrations of O_2 at levels below atmosphere level (21%) and the ability of the respiratory chain to function effectively at these low levels of O_2. The ROS/RNS generated in these conditions is dealt with by the antioxidant defenses of organisms present on three basic defense levels [1]: (i) limiting the availability of transition metals and other pre-oxidizing substances which promote oxidative destruction of biomolecules by

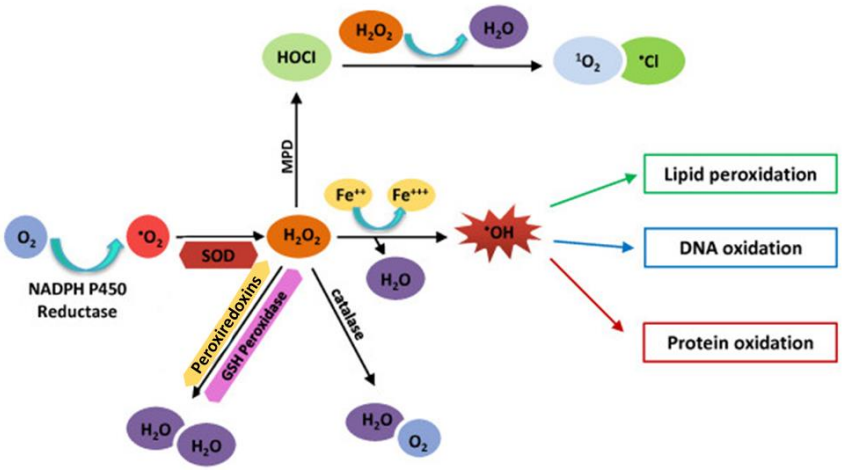

Figure 4. The main antioxidant enzymes in cells and their reactions to eliminate ROS. Cells generate aerobic energy by reducing molecular oxygen (O_2) to water. During the metabolism of oxygen, superoxide anion ($O_2^{\bullet -}$) is formed in presence of NADPH P450 reductase. After superoxide dismutase (SOD) is added to the system, superoxide undergoes dismutation to hydrogen peroxide (H_2O_2), which is converted by glutathione peroxidases, peroxiredoxins or catalase to H_2O. MPD (myeloperoxidase) converts H_2O_2 in neutrophils to hypochlorous acid (HOCl), a strong oxidant that acts as a bactericidal agent in phagocytic cells. During a Fenton reaction, Fe^{2+} is oxidized to Fe^{3+} and H_2O_2 is converted in the highly reactive hydroxyl radical $OH^{\bullet}$. This radical is involved in lipid peroxidation, DNA and protein oxidation. [332]

ROS/RNS or other oxidative stress products. In this group, there are proteins called metalloproteins that bind transition metals and therefore reduce their availability. The most known metalloproteins are transferrin and ferritin [85]–[87]; (ii) scavenging ROS/RNS and other reactive molecules before they attack biomolecules. This step is achieved with the help of enzymes with antioxidant activity, such as superoxide dismutases (SODs), catalase (CAT), GPxs (with or without selenium) and Prdxs (Fig.4). Different low molecular weight organic compounds can also act as free radical scavengers such as glutathione, bilirubin, lipoic acid, uric acid, ubiquinone, melanins, ascorbic acid (vitamin C), tocopherols, tocotrienols, carotenoids, butylated hydroxytoluene (BHT) and butylated hydroxyanisole (BHA) [5], [23]; (iii) repairing affected molecules and repairing damages, using DNA repair mechanisms (DNA glycosylases, DNA methylases, endonucleases, exonucleases), reducing oxidized sulfhydryl groups of proteins and repairing lipid peroxides [23], [24]. Without these mechanisms, living organisms would accumulate oxidative damage to a degree that would not allow their survival.

2.1. Non-cysteine-based enzymes

The non-cysteine enzymes that participate in antioxidant cell defense are superoxide dismutases (SODs) and catalase (CAT) [1], [5], [23].

2.1.1. Superoxide dismutases

Superoxide dismutases are enzymes that catalyze dismutation of $O_2^{\bullet-}$ to H_2O_2 (Table 4, Reactions 6-8). All SODs use a transition metal in their active site, such as Cu, Mn, Fe or Zn. In bacteria, there exist only Fe-SOD and a Mn-SOD. In mammals, there are two Cu/Zn-SOD, a cytoplasmic (SOD1) and an extracellular form (SOD3), but the cytoplasmic Cu/Zn-SOD is also present in lysosomes, peroxisomes and nucleus. The Mn-SOD (SOD2) is mitochondrial [88], [89].

Table 4. Dismutation of $O_2^{\bullet-}$ to H_2O_2 catalyzed by SODs. X= Cu, Mn, Fe. The n represents the number of oxidations. For Cu, n=1 and for Mn and Fe, n=2.

$X^{(n+1)+}\text{-SOD} + O_2^{\bullet-} \rightarrow X^{n+}\text{-SOD} + O_2$	(6)
$X^{n+}\text{-SOD} + O_2^{\bullet-} + 2H^+ \rightarrow X^{(n+1)+}\text{-SOD} + H_2O_2$	(7)
$2\ O_2^{\bullet-} + 2H^+ \rightarrow H_2O_2 + O_2$	(8)

The cytoplasmic Cu/Zn-SOD uses the copper ions to catalyze the dismutation of $O_2^{\bullet-}$, while the zinc ions are more involved in enzyme stabilization. The mitochondrial Mn-SOD assumes the largest load of $O_2^{\bullet-}$ clearance, which leaks from the respiratory chain. A different type of Cu/Zn-SOD is extracellular (EC-SOD or SOD3) and minimizes interaction of $O_2^{\bullet-}$ and $^{\bullet}NO$ to form $ONOO^-$ [89].

Deletions or mutations of SOD genes have been shown to be lethal in lower organisms or causes severe diseases in higher organisms, underpinning the essential importance of this enzyme family. Mutations in SOD1 can cause familial amyotrophic lateral sclerosis (ALS) [90]. Mice lacking SOD1 are more sensitive to ethanol and paraquat exposure. SOD1 knockout mice present muscle wasting, neurological damage and cancers [1]. Complete inactivation of SOD2 in mice causes perinatal lethality [91].

2.1.2. Catalase

Catalase (CAT) is an antioxidant enzyme that catalyzes the reduction of the H_2O_2 to H_2O and O_2 (Table 5, Reactions 9-11). This enzyme forms a homotetramer with one heme group bound in the active site of each monomer. Each subunit has usually one molecule of NADPH bound to it, as a reducing equivalent to prevent oxidative inactivation of the enzyme by H_2O_2 [92]. CAT is very often considered as the main antioxidant enzyme localized in peroxisomes although other peroxidases such as Prdx5 are also present in these organelles. CAT removes H_2O_2 generated by β-oxidation of long-chain fatty acids and H_2O_2 produced by the activity of SODs [1], [5], [23].

CAT could be inactivated by azide, cyanide, $ONOO^-$, HOCl and aminotriazole by inhibiting Compound 1 [1]. CAT can also catalyze other reactions, such as the oxidation of methanol and ethanol to their corresponding aldehydes.

Table 5. Reduction of H_2O_2 to H_2O and O_2 catalyzed by CAT.
Compound I = Fe-O

Catalase-Fe^{3+} + H_2O_2 → Compound I + H_2O	(9)
Compound I + H_2O_2 → Catalase-Fe^{3+} + H_2O + O_2	(10)
$2H_2O_2 \rightarrow 2H_2O + O_2$	(11)

Additionally, CAT can use H_2O_2 to oxidize $^{\bullet}NO$ to NO_2^- and NO_3^- [14]. Mutations of CAT gene in humans results in acatalasemia, condition that is linked to increased incidence of gum disease (Takahara's disease) [93]. In general, CAT deficiency does not cause severe phenotypes, like the SOD deficiencies, probably because of the present of other antioxidant enzymes that eliminate H_2O_2 in peroxisomes.

2.2. Cysteine-based enzymes

Additionally to non-cysteine enzymes, cells have evolved a number of peroxidase cysteine-based enzymes to reduce peroxides. These enzymes are

classified in different families including the glutathione peroxidase family, the glutathione reductase family, the peroxiredoxin family and the thioredoxin family.

2.2.1. Glutathione peroxidase family (GPxs)

The most representative enzymes of this family are the glutathione peroxidases (GPxs), which catalyze the reduction of H_2O_2 to H_2O through the oxidation of two reduced glutathione (GSH), a thiol-containing tripeptide (Table 6, Reactions 12 and 13) [94]. GPxs catalyze the same reaction in the presence of fatty acid hydroperoxides and simple organic hydroperoxides (LOOH and ROOH, respectively) to reduce them to an alcohol. The oxidized GSH is then reduced back by the glutathione reductase (GR), using the NADPH as an electron donor [7], [94].

Table 6. Reduction of the H_2O_2 to H_2O catalyzed by the GPxs.

$H_2O_2 + 2GSH \rightarrow GSSG + 2H_2O$	(12)
$ROOH + 2GSH \rightarrow GSSG + H_2O + ROH$	(13)

In mammals, there are eight different GPxs identified and characterized [95]. The first four GPxs (GPx1-4, also called classical GPxs) have been more studied in depth, while the other GPxs (GPx5-8) have been less investigated

so far. The classical GPxs and the GPx6 contain a selenocysteine (Sec) in their active site. They are reduced by GSH following their oxidation by peroxides. GPx5, GPx7 and GPx8 contain a cysteine in their catalytic site and they are reduced by thioredoxins [95], [96].

Only GPx1 and GPx4 are expressed in all mammalian tissues. GPx1 is mainly cytosolic but also mitochondrial, while GPx4 is cytosolic, mitochondrial, nucleic and present in membrane fractions [97]. GPx2 is gastrointestinal-specific, GPx3 is present in plasma and GPx6 is expressed in olfactory epithelium and embryonic tissues. GPx1-3 are homo-tetramers and reduce H_2O_2 and ROOH, although GPx4 is monomeric and reduces mainly ROOH [96], [98]–[100].

GPx1 KO mice are healthy, fertile and not sensitive to hyperoxia. However, GPx1 KO mice are sensitive to oxidative stress caused by paraquat, H_2O_2 and MPTP [101]–[104]. Additionally, GPx1 and GPx2 double KO mice are more prone to inflammation and cancer development [105]. Interestingly, it was also reported recently that GPx3 suppresses proliferation of lung cancer cells by modulating redox-mediated signals [106]. GPx4 KO mice present prenatal lethality, caused by triggering apoptosis-inducing factor (AIF)-mediated cell death [95], [96], [107], [108]. Additionally, it was shown that GPx4 is a key regulator of ferroptosis, a non-apoptotic form of cell death due to lipid peroxidation [109], [110]. Moreover, conditional GPx4 deletion in

dopaminergic neurons induces anxiety behavior, while double mutant mice for GPx4 and DJ-1, a Parkinson Disease related protein, present diminished spontaneous locomotor activity [111].

2.2.2. Glutathione reductase family

Glutathione reductases (GRs) catalyze the reaction of the oxidized glutathione (GSSG) to the reduced form (GSH) (Table 7, Reaction 14) [112], [113]. Functionally, GR is an NADPH:GSSG oxidoreductase. The GRs consist in two subunits with a FAD-binding site in each active site, which are reduced by the NADPH to FADH. The 2FADH then reduce the GSSG to 2GSH. The main source of NADPH for this reaction is the pentose phosphate pathway [113]–[115]. Different GR isoforms are found in the cytosol, but also in mitochondria and chloroplasts [115].

Table 7. Reduction of the GSSG to 2 GSH catalyzed by the GRs.

$GSSG + NADPH + H^+ \rightarrow 2GSH + NADP^+$	(14)

The importance of GRs in cells has been studied by using knockout models. Yeast GR knockout strains are viable with higher GSSG levels, while the *E.coli* GR knockout have no clear phenotype and normal levels of GSSG [115]. Up-regulation of mitochondrial GR increases the resistance of lung cells to

exogenous hydroperoxides and hyperoxia *in vitro* in cell culture but not in mice [116], [117].

2.2.3. Thioredoxin family

Thioredoxins (Trxs) are ubiquitous enzymes, present in all living organisms, with three isoforms in human [118]. The reduced Trx contains two cysteines in their active site that form a disulfide bond in the oxidized Trx. Trxs bind to target oxidized proteins, such as peroxiredoxins (Prdxs) and transcription factors, reduce their disulfide bridge, while they oxidize themselves (Table 8, Reaction 15) [118], [119]. The oxidized Trxs are reduced back by the Trx reductase (TrxR), using the NADPH as an electron donor (Table 8, Reaction 16). The TrxR contains two selenocysteines with a FAD in each active site, which are reduced by the NADPH to FADH. The two FADH then reduce the oxidized Trx to its reduced form [115], [118], [119].

Table 8. Reduction of oxidized proteins by the Trxs and reduction of the Trxs.

$Trx - - - (SH)_2 + Protein - - - S_2 \rightarrow Trx - - - S_2 + Protein - - - (SH)_2$	(15)
$Trx - - - S_2 + NADPH + H^+ \rightarrow Trx - - - (SH)_2 + NADP^+$	(16)

In vertebrates, there are mainly two Trxs, the Trx1 which is cytosolic, nuclear and also extracellular in some situations [120] and the Trx2 which is only mitochondrial [121]. There is a third Trx (SpTrx), which is a variant highly expressed in spermatozoa [122]. In mice, the homozygous mutation of the Trx1 and Trx2 causes early embryonic lethality [123], [124]. In human, homozygous mutation of Trx2 causes early-onset neurodegeneration [125].

2.2.4. Glutaredoxin family

Glutaredoxins (Grxs) are small redox enzymes of approximately one hundred amino-acid residues that use GSH as a cofactor and reduce back the oxidized proteins (Table 9, Reaction 17) [126]. In contrast to thioredoxins, which are reduced by TrxR, Grxs are reduced by the oxidation of GSH (Table 9, Reaction 18). Oxidized glutathione is then regenerated by GR with the help of $NADPH^+$ (Table 7, Reaction 14). Based on the number of cysteines in their active site, Grxs are divided in dithiol Grxs containing the characteristic Cys-Pro-Tyr-Cys active site motif, and in monothiol Grxs lacking the C-terminal active site thiol

Table 9. Reduction of oxidized proteins by Grxs and reduction of Grxs.

$Grx - - - (SH)_2 + Protein - - - S_2 \rightarrow Grx - - - S_2 + Protein - - - (SH)_2$	(17)
$Grx - - - S_2 + 2GSH \rightarrow Grx - - - (SH)_2 + GSSG$	(18)

in its Cys-Gly-Phe-Ser active site [115], [119], [126]. In mammals, there are 4 isoforms: dithiol Grx1 and Grx2 and monothiol Grx3 and Grx5. Grx1 is localized in the cytosol, nucleus and mitochondria but is also extracellular. Grx2 is mainly present in mitochondria, but also in cytosol. Grx3 is localized in cytosol and nuclear. Grx5 is targeted to mitochondria [126].

2.2.5. Sulfiredoxin

The sulfiredoxin (Srx) is a cysteine sulfinic acid reductase that catalyzes the reduction of Prdx hyperoxidized forms in presence of ATP [127]. Among the Prdxs, only the sulfinic forms of 2-Cys Prdxs (Prdx 1–4) were found to be reduced by Srx but not atypical 2-Cys or 1-Cys Prdxs (Prdx5 and 6).. The conserved cysteine of Srx serves as a phosphate carrier from ATP to sulfinic Prdx. The resulting Prdx sulfinic phosphoryl ester is converted to a disulfide-S-monoxide by a thiol in solution. The disulfide-S-monoxide reacts with three thiols sequentially to yield reduced Prdx. [127]–[129].

3. Peroxiredoxins

Peroxiredoxins (Prdxs or Prxs) are a family of highly conserved thiol-dependent peroxidases [130]–[132]. Prdxs are able to reduce hydrogen peroxide, alkyl hydroperoxydes and the peroxynitrite with different catalytic efficiency between 10^5 and 10^7 M^{-1} s^{-1} [131], [133], [134]. Prdxs represent 1% of total soluble proteins in yeast [135] and they are present in bacteria, archaea and eukaryotes [132]. The first Prdx was identified in yeast and was named thiol-specific antioxidant (TSA) [136], [137]. In *E.coli* the first Prdx to be characterized was named alkyl hydroperoxide reductase (AhpC) [138]. The name peroxiredoxin was proposed by Chae *et al*. in 1994 [139]. In mammals, the Prdx family is represented by six members (Prdx1-6) encoded by six different genes [131], [132].

Prdxs are localized in all subcellular compartments but with different subcellular distributions depending on the isoform [36]. Prdx1, Prdx2, Prdx5 and Prdx6 are cytosolic, while the Prdx1, Prdx2 and Prdx5 can be also present in the nucleus [140]–[145]. Prdx4 is localized in the endoplasmic reticulum and it could be also extracellular, as it possesses a N-terminal domain signal sequence for secretion [146]. Prdx3 and Prdx5 are addressed to mitochondria, thanks to their N-terminal mitochondrial targeting sequence

[147], [148]. Additionally, Prdx5 can be addressed to peroxisomes [36]. Prdx6 was also reported to be localized in lysosomes and the lamellar bodies [149].

Based on their catalytic mechanism and the number of the active cysteines, Prdxs have been classified in three different subgroups [141]: the typical 2-Cys Prdxs (Prdx1-4 in mammals), the atypical 2-Cys Prdxs (Prdx5 in mammals) or the 1-Cys Prdxs (Prdx6 in mammals). One catalytic cysteine is necessary for the attack of the O-O bound of peroxides by all Prdxs, the peroxidatic (Cp) in the N-terminal domain of the enzyme. When the Cp attacks the peroxide, a sulfenic acid (R-SOH) is formed [128], [150]. The sulfenic acid can form a disulfide bond with a second cysteine (R-S-S-R), the resolving cysteine (Cr), which is localized in the C-terminal domain of the enzyme in typical and atypical 2-Cys Prdxs (Prdx1-5) (Fig.5) [131], [133], [141], [151]. In the typical 2-Cys Prdxs, the disulfide bond is intermolecular as it is formed between the sulfenic acid of one subunit with the Cr of a second subunit of the protein (Fig.5a). However, in atypical 2-Cys Prdxs, the disulfide bond is intramolecular, with the Cr localized in the same molecule (Fig.5b). The disulfide can be then reduced by a thiol-dependent enzyme, like thioredoxins or glutaredoxins [131], [152]. In Contrast, in the 1-Cys Prdxs, the sulfenic acid interacts with the π isoform of glutathione S-transferase (πGST) to form the disulfide bond [133], which is reduced afterwards by a glutathione (GSH)

(Fig.5c) [131], [133], [141].

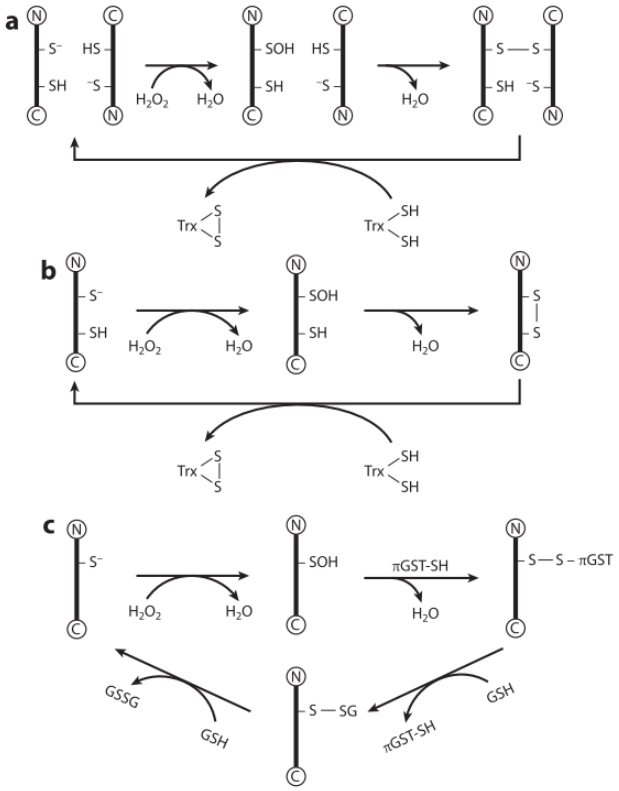

Figure 5. Reaction mechanisms of peroxiredoxin (Prdx) enzymes. The reaction mechanisms of (a) 2-Cys Prdx, (b) atypical 2-Cys Prdx, and (c) 1-Cys Prdx enzymes are shown. All three types of Prdx enzymes share a common first step, in which the peroxidatic Cys (Cp) attacks the peroxide substrate and is oxidized to sulfenic acid (Cp–SOH). The next resolving step (disulfide formation) for Cp–SOH distinguishes the three Prdx types. (a) For Prdx1 to Prdx4, the Cp–SOH in the NH_2-terminal region of one subunit of the homodimer is attacked by the resolving Cys (Cr) located in the COOH-terminal region of the second subunit, resulting in the formation of an intermolecular disulfide bond that is subsequently reduced by thioredoxin (Trx). (b) In Prdx5, both Cp and Cr are present in the same polypeptide and therefore form an intramolecular disulfide bond, which is also reduced by Trx. (c) Given that Prdx6 lacks a Cr residue, the Cp–SOH is resolved by a cysteine thiol (Cr–SH) provided by the π isoform of glutathione S-transferase (πGST). The heterodimeric disulfide formed between the 1-Cys Prdx and πGST is reduced by the successive action of two glutathione (GSH) molecules that are converted to oxidized glutathione (GSSG). Whereas 2-Cys Prdxs and 1-Cys Prdxs form antiparallel homodimers, Prdx5 forms a non-antiparallel homodimer. Both 1-Cys Prdx and atypical 2-Cys Prdx enzymes are indicated by a single chain because they both function as monomers. [133]

Based on sequence alignment of Prdxs from all biological kingdoms, six major clusters or subfamilies can be distinguished among Prdxs [128], [153]–[155].

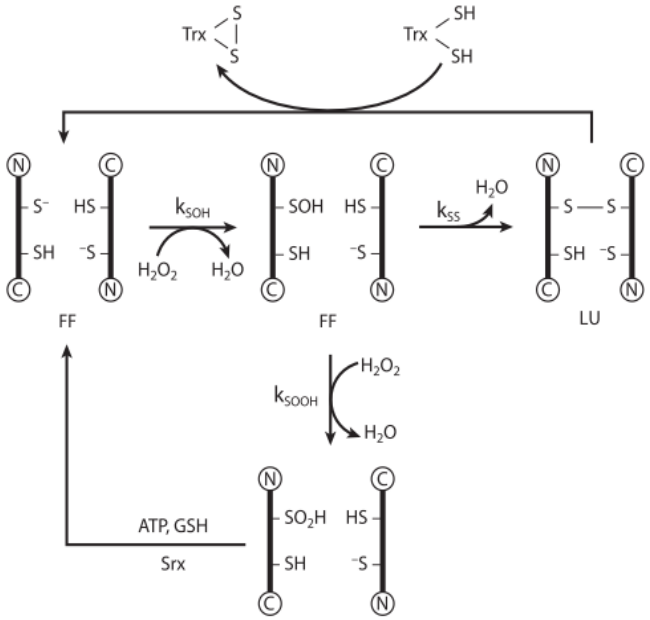

Figure 6. Model for the catalytic cycle and reversible hyperoxidation of 2-Cys Prdx. The Cp thiolate of 2-Cys Prdx, which is located at the bottom of the active site pocket in the FF conformation, is oxidized by H_2O_2 to Cp–SOH, which in turn enters two competitive pathways either to form a disulfide with Cr–SH or to undergo further oxidation to Cp–SO_2H. For the former pathway, a structural rearrangement must occur to generate an LU conformation in which the Cp–SOH is exposed and reacts with Cr–SH. The resulting disulfide is reduced by Trx to restore the Cp–SH in the FF state, completing the catalytic cycle. The Cp–SOH in the FF state can enter the second pathway to undergo further oxidation by H_2O_2 to Cp–SO_2H, resulting in catalytic inactivation. The inactivated, hyperoxidized Prdx is reactivated through a reduction reaction catalyzed by the ATP-dependent activity of Srx. Rate constants: kSOH, the second-order rate constant for the reaction of Cp–SH with H_2O_2; kSS, the first-order rate constant for disulfide formation between Cp–SOH and Cr–SH; and kSOOH, the second-order rate constant for the further oxidation of Cp–SOH to Cp–SO_2H. Abbreviations: ATP, adenosine triphosphate; Cp, peroxidatic cysteine; Cr, resolving cysteine; Cys, cysteine; FF, fully folded; GSH, glutathione; H_2O_2, hydrogen peroxide; LU, locally unfolded; Prdx, peroxiredoxin; Srx, sulfiredoxin; Trx, thioredoxin. [133]

The Prdx1 subfamily comprises the mammalian Prdx1-4, some of the plant peroxiredoxins, thioredoxin peroxidases of yeast, the tryparedoxin peroxidases of kinetoplastida and bacterial AhpCs. The Prdx5 subfamily is also seen in bacteria, lower fungi and higher plants. The Prdx6 subfamily appears prominent in archaea. This subfamily includes the mammalian Prdx6. The TPX subfamily stands for bacterial periplasmic "thiol peroxidases". The BCP subfamily includes 1-Cys Prdxs of ill-defined function originally described as "bacterioferritin-comigratory-protein". The AhpE subfamily includes all 1-Cys Prdxs found in mycobacterial and closely related bacterial species [128], [154], [155].

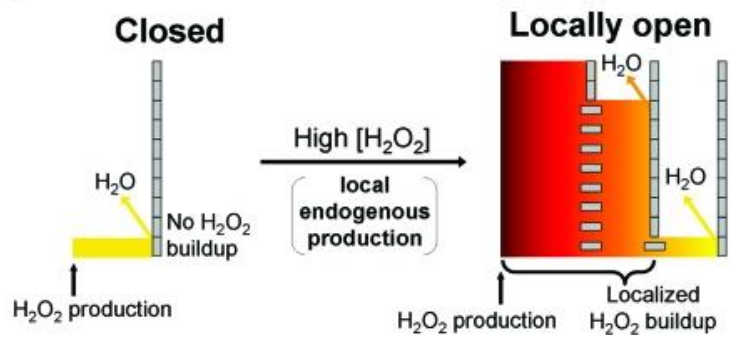

Figure 7. The floodgate model. Prxs are represented as tall barriers made up of gray rectangles—vertical for active, horizontal for overoxidized and inactive. The multiple barriers on the right reflect the cell-wide Prx distribution; Prxs that are close to the peroxide generation site (marked by an arrow) are overwhelmed and inactivated, whereas those at increasing distances away are not. This creates a steep peroxide gradient and allows for localized peroxide build-up after endogenous peroxide generation. The level of hydrogen peroxide is represented by both color gradient and height. [333]

Under high oxidative stress conditions, the typical 2-Cys Prdxs can be inactivated by overoxidation or even hyperoxidation [131] (Fig.6). Typical 2-Cys Prdxs carry a C-terminal domain YF motif that interacts with a GGLG motif in a loop neighboring the Cp, resulting a kinetic pause in the formation of the disulfide bond which can lead to over- or hyperoxidation of the Cp [151], [156]. Indeed, the sulfenic acid (R-SOH) of one Prdx can react with one or two molecules of H_2O_2 and a sulfinic (R-SO_2H) or sulfonic (R-SO_3H) acid is formed, respectively (Fig.6). The sulfinic acid formation of typical 2-Cys Prdxs is reversible, thanks to the sulfiredoxin reduction using ATP [157]. On the other hand, the sulfonic form is irreversible [158]. This inactivation of Prdxs is linked to H_2O_2-mediated redox signaling, as part of the "floodgate hypothesis" mechanism (Fig.7) [33], [35], [131], [156], [159], [160]. The floodgate theory proposes that when H_2O_2 accumulates at high levels, the C_P of Prdxs is hyperoxidized to sulfinic or sulfonic states. This allows accumulation of H_2O_2, which could then attack other targets and cause direct oxidation of other critical cysteine residues in redox-sensitive signaling proteins, permitting its function as intracellular messenger. In that manner, Prdxs have been proposed to play the role of redox sensors. The slow rate of Prdx reactivation via Srx-dependent reduction would be a built-in mechanism that would allow sufficient time for H_2O_2 to accumulate and propagate its signal [159]. It must be noted that the atypical 2-Cys Prdx5 and the 1-Cys

Prdx6 are overoxidized with very slow rate, thanks to their different C-terminal domain [131], [161].

There are many other post-translational modifications in Prdxs, except the hyperoxidation. These modifications play a role in cell signaling, regulating their peroxidatic activity [36], [162]. Tyrosine nitration has been reported as a post-translational modification of non-catalytic residues of Prdxs, which increases the peroxidatic activity of the enzyme [21]. Phosphorylation of a Thr90 in Prdx1 reduces the peroxidatic activity and inactivates the enzyme, while phosphorylation of a Ser32 residue increases it [163], [164]. Acetylation of Prdx1 and Prdx2 increases their activity in reducing H_2O_2 and increases their resistance to hyperoxidation [165], [166]. Additionally, C-terminal truncation has been shown to modulate Prdx activity, by eliminating the YF motif and making Prdxs more resistant to hyperoxidation [167], [168]. S-nitrosylation of Prdx2 inhibits both its enzymatic activity and protective function from oxidative stress [20], [169]. Finally, glutathionylation of Prdxs has been shown to support their peroxidase activity but also to protect them from irreversible hyperoxidation [170]–[172].

A major function of Prdxs would be to act as antioxidant enzymes to protect the cells from oxidative damages caused by high levels of reactive oxygen (ROS) and nitrogen (RNS) species, as it is well documented in the literature [141], [142], [173]–[180]. Additionally, as also discussed before, Prdxs could

have an essential role in redox signaling notably thanks to their over-/hyperoxidation and the subsequent local accumulation of H_2O_2 [10], [133], [156], [160], [162], [181]–[183]. Modulation of Prdx activity and expression by •NO could contribute also to the antioxidant response and control of H_2O_2-mediated signal transduction [183]. Moreover, it was proposed that the local inactivation of Prdx1 by phosphorylation could allow the transient accumulation of H_2O_2 around membranes of cells and play a role in local redox signaling [181]. Also, the expression of different Prdxs is dramatically increased in mouse and murine bone marrow-derived macrophages (BMMs) upon stimulation with IFN-γ and lipopolysaccharide (LPS), suggesting that Prdxs should play important roles in defense mechanisms or in redox-dependent signaling during inflammation [183]–[185].

Also, more recently, a novel role for Prdxs has emerged as pathogen-associated molecular patterns (PAMPs) and damage-associated molecular patterns (DAMPs) triggering inflammation via TLR2-TLR4 binding and signaling [186]–[194].

The Table 10 summarizes the different roles of Prdxs in cancer and the Table 11 in inflammation (end of the chapter).

3.1. Prdx1

As mentioned previously, Prdx1 is mainly localized in the cytosol of mammalian cells. Prdx1 exhibits a conserved Cys^{51} in the N-terminal domain and a conserved Cys^{172} in the C-terminal domain [195]. Prdx1 can appear in a pentameric arrangement of dimers to form a decamer or even form higher molecular complexes when exposed to high levels of H_2O_2 [131], [195].

Prdx1 expression is under the control of Ets and HMGB1 transcription factors during oxidative stress conditions [196]. Loss of Prdx1 expression in mouse T cells and fibroblasts results to high level of ROS and may promote mutations [197]. It was shown also that Prdx1 protects the telomeres from ROS and preserves their elongation during the S phase [198]. Prdx1 interacts with the six-transmembrane protein GDE2 to drive motor neuron differentiation, while the loss of Prdx1 causes motor neuron deficits [199].

Prdx1 KO mice are viable and fertile but they have reduced life span, they develop haemolytic anaemia and several malignant cancers [200]. Prdx1 protects the redox-sensitive PTEN from oxidation-induced inactivation, which appears to be essential for its tumor suppressive function [201]. Under high oxidative stress conditions, Prdx1 is oxidized and this leads to MAPK phosphatase inactivation, acting as a sensor in redox-regulated senescence in breast cancer [202]. Prdx1 was also shown to modulate the activity of the

p38 MAPK and to promote pancreatic cancer cell invasion [203]. Prdx1 can promote tumor metastasis and angiogenesis through the MMP and VEGF signaling pathway in colorectal cancer [204]. Prdx1 was reported to modulate respiratory syncytial virus (RSV)-induced ROS signaling, functioning as non-redundant inhibitor of basal NF-κB-dependent gene expression [205]. Prdx1 KO mice are also sensitive to bleomycin-induced pulmonary inflammation and fibrosis, caused by increased ROS levels [206]. Prdx1 KO mouse embryonic fibroblasts are more susceptible to Ras transformation and DNA damage is higher [207].

It was shown that Prdx1 and other Prdxs are released from necrotic brain cells in post-ischemic inflammation in the brain to act as DAMPs, inducing the expression and release of inflammatory cytokines by macrophages [186]. Also, extracellular Prdx1 increases the production of proinflammatory mediators under hypoxia in cardiogenic shock patients or after exposure to LPS and TNF-α [188], [208], [209].

3.2. Prdx2

Prdx2 is a 2-Cys typical Prdx localized in the cytosol, carrying a conserved Cys^{51} in the N-terminal domain and a conserved Cys^{172} in its C-terminal domain [210]. Prdx2 uses H_2O_2 or peroxynitrite as substrates. The minimal

functional unit of Prdx2 is a dimer, but well-resolved crystal structures of erythrocyte Prdx2 show that the protein is organized in a decamer formed by a doughnut arrange of 5 dimers [210], [211].

Prdx2 KO mice are also viable and fertile. However, Prdx2 KO mice present hemolytic anemia with decreased hematocrit levels and splenomegaly. Moreover, the lack of Prdx2 leads to carcinogenesis [212], [213]. In another study, it was reported that Prdx2 is upregulated in B cell tumors, while the knockdown of Prdx1 and Prdx2 decreases the growth rate of lymphoma cells [214]. It was shown also that Prdx2 (and Prdx4) inhibits the binding of the hypoxia-inducible factors (HIFs) to the hypoxia response elements of target genes (SLC2A3, GPI, and PDK3), inhibiting their transcription. These genes are crucial for the pathogenesis of cancer and other human diseases in prolonged hypoxia environment. Therefore, Prdx2 is involved in a new mechanism for gene feedback inhibition [215].

The role of Prdx2 in central nervous system has been studied using transgenic mouse model overexpressing Prdx2. These mice present reduced brain injury and improved neurological recovery up to three weeks after transient focal cerebral ischemia compared to wildtype littermates [216]. The role of Prdx2 in the central nervous system is also revealed by the protection that Prdx2 offers to hippocampal synaptic plasticity against age-related oxidative damage [217]. Prdx2 expression levels are higher in astrocytes in white

matter multiple sclerosis lesions, suggesting that Prdx2 could be upregulated to provide resistance against oxidative stress in brain [218].

Prdx2 is also involved in inflammation in different ways. Prdx2 can inhibit the immune cell responsiveness of T lymphocytes and dendritic cells, through regulation of the scavenging of low amount of ROS [219]. Prdx2 expression is increased in naive $CD8^+$ T cells after T cell receptor stimulation by phorbol myristate acetate (PMA) and ionomycin (ION), the number of effector $CD8^+$ T cells in Prdx2-deficient mice was increased, suggesting that Prdx2 modulation could increase recruitment and expansion of $CD8^+$ T cells during chronic infection [220]. Additionally, LPS causes lethal shock in Prdx2 KO mice compared to their wildtype littermates, because of greater ROS generation and activation of NADPH oxidases, while the Prdx2-deficient macrophages produce higher levels of pro-inflammatory cytokines and present lower activation of NF-κB and MAPK signaling pathways, suggesting an important role for Prdx2 in the prevention of excessive host responses to microbial products [221]. Prdx2 decreases the activation of JNK and p38 but increases that of Erk, during TNF-α activation in HeLa cells, showing that Prdx2 is an important regulator of TNF signaling pathways [222]. Prdx2 deficiency decreases the colonic inflammation *in vivo*, through the increase in $Foxp3^+$ Treg cells [223].

The role of Prdx2 in inflammation is also linked to its function as a DAMP. Intracellular but also extracellular levels of Prdx2 are increased in lymphocytes and serum of rheumatoid arthritis patients, suggesting that Prdx2 may be involved in the activation of the pro-inflammatory cells [224]. Extracellular Prdx2 acts as a DAMP, by triggering macrophages to produce and release TNF-α and other inflammatory cytokines [192], [208], [225]. Additionally, extracellular Prdx2 activates microglia via TLR4/MyD88/NF-κB pathway and leads to neuronal apoptosis in subarachnoid hemorrhage (SAH) patients [191].

3.3. Prdx3

Prdx3 is addressed to mitochondria [174]. Prdx3 exhibits a peroxidatic Cys^{47} in its N-terminal domain and a resolving Cys^{168} in the C-terminal domain of the protein [226]. The enzyme can form a decamer or a dodecamer [226], [227].

Prdx3 KO mice are viable, fertile but they present higher DNA damage, higher protein carbonylation and higher ROS levels [228] compared to wildtype animals. They are also more sensitive to lung inflammation induced by LPS with more severe inflammatory cell infiltration and airway wall thickening as well as increased oxidative stress damages [228].

Prdx3 is linked to the protection of cells from apoptosis in many cases. Prdx3 depletion in HeLa cells results in increased intracellular levels of H_2O_2 and sensitizes cells to induction of apoptosis by staurosporine or TNF-α [174]. Prdx3 overexpression protects cells against apoptosis caused by H_2O_2, *t*-butylhydroperoxide (TBH), and the anticancer drug imexon [173]. Overexpression of Prdx3 attenuates lactate dehydrogenase (LDH) release and neuronal apoptosis after traumatic neuronal injury, by preserving mitochondrial function and mitochondrial biogenesis [229]. On the other hand, silencing of Prdx3 in human neuroblastoma SH-SY5Y cells makes the cells more sensitive to oxidative stress and apoptosis induced by MPP+ [230]. Additionally, Prdx3 suppression leads to decreased MCF-7 cell survival in the absence of doxorubicin and increases the doxorubicin-induced toxicity leading to apoptosis [231].

Prdx3 is also linked to age-related diseases, such as osteoarthritis and Alzheimer's disease [232], [233]. Chondrocytes from old human adults presents higher basal levels of hyperoxidized Prdx3 and under conditions of oxidative stress, which is associated with inhibition of pro-survival Akt signaling and stimulation of pro-death p38 signaling [232]. H_2O_2 scavenging function of Prdx3 is associated also to Alzheimer's disease. Indeed, aged double transgenic mice overexpressing amyloid precursor protein (APP) and Prdx3 have improved cognition, reduced brain amyloid beta levels and

decreased amyloid beta production, compared to aged APP transgenic mice [233]. The double transgenic mice APP/Prdx3 present also reduced mitochondrial oxidative stress damage and increased mitochondrial function, while the CREB signaling, which is important for cognition, is enhanced.

There are a few data in the literature suggesting a link between Prdx3 and carcinogenesis. As it is mentioned above, Prdx3 KO mice are viable and they do not develop cancer, as it happens in the Prdx1 and Prdx2 KO mice [228]. Prdx3, among the other Prdxs, is highly expressed in endometrial cancer tissues. Prdx3 is associated with advanced stage and poor prognosis of endometrial cancer, suggesting that it could be used as a prognostic marker for endometrial cancer [234].

Recombinant Prdx3 from *Toxoplasma gondii* partially protects mice against lethal infections with *T. gondii*, by promoting IL-12 release by macrophages, establishing a new role of Prdx3 as a PAMP [235]. The role of Prdx3 as a DAMP was tested in macrophages treated with exogenous recombinant Prdx3 but it was shown that Prdx3 causes mainly increased cytotoxicity [225].

3.4. Prdx4

As a member of the typical 2-Cys Prdx subgroup, Prdx4 forms homodimers with the two subunits in a head-to-tail manner [236]. Five dimers of Prdx4 can be organized also as homodecamers. Prdx4 exhibits a conserved peroxidatic Cys^{52} in its N-terminal domain and a conserved Cys^{173} in the C-terminal domain [175], [237]. The localization of Prdx4 is mainly in the endoplasmic reticulum (ER) [237]. It was shown that Prdx4 can be secreted, thanks to a signal peptide at the N-terminus, that is responsible for translocation across the ER membrane into the luminal space [236]. This sequence is cleaved, allowing the Prdx4 being extracellularly released.

The antioxidant role of Prdx4 in apoptosis has been studied in relation with different diseases. It appears that Prdx4 could be found as a membrane-associated form, playing a role in the acrosome formation during spermiogenesis in rats [146]. In accordance with this study, Prdx4 KO mice are viable, fertile but present testicular atrophy caused by an abnormally high incidence of spermatogenic cell death associated to increased ROS levels [238]. Also, overexpression of Prdx4 can suppress the progress of the atherosclerosis in Apolipoprotein E KO mice, by reducing oxidative damage and apoptosis [239]. It was also shown that Prdx4 overexpression prevents ROS generation stimulated by EGF and p53 in A431 and NIH-3T3 cells [175].

Prdx4 expression and Akt phosphorylation are increased in oligodendrocytes that are co-incubated with human umbilical cord blood cells (HUCB) [240], [241]. These studies show that secreted Prdx4 mediates the protective effects of HUCB cells, either through its antioxidant properties, either with activation of survival signaling, or both. Prdx4 is also upregulated in dorsal root ganglia (DRGs) during sciatic nerve injury which suggests its role as an endogenous HIF1α-dependent, transcriptionally regulated cytoprotective antioxidant enzyme in nerve injury that may be important for neuronal survival and regeneration [242].

Prdx4 is also linked to immune response in different situations. Indeed, Prdx4 modulates respiratory syncytial virus (RSV)-induced NF-κB signaling, reducing the virus-inducible ROS and protein carbonylation [205]. Additionally, Prdx4 negatively regulates the activity of the NF-κB in large yellow croaker, while in the same study, in zebrafish, suppression of Prdx4 expression by siRNA significantly increases animal mortality after mixed bacterial infection, proposing a novel antibacterial mechanism in fish [243]. Prdx4 localized in the ER plays a critical role in controlling inflammatory response in Drosophila [244]. The extracellular form of Prdx4, acting as a DAMP, activates the JAK/STAT pathway and upregulates the downstream response genes. On the other hand, the cytosolic form of Prdx4 promotes apoptotic cell death due to interaction with the inhibitor of apoptosis protein

1 (IAP1) in Drosophila [244]. From this study, it was shown that the inflammatory and pro-apoptotic effects of Prdx4 in response to sterile stimuli are mediated via the NF-κB analog Relish by the activation of the ER/Relish signaling branch. Prdx4 was also reported to act as an inflammatory DAMP, inducing TLR4 activation and inflammatory response in macrophages, contributing to post-ischemic neuroinflammation and brain injury [225].

The role of Prdx4 in carcinogenesis has been briefly studied. Prdx4 interacts with Srx and the disruption/enhancement of this Srx–Prdx4 axis reduces or accelerates respectively the formation of tumor metastases in a mouse model of lung tumor metastasis [245]. This Srx–Prdx4 axis is required for the activation of specific intracellular phosphokinase signaling including the AP-1/MMP9 axis and MAPK signaling. [245].

3.5. Prdx6

Prdx6 is the only 1-Cys Prdx in mammals. It exhibits only a peroxidatic Cys^{47} in its N-terminal domain and Prdx6 lacks a resolving Cys [182]. After the sulfenic acid is formed on the Cys^{47}, the π isoform of glutathione S-transferase (πGST) interacts with Prdx6 to form a disulfide bond. The resulting heterodimeric disulfide is reduced by glutathione (GSH) [133], [246]. The GSH is bound to πGST, resulting in glutathionylation of Prdx6 Cp

and πGST release. A second molecule of GSH is used that results in Prdx6 deglutathionylation, completing the cycle [133], [246]. Prdx6 does not form decamers as typical 2-Cys Prdxs [247].

Prdx6 is a bifunctional protein with both GSH peroxidase and phospholipase A_2 (PLA_2) activities, which allow it to play a role in the recycling and the synthesis of the phospholipids [149], [248]–[250]. The PLA_2 activity of Prdx6 has been implicated in dipalmitoyl phosphatidyl-choline (DPPC) turnover, a major phospholipid component of lung surfactant, a secretion that stabilizes lung alveoli during respiration [250]. Indeed, Prdx6 KO mice present reduced degradation of internalized DPPC in the lung epithelium and a decreased rate in DPPC synthesis [251].

Prdx6 expression can be regulated in different ways in different cell types. The B cell-specific activator protein, Pax5 binds to Prdx6 promoter region, regulating the transcription of Prdx6 in mouse cells [252]. Additionally, Prdx6 upregulation in reactive astrocytes inhibits microglial activation, MMP9 expression and experimental autoimmune encephalomyelitis (EAE) via reduction of ROS and $^{\bullet}NO$ [253]. Prdx6 expression is upregulated through growth differentiation factor-9 (GDF-9) in oocytes and cumulus cells during *in vitro* maturation, regulated by both cell types at the same time [254].

The pro-inflammatory cytokines IFN-γ and TNF-α downregulate Prdx6 expression in insulin-producing RINm5F cells, while the anti-inflammatory cytokine IL-4 is able to counteract this downregulation, suggesting that Prdx6 modulation could be important for β-cells protection against oxidative stress [255]. Additionally, upregulation of Prdx6 by LPS and IFNγ was associated with the activation of multiple protein kinases, most notably JAK2, PI3K, and p38 MAPK and also in an NO-independent manner by cyclooxygenases and prostaglandin E2, suggesting a possible role of Prdx6 in defense mechanisms in activated macrophages against oxidative stress during inflammation or infection [185]. Prdx6 can be phosphorylated by MAPKs (ERK2, p38), increasing its PLA_2 activity and affinity for the membrane that leads to the activation of NOX2, regulating the prostaglandin D2 and E2 production in acute inflammation in macrophages [256].

Prdx6 is implicated in diseases' development, through the inactivation of its two activities. Overexpression of Prdx6 could accelerate the development of Alzheimer's disease through independent PLA_2 activation and nuclear respiratory factor 2 (Nrf2) transcription, causing the increase of amyloidogenesis [257]. Prdx6 expression is decreased in patients with childhood cortical dysplasia (CCD), probably as a result of enhanced oxidative stress that is associated with developmental brain disorders and epileptogenesis [258]. Prdx6 expression is increased in satellite glial cells

after sciatic nerve injury, as a result of activation of endogenous defense against ROS imbalance caused by upregulations of pro-oxidative enzymes in injured neurons [242]. On the other hand, Prdx6 overexpression is not associated with significant protection against ethanol-mediated liver injury, suggesting that antioxidant function of Prdx6 would not be involved in the initiation and/or progression of alcoholic liver disease (ALD) [259]. It is worth to mention that both peroxidase and phospholipase A_2 activities of Prdx6 are required to promote the invasion and the metastasis of lung cancer cells, by promoting the accumulation of arachidonic acid and inducing the invasive pathway involving p38 kinase, phosphoinositide 3-kinase, Akt, and urokinase-type plasminogen activator [260].

Prdx6 KO mice are viable, fertile but they are sensitive to oxidative stress caused by paraquat treatment [179], [261]. It was also shown that Prdx6 protects ARPE-19 cells from oxidative damage caused by H_2O_2 and blue light via PI3K/AKT signaling pathway, while the Prdx6 knockdown enhances oxidative stress damage [262]. Additionally, Prdx6 overexpression in mice makes them more resistant to lung injury in hyperoxia, with less epithelial cell necrosis, perivascular edema, and inflammatory cell recruitment [263].

Prdx6 is also acting as a DAMP. Indeed Prdx6 released from ischemic cells is an endogenous ligand for TLR2 as well as TLR4, and initiates destructive immune responses in ischemic brain, by upregulating pro-inflammatory

cytokines (TNF-α, Il-1β, Il-23, Il-17) [186], [187]. Ligustilide (LIG) may provide an early and direct neuroprotection by inhibiting TLR4/Prx6 signaling and subsequent immunity and neuroinflammation after cerebral ischemia, proposing that the blocking of this signaling could be used as a treatment for ischemic stroke [187].

Table 10. Prdxs involvement in cancer

Prdx1	Prdx1 KO mice present hemolytic anaemia and malignant tumors [190]	Prdx1 prevents ROS-induced senescence in breast cancer cells [192]	Prdx1 interaction with p38 MAPK promotes pancreatic cancer cell invasion [193]	Prdx1 promotes tumor metastasis and angiogenesis in colorectal cancer [194]
Prdx2	Prdx2 KO mice present hemolytic anemia with decreased hematocrit levels and splenomegaly [202], [203]	Prdx2 is upregulated in B cell tumors while Prdx2 knockdown decreases the growth rate of lymphoma cells [204]	Prdx2 inhibits the transcription of genes related to the pathogenesis of cancer under hypoxia [205]	
Prdx3	Prdx3 is highly expressed in endometrial cancer tissues [224]			
Prdx4	The dissruption of Prdx4-Srx interaction reduces the formation of tumor metastasis in lung tumor mouse model [235]			
Prdx6	Prdx6 peroxidase and PLA_2 activities are required to promote invasion and metastasis of lung cancer cells [250]			

Table 11. Prdxs involvement in inflammation

Prdx1	Prdx2	Prdx3	Prdx4	Prdx6
	Prdx2 inhibits T lymphocytes and dendritic cells resposiveness through its ROS scavenging activity [209]			Prdx6 is downregulated in β cells by IFN-γ, TNF-α and Il-4 [245]
Prdx1 KO mice are more sensitive to bleomycin-induced pulmonary inflammation and fibrosis, caused by increased ROS levels [196]	Prdx2 expression is increased in naïve $CD8^+$ T lymphocytes, while in Prdx2 KO mice the number of the effector CD8+ T lymphocytes is increased [210]	Prdx3 KO mice are sensitive to lung inflammation induced by LPS [218]	Prdx4 modulates NF-κB signaling by reducing ROS levels and protein carbonylation [195]	Prdx6 is upregulated in macrophages by IFN-γ and LPS [175]
	Prdx2 KO mice are more sensitive to inflammation caused by LPS, while Prdx2 KO macrophages produce high levels of pro-inflammatory cytokines [211]		Prdx4 negatively regulates NF-κB activity and Prdx4 suppression increases animal mortality after bacterial infection [233]	Prdx6 is phosphorylated by MAPKs, increasing its PLA2 activity and regulating the prostaglandin D2 and E2 production during acute inflammation in macrophages [246]
Extracellular Prdx1 acts as a DAMP, increasing the expression and release of inflammatory cytokines in macrophages [176]	Prdx2 decreases the activation of JNK and p38, and increases Erk during TNF-α activation in HeLa cells [212]	Recombinant Prdx3 acts as a PAMP, protecting mice from lethal infections caused by *T. gondii*, by promoting Il-12 release [225]	Extracellular Prdx4 acts as a DAMP, activating JAK/Stat and TLR4 pathways [215], [234]	Overexpressed Prdx6 in mice makes them more resistant to lung injury caused by hyperoxia, associated with inflammatory cell recruitment [253]
	Prdx2 deficiency decreases colonic inflammation *in vivo* [213]			Extracellular Prdx6 acts as a DAMP, upregulating pro-inflammatory cytokines [176], [177]
	Extracellular Prdx2 acts as a DAMP, activating the expression of inflammatory cytokines in macrophages [182], [198], [215]			

4. Peroxiredoxin-5

Peroxiredoxin-5 was the last Prdx isoform to be characterized [141], [143], [148], [264]–[266]. It is a peroxidase that reduces peroxynitrite and alkyl hydroperoxides with high rate constants (respectively 10^7 M^{-1} s^{-1} and 10^6 M^{-1} s^{-1}) but also H_2O_2 although with more modest rate constant (10^5 M^{-1} s^{-1}) [161], [267], [268]. The amino-acid sequence of Prdx5 diverges from the other members of the family, sharing only 28-30% amino-acid sequence identity [269]. Prdx5 protein is conserved from bacteria to mammals, with notable exceptions in birds, while dog and pig have lost the mitochondrial Prdx5 form [270]–[273].

Prdx5 protein is localized in different subcellular compartments in most living organisms depending on different transcriptional and translational start sites [148], [269], [270], [274], [275]. Indeed, human Prdx5 mRNA for example possesses two AUGs in the same reading frame and several transcription start sites have been identified [270]. The translation from the first AUG leads to the production of a 214-amino acid protein that corresponds to the long mitochondrial form of Prdx5. The translation from the second AUG produces a 162-amino acid protein, which is the cytosolic/peroxisomal/nuclear short form of Prdx5 (Fig.7). Thus, the long form (L-Prdx5) is addressed to mitochondria, thanks to the 52 extra amino acids that form the

mitochondrial targeting sequence (MTS) in the N-terminal domain of the enzyme. When addressed to mitochondria, the MTS is cleaved and the processed active Prdx5 protein exhibits the same size as the short form of Prdx5 (S-Prdx5) [148]. The S-Prdx5 which is localized in the cytosol, and addressed to peroxisomes and the nucleus, lacks the MTS [140], [141], [143], [145], [148], [270], [274]. Both the L-Prdx5 and S-Prdx5 contain a peroxisomal targeting sequence 1 (PTS1) SQL tripeptide in their C-terminal domain [148], [264] (Fig.8). Although L-Prdx5 has both targeting sequences (MTS and PTS1), the enzyme is targeted only to mitochondria [142], [180]. It must be noted that only a short Prdx5 is detected in human and mouse cell lines and tissues by Western blotting, suggesting that L-Prdx5 is, upon mitochondrial

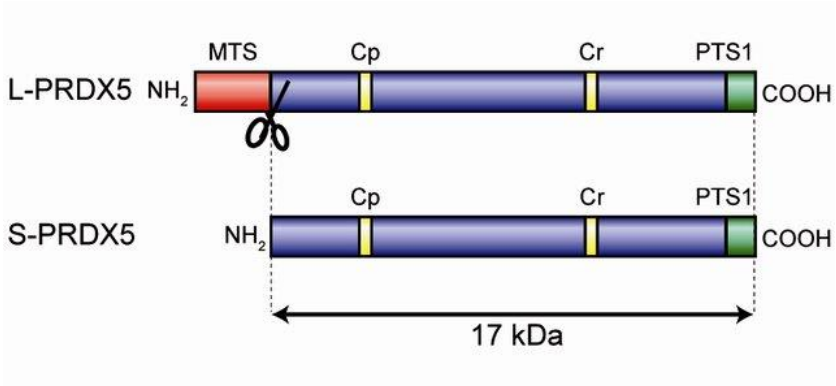

Figure 8. Representation of the long (L-PRDX5) and short (S-PRDX5) forms of human Prdx5. They are both produced by alternative use of two translation-initiation sites. The L-PRDX5 possesses a mitochondrial targeting sequence (MTS) that is cleaved upon translocation into mitochondria. Both mature forms have the same molecular mass and exhibit a peroxisomal targeting sequence type 1 (PTS1) at their C-terminus. The peroxidatic (Cp) and resolving (Cr) cysteines are indicated in yellow. [161]

internalization, rapidly converted to a short Prdx5 which is the active form of the enzyme [141], [142].

As it was mentioned previously, Prdx5 is an atypical 2-Cys Prdx that forms an intramolecular disulfide bond upon oxidation. The peroxidatic Cys^{47} reduces hydrogen peroxide, organic peroxides or the peroxynitrite to form a sulfenic acid. Then, the sulfenic acid is attacked by the resolving Cys^{151} to form an intramolecular disulfide bond. Trx1 in the cytosol and the nucleus or Trx2 in the mitochondria are able to reduce the disulfide bond to recycle the enzyme [161], [247], [276], [277]. Structurally, Prdx5 form a different type of dimers (A dimers) compared to typical 2-Cys or 1-Cys Prdxs (B dimers). In A dimers, alpha3 helix of one monomer comes in close contact with the alpha5 helix of the other monomer [161]. Overoxidized Prdx5 is not reduced by sulfiredoxin as the typical 2-Cys Prdxs. Moreover, Prdx5 lacks GGLG motif in the C-

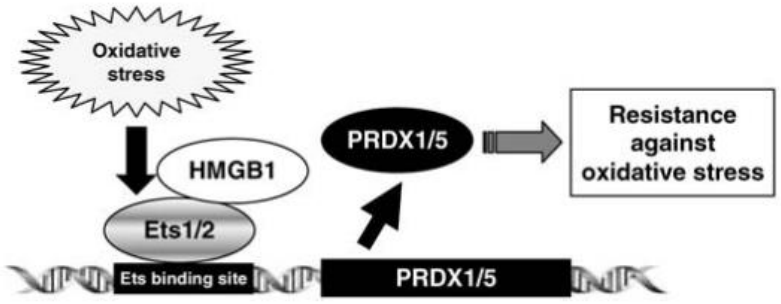

Figure 9. Prdx1/5 regualtion by Ets/HMGB1 transcription system. Oxidative stress induces the expression of Ets transcription factors. Then, Ets transcription factors induce both Prdx1 and Prdx5 expression via binding to Ets binding site. HMG proteins enhance the DNA binding ability of Ets transcription factors and function as a coactivator. Increased Prdxs lead to resistance against oxidative stress. [196]

terminal domain, making the enzyme more resistant to over- or hyperoxidation [157], [161]. A few reports show other Prdx5 post-translational modifications. Prdx5 can undergo glutathionylation in rat hepatocytes and human hepatoma cells [278]. There are no data in the literature for other Prdx5 modifications.

Prdx5 gene expression can be controlled by the Ets transcription factors and the high-mobility group protein B1 (HMGB1) [196]. Under oxidation stress conditions, the expression of Ets transcription factor is induced and then they bind in the Ets binding site upstream the Prdx5 gene region, using HMGB1 as a coactivator (Fig.9). Prdx5 expression is constitutive in almost all cell types but can also be upregulated to provide protection against oxidative stress, to modulate redox-dependent signaling pathways and pro-inflammatory responses [196]. Additionally, Prdx5 gene is negatively regulated by the transcription factor GATA1, which leads to protection loss against apoptosis (Fig.10) [279]. Moreover under oxidative stress, it was shown that c-Myc oncoprotein is able to increase Prdx5 expression in the absence of Prdx1, by direct transcriptional activation, although when Prdx1 is present, it serves to dampen this upregulation [280]. It was also reported that human Prdx5 promoter exhibits binding sites for nuclear respiratory factor 1 (Nrf1) and 2 (Nrf2), which regulate the biogenesis of mitochondria at basal levels activity in the absence of oxidative stress [274].

In a very recent study, it was reported that Prdx5 KO in *Xenopus* leads to reduced expression levels of pyruvate kinase (PK) and is associated with excessive production of ROS in epithelial cells, resulting in mitochondrial dysfunction and abnormal ciliogenesis in *Xenopus* embryos [281]. In a study published in 2018 increased fat mass, adipocyte hypertrophy, severe fatty liver disease and high levels of triglyceride in serum was reported in a Prdx5 KO mouse [282]. Moreover, in a previous proteomic analysis of mouse kidney under hypoxia in Prdx5 knockdown mice, it was shown that proteins related to oxidative stress, fatty acid metabolism and mitochondrial dysfunction were both significantly up- and down-regulated [283].

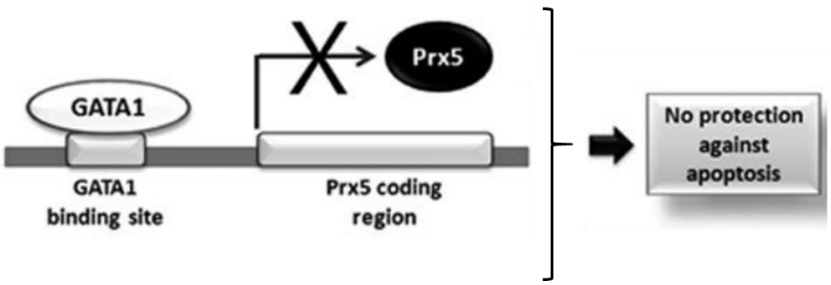

Figure 10. Regulation of Prdx5 gene expression via GATA1 in breast cancer cells. The transcription factor binds to its binding site in the Prdx5 promoter region and negatively regulates Prdx5 expression. GATA1 binding to promoter region leads to reduction of *Prdx5* transcription and Prdx5 protein expression. Cells under oxidative stress may undergo apoptosis due to loss of Prdx5-mediated protection against apoptosis. [279]

The cytoprotective role of Prdx5 against oxidative stress damages has been extensively studied in the literature. Overexpression of Prdx5 protects

chinese hamster ovary (CHO) cells from peroxidation, thus reducing cell death and DNA damages [142], [180]. Moreover, yeast cells are protected from cell death and lipid peroxidation induced by paraquat, thanks to mitochondrial and cytosolic expression of human Prdx5 [284]. Additionally, peroxisomal Prdx5 protects 158N oligodendrocytes from lipid peroxidation which is induced by Killer-Red phototoxicity and H_2O_2 [285].

Prdx5 is highly expressed in osteoarthritic cartilage, while knockdown of Prdx5 in the osteoarthritic chondrocytes increases apoptosis caused by the decreased ROS scavenging, via activation of Wnt/β-catenin signaling [286], [287]. Additionally, Prdx5 is upregulated in degenerative human tendon, protecting human tendon cells against apoptosis, suggesting also that oxidative stress is involved in the pathogenesis of the disease [288], [289].

Prdx5 is also reported to be involved in intracellular redox signaling, preventing p53-dependent generation of ROS, and resulting in apoptosis inhibition [290]. Additionally, Prdx5 overexpression in 3T3L1 cells significantly reduced adipogenesis by suppressing the expression of the adipogenic genes C/EBPa, PPARγ, aP2 and GLUT4 and decreasing the phosphorylation levels of Akt [282]. In the same study, Prdx5 decreases insulin-induced intracellular and mitochondrial ROS generation which is linked closely to adipogenesis [282].

As a DAMP, Prdx5 was shown to induce the expression and release of Il-23, II-12β and TNF-α after post-ischemic inflammation in the brain, via binding to TLR2 and TLR4 receptors [186]. In the same study, Prdx5 was reported to activate the NF-κB pathway through TLR4. Also, it was recently shown by atomic force microscopy (AFM) that extracellular Prdx5 specifically binds to TLR4 receptors on macrophage-differentiated THP-1 cells, and on human TLR4-transfected CHO cells, triggering a proinflammatory response [190].

4.1. Prdx5 in the Central Nervous System

Several studies on Prdx5 have been carried out, in order to understand the role of this enzyme in the central nervous system. In a systematic histological study, it was shown that Prdx5 is highly expressed in the mouse brain, mainly in neurons but also in choroid plexus and in ependymal layer [291]. In the peripheral nervous system, Prdx5 expression levels are higher in dorsal root ganglia (DRGs) neurons after sciatic nerve injury, while its expression is reduced in deficient mice for the hypoxia inducible factor 1 alpha (HIF-1α), suggesting that Prdx5 could be an endogenous HIF1α-dependent cytoprotective antioxidant enzyme during nerve injury [242]. The most representative studies of Prdx5 in CNS are listed in table 12.

The cytoprotective role of Prdx5 in central nervous system is linked to the development of different diseases. Mitochondrial Prdx5 silencing in human neuroblastoma SH-SY5Y cells causes increased oxidative damages and apoptosis induced by 1-methyl-4-phenylpyridinium ion (MPP+), a complex I inhibitor which provides an experimental paradigm of Parkinson's disease [230]. On the opposite, overexpression of mitochondrial Prdx5 in the same cell model exposed to MPP+ prevents Ca^{+}-dependent apoptosis by removal of mitochondrial ROS/RNS, which are necessary to induce redox activation of IP_3R and subsequent Ca^{2+} release in the cytosol to pursue apoptosis [292]. Altogether, these data suggest that Prdx5 could be a molecular link between ROS/RNS generation and Ca^{2+} dysregulation in some neurodegenerative processes. Additionally, the neuroprotective effects of Prdx5 against neonatal ibotenate-induced excitotoxic challenge was shown by the administration of recombinant Prdx5 in newborn mice resulting in the elimination of ROS and providing protection in brain lesions [293].

More recently, it was shown that Prdx5 expression is induced by LPS in activated microglia cells. Prdx5 would act as a negative regulator of excessive mitochondrial fission and a modulator of pro-inflammatory responses by inhibiting ROS-dependent Ca^{2+}/calcineurin but also de-phosphorylation of Drp1(Ser637) [294]. In addition, it was reported that Prdx5 can prevent ERK–Drp1-mediated mitochondrial fragmentation and neuronal cell death caused

by amyloid-beta oligomers (AβO)-induced oxidative stress by decreasing ROS levels [295]. Taking together these data, it was proposed that regulation of Prdx5 expression could be a useful therapeutic target for preventing neuroinflammation, and neuronal cell death.

4.2. Prdx5 in inflammation

Prdx5 gene expression has been reported to be regulated by two main signaling pathways in immunostimulated primary macrophages [184]. In the first pathway, LPS stimulates Prdx5 gene expression by a TLR4- and TRIF-dependent signaling. The second pathway is activated by IFN-γ, MyD88 and TNFα. In both cases, MAPK signaling pathway is activated downstream, leading to Prdx5 gene expression [184]. It was confirmed in another study that Prdx5 expression is induced by both LPS and IFN-γ but Prdx5 induction is independent of NO production, as it happens for other Prdxs [185]. PI3K, p38 MAPK and JAK2 take part in the signaling pathway leading to upregulation of *Prdx5* transcripts [185]. *Prdx5* is induced by cooperative action among the ROS, RNS, and JNK signaling cascades in LPS- stimulated microglia [296]. In contrast, it was shown recently that phagocyte NO production induces a Keap1-Nrf2-mediated antioxidant response leading to Prdx5 expression [297]. Prdx5 then is able to reduce the NO production and

the Toll-like receptor (TLR)-induced cytokine production, acting as a negative regulator of inflammation. In the same study, *Prdx5* KO dendritic cells present elevated NO production and oxidative stress. This oxidative stress can be ameliorated by the iNOS inhibition, suggesting an important role of Prdx5 in the regulation of ROS and RNS during inflammation [297]. Prdx5 also interacts with Jak2 via its catalytic Cys^{48} residue, inhibiting the sequential phosphorylation of Jak2 and Stat5 induced by LPS, in turn diminishing IL-6 production [298].

The role of Prdx5 in inflammation has been also studied in other organisms such as invertebrates. Interestingly in insects, Prdx5 damps activation of the immune response, acting as a negative regulator of the Tak1-JNK signaling pathway in *Drosophila* [299]. Overexpression of drosophila Prdx5 increases resistance of flies to oxidative stress and extends their life span by up to 30% [300], while its inactivation decreases life span and induces apoptosis in muscle and digestive system tissues [301]. Table 12 summarizes the implication of Prdx5 in inflammation.

4.3. Prdx5 in Cancer

Most of Prdxs have been associated to several types of cancers [302]–[305] but the role of each Prdx in the development and the progression of

carcinogenesis is not always clear. Loss of Prdx expression in mice leads to an increased incidence of carcinogenesis, while many human tumors display increased levels of Prdxs [304], [305]. Increased mitochondrial ROS generation and disturbance of Prdx production in cancer cells may lead the cells to oxidative stress conditions and induction of apoptosis. However, Prdx expression in cancer cells able to scavenge ROS/RNS supports the survival and tumor maintenance by protecting cells from oxidative stress-induced apoptosis [305]. The specific role of Prdx5 in carcinogenesis is not clear either, due to few data of mechanistical studies. Some of these studies are presented below and in the Table 12.

Prdx5 overexpression was reported to significantly enhance cell proliferation, migration and invasion, promoting colon [306] and gastric cancer [307]. Prdx5 would enhance epithelial-to-mesenchymal transition (EMT), a procedure very critical for tumorigenesis and metastasis. It was reported that Prdx5 regulates the expression of two hallmark EMT proteins and two EMT-inducing transcription factors. Prdx5 would downregulate E-cadherin and upregulate Vimentin. Additionally Prdx5 upregulates the EMT-inducing transcription factors Snail and Slug, inducing the cell invasion. In addition, Prdx5 suppression was shown to markedly inhibit these EMT properties [306], [307]. In C26-injected mice with colon cancer and melanoma B16-bearing mice, the treatment with human Prdx5 decreases

tumor growth in a dose-dependent manner [308]. In the same study, programmed death ligand 1 (PD-L1) is proposed as one target of Prdx5 to inhibit the tumorigenesis [308].

Cytoplasmic Prdx5 is highly expressed in patients with endometrial cancer, suggesting that Prdx5 is associated with advanced-stage endometrial cancer and lymph node metastasis. Therefore, it was proposed that Prdx5 could be used as a prognostic marker in patients with endometrial cancer [234]. In the same manner, Prdx5 is highly expressed in human thyroid gland, suggesting that it could play a role in regulating intracellular levels of ROS/RNS, acting as antioxidant [144]. In hyperthyroid tissues such as Graves' disease, hot nodules, multinodular goiters (MNG) and Hürthle cell adenoma, Prdx5 expression is upregulated [144]. This upregulation supports that when the thyroid hormone synthesis is turned on, antioxidant defenses are also strengthened to face increased amounts of ROS/RNS [144]. Additionally, Prdx5 is expressed in malignant mesothelioma [140]. Prdx5 is mostly expressed in mitochondria of these tumors and is associated with longer survival of patients. This study points out the importance of further investigation for the implication of this enzyme in the mechanisms of tumor progression and primary drug resistance of malignant cells. All these cases emphasize a positive correlation between Prdx5 expression and

carcinogenesis in different cell types although further mechanistic investigation would be necessary.

Prdx5 was significantly downregulated in tumors obtained from Sudanese breast cancer patients, suggesting that the loss of Prdx5 affects the ability of ROS scavenging and apoptosis during tumorigenesis [309]. In the same study, Prdx5 mRNA was found to be overexpressed in tumors obtained from Chinese breast cancer patients. Prdx5 downregulation correlated with the development of breast cancer only in Sudanese patients, suggesting that Prdx5 could be a prognostic marker of population specifically for breast cancer [309]. As it was mentioned before, GATA-binding protein 1 (GATA1) is proposed as a negative transcription regulator of Prdx5 in human breast cancer cells [279]. GATA1 binds to the GATA1 binding sites of Prdx5 promoter region, decreasing Prdx5 expression and reducing the protection against apoptosis [279]. In another study the results were contradictory, showing that Prdx5 is increased in breast malignancy [310]. This increased expression is associated to a larger tumor size, positive lymph node status and shorter survival [310]. Prdx5 has been also implicated in the resistance against doxorubicin treatment in MCF-7 breast cancer cells, while Prdx5 inactivation makes MCF-7 breast cancer cells more sensitive in doxorubicin-induced toxicity [231]. As a matter of fact, the role of Prdx5 in the breast cancer

development is not clear, possibly because of the potential biphasic/dual or even pleiotropic role Prdx5 may play during carcinogenesis.

Prdx5 was also reported to protect human lung carcinoma cells from apoptosis that is induced by the anticancer drugs etoposide and adriamycin [311]. Prdx5 downregulation makes these cells more sensitive to apoptosis [311]. ROS production did not play a significant role in the adriamycin-induced cell death, so it was proposed that Prdx5 peroxidase activity was not responsible for the protection against adriamycin-induced apoptosis. These peroxidase-independent activities may include Prdx5 involvement in DNA protection against alkylation and supercoiling, which would require further investigation.

Table 12. Prdx5 involvement in cancer, inflammation and CNS

Cancer	Inflammation	CNS
Prdx5 overexpression enhances cell proliferation, migration and invasion, promoting colon and gastric cancer [295], [296]		
Human Prdx5 decreases tumor growth in mice with colon cancer and melanoma [297]	Prdx5 is upregulated by LPS, IFN-γ, MYD88 and TNF-α pathways in macrophages [174], [175]	Silencing/overexpression of mtPrdx5 increases/prevents oxidative damage and apoptosis induced by MPP+ in SH-SY5Y neuroblastoma cells [220], [281]
Prdx5 is highly expressed in endometrial cancer [224], hyperthyroid tissues [144], malignant mesothelioma [140] and in breast malignancies [299]	Prdx5 is upregulated by LPS in microglia [285]	Recombinant Prdx5 eliminates ROS in newborn mice, providing protection in brain lesions [282]
Prdx5 is downregulated in sudanese but overexpressed in chinese breast cancer patients [298]	Prdx5 expression is induced by NO production and this induction leads to reduced NO and cytokine production [286]	Prdx5 acts as negative regulator of excessive mitochondrial fission in microglial cells [283]
Prdx5 inactivation makes MCF-7 breast cancer cells more sensitive to doxorubicin-induced toxicity [221]	Prdx5 inhibits Jak2 and Stat5 phosphorylation induced by LPS and diminishes Il-6 production [287]	Prdx5 prevents ERK-Drp1-mediated mitochondrial fragmentation and neuronal cell death caused by ABO-induced oxidative stress [284]
Prdx5 downregulation makes human lung carcinoma cells more sensitive to apoptosis [300]		

PART II: Aim of the study

Prdx5 has a central role in the antioxidant system as well in the regulation of redox signaling in mammalian cells. Several studies on Prdx5 have been carried out, in order to understand the role of this enzyme in the central nervous system. Prdx5 is highly expressed in the mouse brain, mainly in neurons but also in choroid plexus and in ependymal layer. Additionally, Prdx5 gene expression is induced by two main signaling pathways in primary macrophages stimulated by LPS and IFN-γ. Finally, Prdx5 has been reported to be upregulated or downregulated in several cancers, suggesting a role of this enzyme during the tumorigenesis.

Therefore, the aim of this study is to figure out the exact role of Prdx5 in the different cell procedures and evolution of diseases *in vivo*. For this purpose, a Prdx5 KO (*Prdx5*$^{-/-}$) mouse model was obtained.

In the chapter 5, we provide a description of the procedure to obtain the *Prdx5*$^{-/-}$ mouse and a complete histological analysis of it. Markers of oxidative stress were measured in *Prdx5*$^{-/-}$ and *Prdx5*$^{+/+}$ mice, as well as a transcriptomic analysis of the model was carried out. Finally, *Prdx5*$^{-/-}$ and *Prdx5*$^{+/+}$ mice were challenged with LPS, in order to study the effect of the Prdx5 gene during inflammation.

In the chapter 6, we report the implication of Prdx5 in cancer development. Several *Prdx5*$^{-/-}$ mice (41.18 %) developed tumors after the age of 12 months.

The tumors of the *Prdx5*$^{-/-}$ mice were fixed and stained with specific markers, in order to identify the type of the tumors. Continuously, the PI3K/Akt/PTEN and MAPK signaling pathways were studies in *Prdx5*$^{-/-}$ and *Prdx5*$^{+/+}$ MEF cells, as well as in the *Prdx5*$^{-/-}$ tumors, to better understand the role of Prdx5 during the tumorigenesis.

In the chapter 7, we studied the role of Prdx5 in the CNS. Behavioral tests and immunostaining with specific markers of neurons and glial cells in different brain areas of young and old adult *Prdx5*$^{-/-}$ and *Prdx5*$^{+/+}$ mice were carried out.

PART III: Results

5. Peroxiredoxin-5 protects mice from lipopolysaccharide-induced endotoxic shock

Vasiliki Argyropoulou[1], Julie Goemaere[1], Charlotte Lefort[1], Laurence Liénard[1], André Clippe[1], Marie-Thérèse Ahn[1], Hervé Degand[3], Pierre Morsomme[3], Fadel Tissir[2], Bernard Knoops[1]*

[1]*Group of Animal Molecular and Cellular Biology, Louvain Institute of Biomolecular Science and Technology (LIBST), Université catholique de Louvain, 1348, Louvain-la-Neuve, Belgium*

[2]*Group of Developmental Neurobiology, Institute of Neuroscience (IoNS), Université catholique de Louvain, 1200, Brussels, Belgium*

[3]*Group of Molecular Physiology, Louvain Institute of Biomolecular Science and Technology (LIBST), Université catholique de Louvain, 1348, Louvain-la-Neuve, Belgium*

Keywords: *Peroxiredoxin, Prdx5, antioxidant, lipopolysaccharide, inflammation*

[*]***Address correspondence to :*** *Prof. Bernard Knoops, Louvain Institute of Biomolecular Science and Technology (LIBST), Université catholique de*

Louvain, place Croix du Sud, 4-5 bte L7.07.02, B-1348 Louvain-la-Neuve, Belgium. ***E-mail :*** *bernard.knoops@uclouvain.be* ***Tel :*** *+32-10-47 37 60 ;* ***Fax :*** *+32-10-47 35 15*

5.1 Abstract

Aims: Peroxiredoxins (Prdxs) are a superfamily of peroxidases widely distributed among prokaryotes and eukaryotes. Prdx5 is ubiquitously expressed in tissues and its roles as cytoprotective antioxidant enzyme, redox modulator and damage-associated molecular pattern (DAMP) have been reported mainly *in vitro*. The purpose of this work was to study Prdx5 function *in vivo* using transgenic mice in which *Prdx5* gene was inactivated with a gene-trap strategy.

Results: *Prdx5* knockout (*Prdx5*$^{-/-}$) mice are viable and fertile. The complete histological analysis of the *Prdx5*$^{-/-}$ mice was performed and did not reveal major tissue abnormalities. Measurements of oxidative stress markers for DNA, lipid and protein in *Prdx5*$^{-/-}$ tissues under normal conditions, revealed that lipid peroxidation is significantly higher in skeletal muscles and protein carbonylation is higher in brain. Additionally, lung and spleen of *Prdx5*$^{-/-}$ mice have shown a tendency in higher DNA oxidation. Transcriptomic analysis in *Prdx5*$^{-/-}$ liver and brain showed that several CYP450 genes are upregulated in

both organs. Also, the vulnerability of *Prdx5*$^{-/-}$ mice to intraperitoneal injection of proinflammatory lipopolysaccharide (LPS) was tested. *Prdx5*$^{-/-}$ mice were more sensitive to LPS compared to wild type animals. Finally, proteomic analysis of *Prdx5*$^{-/-}$ peritoneal phagocytes exposed to 1 μg/ml of LPS for 24 hours showed that different pathways related to immune system, apoptosis, metabolism and cell cycle regulation were significantly affected, pointing to a more complex role of Prdx5 in inflammation than anticipated.

Innovation/Conclusion: *Prdx5*$^{-/-}$ mice are more prone to LPS-induced endotoxic shock, suggesting that Prdx5 protein may play a major role in inflammation.

5.2 Introduction

Peroxiredoxins (Prxs or Prdxs) are a superfamily of peroxidases well conserved from prokaryotes to eukaryotes throughout evolution [1], [2]. Prdxs, with superoxide dismutases (SODs), the catalase (CAT) and glutathione peroxidases (GPXs), constitute the major enzymatic antioxidant defense system in mammals against peroxides [3]. Prdxs are able to reduce H_2O_2, alkyl hydroperoxides and peroxynitrite with high rate constants [4]. There exist 6 isoforms of Prdxs in mammals [5]. In most Prdxs, two catalytic

cysteines (Cys) are involved in the catalytic mechanism, the peroxidatic Cys (Cp) localized in the N-terminal region and the resolving Cys (Cr) in the C-terminal region. The Cp attacks the peroxide and a sulfenic acid (R-SOH) is formed [6]. Afterwards, the sulfenic acid forms a disulfide bond with the resolving cysteine (R-S-S-R) [7]. Finally, the disulfide bond is reduced (R-SH) by a thiol-containing reductant such as thioredoxin (Trx) [1]. Based on their catalytic mechanism and the number of active Cys in their molecule, mammalian Prdxs are classified in three subgroups. Prdx1-4 are classified among the typical 2-Cys Prdxs, in which the Cp of the first Prdx forms an intermolecular disulfide bond with the Cr from the second molecule of Prdx. Prdx5 is the only atypical 2-Cys Prdx in which the Cp forms an intramolecular disulfide bond with the Cr in the same molecule. Finally, Prdx6 is the 1-Cys Prdx that carries only the Cp [7], [1]. In this case, the sulfenic acid can be reduced by glutathione (GSH) in presence of glutathione S-transferase pi [8]. Mammalian Prdxs are distributed in all subcellular compartments but with different or common localizations depending on the cell type and the Prdx isoform [1]. Prdx1 and Prdx2 are localized in the cytosol and the nucleus, Prdx3 in the mitochondria, Prdx4 in the endoplasmic reticulum and is also extracellular, Prdx5 in the cytosol, the nucleus, the mitochondria and the peroxisomes and Prdx6 in the cytosol [1], [3], [9]. Moreover, several Prdxs

have been reported to play the role of damage-associated molecular pattern (DAMP) in inflammation after their release in the extracellular milieu [10].

Prdx5 reduces alkyl hydroperoxides and peroxynitrite with high rate constants but less efficiently H_2O_2 compared to typical 2-Cys Prdxs [11]. Prdx5 was the last isoform of the mammalian Prdxs to be characterized [12]–[14]. As it was mentioned previously, Prdx5 is an atypical 2-Cys Prdx that forms an intramolecular disulfide bond. Thioredoxin-1 (Trx1) reduces the intramolecular disulfide bond of Prdx5 in the cytosol and the nucleus and thioredoxin-2 (Trx2) in mitochondria. The amino-acid sequence of Prdx5 diverges from the sequence of the other members of the mammalian family, sharing only 28-30 % amino-acid sequence identity [15]. Human Prdx5 can be expressed as a long form (L-Prdx5) which is targeted to mitochondria, thanks to the mitochondrial targeting sequence (MTS) [12], [16]. Once imported into mitochondria, L-Prdx5 is cleaved into a short form which is identical to the short form (S-Prdx5) localized in the cytosol, peroxisomes and nucleus, that lacks the MTS. S-Prdx5 like L-Prdx5 contains a weak peroxisomal targeting sequence 1 (PTS1) SQL tripeptide at the C-terminus of the protein [11], [14].

Several studies investigated Prdx5 functions in different cell types and living organisms [11], [17], [18]. As mentioned previously, Prdx5 was reported to be an antioxidant enzyme with cytoprotective role against oxidative attacks,

like other members of this family of peroxidases. Indeed, Prdx5 overexpression in different subcellular compartments of chinese hamster ovary (CHO) cells protects them against exposure to extracellular peroxides [19], [20]. Prdx5 also prevents MPP+-mediated apoptosis in SH-SY5Y neuroblastoma cells and in this context it was proposed that Prdx5 may act as a modulator of mitochondria–ER crosstalk [21], [22]. It was also reported that peroxisomal Prdx5 protects 158N oligodendrocytes against peroxisomal and mitochondrial oxidative stress [23]. Moreover, Prdx5 plays a protective role in human tendon cells against oxidative stress by reducing apoptosis and maintaining collagen synthesis [24], [25]. Prdx5 expression was shown to be higher in the thyroid gland of patients with Graves' disease, an autoimmune disease that affects the thyroid and causes hyperthyroidism, suggesting that Prdx5 could act as antioxidant [26]. Prdx5 knockdown (KD) in mouse using RNA interference has been reported *in vivo* [27]. Although Prdx5 expression has been decreased by ~70 % in liver and kidneys, these transgenic mice appear physiologically normal, with survival and fertility similar to wild type mice. A proteomic analysis has been performed on the hypoxic kidneys to identify genes with altered expression in Prdx5 KD mice. Proteins with modified expression were mainly involved in oxidative stress, fatty acid metabolism and mitochondrial dysfunction [27]. More recently, it was shown in *Prdx5* KO mice that Prdx5 could act as an inhibitor of adipogenesis, through

its ability to scavenge insulin-induced ROS [17]. It is worth mentioning that the cytoprotective role of Prdx5 was also shown in invertebrates [28]. Indeed, *Prdx5* KO *Drosophila melanogaster* flies are more susceptible to oxidative stress and show a higher incidence of apoptosis [29].

As for other pleiotropic enzymes, it was proposed that Prdxs may act as modulators of peroxide signaling notably during inflammation [30]–[32]. The expression of different Prdxs, including Prdx5, is dramatically increased in mouse and murine bone marrow-derived macrophages (BMMs) upon exposure to IFN-γ and LPS [33]–[35]. Specifically, it was shown that Prdx5 expression is upregulated via LPS/TLR4, the Th1 cytokine IFN-γ and the TRIF-dependent/INF-γ-independent pathways [34]. Prdx5 expression can be also induced in microglia under the control of ROS/RNS and JNK signaling cascades [36]. Another study showed that Prdx5 is able to interact with jak2 via its Cp. This interaction causes the inhibition of the phosphorylation of jak2 and stat5, resulting in the reduction of IL-6 production [37]. Induced expression of Prdx5 by LPS in activated microglia can act as a negative regulator of excessive mitochondrial fission and a modulator of pro-inflammatory responses by inhibiting ROS-dependent Ca^{2+}/calcineurin and de-phosphorylation of dynamin-related protein 1 (Drp1) [38].

As mentioned before, it was also shown that several Prdxs can act as DAMPs but also pathogen-associated molecular patterns (PAMPs) [39], [40]. In post-

ischemic inflammation in the brain, Prdx1, Prdx2, Prdx5 and Prdx6 are released from the necrotic brain cells and may act as DAMPs, inducing the expression and the release of pro-inflammatory cytokines by macrophages [41]. In another study, Prdx1 and Prdx2 dimeric forms were reported to trigger the production of inflammatory cytokines by macrophages, after exposure to LPS and TNF-α [42], [43]. Finally, our group showed, using atomic force microscopy (AFM), that extracellular Prdx5 binds to purified TLR4 receptors, on macrophage-differentiated THP-1 cells, and on human TLR4-transfected CHO cells, triggering a pro-inflammatory response [44].

So far, all *Prdx* knockout (KO) mice reported in the literature are viable and fertile but develop different phenotypes related to enhanced levels of ROS/RNS. *Prdx1* and *Prdx2* KO mice acquire severe haemolytic anemia [45], [46] and several malignant tumors. *Prdx3* and *Prdx6 KO* mice are more susceptible to oxidative stress induced by LPS, paraquat and hyperoxia [47]–[49]. Analysis of the *Prdx4* KO mice has revealed atrophy of testes and enhanced oxidative damage in spermatogenic cells [50]. In the literature, only very recent papers report on the *in vivo* functions of Prdx5 with generation of KO mice models. The analysis of *Prdx5* KO models showed that *Prdx5* KO mice are more sensitive to high fat diet-induced obesity [17], that Prdx5 modulates cytokine production [18] and controls ciliogenesis via mitochondrial ROS reduction [51].

Thus, the purpose of this work was to provide a general phenotypic analysis of a *Prdx5* KO mouse model with emphasis on Prdx5 role in inflammation.

5.3 Results

5.3.1 General features of the Prdx5 knockout mice

The confirmation of the genotype for each mouse was performed by PCR on genomic DNA from tail and ear biopsies (Fig.1A-B). Three different primers were used (*Intron1afw*, *Intron1arv* and *K7a1fw,* Fig.1A, and see materials and methods) in the same PCR mix, to amplify the different DNA sequences that correspond to the different alleles/genotypes. The PCR product for the wt allele is 854 bp long and the amplicon for the gt allele is 675 bp long (Fig.1B). The presence of both PCR products corresponds to heterozygous *Prdx5*$^{+/-}$ mice.

Western blotting analysis with total proteins from tail lysates confirmed the lack of *Prdx5* expression at the protein level in the *Prdx5*$^{-/-}$mice and a half decrease in *Prdx5*$^{+/-}$ mice (Fig.1C and 1D).

Prdx5 mRNA expression was also examined by RT-PCR in seven different organs (Fig.1E). A 131bp RT-PCR product corresponding to wt *Prdx5* mRNA

was detected in all the *Prdx5*$^{+/+}$ tissues, as expected. A weak Prdx5 RT-PCR product of 131bp was detected in *Prdx5*$^{-/-}$ heart, muscle and spleen. A second RT-PCR product of 246 bp was detected in the *Prdx5*$^{-/-}$ tissues. These PCR products were cloned and sequenced and corresponded to mRNA splicing products depicted in green and yellow in supplementary data (SFig.1). However, Western blotting analyses of proteins for the same organs (Fig.1F) confirmed that Prdx5 protein was not expressed in *Prdx5*$^{-/-}$ mice.

The distribution of the three different genotypes among animals obtained from the crossing of heterozygotes followed the Mendel's 2nd law. In a total of 735 offspring, we obtained 181 Prdx5$^{+/+}$ (25%), 355 *Prdx5*$^{+/-}$ (48%) and 199 *Prdx5*$^{-/-}$ (27%) mice, that is very close to the expected distribution of 25% for *Prdx5*$^{+/+}$, 50% for *Prdx5*$^{+/-}$ and 25% of *Prdx5*$^{-/-}$ mice. The distribution of the

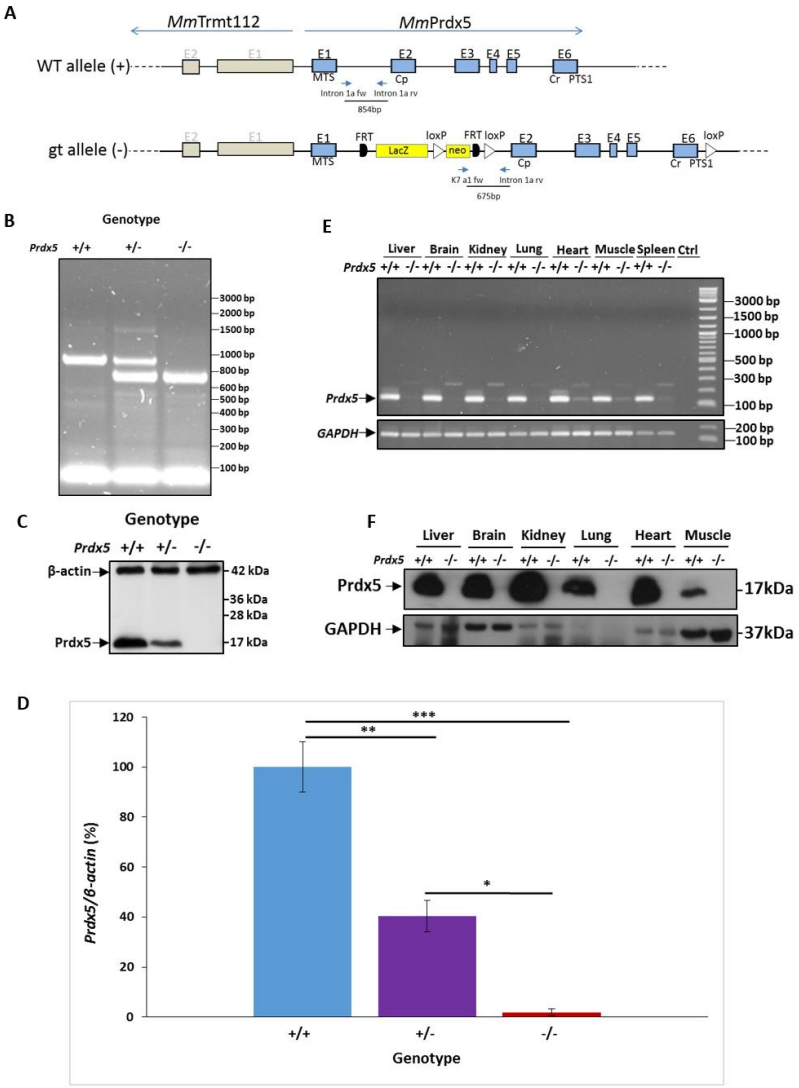

Figure 1. Prdx5 KO mice characterization. (*A) Schematic representation of the Prdx5 wild-type (WT) and the gene-trap Prdx5 (gt) alleles. The gene-trap knockout construct (gt allele) consists of the lacZ gene as a reporter and the neomycin phosphotransferase gene. Exons (E) 1 to 6, FRT and LoxP recombination sites are depicted. Intron1afw, Intron1arv and K7a1fw are the primers used for genotyping mice. Trmt112 gene is located upstream the Prdx5 gene. It consists from 2 exons (E1 and E2) but its expression is not affected from the gt construct (data not shown). (B) PCR was performed using primers indicated before. The PCR amplification gives a product of 854bp on Prdx5$^{+/+}$ allele and a product of 675bp on mutant allele. (C) Western blotting analysis (Prdx5 and β-actin) of tail lysates from Prdx5$^{+/+}$ and transgenic mice (Prdx5$^{+/-}$ and Prdx5$^{-/-}$). (D) Prdx5 protein levels were normalized to β-actin and were expressed in arbitrary units. Values represented the mean ± S.E.M. from triplicates. Significant is designed by * (p<0.05), ** (p<0.01), *** (p<0.005). (E) RT-PCR in 7 different organs shows that Prdx5 mRNA Prdx5 in the Prdx5$^{-/-}$ mice decreased compare to Prdx5$^{+/+}$ animals. The 2 weak RT-PCR products are coming from alternative splicing but there are not translating into proteins. GAPDH was used as a reference gene in this experiment. (F) Western blotting in the same organs shows that indeed the Prdx5 protein is not existed in the Prdx5$^{-/-}$ mice, compare with the Prdx5$^{+/+}$. The GAPDH protein is used as a marker of the expression.*

gender was also normal with 382 females and 353 males. The *Prdx5*$^{-/-}$ mice are viable and grow without any obvious problems. The crossing of 5 different couples of *Prdx5*$^{-/-}$ mice revealed that they are also fertile (3-8 newborns/littermate).

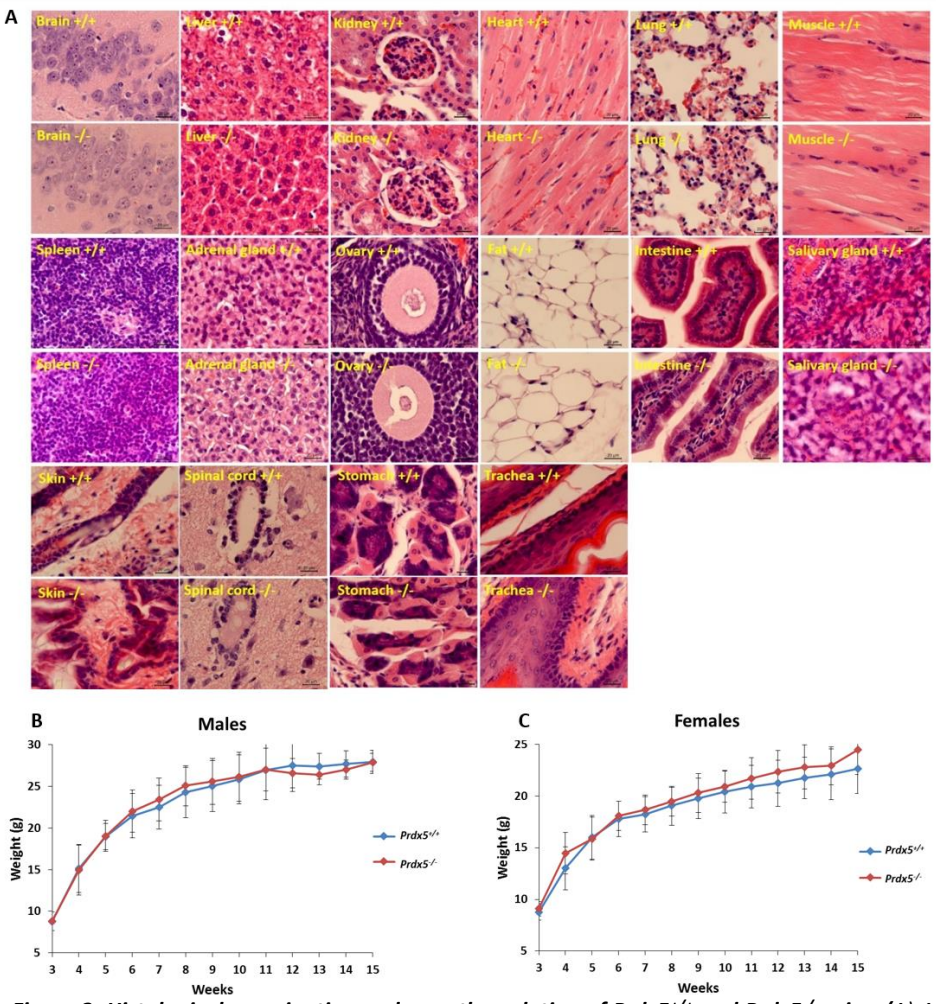

Figure 2. Histological examination and growth evolution of Prdx5$^{+/+}$ and Prdx5$^{-/-}$ mice. (*A) A classical hematoxylin-eosin staining in the slides of the tissues from a Prdx5$^{+/+}$ and Prdx5$^{-/-}$ 3-month old female mouse was performed. Brain, liver, kidney, heart, lung, muscle, spleen, adrenal gland, ovary, fat, intestine, salivary gland, skin, spinal cord, stomach, trachea-esophagus. We do not observe any difference between the 2 genotypes. (B-C) The weight was measured between the 3rd and the 15th week of male and female Prdx5$^{+/+}$ and Prdx5$^{-/-}$ mice. There was no statistically significant differences for both genders.*

A complete and systematic histological examination of different tissues of the *Prdx5*$^{+/+}$ and *Prdx5*$^{-/-}$ young female mice (3 month-old) was performed. Hemalun-eosin staining was performed for a variety of organs and tissues (Fig.2A). No clear abnormalities nor dysplasia were observed in the *Prdx5*$^{-/-}$ tissues compared to *Prdx5*$^{+/+}$ tissues at this age. In all the tissues examined, the morphology of the tissue or the cells did not appear affected.

The growth of 21 *Prx5*$^{+/+}$ and 20 *Prdx5*$^{-/-}$ male and 20 *Prdx5*$^{+/+}$ and 21 *Prdx5*$^{-/-}$ female mice was measured between the 3rd and the 15th week (Fig.2B-C). No statistically significant difference between the two genotypes was detected in any gender.

5.3.2 Oxidative stress damage in the *Prdx5*$^{-/-}$ mice

The DNA oxidation damages were evaluated in the liver, brain, kidney, lung, skeletal muscle and spleen of young *Prdx5*$^{+/+}$ and *Prdx5*$^{-/-}$ mice (3 month-old), by measuring the level of 8-OHdG/mg of total protein (Fig.3A). We observed a higher DNA oxidation in the lung and spleen of the *Prdx5*$^{-/-}$ mice. However these differences were not statistically significant. Protein carbonylation was measured in the liver, brain, kidney, and lung of young *Prdx5*$^{+/+}$ and *Prdx5*$^{-/-}$ mice (3 month-old) (Fig.3B). We observed a significant higher level of protein

carbonylation (nmoles of carbonyls/mg total protein) in the brain of the *Prdx5*$^{-/-}$ mice. The level of lipid peroxidation was estimated in the liver, brain, kidney, lung, heart, skeletal muscle and spleen of young *Prdx5*$^{+/+}$ and *Prdx5*$^{-/-}$ mice (6 month-old) (Fig.3C). We observed a significant higher lipid peroxidation (nmoles LOOH/mg of total protein) in skeletal muscles of the *Prdx5*$^{-/-}$ mice. The expression of the other antioxidant enzymes Prdx1, Prdx2, Prdx3, Prdx4, Prdx6, Catalase, SOD2 and the overoxidized forms of the Prdx1-4 (Prdx-SOx), were analyzed by Western blotting in *Prdx5*$^{+/+}$ and *Prdx5*$^{-/-}$ liver, brain, kidney, lung, heart and muscle (Fig.3D-E). The expression of the Prdx1, Prdx6, SOD2 and catalase are decreased in the *Prdx5*$^{-/-}$ lung. On the other hand, Prdx6 is increased in the *Prdx5*$^{-/-}$ liver, Prdx-SOx is increased in *Prdx5*$^{-/-}$ liver and heart and SOD2 is increased in *Prdx5*$^{-/-}$ heart.

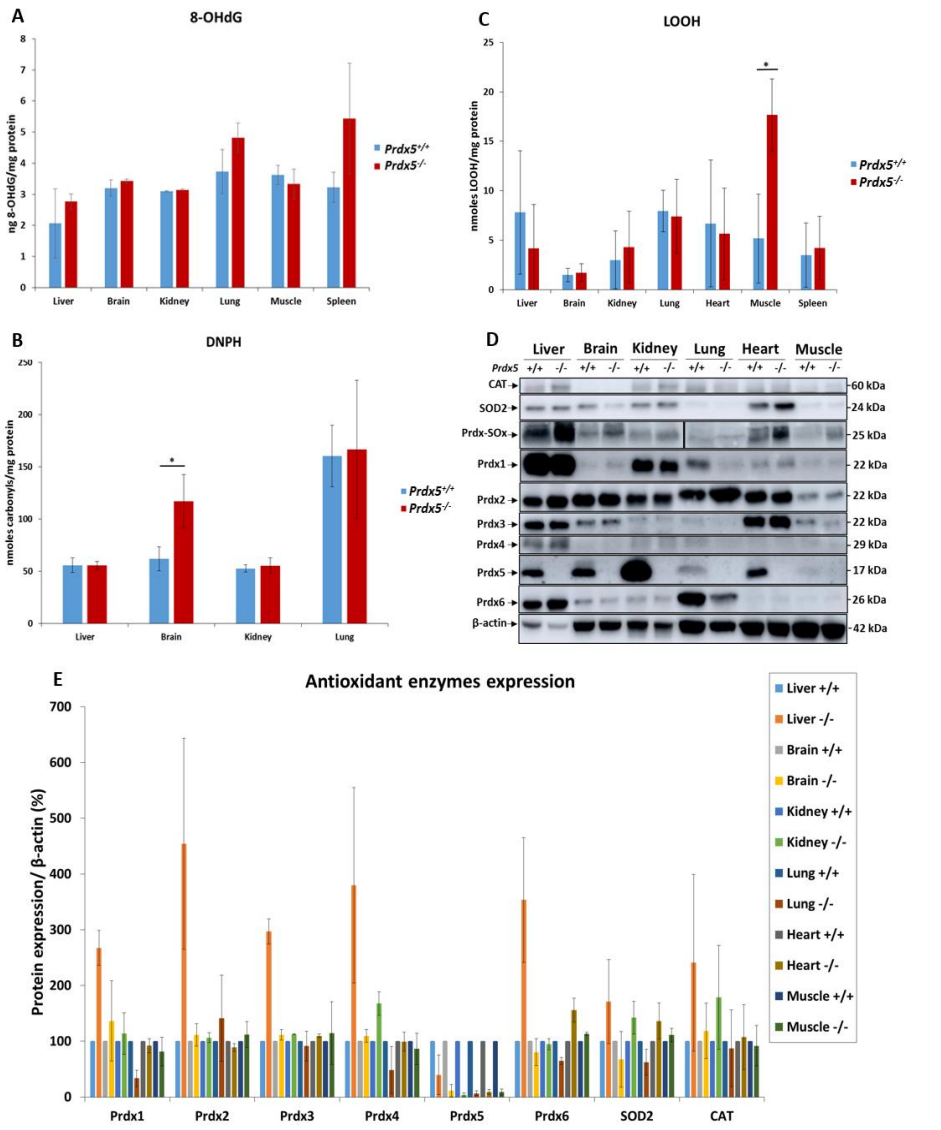

Figure 3. Oxidative stress damage in Prdx5$^{+/+}$ and Prdx5$^{-/-}$ mice. *(A) DNA oxidation was measured in liver, brain, kidney, lung, muscle and spleen homogenates of Prdx5$^{+/+}$ and Prdx5$^{-/-}$ mice, using the 8-OHdG ELISA kit. (B) The protein oxidation was measured in liver, brain, kidney and lung homogenates of Prdx5$^{+/+}$ and Prdx5$^{-/-}$ mice, using the DNPH marker. Higher protein carbonylation is detected in Prdx5$^{-/-}$ brain compare to the Prdx5$^{+/+}$ brain. (C) The lipid peroxidation was measured in liver, brain, kidney, lung, heart, muscle and spleen homogenates of Prdx5$^{+/+}$ and Prdx5$^{-/-}$ mice, using the LOOH marker. We observed higher lipid peroxidation in Prdx5$^{-/-}$ muscle compare to the Prdx5$^{+/+}$ muscle. (D) Expression of the antioxidant enzymes and oxidized forms of Prdxs in liver, brain, kidney, lung, heart and muscle of Prdx5$^{+/+}$ and Prdx5$^{-/-}$ mice. (E) Antioxidant protein levels were normalized to β-actin and were expressed in arbitrary units. Values represented the mean ± S.E.M. from triplicates. Significant is designed by * (p<0.05), ** (p<0.01), *** (p<0.005).*

5.3.3 Gene expression analysis using microarrays

In order to investigate the effects of the Prdx5 absence in the mouse model on gene expression, we performed microarray analysis of mRNA extracted from liver and brain of *Prdx5*$^{+/+}$ and *Prdx5*$^{-/-}$ young female mice (3 month-old). Several genes were significantly up- and down-regulated in the *Prdx5*$^{-/-}$ liver and brain (Fig.4, suppl. table 1-4). As expected, *Prdx5* gene expression was dramatically decreased in both liver and brain of *Prdx5*$^{-/-}$ mice (70 and 23 fold change respectively, Fig.4A-B). Genes coding for proteins involved in the immune system, like serum amyloid A1 and A2 (Saa1 and Saa2), lipocalin 2 (Lcn2) and orosomucoid 2 (Orm2) were significantly downregulated in *Prdx5*$^{-/-}$ liver (Fig.4A). In *Prdx5*$^{-/-}$ brain, several genes were also significantly downregulated, such as genes coding for glutamate decarboxylase-like 1 (Gadl1), visual system homeobox 1 homolog (Vsx1), hydrolethalus syndrome 1 (Hysl1) and dystrotelin (Dytn) (Fig.4B). Several genes coding for proteins of the same family were up- or downregulated. For example, the gene coding for collagen type XVI alpha1 (Col16a1) was upregulated but the transcripts coding for collagen type VI alpha5 (Col6a5) and collagen type IV alpha3 (Col4a3) were downregulated in the *Prdx5*$^{-/-}$ liver (suppl. table 1-2). The most striking result in this transcriptional analysis was the significant upregulation of genes coding for different isoforms of cytochrome P450 in both *Prdx5*$^{-/-}$

liver and *Prdx5*$^{-/-}$ brain (Fig.4A-B, suppl. table 1 and 3). Genes coding for four isoforms (Cyp4a32, Cyp2g1, Cyp2a4, Cyp7b1) in liver (suppl. table 1) and 16 isoforms (Cyp2c39, Cyp2c54, Cyp2c37, Cyp2f2, Cyp2c54, Cyp2c67, Cyp2c29, Cyp8b1, Cyp2c68, Cyp2a4, Cyp2c50, Cyp4a10, Cyp2a12, Cyp1a2, Cyp3a44, Cyp2e1) of cytochrome P450 in brain (suppl. table 3) were significantly upregulated in the *Prdx5*$^{-/-}$ mouse. We also observed that genes coding for members of the apolipoprotein (Apoa2, Apoc3, Apoc1, Apoh and Apob) and the aldo-keto reductase family (Akr1c12, Akr1c20, Akr1c6 and Akr1d1) were upregulated in the *Prdx5*$^{-/-}$ brain (suppl. table 3). No significant differences of expression were observed for genes coding for antioxidant enzymes, except for the gene coding for the extracellular SOD3 that was significantly upregulated in *Prdx5*$^{-/-}$ brain (suppl. table 3).

Figure 4. Up- and Down-regulated genes between Prdx5$^{+/+}$ and Prdx5$^{-/-}$ liver and brain. *Volcano plot of the quantification of transcripts identified between Prdx5$^{+/+}$ and Prdx5$^{-/-}$ liver (A) and brain (B). Y-axis indicates −log10 (p value) while the horizontal axis indicates base 2 logarithmic value of mean peptide abundance ratio (Prdx5$^{+/+}$ vs. Prdx5$^{-/-}$). The horizontal black line represents the threshold of significance assigned for subsequent analysis of transcripts. The two vertical black lines represent the threshold of fold change 2. Transcripts significantly decreased in Prdx5$^{-/-}$ are indicated in blue, those significantly increased in abundance are indicated in red.*

5.3.4 Prdx5 knockout mice are more vulnerable in LPS-induced inflammation

The vulnerability of *Prdx5*$^{-/-}$ mice to LPS-induced endotoxic shock was examined. *Prdx5*$^{+/+}$ and *Prdx5*$^{-/-}$ male mice were intraperitoneally injected with two concentrations of LPS (20 mg/kg or 10 mg/kg) or vehicle. Animal survival was monitored every 3 hours after injection. 72 hours after injection all *Prdx5*$^{-/-}$ mice exposed to a high dose of LPS (20 mg/kg) died and 40 % of *Prdx5*$^{+/+}$ mice survived (Fig.5A). For the groups of mice that received 10 mg/kg of LPS, 100 % survival of *Prdx5*$^{+/+}$ and 80 % survival of *Prdx5*$^{-/-}$ animals was observed.

Peritoneal cells collected from *Prdx5*$^{+/+}$ mice and cultured *in vitro* were characterized by immunofluorescence, using anti-CD11b and anti-F4/80 antibodies as markers of phagocytes and macrophages respectively, and anti-Prdx5 antibody to examine Prdx5 expression in *Prdx5*$^{+/+}$ cells. More than 90% of these cells expressed CD11b identified as phagocytes (suppl. Fig.2a-c), while 50% of cells expressed F4/80, identified as macrophages (suppl. Fig.2d-f). In both cases, these cells co-express Prdx5 (suppl. Fig.3). The level of Prdx5 expression in *Prdx5*$^{+/+}$ phagocytes stimulated with 1 µg/ml LPS for different time points was measured by Western blotting (Fig.5B). These results confirm that Prdx5 expression is increased in peritoneal phagocytes

exposed to LPS as reported before [37]. The release of the pro-inflammatory cytokines Il-1β and TNF-α from the *Prdx5*$^{+/+}$ and *Prdx5*$^{-/-}$ phagocytes exposed to 1μg/ml LPS or PBS (vehicle) for 24 hours, was measured by ELISA (Fig.5C-D). The release of the two pro-inflammatory cytokines is higher for both genotypes, although not statistically significant for IL-1β, under LPS stimulation after 24 hours compared to the control conditions. Notably, TNF-α release is significantly higher (p-value 0.0066) from *Prdx5*$^{-/-}$ phagocytes than from *Prdx5*$^{+/+}$ cells exposed to 1μg/ml LPS although the difference is not dramatic (Fig. 5D).

5.3.5 Oxidative stress damage in *Prdx5*$^{-/-}$ mice upon intraperitoneal LPS exposure

Prdx5$^{+/+}$ and *Prdx5*$^{-/-}$ mice (5 month-old) were intraperitoneally exposed to 20 mg/kg LPS for 18 hours and their liver, brain, kidney, lung and spleen were collected to measure oxidative damage of DNA, proteins and lipids. The DNA oxidation damage was measured (8-OHdG/mg total protein) (Fig.5E) and no significant difference was observed between the two genotypes. Protein carbonylation

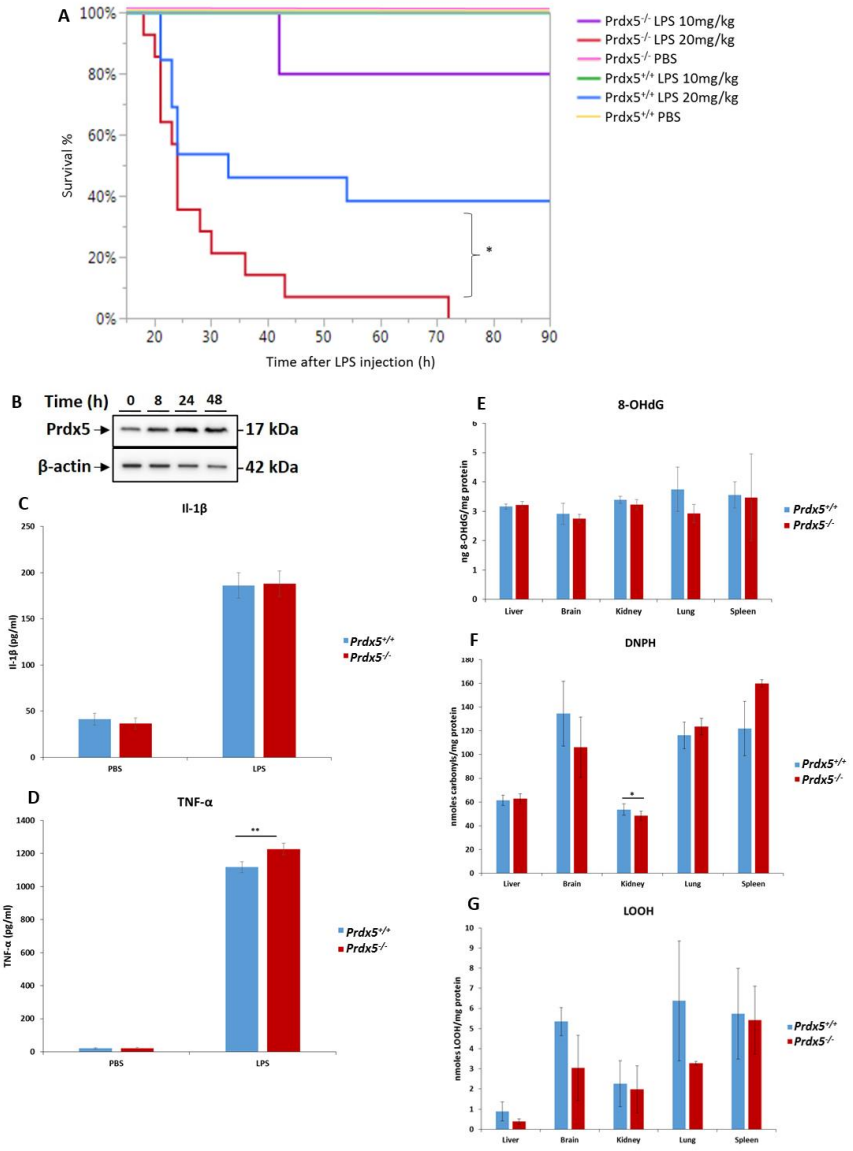

Figure 5. LPS challenge in Prdx5 KO mice in vivo and in vitro. *(A) Mice were exposed to different concentrations of LPS (20, 10 and 0 mg/kg, i.p.). There is 100% mortality of the Prdx5$^{-/-}$ mice for the LPS 20 mg/kg condition after 72h and 60% of the Prdx5$^{+/+}$ mice. Moreover, there is 20% mortality for the Prdx5$^{-/-}$ mice with the 10 mg/kg of LPS and 0% of the Prdx5$^{+/+}$ mice. (B) The Prdx5$^{+/+}$ peritoneal cells were stimulated by 1µg/ml LPS for 0 to 48 hours and the Prdx5 expression was measured by Western blotting. Il-1beta (C) and Tnf-alpha (D) release from Prdx5$^{+/+}$ and Prdx5$^{-/-}$ macrophages stimulated by 1µg/ml LPS or PBS (control). (E) DNA oxidation was measured in liver, brain, kidney, lung and spleen homogenates of Prdx5$^{+/+}$ and Prdx5$^{-/-}$ mice stressed by LPS during 18 hours, using the 8-OHdG ELISA kit. (F) The protein oxidation was measured in liver, brain, kidney, lung and spleen homogenates of Prdx5$^{+/+}$ and Prdx5$^{-/-}$ mice stressed by LPS during 18 hours, using the DNPH marker. Higher protein carbonylation is detected in Prdx5$^{+/+}$ kidney compare to the Prdx5$^{-/-}$ kidney. (G) The lipid peroxidation was measured in liver, brain, kidney, lung and spleen homogenates of Prdx5$^{+/+}$ and Prdx5$^{-/-}$ mice, using the LOOH marker.*

(carbonyls/mg total protein) and lipid peroxidation (LOOH/mg total protein) were also measured (Fig.5F-G). Only significant slightly lower protein carbonylation was measured in kidneys of *Prdx5*$^{-/-}$ mice (Fig.5F). On the other hand, the *Prdx5*$^{-/-}$ brain showed non-significant lower protein carbonylation. For lipid peroxidation, all the tissues presented lower levels of LOOH/mg total protein compared to *Prdx5*$^{+/+}$ mice although these results were not statistically significant (Fig.5G).

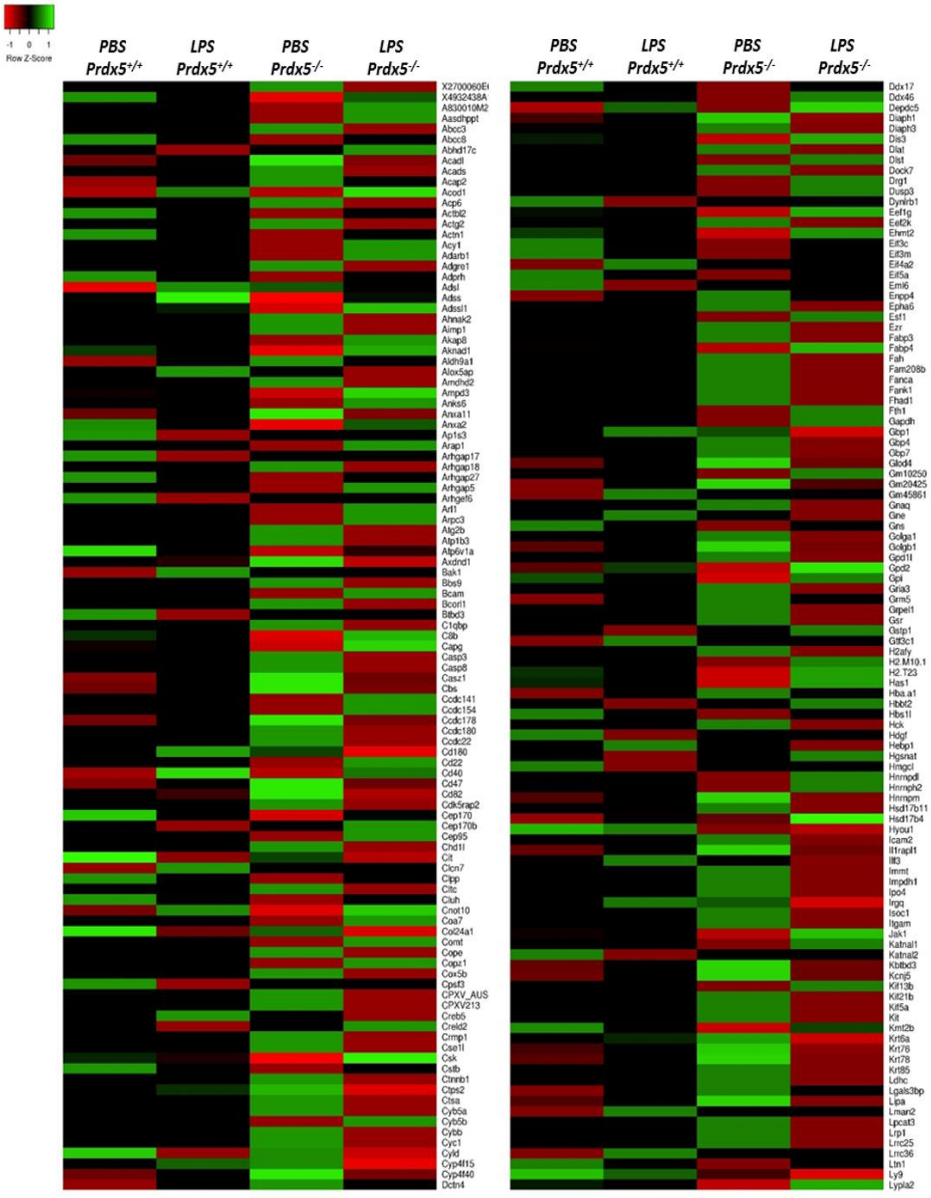

Figure 6. Heatmap showing the significantly downregulated (red) and upregulated (green) proteins (p-value <0.05) in the Prdx5$^{+/+}$ and Prdx5$^{-/-}$ macrophages in LPS or PBS conditions. *See supplementary tables for complete list of proteins. (Continue in the next page)*

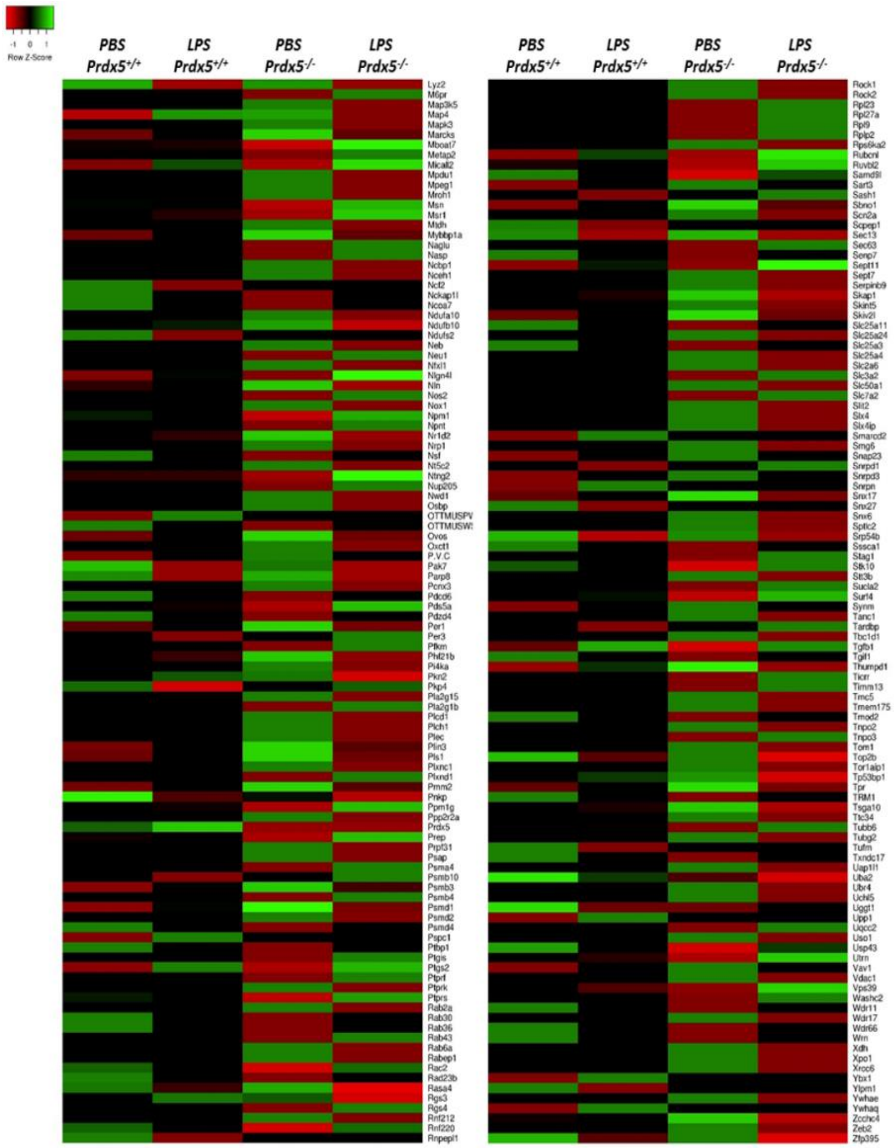

Figure 6. Heatmap showing the significantly downregulated (red) and upregulated (green) proteins (p-value <0.05) in the Prdx5$^{+/+}$ and Prdx5$^{-/-}$ macrophages in LPS or PBS conditions. *See supplementary tables for complete list of proteins.*

5.3.6 Proteomic analysis of *Prdx5*$^{+/+}$ and *Prdx5*$^{-/-}$ peritoneal phagocytes exposed to LPS

The protein content of the *Prdx5*$^{+/+}$ and *Prdx5*$^{-/-}$ peritoneal phagocytes was examined after 24 hours with or without exposure to 1 μg/ml LPS using nanoUPLC HDMS^{E} analysis. The proteomic analysis revealed that several proteins are up- and down-regulated significantly in *Prdx5*$^{+/+}$ and *Prdx5*$^{-/-}$ peritoneal phagocytes without or with LPS exposure (Fig.6). Specific filters for p-value were applied (see materials and methods and Fig.7) and proteins were compared by condition (suppl. Tables 5-12). Also, proteins which expression was significantly regulated were analyzed with PANTHER software, in order to identify signaling pathways that were altered.

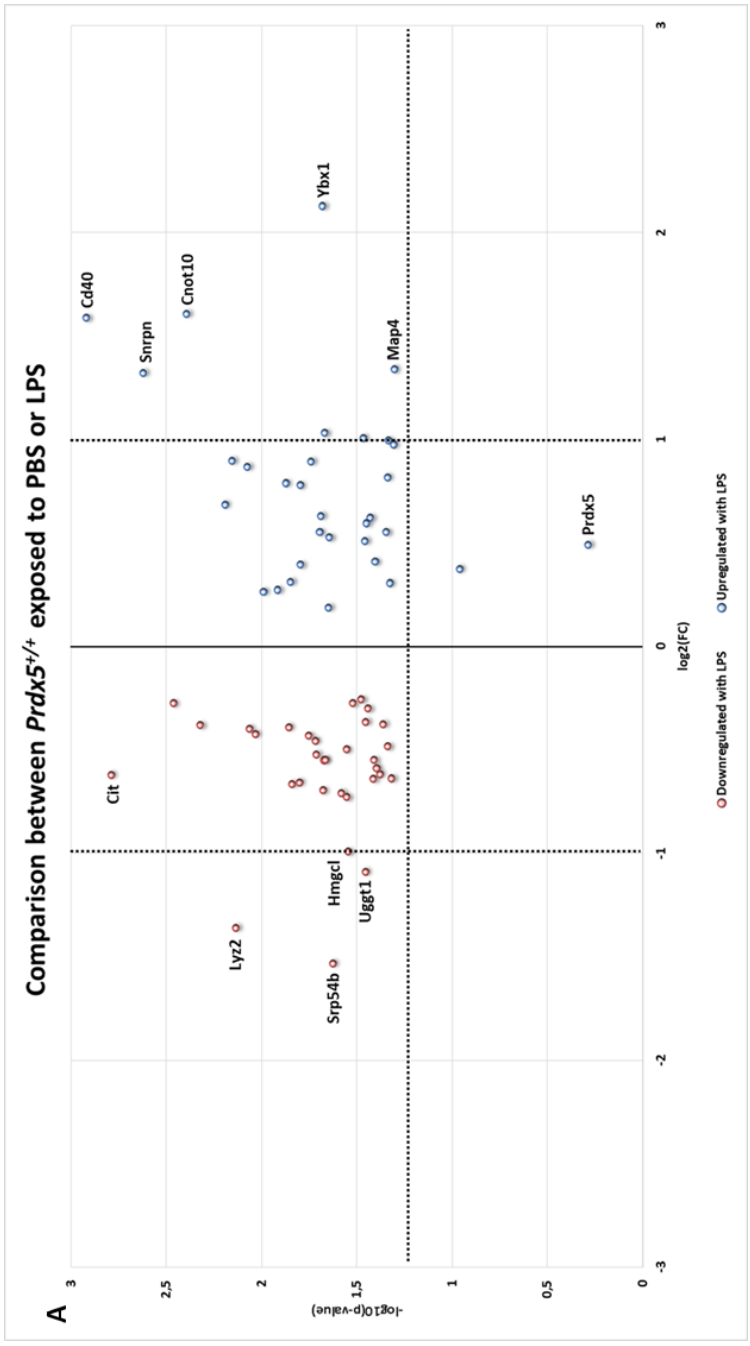
A
Comparison between Prdx5+/+ exposed to PBS or LPS
-log10(p-value)
log2(FC)
Cd40
Snrpn
Cnot10
Ybx1
Map4
Prdx5
Cit
Lyz2
Srp54b
Hmgcl
Uggt1
Downregulated with LPS
Upregulated with LPS

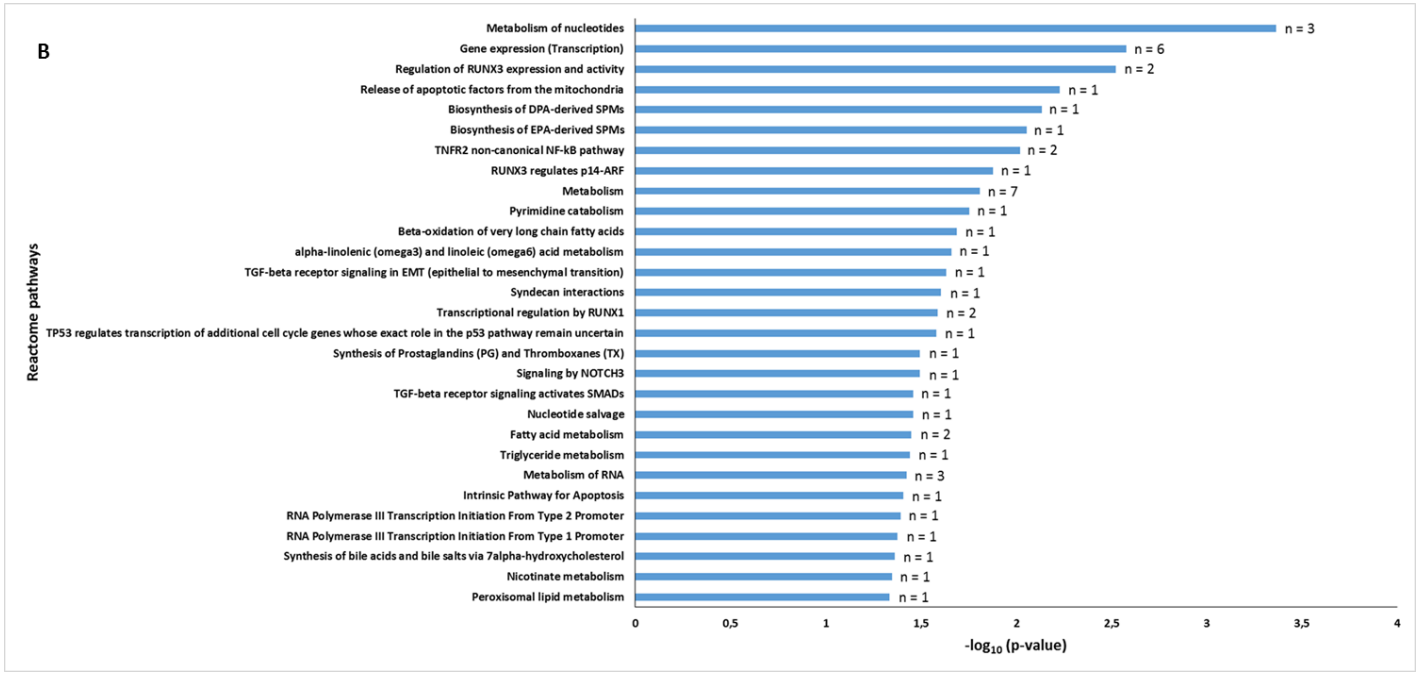
B
Reactome pathways
Metabolism of nucleotides
Gene expression (Transcription)
Regulation of RUNX3 expression and activity
Release of apoptotic factors from the mitochondria
Biosynthesis of DPA-derived SPMs
Biosynthesis of EPA-derived SPMs
TNFR2 non-canonical NF-kB pathway
RUNX3 regulates p14-ARF
Metabolism
Pyrimidine catabolism
Beta-oxidation of very long chain fatty acids
alpha-linolenic (omega3) and linoleic (omega6) acid metabolism
TGF-beta receptor signaling in EMT (epithelial to mesenchymal transition)
Syndecan interactions
Transcriptional regulation by RUNX1
TP53 regulates transcription of additional cell cycle genes whose exact role in the p53 pathway remain uncertain
Synthesis of Prostaglandins (PG) and Thromboxanes (TX)
Signaling by NOTCH3
TGF-beta receptor signaling activates SMADs
Nucleotide salvage
Fatty acid metabolism
Triglyceride metabolism
Metabolism of RNA
Intrinsic Pathway for Apoptosis
RNA Polymerase III Transcription Initiation From Type 2 Promoter
RNA Polymerase III Transcription Initiation From Type 1 Promoter
Synthesis of bile acids and bile salts via 7alpha-hydroxycholesterol
Nicotinate metabolism
Peroxisomal lipid metabolism
n = 3
n = 6
n = 2
n = 1
n = 1
n = 1
n = 2
n = 1
n = 7
n = 1
n = 1
n = 1
n = 1
n = 2
n = 1
n = 1
n = 1
n = 1
n = 1
n = 2
n = 1
n = 3
n = 1
n = 1
n = 1
n = 1
n = 1
0
0,5
1
1,5
2
2,5
3
3,5
4
-log10 (p-value)

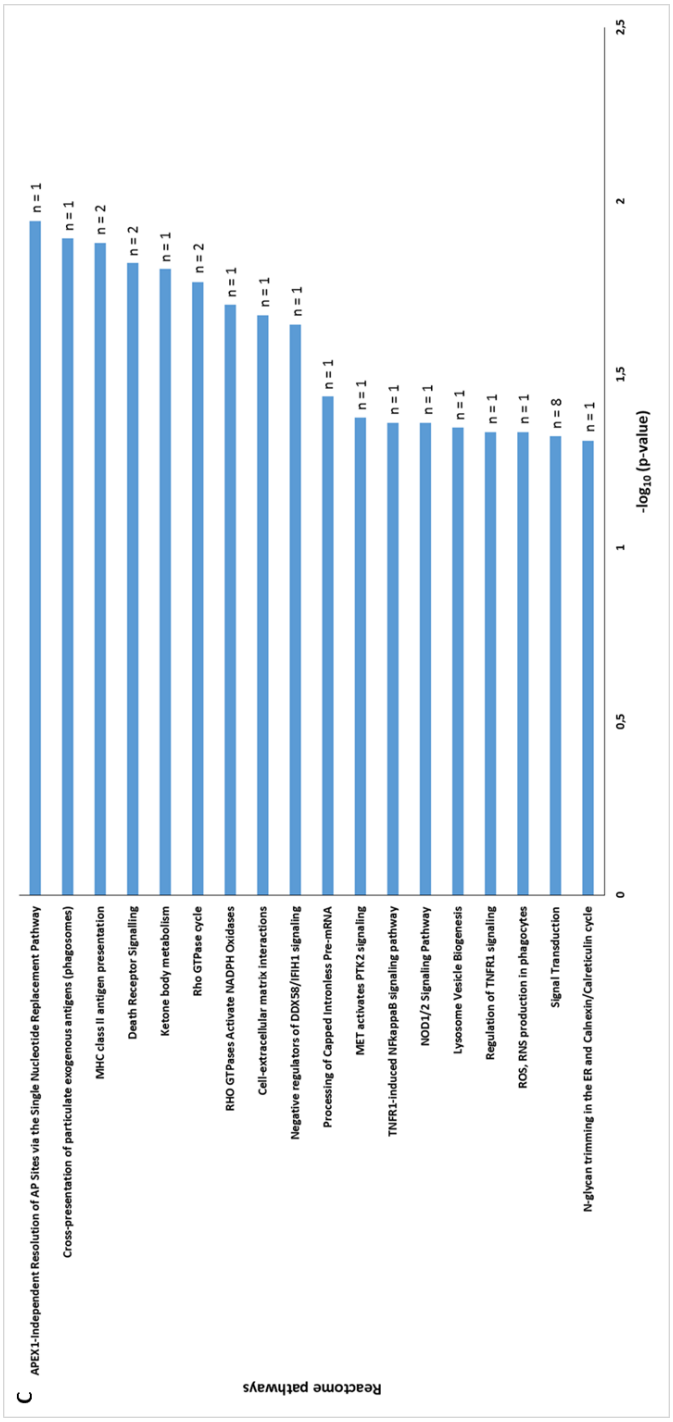
C
Reactome pathways
APEX1-Independent Resolution of AP Sites via the Single Nucleotide Replacement Pathway
Cross-presentation of particulate exogenous antigens (phagosomes)
MHC class II antigen presentation
Death Receptor Signalling
Ketone body metabolism
Rho GTPase cycle
RHO GTPases Activate NADPH Oxidases
Cell-extracellular matrix interactions
Negative regulators of DDX58/IFIH1 signaling
Processing of Capped Intronless Pre-mRNA
MET activates PTK2 signaling
TNFR1-induced NFkappaB signaling pathway
NOD1/2 Signaling Pathway
Lysosome Vesicle Biogenesis
Regulation of TNFR1 signaling
ROS, RNS production in phagocytes
Signal Transduction
N-glycan trimming in the ER and Calnexin/Calreticulin cycle
n = 1
n = 1
n = 2
n = 2
n = 1
n = 2
n = 1
n = 1
n = 1
n = 1
n = 1
n = 1
n = 1
n = 1
n = 1
n = 8
n = 1
0
0,5
1
1,5
2
2,5
-log10 (p-value)

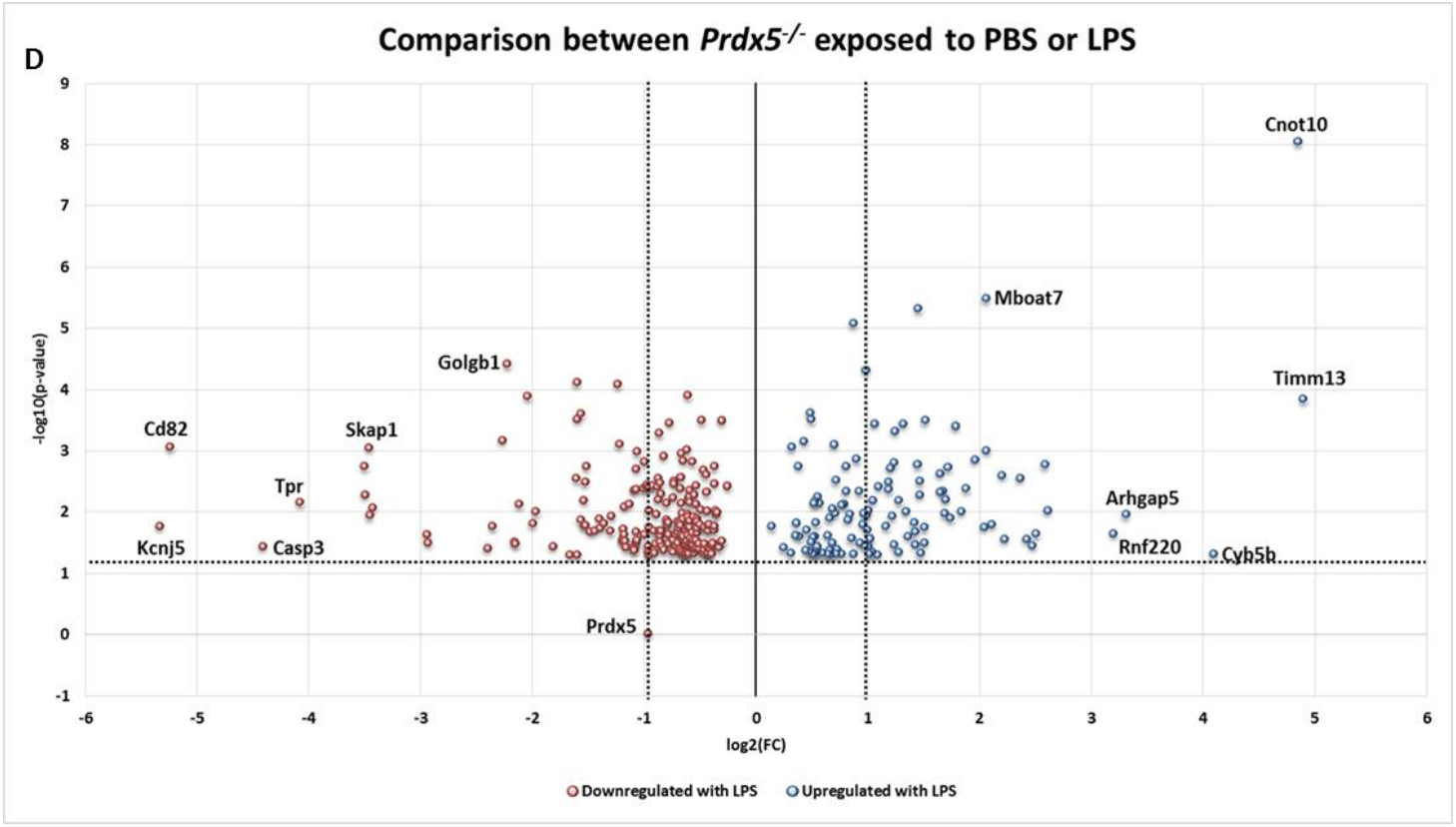
D
Comparison between Prdx5-/- exposed to PBS or LPS
-log10(p-value)
log2(FC)
Cnot10
Mboat7
Timm13
Golgb1
Cd82
Skap1
Tpr
Arhgap5
Kcnj5
Casp3
Rnf220
Cyb5b
Prdx5
Downregulated with LPS
Upregulated with LPS

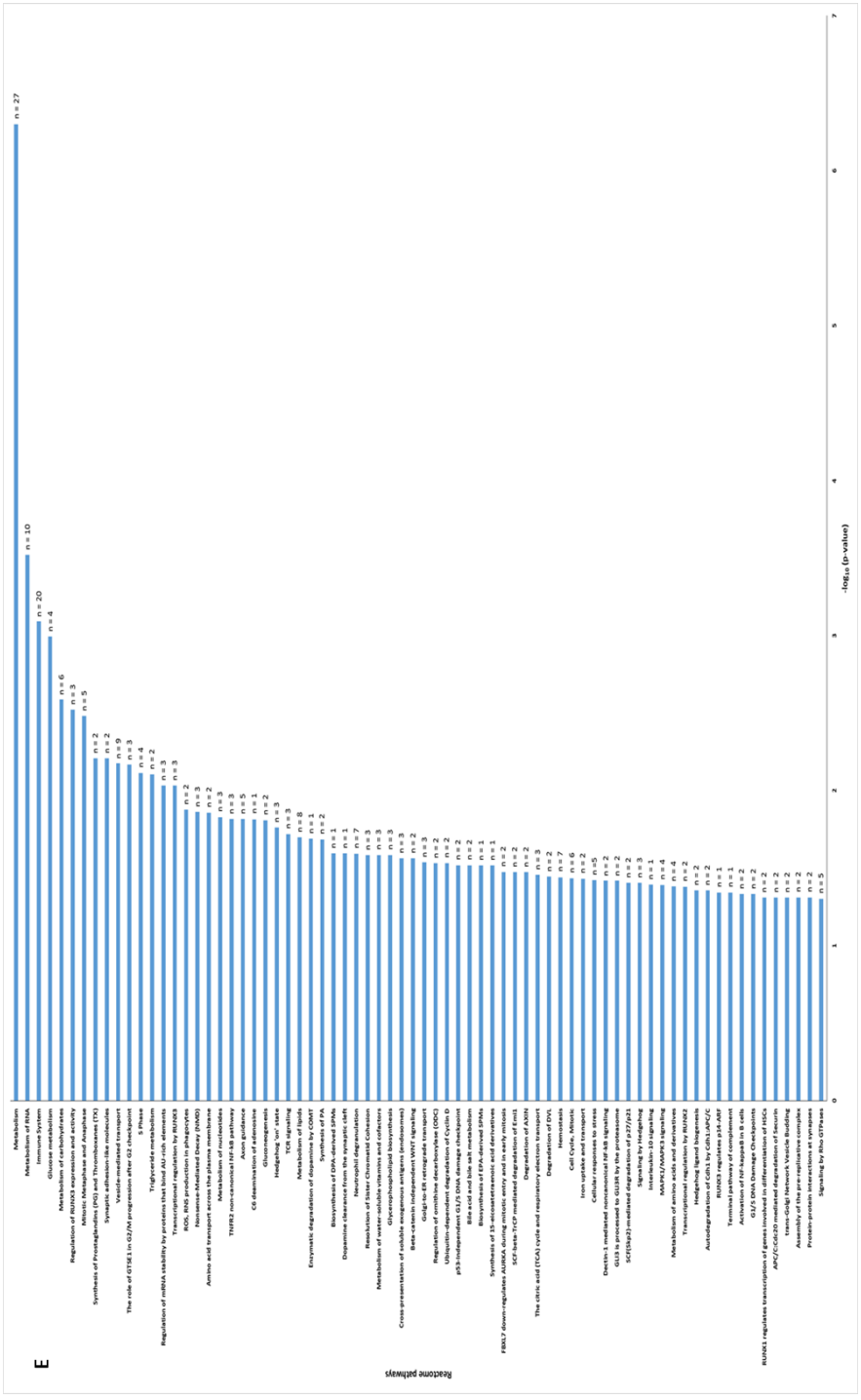
E
Reactome pathways
-log10 (p-value)
0
1
2
3
4
5
6
7
Metabolism n = 27
Metabolism of RNA n = 10
Immune System n = 20
Glucose metabolism n = 4
Metabolism of carbohydrates n = 6
Regulation of RUNX3 expression and activity n = 3
Mitotic Metaphase and Anaphase n = 5
Synthesis of Prostaglandins (PG) and Thromboxanes (TX) n = 2
Synaptic vesicle cycle n = 2
Vesicle-mediated transport n = 9
The role of GTSE1 in G2/M progression after G2 checkpoint n = 3
S Phase n = 4
Triglyceride metabolism n = 2
Regulation of mRNA stability by proteins that bind AU-rich elements n = 3
Translation of Structural Proteins n = 3
ROS, RNS production in phagocytes n = 2
Nonsense-Mediated Decay (NMD) n = 3
Amino acid transport across the plasma membrane n = 2
Metabolism of nucleotides n = 3
TNFR2 non-canonical NF-kB pathway n = 3
Apoptosis n = 5
Cit deamination of adenosine n = 1
Gluconeogenesis n = 2
Hedgehog 'on' state n = 3
TCR signaling n = 3
Metabolism of lipids n = 8
Enzymatic degradation of Kaposin mRNA by eIF4H n = 1
Synthesis of PA n = 2
Biosynthesis of EPA-derived SPMs n = 1
Dopamine clearance from the synaptic cleft n = 1
Neutrophil degranulation n = 7
Resolution of Sister Chromatid Cohesion n = 3
Metabolism of steroids - Cholesterol biosynthesis n = 3
Glycerophospholipid biosynthesis n = 3
Cross-presentation of soluble exogenous antigens (endosomes) n = 3
Beta-catenin independent WNT signaling n = 2
Golgi-to-ER retrograde transport n = 3
Regulation of activated PAK-2p34 by proteasome mediated degradation n = 2
Ubiquitin-dependent degradation of Cyclin D n = 2
p53-Independent G1/S DNA damage checkpoint n = 2
Bile acid and bile salt metabolism n = 2
Biosynthesis of EPA-derived SPMs n = 1
Synthesis of 15-eicosatetraenoic acid derivatives n = 1
FBXL7 down-regulates AURKA during mitotic entry and in early mitosis n = 2
SCF-beta-TrCP mediated degradation of Emi1 n = 2
Degradation of AXIN n = 2
The citric acid (TCA) cycle and respiratory electron transport n = 3
Degradation of DVL n = 2
Hemostasis n = 7
Cell Cycle Checkpoints n = 6
Iron uptake and transport n = 2
Cellular responses to stress n = 5
Electron transport from NADPH to Ferredoxin n = 2
GLI3 is processed to GLI3R by the proteasome n = 2
SCF(Skp2)-mediated degradation of p27/p21 n = 2
Vesicle-mediated transport n = 3
Interleukin-10 signaling n = 1
MAPK1/MAPK3 signaling n = 4
Metabolism of amino acids and derivatives n = 4
Transcriptional regulation by RUNX2 n = 2
Hedgehog ligand biogenesis n = 2
Autodegradation of the E3 ubiquitin ligase COP1 n = 2
RUNX3 regulates p14-ARF n = 1
Terminal pathway of complement n = 1
Activation of NF-kappaB in B cells n = 2
G1/S DNA Damage Checkpoints n = 2
RUNX1 regulates transcription of genes involved in differentiation of HSCs n = 2
APC/C:Cdc20 mediated degradation of Cyclin B n = 2
trans-Golgi Network Vesicle Budding n = 2
Assembly of the pre-replicative complex n = 2
Protein-protein interactions at synapses n = 2
Signaling by Rho GTPases n = 5

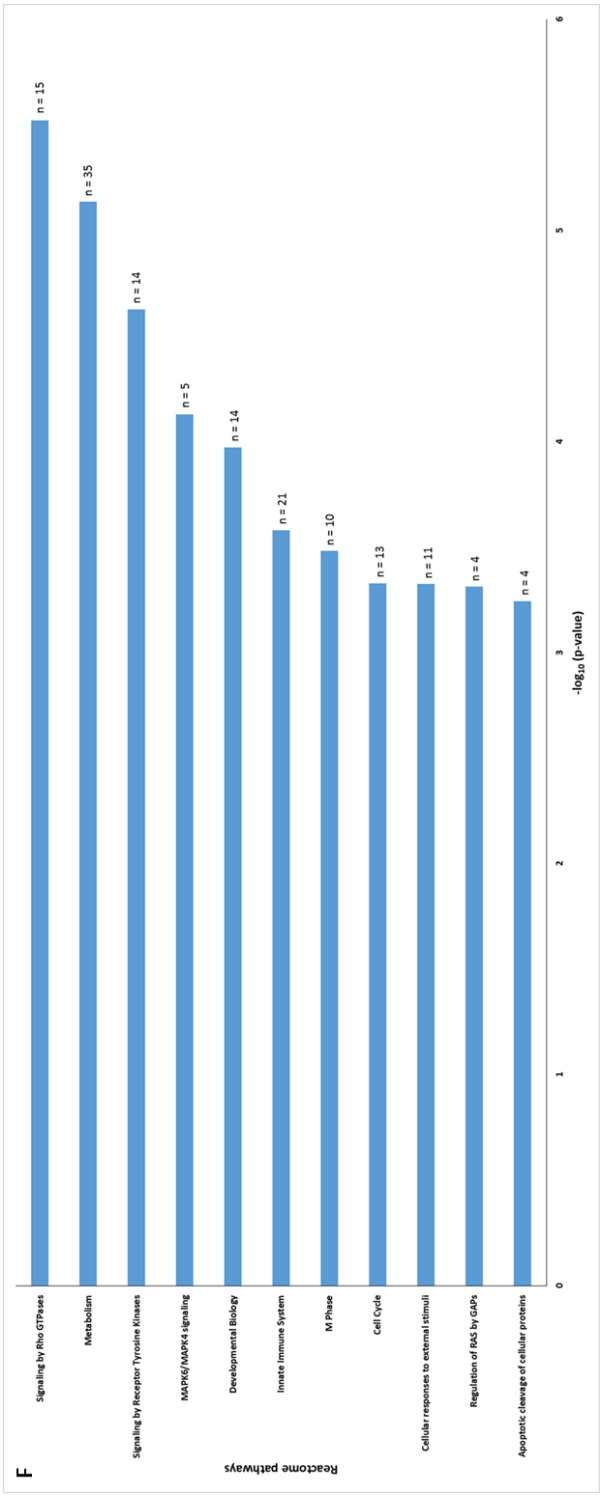
F
Signaling by Rho GTPases
Metabolism
Signaling by Receptor Tyrosine Kinases
MAPK6/MAPK4 signaling
Developmental Biology
Innate Immune System
M Phase
Cell Cycle
Cellular responses to external stimuli
Regulation of RAS by GAPs
Apoptotic cleavage of cellular proteins
n = 15
n = 35
n = 14
n = 5
n = 14
n = 21
n = 10
n = 13
n = 11
n = 4
n = 4
Reactome pathways
0
1
2
3
4
5
6
-log10 (p-value)

Figure 7. Up- and Down-regulated proteins under LPS and PBS conditions in Prdx5$^{+/+}$ or Prdx5$^{-/-}$ macrophages. *(A) Volcano plot of the quantification of peptides identified between LPS or PBS stimulated Prdx5$^{+/+}$ peritoneal macrophages. Y-axis indicates −log10 (p value) while the horizontal axis indicates base 2 logarithmic value of mean peptide abundance ratio (LPS vs. PBS). The horizontal black line represents the threshold of significance assigned for subsequent analysis of peptides. The two vertical black lines represent the threshold of fold change 2. Peptides significantly decreased in Prdx5$^{+/+}$ macrophages following LPS treatment are indicated in red, those significantly increased in abundance are indicated in blue. (B) Upregulated signaling pathways in Prdx5$^{+/+}$ macrophages treated with LPS compared to PBS analyzed by Panther. The number of genes for each pathway in indicated on the right. (C) Downregulated signaling pathways in Prdx5$^{+/+}$ macrophages treated with LPS compared to PBS analyzed by Panther. The number of genes for each pathway in indicated on the right. (D) Volcano plot of the quantification of peptides identified between LPS or PBS stimulated Prdx5$^{-/-}$ peritoneal macrophages. Y-axis indicates −log10 (p value) while the horizontal axis indicates base 2 logarithmic value of mean peptide abundance ratio (LPS vs. PBS). The horizontal black line represents the threshold of significance assigned for subsequent analysis of peptides. The two vertical black lines represent the threshold of fold change 2. Peptides significantly decreased in Prdx5$^{-/-}$ macrophages following LPS treatment are indicated in red, those significantly increased in abundance are indicated in blue. (E) Upregulated signaling pathways in Prdx5$^{-/-}$ macrophages treated with LPS compared to PBS analyzed by Panther. The number of genes for each pathway in indicated on the right. (F) Downregulated signaling pathways in Prdx5$^{-/-}$ macrophages treated with LPS compared to PBS analyzed by Panther. The number of genes for each pathway in indicated on the right.*

In a first comparison, *Prdx5$^{+/+}$* peritoneal phagocytes were exposed for 24 hours to 1 µg/ml LPS or vehicle. Prdx5 was only slightly upregulated (but the p-value is 0.52) in the LPS condition compared to the control (Fig.7A) and this upregulation was confirmed by Western blotting (Fig.5B). Also, CD40 was highly and significantly upregulated in the *Prdx5$^{+/+}$* phagocytes exposed to LPS (Fig.7A). CD40 is a member of the TNF family receptors that is expressed in antigen presenting cells and induced upon exposure to LPS [52]. Additionally, we observed that Bak1, a pro-apoptotic protein from the Bcl-2 family is slightly upregulated in the *Prdx5$^{+/+}$* phagocytes exposed to LPS (suppl. table 5). Several pathways involved in the metabolism of different macromolecules, such as nucleotides, fatty acids, organic compounds, but

also pathways involved in apoptosis were upregulated in the *Prdx5*$^{+/+}$ macrophages exposed to LPS (Fig.7B). Fewer pathways with a lower number of involved proteins were downregulated in the *Prdx5*$^{+/+}$ phagocytes exposed to LPS (Fig.7C). Among these pathways we can point out pathways related to inflammation and apoptosis, such as the MHC class II antigen presentation, death receptor signaling and TNFR1-induced NF-kappaB signaling, but also pathways involved in ROS and RNS production in phagocytes.

Prdx5$^{-/-}$ phagocytes were also exposed to 1 μg/ml LPS or vehicle for 24 hours. In *Prdx5*$^{-/-}$ phagocytes, the number of proteins which expression was significantly altered upon LPS exposure, was higher compared to *Prdx5*$^{+/+}$ phagocytes (Fig.7D). Several proteins with different functions were significantly upregulated in *Prdx5*$^{-/-}$ peritoneal phagocytes upon LPS exposure. Among those, Cnot10, Timm13, Cyb5b, Mboat7, Rnf220 and Arhgap5 are the proteins for which their expression was the most upregulated (Fig.7D). All these proteins and others are involved in the immune system and inflammation, in the metabolism of macromolecules, in cell cycle and mitosis, in apoptosis, in cell expression and transport (Fig.7E). Interestingly, Jak1, an important tyrosine kinase essential for cytokine signaling was highly upregulated in the *Prdx5*$^{-/-}$ phagocytes after LPS exposure. Among the proteins which expression was downregulated in *Prdx5*$^{-/-}$ phagocytes under LPS exposure, we identified Cd82, Casp3, Kcnj5,

Tpr, Skap1 and Golgb1 (Fig.7D). Most of downregulated proteins are involved in metabolism, in innate immune system, in apoptosis, in MAPK signaling and in cell cycle (Fig.7F).

Proteomic comparison of *Prdx5*$^{+/+}$ and *Prdx5*$^{-/-}$ peritoneal phagocytes not exposed to LPS, revealed that expression of fewer proteins is altered (Fig.8A). Among these proteins, Kcnj5, Ccdc178, Synm and Mybbp1a are highly upregulated in the *Prdx5*$^{-/-}$ phagocytes. Most of upregulated proteins in *Prdx5*$^{-/-}$ phagocytes are involved in apoptosis, p53 signaling pathway, MAPK signaling pathway, regulation of the cell cycle and immune system (Fig.8B). It must be noted that among downregulated proteins in the *Prdx5*$^{-/-}$ phagocytes Prdx5 is highly and significantly decreased but surprisingly still detectable (Fig.8A). Moreover, Pdcd6, Wdr66 and Rnf220 among other proteins were also significantly downregulated in *Prdx5*$^{-/-}$ phagocytes. These proteins are mainly involved in immune system and apoptosis signaling pathways (Fig.8C).

Finally, the comparison between *Prdx5*$^{+/+}$ and *Prdx5*$^{-/-}$ peritoneal phagocytes exposed to LPS, showed that altered proteins are less abundant (Fig.8D). However, Sash1 and Hbbt2 were significantly upregulated in the *Prdx5*$^{-/-}$ phagocytes. The few proteins which expression was upregulated in*Prdx5*$^{-/-}$ macrophages are members of metabolic, immune system and cell cycle pathways (Fig.8E). In this comparison, as expected, Prdx5 is indeed strongly

decreased in *Prdx5*$^{-/-}$ phagocytes. Cd82 is also downregulated in the *Prdx5*$^{-/-}$ phagocytes as well as the Skap1, Ilf3 and Hebp1 (Fig.8D). Pathways that are downregulated in *Prdx5*$^{-/-}$ macrophages upon LPS exposure are mainly related to SUMOylation, metabolism of macromolecules and detoxification of ROS (Fig.8F).

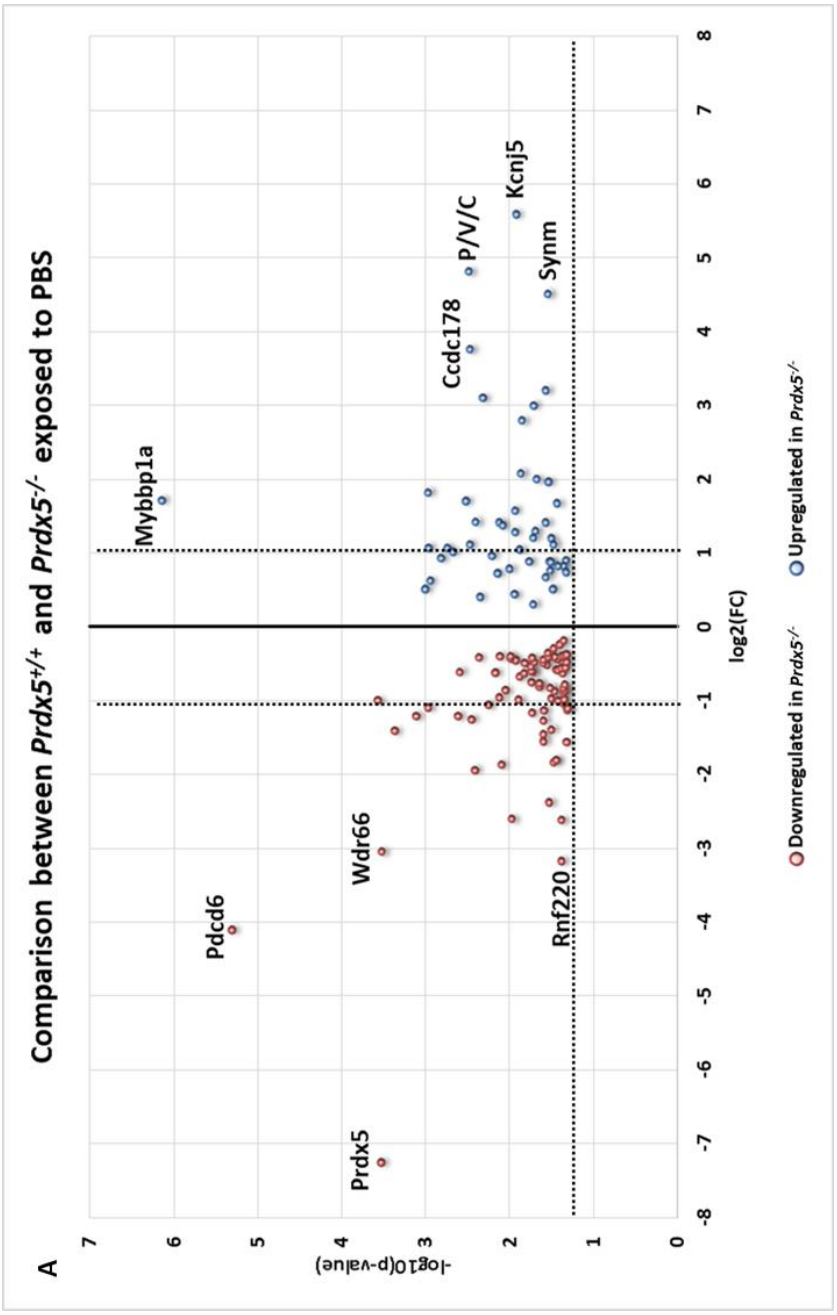
A
Comparison between Prdx5+/+ and Prdx5-/- exposed to PBS
-log10(p-value)
log2(FC)
Mybbp1a
Pdcd6
Wdr66
Prdx5
Rnf220
Ccdc178
P/V/C
Kcnj5
Synm
Downregulated in Prdx5-/-
Upregulated in Prdx5-/-

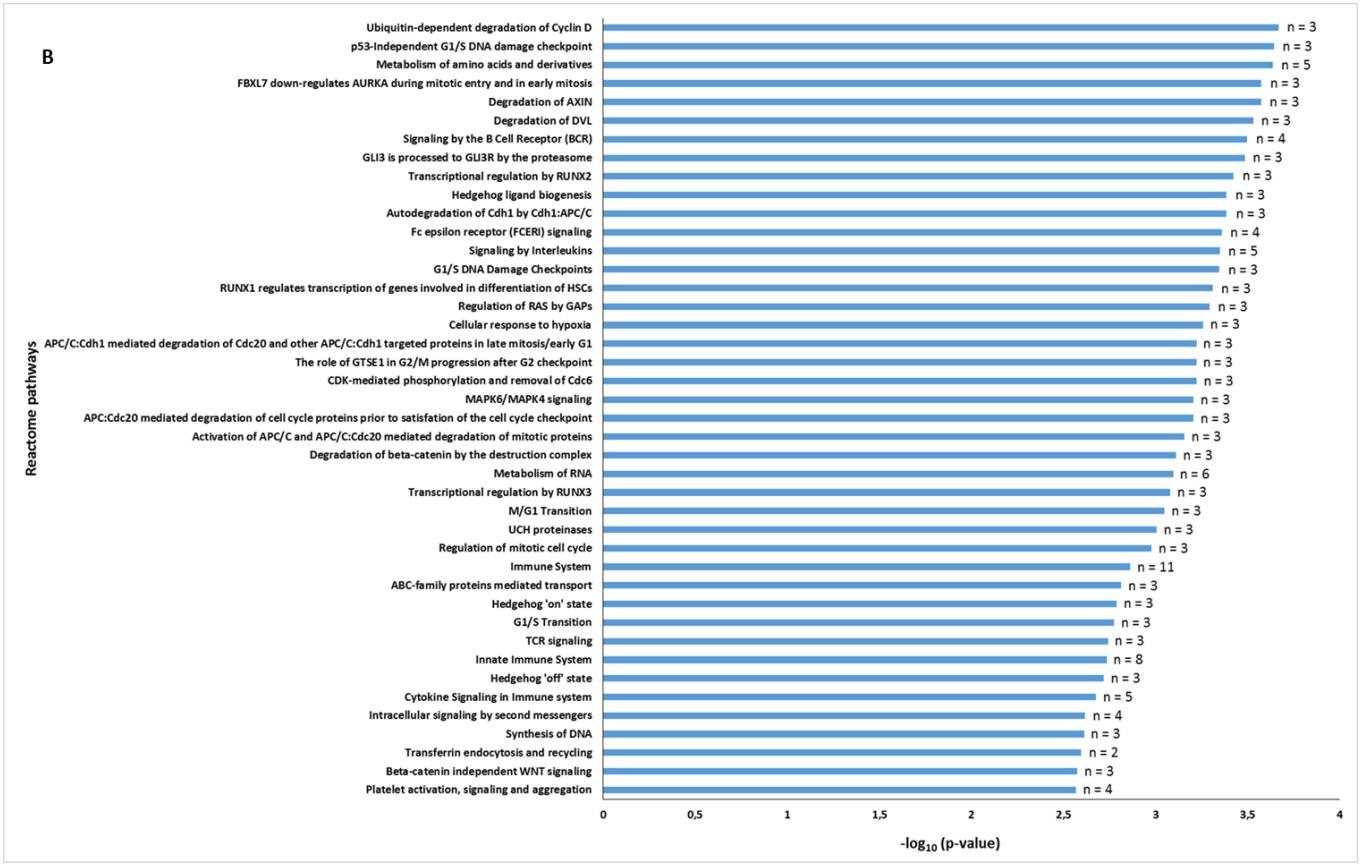
B
Reactome pathways
Ubiquitin-dependent degradation of Cyclin D
p53-Independent G1/S DNA damage checkpoint
Metabolism of amino acids and derivatives
FBXL7 down-regulates AURKA during mitotic entry and in early mitosis
Degradation of AXIN
Degradation of DVL
Signaling by the B Cell Receptor (BCR)
GLI3 is processed to GLI3R by the proteasome
Transcriptional regulation by RUNX2
Hedgehog ligand biogenesis
Autodegradation of Cdh1 by Cdh1:APC/C
Fc epsilon receptor (FCERI) signaling
Signaling by Interleukins
G1/S DNA Damage Checkpoints
RUNX1 regulates transcription of genes involved in differentiation of HSCs
Regulation of RAS by GAPs
Cellular response to hypoxia
APC/C:Cdh1 mediated degradation of Cdc20 and other APC/C:Cdh1 targeted proteins in late mitosis/early G1
The role of GTSE1 in G2/M progression after G2 checkpoint
CDK-mediated phosphorylation and removal of Cdc6
MAPK6/MAPK4 signaling
APC:Cdc20 mediated degradation of cell cycle proteins prior to satisfation of the cell cycle checkpoint
Activation of APC/C and APC/C:Cdc20 mediated degradation of mitotic proteins
Degradation of beta-catenin by the destruction complex
Metabolism of RNA
Transcriptional regulation by RUNX3
M/G1 Transition
UCH proteinases
Regulation of mitotic cell cycle
Immune System
ABC-family proteins mediated transport
Hedgehog 'on' state
G1/S Transition
TCR signaling
Innate Immune System
Hedgehog 'off' state
Cytokine Signaling in Immune system
Intracellular signaling by second messengers
Synthesis of DNA
Transferrin endocytosis and recycling
Beta-catenin independent WNT signaling
Platelet activation, signaling and aggregation
n = 3
n = 3
n = 5
n = 3
n = 3
n = 3
n = 4
n = 3
n = 3
n = 3
n = 3
n = 4
n = 5
n = 3
n = 3
n = 3
n = 3
n = 3
n = 3
n = 3
n = 3
n = 3
n = 3
n = 3
n = 6
n = 3
n = 3
n = 3
n = 3
n = 11
n = 3
n = 3
n = 3
n = 3
n = 8
n = 3
n = 5
n = 4
n = 3
n = 2
n = 3
n = 4
0
0,5
1
1,5
2
2,5
3
3,5
4
-log10 (p-value)

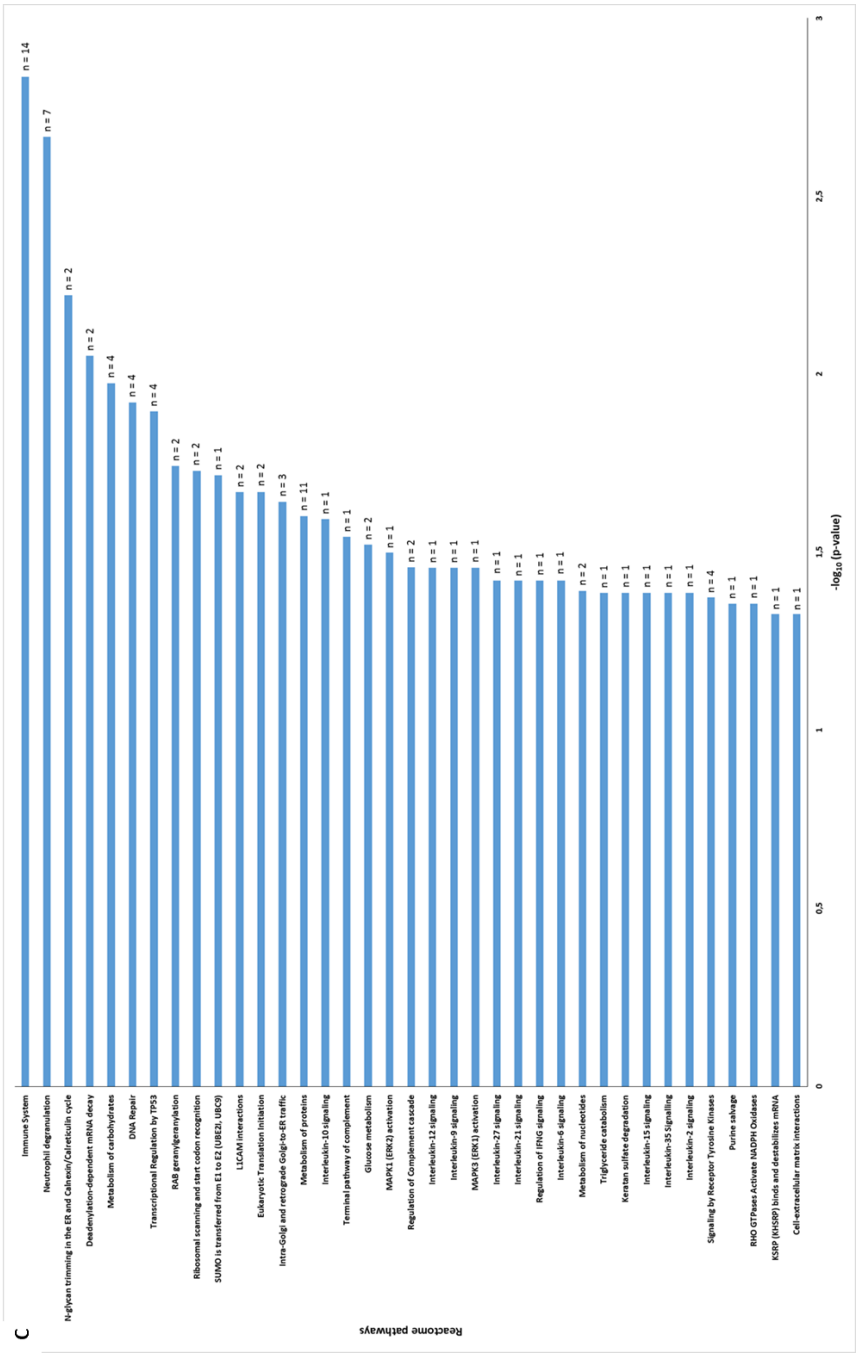
C
Reactome pathways
Immune System
Neutrophil degranulation
N-glycan trimming in the ER and Calnexin/Calreticulin cycle
Deadenylation-dependent mRNA decay
Metabolism of carbohydrates
DNA Repair
Transcriptional Regulation by TP53
RAB geranylgeranylation
Ribosomal scanning and start codon recognition
SUMO is transferred from E1 to E2 (UBE2I, UBC9)
L1CAM interactions
Eukaryotic Translation Initiation
Intra-Golgi and retrograde Golgi-to-ER traffic
Metabolism of proteins
Interleukin-10 signaling
Terminal pathway of complement
Glucose metabolism
MAPK1 (ERK2) activation
Regulation of Complement cascade
Interleukin-12 signaling
Interleukin-9 signaling
MAPK3 (ERK1) activation
Interleukin-27 signaling
Interleukin-21 signaling
Regulation of IFNG signaling
Interleukin-6 signaling
Metabolism of nucleotides
Triglyceride catabolism
Keratan sulfate degradation
Interleukin-15 signaling
Interleukin-35 Signalling
Interleukin-2 signaling
Signaling by Receptor Tyrosine Kinases
Purine salvage
RHO GTPases Activate NADPH Oxidases
KSRP (KHSRP) binds and destabilizes mRNA
Cell-extracellular matrix interactions
n = 14
n = 7
n = 2
n = 2
n = 4
n = 4
n = 4
n = 2
n = 2
n = 1
n = 2
n = 2
n = 3
n = 11
n = 1
n = 1
n = 2
n = 1
n = 2
n = 1
n = 1
n = 1
n = 1
n = 1
n = 1
n = 1
n = 2
n = 1
n = 1
n = 1
n = 1
n = 4
n = 1
n = 1
n = 1
n = 1
0
0,5
1
1,5
2
2,5
3
-log10 (p-value)

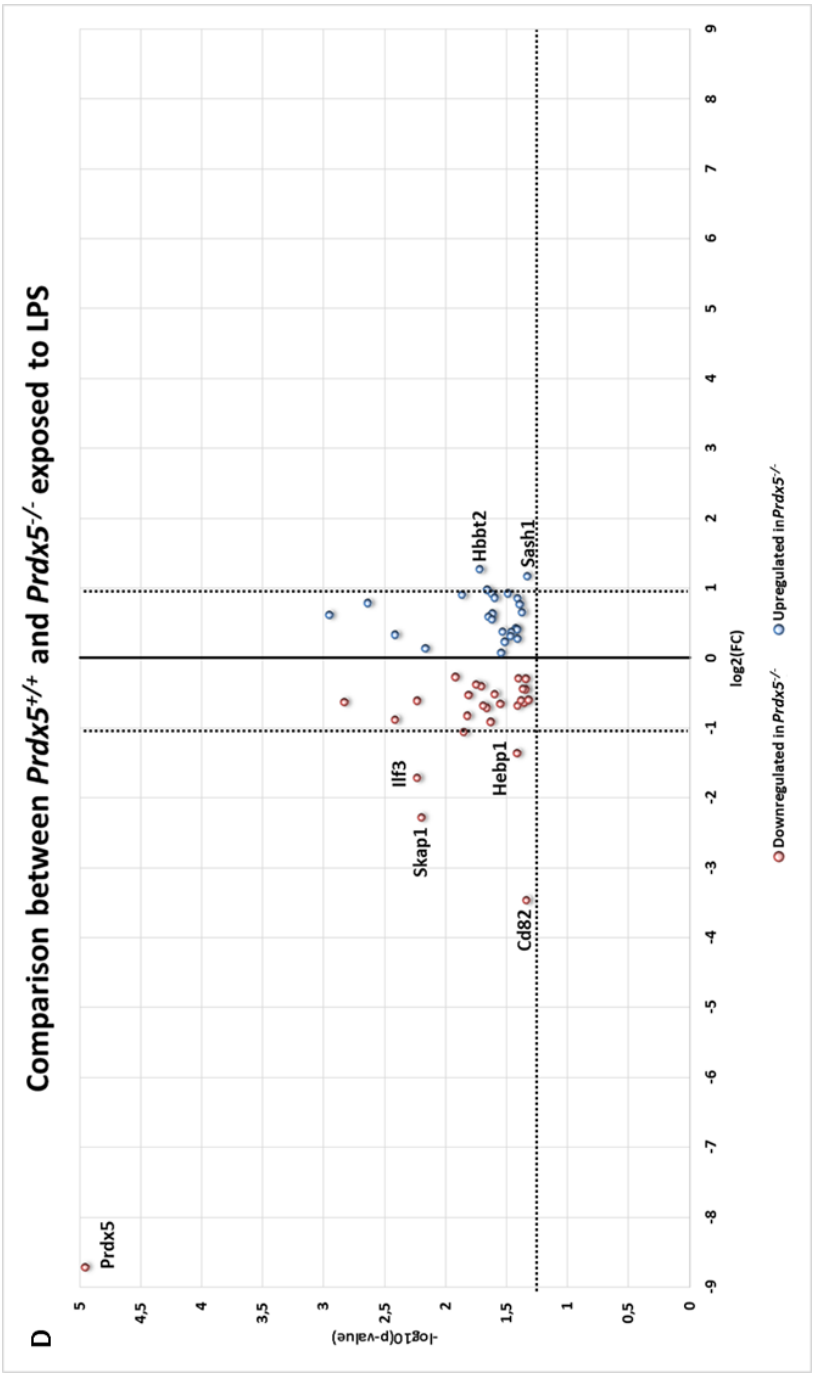
D
Comparison between Prdx5+/+ and Prdx5-/- exposed to LPS
-log10(p-value)
log2(FC)
Prdx5
Ilf3
Skap1
Hebp1
Cd82
Hbbt2
Sash1
Downregulated in Prdx5-/-
Upregulated in Prdx5-/-

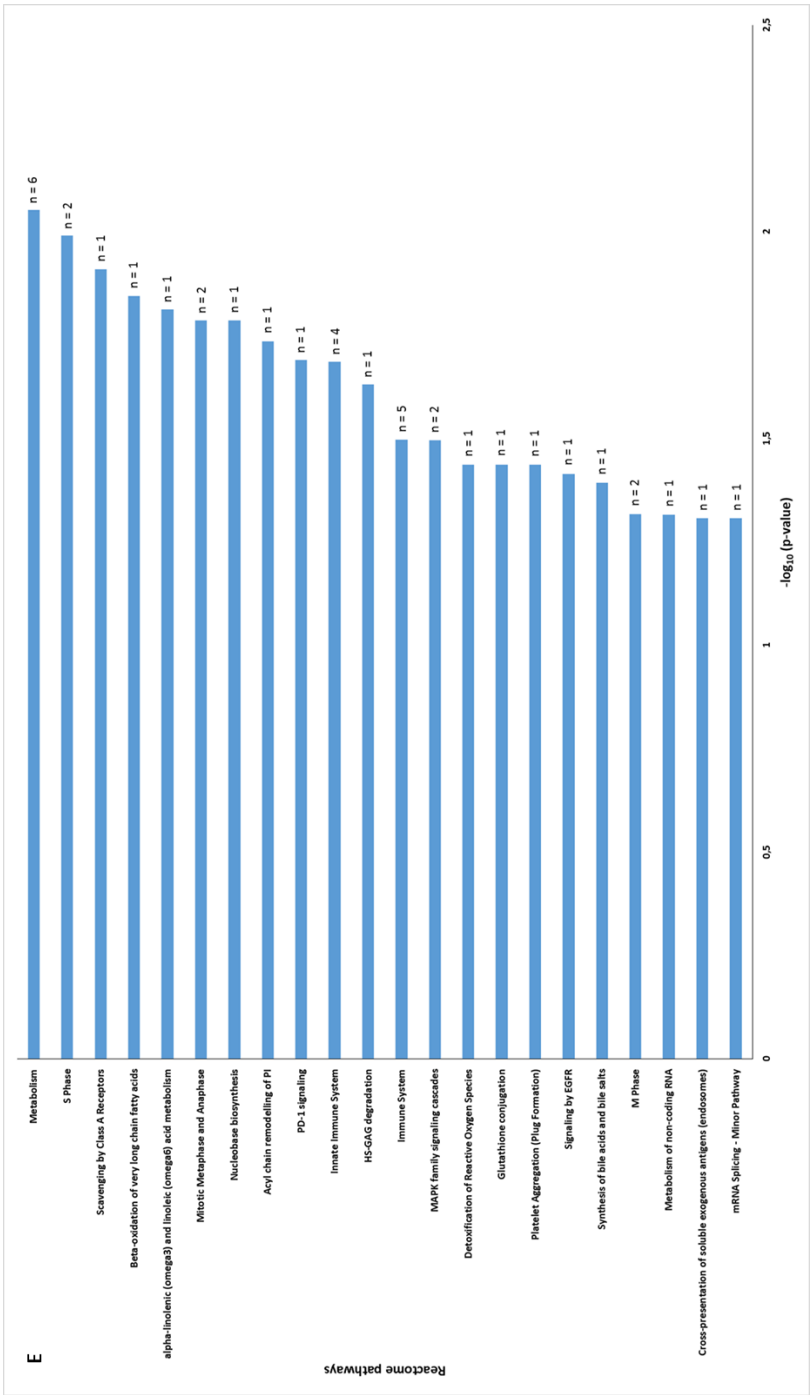
E
Reactome pathways
Metabolism
S Phase
Scavenging by Class A Receptors
Beta-oxidation of very long chain fatty acids
alpha-linolenic (omega3) and linoleic (omega6) acid metabolism
Mitotic Metaphase and Anaphase
Nucleobase biosynthesis
Acyl chain remodelling of PI
PD-1 signaling
Innate Immune System
HS-GAG degradation
Immune System
MAPK family signaling cascades
Detoxification of Reactive Oxygen Species
Glutathione conjugation
Platelet Aggregation (Plug Formation)
Signaling by EGFR
Synthesis of bile acids and bile salts
M Phase
Metabolism of non-coding RNA
Cross-presentation of soluble exogenous antigens (endosomes)
mRNA Splicing - Minor Pathway
n = 6
n = 2
n = 1
n = 1
n = 1
n = 2
n = 1
n = 1
n = 1
n = 4
n = 1
n = 5
n = 2
n = 1
n = 1
n = 1
n = 1
n = 1
n = 2
n = 1
n = 1
n = 1
0
0,5
1
1,5
2
2,5
-log10 (p-value)

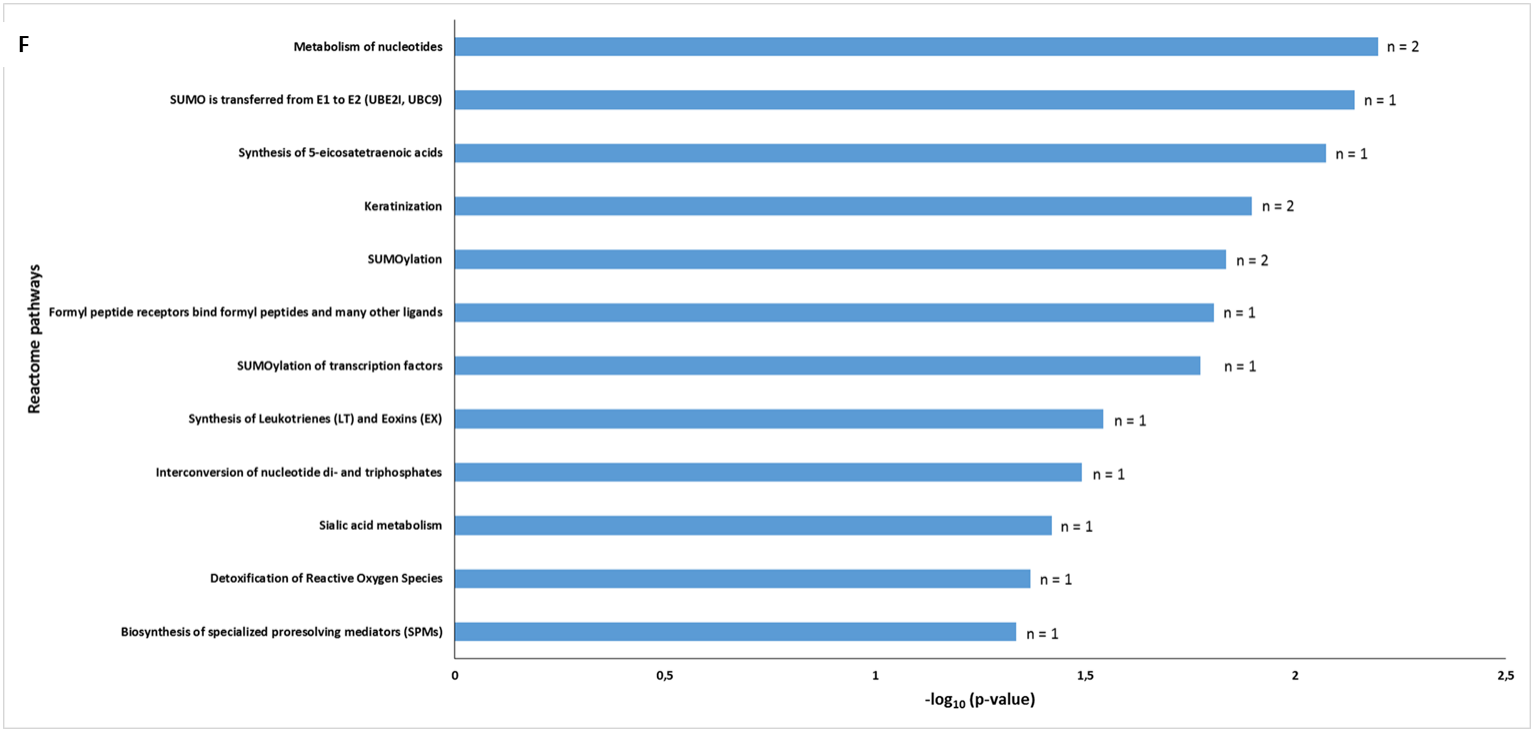
F
Metabolism of nucleotides
SUMO is transferred from E1 to E2 (UBE2I, UBC9)
Synthesis of 5-eicosatetraenoic acids
Keratinization
SUMOylation
Formyl peptide receptors bind formyl peptides and many other ligands
SUMOylation of transcription factors
Synthesis of Leukotrienes (LT) and Eoxins (EX)
Interconversion of nucleotide di- and triphosphates
Sialic acid metabolism
Detoxification of Reactive Oxygen Species
Biosynthesis of specialized proresolving mediators (SPMs)
n = 2
n = 1
n = 1
n = 2
n = 2
n = 1
n = 1
n = 1
n = 1
n = 1
n = 1
Reactome pathways
0
0,5
1
1,5
2
2,5
-log10 (p-value)

Figure 8. Up- and Down-regulated proteins between Prdx5$^{+/+}$ and Prdx5$^{-/-}$ macrophages under LPS or PBS conditions. *(A) Volcano plot of the quantification of peptides identified between Prdx5$^{+/+}$ and Prdx5$^{-/-}$ peritoneal macrophages treated by PBS. Y-axis indicates –log10 (p value) while the horizontal axis indicates base 2 logarithmic value of mean peptide abundance ratio (Prdx5$^{+/+}$ vs. Prdx5$^{-/-}$). The horizontal black line represents the threshold of significance assigned for subsequent analysis of peptides. The two vertical black lines represent the threshold of fold change 2. Peptides significantly decreased in Prdx5$^{-/-}$ macrophages following PBS treatment are indicated in red, those significantly increased in abundance are indicated in blue. (B) Upregulated signaling pathways in Prdx5$^{-/-}$ macrophages treated with PBS compared to Prdx5$^{+/+}$ macrophages analyzed by Panther. The number of genes for each pathway in indicated on the right. (C) Downregulated signaling pathways in Prdx5$^{-/-}$ macrophages treated with PBS compared to Prdx5$^{+/+}$ macrophages analyzed by Panther. The number of genes for each pathway in indicated on the right. (D) Volcano plot of the quantification of peptides identified between Prdx5$^{+/+}$ and Prdx5$^{-/-}$ peritoneal macrophages treated by LPS. Y-axis indicates –log10 (p value) while the horizontal axis indicates base 2 logarithmic value of mean peptide abundance ratio (Prdx5$^{+/+}$ vs. Prdx5$^{-/-}$). The horizontal black line represents the threshold of significance assigned for subsequent analysis of peptides. The two vertical black lines represent the threshold of fold change 2. Peptides significantly decreased in Prdx5$^{-/-}$ macrophages following LPS treatment are indicated in red, those significantly increased in abundance are indicated in blue. (E) Upregulated signaling pathways in Prdx5$^{-/-}$ macrophages treated with LPS compared to Prdx5$^{+/+}$ macrophages analyzed by Panther. The number of genes for each pathway in indicated on the right. (F) Downregulated signaling pathways in Prdx5$^{-/-}$ macrophages treated with LPS compared to Prdx5$^{+/+}$ macrophages analyzed by Panther. The number of genes for each pathway in indicated on the right.*

5.4 Discussion

In this study, we report the generation of *Prdx5*$^{-/-}$ mice using a gene-trap strategy to examine the consequences of non-conditional *Prdx5* inactivation *in vivo* in a mouse model. Indeed, when this study started, no mouse line with inactivated *Prdx5* gene was reported in the literature. In the meantime, two papers were published reporting generation and analysis of two different *Prdx5*$^{-/-}$ mouse lines [17], [18]. In the mouse model of *Prdx5* inactivation generated in our study, a gene-trap cassette was inserted in intron 1 of the mouse *Prdx5* gene. WT *Prdx5* gene inactivation was confirmed

at mRNA level by RT-PCR and at the protein level by Western blotting. However, it must be noted that in the RT-PCR analyses, weak bands of 246bp and of 131bp were detected, products of alternative splicing of the gt allele during the post-transcriptional modifications as determined by the sequencing of cloned RT-PCR products. Based on Western blotting analyses of different tissues, it appeared that these mRNAs were not translated into detectable Prdx5 proteins although very low levels of peptides corresponding to fragments of Prdx5 were detected in *Prdx5*$^{-/-}$ phagocytes by mass spectrometry (see discussion below). The ratio between the two genders is 1:1 and the distribution of the three genotypes (*Prdx5*$^{+/+}$, *Prdx5*$^{+/-}$, *Prdx5*$^{-/-}$) follows the 1:2:1 ratio as expected from the Mendelian inheritance. *Prdx5*$^{-/-}$ embryos developed normally. It must be noted that all the knockout models for the other Prdxs are also viable [47], [48], [53]–[55].

LPS triggers a massive inflammation and oxidative stress [47], [69]. LPS inflammation is initiated when LPS binds to TLR4 on monocyte cells, leading to an increase of ROS produced by the membrane NADPH oxidase [70]. The immune response triggered by LPS-TLR4 signaling is primarily regulated by NF-κB [71]. It was also shown previously that LPS up-regulates Prdx5 expression in macrophages and microglia [34]. Based on these studies, *Prdx5*$^{+/+}$ and *Prdx5*$^{-/-}$ mice were injected intraperitoneally with LPS to induce endotoxic shock. LPS injection induced a significant increase in the mortality

in the *Prdx5*$^{-/-}$ mice compared to the *Prdx5*$^{+/+}$ mice for both LPS concentrations used. These results suggest that Prdx5 protects mice from lethality caused by an endotoxic shock. These results are in agreement with other data from the literature. For instance, *Srxn*$^{-/-}$ mice are hypersensitive to LPS-induced endotoxic shock [72]. A high mortality of *Nrf2*$^{-/-}$ mice is also reported after LPS injection at different concentrations [73]. A complete proteomic analysis was performed in *Prdx5*$^{+/+}$ and *Prdx5*$^{-/-}$ macrophages, in order to examine major differences of the absence of Prdx5 during inflammation. Among the proteins that were upregulated in the *Prdx5*$^{-/-}$ macrophages under LPS exposure, proteins related to the inflammatory response were affected differently. Previously, it was shown that Prdx5 is a negative regulator of excessive mitochondrial fission and a modulator of pro-inflammatory responses in activated microglia cells by LPS [38]. Prdx5 inhibits the ROS-dependent Ca^{2+}/calcineurin and de-phosphorylation of dynamin-related protein 1 (Drp1). It is also reported that Prdx5 is implicated in the regulation of LPS/TLR4-induced IL-6 production in mouse macrophages, by modulating the jak-stat5 signaling pathway [37]. In a KO study of Prdx5 *in vitro*, microglia was shown to be activated with high increase of ROS/RNS levels through the JNK-dependent NO production, suggesting that Prdx5 modulates a ROS-dependent signaling cascade [36]. However, other proteins related to inflammation process are downregulated in the *Prdx5*$^{-/-}$

macrophages, such as the CD82 antigen and the Interleukin enhancer-binding factor 3, while the TNF-α release measured by ELISA is higher. Prdx5 knockdown dendritic cells resulted in increased cytokine expression relative to control knockdown, suggesting an increase in inflammatory cytokine and chemokine production [18]. The programmed cell death protein 6 was also downregulated in *Prdx5*$^{-/-}$ macrophages control conditions, suggesting that Prdx5 may be implicated in apoptosis as well, but the mechanism is not clear. Overexpression of Prdx5 was reported to protect tendon cells against H_2O_2-induced apoptosis [25]. This role of Prdx5 could be linked to the downregulation of the programmed cell death protein 6.

In the transcriptomic analysis in the *Prdx5*$^{-/-}$ liver and brain, we noticed a number of genes with altered expression between the *Prdx5*$^{+/+}$ and the *Prdx5*$^{-/-}$ mice. Genes related to the immune system, such as the serum amyloid protein 1 and 2 (Saa1 and Saa2), were significantly downregulated in the *Prdx5*$^{-/-}$ liver. Saa1 and Saa2 genes are involved in activation of MAPKs activity, in macrophages and neutrophils chemotaxis, platelet activation and they are regulated in liver cells by the proinflammatory cytokines IL-1, IL-6, and TNF-α. They are both induced up to a 1000-fold in mice under acute inflammatory conditions following exposure to LPS [57]. Lipocalin 2 was also downregulated in *Prdx5*$^{-/-}$ liver. The binding of lipocalin 2 to bacterial siderophores is important in the innate immune response to bacterial

infection. The toll-like receptors on immune cells stimulate the synthesis and secretion of lipocalin 2. Secreted lipocalin 2 then limits bacterial growth by sequestering iron-containing siderophores [58]. The orosomucoid 2 (orm2) is an acute-phase protein that belongs to the immunocalin subfamily, a group of small-molecule-binding proteins with immunomodulatory functions, that is also downregulated in *Prdx5*$^{-/-}$ liver. Expression of Orm2 is highly induced in the mouse brain after systemic injection of LPS [59]. Prdx5 could be implicated in the decreased expression of these proteins, since its absence affected them. Additionally, a number of proteins are downregulated in the *Prdx5*$^{-/-}$ brain. Visual system homeobox 1 may regulate expression of the cone opsin genes early in development [60]. Mutations in this gene can cause posterior polymorphous corneal dystrophy (PPCD) and keratoconus [61]. The hydrolethalus syndrome 1 protein (hyls1) plays an essential role in the formation of the primary cilium [62]. The p.Asp211Gly homozygous HYLS1 mutation is so far known to cause only hydrolethalus syndrome, a lethal malformation syndrome. Dystrotelin, an entirely novel branch of the Dystrophin superfamily, present in most vertebrates examined. Dystrotelin is expressed in the central nervous system, and is a possible orthologue of Drosophila DAH [63]. It is known that Prdx5 is highly expressed in the brain [64], so its absence could cause the downregulation of these proteins in the

brain. Based partly on these observations, the role of Prdx5 in the brain has been studied also in the framework of this thesis (see chapter 7).

Interestingly, members of the Aldo-keto reductases, apolipoproteins and Cytochrome P450 families were significantly upregulated in the *Prdx5*$^{-/-}$ brain and liver at the transcriptional level. The Aldo-keto reductases (AKRs) are a major superfamily of NAD(P)H-dependent oxidoreductases. There are 15 human AKRs of these AKR1B1, AKR1C1–1C3, AKR1D1, and AKR1B10 have been implicated in diabetic complications, steroid hormone dependent malignancies, bile acid deficiency and defects in retinoic acid signaling, respectively [65]. Exchangeable apolipoproteins function in lipid transport as structural components of lipoprotein particles, cofactors for enzymes and ligands for cell-surface receptors [66]. Type I collagen is the most abundant protein in humans, and it helps to maintain the integrity of many tissues via its interactions with cell surfaces, other extracellular matrix molecules, and growth and differentiation factors [67]. Additionally, most of the genes in the CYP1, CYP2, CYP3 and CYP4 families encode enzymes involved in eicosanoid metabolism [68]. Upregulation of all these families in the *Prdx5*$^{-/-}$ brain and liver suggests that Prdx5 plays a role in lipid metabolism and transportation. More data will be necessary to confirm this hypothesis.

In order to determine whether there is a compensation of Prdx5 absence, the expression of the other antioxidants enzymes was examined. It appeared

that *Prdx5* inactivation, did not affect dramatically the expression of the antioxidant enzymes. Prdx1, Prdx6, SOD2 and catalase were decreased in the *Prdx5*$^{-/-}$ lung, while Prdx6 is increased in the *Prdx5*$^{-/-}$ liver, Prdx-SOx was increased in *Prdx5*$^{-/-}$ liver and heart and SOD2 is increased in *Prdx5*$^{-/-}$ heart. The Prdx6 increase in the *Prdx5*$^{-/-}$ liver was not confirmed at the mRNA level in the transcriptomic analysis. Interestingly, in *Prdx6*$^{-/-}$ mice also, no significant differences in the expression of the other antioxidant enzymes was observed [48].

The development of the *Prdx5*$^{-/-}$ young adults mice appeared as normal compared to the *Prdx5*$^{+/+}$ mice. The growth of the mice was not significantly different between the *Prdx5*$^{+/+}$ and *Prdx5*$^{-/-}$ in the two genders, suggesting that at this stage, the absence of Prdx5 protein does not play a major role in the development and the growth of the mice under normal diet. Similar analyses were made for Prdx1 [53], Prdx3 [47] and Prdx6 [48] knockout mouse lines. However, recently, for another *Prdx5*$^{-/-}$ mouse model, it was reported that high fat diet-induced obesity was more often present in these *Prdx5*$^{-/-}$ mice, with increased fat mass and adipocyte hypertrophy [17]. The authors of this study proposed that Prdx5 inhibits adipogenesis by modulating ROS generation and adipogenic gene expression.

However, in our study, the complete histological analysis of the young *Prdx5*$^{-/-}$ and *Prdx5*$^{+/+}$ mice did not reveal any significant difference in the tissues due

to the absence of Prdx5 protein. As Prdx5 protein is ubiquitously expressed in all the tissues in mammals and highly expressed in organs exposed metabolically to ROS/RNS [12], it was expected that the absence of this protein could affect organs such as the liver, kidneys or the brain. This was not observed for *Prdx5*$^{-/-}$ young adults under normoxia. Although histological examinations did not reveal any significant differences, higher lipid peroxidation was measured in the *Prdx5*$^{-/-}$ muscles compared to the *Prdx5*$^{+/+}$ mice in normal conditions. Higher lipid peroxidation has also been shown in lungs of *Prdx6* KO mice challenged with paraquat [49] and in neurons of *Prdx2* KO mice during aging [56]. In our mouse model, higher protein oxidation in *Prdx5*$^{-/-}$ brain was measured but no significant differences were observed in DNA oxidation. It must be pointed out that *Prdx3* KO mice present higher DNA oxidation and protein carbonylation in lungs after LPS exposure [47], *Prdx2* KO higher protein carbonylation in neurons during aging [56] and *Prdx6* KO mice higher protein carbonylation in liver after paraquat exposure [48]. It appears that oxidative damages are mainly detected in young *Prdx* KO mice when animals are challenged by pro-oxidative compounds.

To conclude, *Prdx5*$^{-/-}$ mice generated in this study were viable, fertile and grow normally. They did not exhibit any abnormality in young age at tissue

level. However, *Prdx5*$^{-/-}$ mice were more vulnerable to LPS-induced endotoxic shock, suggesting that Prdx5 protein may play a major role in inflammation.

5.5 Innovation

To fully understand the role of the antioxidant enzyme Prdx5 during inflammation, a new *Prdx5*$^{-/-}$ mouse model was generated and studied. Within this study, we showed that Prdx5 is protecting the mice from LPS-induced endotoxic shock, while its absence make the mice more prone to inflammation and lethality.

5.6 Materials and Methods

5.6.1 Prdx5 knockout mouse generation

The plasmid with the gene-trap (gt) *Prdx5* construct (Fig. 1A) was obtained from the EUCOMM consortium and used for homologous recombination in ES cells (129 Sv cells, XY caryotype and A/A agouti phenotype). ES cells were microinjected into C57BL6cBrd/cBrd blastocysts. The blastocysts were hosted by CBA;C57BL6/J F1 hybrid females and male chimeras were produced. Four generated chimeric males were then intercrossed with C57BL/6N (a/a, Tyr+/+, black phenotype) or C57BL/6-Tyrc-Brd (a/a, Tyrc/c, albino phenotype) females to generate F1 offspring. Once the germline of the chimera was transmitted, all the F1 offsprings were $Prdx5^{+/-}$ agouti (A/a genotype, Tyr+/+ or Tyrc/c), carrying one wt allele (+) and one gt allele (-). Heterozygous mice $Prdx5^{+/-}$ were crossed in our animal facility to obtain homozygous $Prdx5^{-/-}$ mice. The F2 offspring was $Prdx5^{+/+}$, $Prdx5^{+/-}$ or $Prdx5^{-/-}$, with all three colors independently of the *Prdx5* genotype. All animal experiments were performed in accordance with the Belgian national guidelines and in agreement with the European directive 2010/63/UE. The protocols used in this study were approved by the animal ethic committee of UClouvain (approval 122801).

5.6.2 DNA extraction

The DNA extraction was performed from pieces of ear or tail, using a Hotshot solution (EDTA 20mM, NaOH 2.5M, pH 11.9). Each sample was incubated with 100µl of the Hotshot solution for 1 hour in 95°C, vortexed every 15min. 100µl of neutralizing buffer (Tris 40mM, pH 5) were added continuously to the samples that were centrifuged at 5000 rpm for 2min at 4°C. Supernatant was collected after centrifugation and stored at -20°C.

5.6.3 Genotyping by PCR

PCR was performed to genotype the offspring obtained from each crossing and detect the presence of the *wt Prdx5* (+) allele and/or the *gt Prdx5* (-) allele. 0.5µl of total DNA was used for the reaction, in a total volume of 20µl. The Go Taq® G2 Hot Start Green Master Mix (Promega, M742A) was used for the reaction. Three primers were used in the same PCR reaction to detect simultaneously *wt* and *gt* alleles (Fig. 1A): *Intron1afw* (5'-CCCCACCATTTTCAAGCGACCGAATGC-3'), *Intron1arv* (5'-TTGGGGTTGAGAAACCGCCTGGTAAC-3') and *K7a1fw* (5'-TCTGGGGTTCGAAATGACCGACCAAG-3'). *Intron1afw*2 and *Intron1arv2* primers hybridize on the *wt* allele, and *Intron1afw* and *K7a1fw* on the *gt*

allele (Fig. 1A). The PCR reactions were performed on a GeneAmp machine (PCR System 9700) for 40 cycles. Each cycle included denaturation at 94^{o}C for 45sec, annealing at 60^{o}C for 45sec, and elongation at 72^{o}C for 1min. The size of the PCR products was determined by 1.5% agarose gel electrophoresis with visualization by ethidium bromide staining. The *wt* allele PCR product of this amplification corresponds to 854bp and the *gt* allele PCR product to 675bp (Fig. 1A and 1B).

5.6.4 RNA extraction

Trizol Reagent (Invitrogen, 15596-026) was used to isolate total RNA from mouse tissues. Specifically, 100 mg of tissue was homogenized in 1.1 ml of Trizol Reagent in an Eppendorf tube and power homogenizer. After incubation for 5 min at room temperature, 0.2 ml of chloroform was added in each sample and the solution was vortexed and incubated 2-3min at room temperature. The aqueous phase (~0.6ml) was separated after centrifugation for 15min at 14000rpm at 4^{o}C and total RNA was precipitated by mixing with 0.5 ml of isopropanol. After washing with 75% ethanol, the RNA pellet was dissolved in 20µl RNase-free H_2O and OD of 1µl was measured in the Nanodrop ND-1000 (Isogen Life Science, De Meern, The Netherlands).

5.6.5 RT-PCR

RT-PCR was performed to detect the mRNA expression of *Prdx5* in *Prdx5*$^{+/+}$ and *Prdx5*$^{-/-}$ tissues. RT-PCR *GAPDH* mRNA expression was used as positive control and the complete procedure without reverse transcription was used as negative control. 1μg of total RNA was used for the reverse transcription with the Quantitect Reverse Transcription Kit (Qiagen, 205311). The primers used for the RT-PCR were 5'-AGTTCACCTTCTTTCCCGGT-3' and 5'-AGAAGCAGGTTGGGAGTGTG-3' for *Prdx5* wt allele, and 5'-TTGAGGTCAATGAAGGGGTC-3' and 5'-TCGTCCCGTAGACAAAATGG-3' for *GAPDH*. RT-PCR was performed on a GeneAmp machine (PCR System 9700) for 35 cycles. Each cycle included denaturation at 94^{o}C for 30sec, annealing at 65^{o}C for 30sec, and elongation at 72^{o}C for 2min. The size of the RT-PCR products was determined by 2% agarose gel electrophoresis with visualization by ethidium bromide staining. The *Prdx5* wt allele product of PCR amplification corresponds to 131bp and the GAPDH product to 132bp.

5.6.6 Western blotting

Mouse tissues were homogenized in lysis buffer (Tris 10mM, NaCl 150mM, EDTA 1mM, Triton X-100 1%) containing protease inhibitors cocktail (Roche,

1836170). Protein concentrations were measured using the Pierce BCA protein assay kit (Thermo-Scientific, 23225) and using bovine serum albumin (BSA) as the standard. Protein samples in loading buffer (Tris 45mM pH 6.8, Glycerol 10%, SDS 1%, BPP 0.25%, DTT 0.5M) were subjected to electrophoresis on 12% Mini-Protean SF TGX gels (Bio-Rad) using electrophoresis buffer (Tris 50mM, Glycine 150mM, SDS 0.1%) and transferred to nitrocellulose membranes (Amersham Protran 0.45 µM NC GE Healthcare, 10.600.002). Membranes were first incubated for 1h at room temperature in blocking solution (0.1% Tween 20 - TBS buffer containing 5% non-fat dry milk). After washing with 0.1% Tween 20 - TBS buffer, the membranes were probed with rabbit anti-Prdx1 polyclonal antibody (Hormonology Laboratory of Marloie, UC232) 1:4000, rabbit anti-Prdx2 polyclonal antibody (Hormonology Laboratory of Marloie, UC198) 1:2000, rabbit anti-Prdx3 polyclonal antibody (AbFrontier, LF-PA0030) 1:2000, rabbit anti-Prdx4 polyclonal antibody (Hormonology Laboratory of Marloie, UC194) 1:5000, rabbit anti-Prdx5 polyclonal antibody (Hormonology Laboratory of Marloie, G234) 1:5000, rabbit anti-Prdx6 polyclonal antibody (AbFrontier, LF-PA0011) 1:2000, rabbit anti-Prdx-SO_3 polyclonal antibody (AbFrontier LF-PA0004) 1:2000, rabbit anti-Prdx6-SO_3 polyclonal antibody (AbFrontier LF-PA0005) 1:2000, mouse anti-Catalase polyclonal antibody (Sigma, C0979) 1:2000, rabbit anti-Mn-SOD polyclonal antibody (Merck Millipore, 06-984)

1:2000, rabbit anti-β-actin polyclonal antibody (Sigma, A2066) 1:1500, followed by horseradish peroxidase-conjugated anti-rabbit secondary antibody (DAKO, p0448) 1:2000 and anti-mouse secondary antibody (DAKO, p0447) 1:2000. The reaction was detected by chemiluminescence using ECL Western Lightning Chemiluminescence Reagent Plus (Perkin Elmer Life Sciences, NEL104) and exposed to film (Amersham Hyperfilm™ ECL, 28-9068-37). The ImageJ software was used for Western blot quantifications.

5.6.7 cDNA cloning and sequence analysis

The PCR products of ~250bp and 131bp were gel purified with the Nucleospin gel and PCR Clean-up extraction kit (Macherey-Nagel, 740609) and cloned into the pcr2.1 TOPO vector with the TOPO TA Cloning kit (Invitrogen, 45-0641), following the manufacturer's instructions. Cloned PCR products were sequenced using primers *Univ5'* 5'-TTGTGAGCGGATAACAATTTC-3' and *Univ3'* 5'-GTTTTCCCAGTCACGACGTTGTA-3'.

5.6.8 Histological analysis

For histological analysis, brain, liver, kidney, heart, lung, muscle, spleen, adrenal gland, ovary, fat, intestine, salivary gland, skin, spinal cord, stomach, trachea and esophagus of *Prdx5*$^{+/+}$ and *Prdx5*$^{-/-}$ young mouse females (3 month-old) were fixed in 10% buffered neutral formalin. Fixed tissues were embedded in paraffin and 7µm sections were cut. The sections were mounted on polylysine slides (VWR, 631-0107) and stained with hemalun-eosin as following: the sections were deparaffinized in xylol, rehydrated in decreasing ethanol solutions (100-30%), stained with Mayer's hemalun (Carl Roth, Karlsruhe, Germany) for 5 min, washed again, and stained with 1% eosin (Carl Roth, Karlsruhe, Germany) for 2 minutes. Continuously, the sections were washed in tab water, dehydrated in increasing ethanol solutions (30-100%), treated with xylol, and mounted with Eukitt Quick-hardening mounting medium (Sigma-Aldrich, 03989). The slides were observed with the Polyvar Reichter-Jung microscope.

5.6.9 DNA oxidation assay

The DNA oxidation damage was measured in different tissue homogenates of *Prdx5*$^{+/+}$ and *Prdx5*$^{-/-}$ mice, using ELISA kit against 8-OHdG (E03H0007, Blue

Gene, Amsbio), according to the manufacturer's protocols. Tissue homogenates were incubated with the HRP conjugated 8-OHdG antibody for 1 hour. Then, the wells were washed and incubated with a substrate for HRP enzyme. The reaction was stopped after 15 minutes and the intensity of the color was measured spectrophotometrically at 450nm in a microplate reader. A standard curve was plotted and the 8-OHdG concentration in each sample was interpolated from this curve.

5.6.10 Protein carbonylation assay

Protein oxidation was determined by the presence of carbonylated proteins, which contain oxidative derivatives of amino acid residues after direct oxidation or indirect modification by reactive aldehydes derived from lipid peroxides, as it described previously [74]. Since carbonylated proteins could bind DNPH, tissue homogenates were incubated with 10mM 2,4-dinitrophenylhydrazine (DNPH) in 2.5M hydrogen chloride for 1 hour. Then the proteins were precipitated in 10% TCA for 5 min, centrifuged and the pellets were washed 3 times with EtOH:Ethyl Acetate (1:1). After the final wash, the pellets were suspend in 6M Guanidine hydrochloride and their optical density was measured spectrophotometrically at 370nm in a microplate reader. The concentration of the protein carbonyls was

determined using the extinction coefficient 22.000 M^{-1} cm^{-1} for the DNPH at 370nm.

5.6.11 Lipid peroxidation assay

Tissue lipid peroxidation was determined by measuring the total hydroperoxides (LOOH) in different tissue homogenates of *Prdx5*$^{+/+}$ and *Prdx5*$^{-/-}$ mice, using the xylenol orange assay, as described previously [75]. The lipid fraction of the homogenates was separated with chloroform:methanol mix (2:1) and was concentrated by vacuum evaporation. Continuously, the lipid pellet was dissolved in methanol and the samples were incubated with the FOX reagent (2mM xylenol orange in 0.25M H_2SO_4) and 8mM Fe^{2+} for 30 min. The optical density of the samples was measured spectrophotometrically at 650nm in a microplate reader. A standard curve was plotted relating the optical density to the concentrations of the cumene standards. The LOOH concentration in each sample was interpolated from this standard curve.

5.6.12 Immunohistochemistry

Immunohistochemistry was performed to analyze lipid peroxidation in tissues slides. Antibody against 4-hydroxy-2-nonenal (4-HNE) was used for detection of lipid oxidation and staining procedure was referred to that described. All the sections were deparaffinized in xylol, rehydrated in decreasing ethanol solutions (100-30%) and heated for 20 min in a microwave with 10mM sodium citrate – 0.05% Tween 20 pH 6.0 and incubated with peroxidase blocking solution (DakoCytomation, Heverlee, Belgium) for 5 min at RT. Then, sections were washed with PBS and incubated with PBS containing 25% non-immune fetal bovine serum and 10% non-fat dry milk for 45 min at RT. The sections were incubated for 1 hour at RT with the monoclonal anti-4-HNE antibody (Merck, 393207) 1:300, washed with PBS for 10 min, incubated with Envision Flex rabbit LINKER (DakoCytomation) for 15 min at RT, and then incubated with an Envision-labeled polymer-HRP anti-rabbit secondary antibody (DakoCytomation) for 30 min at RT. The peroxidase reaction was visualized by incubating the sections for 5 min with diaminobenzidine (DAB, DakoCytomation) and then stained with hematoxylin as described before. The slides were observed using a Polyvar Reichter-Jung microscope.

5.6.13 Microarray analysis

The Mouse Gene Expression Microarray 4x44K plates (Agilent Technologies, Santa Clara, CA, USA) containing 43.803 mouse probes was used to identify expressed and differently regulated genes in the *Prdx5*$^{+/+}$ and *Prdx5*$^{-/-}$ liver and brain homogenate samples (2 females per genotype). The RNA labelling and the microarray hybridization and scanning were performed at the transcriptomic platform of the Louvain Institute of Biomolecular Science. In brief, total RNA was extracted using the TRIZOL/Chlorofom extraction protocol (Invitrogen, 15596-026). The concentration and the quality of RNA were checked using a NanoDrop ND-1000 (Isogen Life Science, De Meern, The Netherlands) and the Bioanalyzer Agilent 2100 (Agilent Technologies), respectively, with the Agilent 6000 RNA Nano kit (Agilent Technologies). Fluorescently labeled cDNA was synthesized from 10µg of total RNA using the SuperScript Plus Indirect cDNA Labeling System (Invitrogen, Paisley, UK) according to manufacturer's instructions. Gene expression analyses were carried out using GeneSpring GX v11.0 software (Agilent Technologies). Data were filtered for outliers, negative and positive controls. To identify statistically significant differentially expressed genes, combined criteria of a two-fold change ratio or greater and a p-value < 0.05 in the t-tests were adopted. Only common probe sets that were present in both experiments

were considered significant. Gene ontology analysis was carried out using PANTHER14.0 Classification System software.

5.6.14 LPS injection

Endotoxic shock was induced by intraperitoneal (IP) injection of LPS (*Escherichia coli*, serotype 0111:B4, Sigma, L2630) at a dosage of 10 mg/kg of body weight in 5 *Prdx5*$^{+/+}$ and 5 *Prdx5*$^{-/-}$ mice that were matched for age (7 month-old) and gender (male) and 20 mg/kg of body weight in 13 *Prdx5*$^{+/+}$ and 14 *Prdx5*$^{-/-}$ mice that were matched for age (7 month-old) and were of both genders. PBS was injected in control animals. Survival was monitored every 3 h for 4 days.

5.6.15 Primary culture of peritoneal cells

Peritoneal cells were collected from the peritoneal cavity of 8 *Prdx5*$^{+/+}$ and *Prdx5*$^{-/-}$ 4 month-old mice in 0.09% NaCl. The cells from the 8 mice were pulled together and centrifuged at 1500rpm for 10 min at 4^{o}C. The cell pellet was suspended in 1ml of DMEM [Dulbecco's Modified Eagle Medium (+) 4.5g/L D-glucose, (+) L-glutamine, (+) pyruvate (Gibco, 41966052)].

Approximately, 400.000 cells were plated in 24-well plates (BectonDickinson Labware, 353047) on cover-slips and 2 millions of cells in 6-well plates (Becton Dickinson Labware, 353046) and they were cultivated with DMEM with 10% fetal bovine serum and 1% penicillin/streptomycin at 37^{o}C with 5% CO_2 overnight. Next day, the non-adherent cells were removed and fresh medium was added to the cells.

5.6.16 Characterization of the peritoneal cells by immunofluorescence

Peritoneal cells in 24-well plates on cover-slips were fixed with 4% PFA for 20 minutes at RT. Cover-slips were washed with PBS for 3 times and 0.05M TBS-0.1% Triton X-100 (TBS-T) for 3 times. The cells were blocked with TBS-T + 10% non-fat dry milk for 30 minutes in RT. Then, the cells were incubated overnight at 4^{o}C with rabbit anti-Prdx5 polyclonal antibody (Hormonology Laboratory of Marloie, G234) 1:750, rat anti-F4/80 monoclonal antibody (BioRad, MCA497GA) 1:200, rat anti-CD11b monoclonal antibody (DSHB, M1/70.15.11.5.2-c) 1:200, followed by the Fluorophore-labeled secondary antibodies, Alexa Fluor 488 donkey anti-rabbit (ThermoFisher, A21206) 1:500 and Alexa Fluor 546 goat anti-rat (ThermoFisher, A11081) 1:500. Continuously, the cells were rinsed in buffer and exposed 10 min to 4',6-

diamidino-2-phenylindole (DAPI) (Roche, 10236276001). The cover-slips were mounted in Fluorescent mounting medium (DAKO, S3023) on microscope slides. The fixed cells were observed with a Polyvar Reichter-Jung fluorescence microscope with dedicated filters.

5.6.17 LPS exposure

The peritoneal cells in 6-well plates were stimulated by 1μg/ml of LPS or PBS (controls) for 0, 8, 24 and 48 hours. The cells were harvested at the specific time points and proteins were extracted, using PBS-1% Triton X-100 with protease inhibitor cocktail (Roche, 1836170). Cell culture medium of each well was also collected.

5.6.18 Enzyme-linked immunosorbent assay (ELISA)

ELISA kits for TNF-α (R&D Systems, MTA00B) and IL-1β measurements (R&D Systems, MLB00C) were used, and inflammatory cytokine levels in cell culture medium were quantitated according to the manufacturer's protocols.

5.6.19 Peptide separation using nanoUPLC

Peptide mixture in 0.1% (v/v) formic acid was separated by reverse phase chromatography on a NanoACQUITY UPLC MClass system (Waters, Milford, MA, USA) working with masslynx V4.1 (Waters) software. Digested proteins were injected into a trap C18, 100Å 5 µm, 180 µm × 20 mm column (Waters) and desalted using isocratic conditions with at a flow rate of 15 µL/min using a 99% formic acid and 1% (v/v) acetonitrile (ACN) buffer for 3 min. Peptide mixture was subjected to reverse phase chromatography on a C18, 100Å 1.8 µm, 75 µm × 150 mm column (Waters) PepMap for 120 min at 35°C at flow rate of 300 nL·min−1 using a two part linear gradient from 1% (v/v) ACN, 0.1% formic acid to 35% (v/v)) ACN, 0.1% formic acid and from 35% (v/v) ACN, 0.1% formic acid to 85% (v/v)) ACN, 0.1% formic acid.

5.6.20 HDMS^E analysis

The IMS-HDMS^E (Ion Mobilty Separation-High Definition Enhanced) analysis was performed on an SYNAPT G2-Si high definition mass spectrometer (Waters). The mass spectrometer was equipped with a NanoLockSpray dual electrospray ion source (Waters). The data were collected from 15 min after injection to 106 min using the HDMS^E method in resolution mode. This

method acquires MS^E in positive and resolution mode over the m/z range from 50 to 2000. Doubly charged monoisotopic ion of [Glu 1]-fibrinopeptide B was used for the postacquisition lock mass correction of the data.

5.6.21 LC-qTOF data processing

$HDMS^E$ data were processed with PROGENESIS QI (Nonlinear DYNAMICS, Waters) software using the relative quantitation using Hi-N3 method and UniProt database containing protein of interest sequence. To identify statistically significant differentially expressed proteins, combined criteria of a two-fold change ratio or greater, a p-value < 0.05 in the t-tests, correlation of peptides > 0.9 and number of unique peptides > 2 were adopted. Protein ontology analysis was carried out using PANTHER14.0 Classification System software.

5.6.22 Statistical analysis

All statistical analyses were performed with JMP 12.1 by SAS. Statistical comparison of differences between groups was performed using a mixed model on the normalized data sets. For both analyses, a probability value of

$p < 0.05$ was considered as statistically significant. Values were expressed as means ± confidence intervals.

5.7 Acknowledgements

Grant sponsor: F.R.S.-FNRS (grant number: PDR T.0090.15 and CDR J.0092.19) and ARC-Actions de Recherche Concertées. Vasiliki Argyropoulou is a holder of a FRIA fellowship (F.R.S.-FNRS). We would like to acknowledge Catherine Rasse of the SMCS platform at UCLouvain for statistical analyses. We also thank Coralie Piget for her contribution in the well-being of the mice in the animal facility.

5.8 Abbreviations

ACN: acetonitrile

AFM: atomic force microscope

Akr: Aldo-keto reductase

Apo: Apolipoprotein

Arhgap5: Rho GTPase-activating protein 5

BCA: Bicinchoninic acid assay

BMM: Bone marrow-derived macrophages

Casp3: Caspase 3

CAT: Catalase

Ccdc178: Coiled-coil domain containing 178

Cd11b: Cluster of differentiation 11b

Cd40: Cluster of differentiation 40

Cd82: Cluster of differentiation 82

CHO: Chinese hamster ovary cells

Cnot10: CCR4-NOT transcription complex subunit 10

Col16a1: collagen type XVI alpha1

Col6a5: collagen type VI alpha5

Col4a3: collagen type IV alpha3

CYP450: cytochrome P450

DAMP: damage-associated molecular pattern

DAPI: 4’,6-diamidino-2-phenylindole

DMEM: Dulbecco's Modified Eagle Medium

DNPH: 2,4-Dinitrophénylhydrazine

Drp1: dynamin-related protein 1

Dytn: dystrotelin

EDTA: Ethylene-diamine-tetra-acetic acid

ER: Endoplasmic reticulum

EtOH: Ethanol

F4/80: Macrophage receptor

Gadl1: glutamate decarboxylase-like 1

GAPDH: Glyceraldehyde 3-phosphate dehydrogenase

Golgb1: Golgin subfamily B member 1

GPx: Glutathione peroxidase

GSH: Glutathione

gt: gene trap

H_2O_2: Hydrogen peroxide

Hbbt2: Beta-globin

HEBP1: Heme binding protein 1

HRP: horseradish peroxidase

Hysl1: hydrolethalus syndrome 1

IFN-γ: interferon gamma

Il-1β: Interleukin 1 beta

Il-6: Interleukin 6

Ilf3: Interleukin Enhancer Binding Factor 3

Jak2: Janus kinase 2

JNK: c-Jun N-terminal kinases

KD: knockdown

Kcnj5: G protein-activated inward rectifier potassium channel 4

KO: knockout

Lcn2: lipocalin 2

LPS: lipopolysaccharide

LOOH: lipid hydroperoxides

MAPK: Mitogen-activated protein kinases

Mboat7: Membrane bound O-acyltransferase domain containing 7

MHC class II: Major histocompatibility complex class II

MPP+: 1-methyl-4-phenylpyridinium

MTS: Mitochondria targeting sequence

Mybbp1a: MYB binding protein 1a

NADPH: nicotinamide adenine dinucleotide phosphate

NF-κB: nuclear factor kappa-light-chain-enhancer of activated B cells

NO: Nitrogen oxide

Nrf2: nuclear factor erythroid-2-related factor 2

Orm2: orosomucoid 2

p53: Tumor protein 53

PAMP: pathogen-associated molecular pattern

PCR: polymerase chain reaction

Pdcd6: Programmed cell death 6

Prdx: Peroxiredoxin

PTS1: Peroxisome targeting signal 1

Rnf220: Ring finger protein 220

RNS: Reactive nitrogen species

ROS: Reactive oxygen species

RT-PCR: Reverse transcription polymerase chain reaction

Saa1: serum amyloid A1

Saa2: serum amyloid A2

Sash1: SAM and SH3 domain containing 1

SDS: Sodium dodecyl sulfate

Skap1: Src kinase-associated phosphoprotein 1

SOD: Superoxide dismutase

Srxn: Sulfiredoxin

Stat5: Signal transducer and activator of transcription 5

SUMO: Small ubiquitin-like modifier

Synm: Synemin

TBS: Tris-Buffered saline

Timm13: Translocase of inner mitochondrial membrane 13

TLR4: Toll-like receptor 4

TNF-α: Tumor necrosis factor alpha

Tpr: Translocated promoter region protein

TRIF: TIR-domain-containing adapter-inducing interferon-β

Trx: Thioredoxin

Vsx1: visual system homeobox 1 homolog

Wdr66: WD Repeat Domain 66

WT: Wild type

4-HNE: 4-hydroxy-2-nonenal

8-OHdG: 8-hydroxy-2' –deoxyguanosine

5.9 References

[1] A. Perkins, K. J. Nelson, D. Parsonage, L. B. Poole, and P. A. Karplus, "Peroxiredoxins: guardians against oxidative stress and modulators of peroxide signaling," *Trends Biochem. Sci.*, vol. 40, no. 8, pp. 435–445, 2015.

[2] S. G. Rhee and I. S. Kil, "Multiple Functions and Regulation of Mammalian Peroxiredoxins," *Annu. Rev. Biochem.*, vol. 86, no. 5, pp.

1–27, 2017.

[3] E.-M. Hanschmann, J. R. Godoy, C. Berndt, C. Hudemann, and C. H. Lillig, “Thioredoxins, glutaredoxins, and peroxiredoxins--molecular mechanisms and health significance: from cofactors to antioxidants to redox signaling.,” *Antioxid. Redox Signal.*, vol. 19, no. 13, pp. 1–200, 2013.

[4] G. Ferrer-Sueta, B. Manta, H. Botti, R. Radi, M. Trujillo, and A. Denicola, “Factors affecting protein thiol reactivity and specificity in peroxide reduction,” *Chem. Res. Toxicol.*, vol. 24, pp. 434–450, 2011.

[5] B. Knoops, E. Loumaye, and V. Van Der Eecken, “Evolution of Peroxiredoxins: Taxonomy, homology and characterization,” *Peroxiredoxin Syst.*, pp. 27–40, 2007.

[6] A. Hall, K. Nelson, L. B. Poole, and P. A. Karplus, “Structure-based Insights into the Catalytic Power and Conformational Dexterity of Peroxiredoxins,” *Antioxid. Redox Signal.*, vol. 15, no. 3, pp. 795–815, 2011.

[7] M. S. Seo, S. W. Kang, K. Kim, I. C. Baines, T. H. Lee, and S. G. Rhee, “Identification of a new type of mammalian peroxiredoxin that forms an intramolecular disulfide as a reaction intermediate,” *J. Biol. Chem.*, vol. 275, no. 27, pp. 20346–20354, 2000.

[8] A. B. Fisher, “Peroxiredoxin 6, a Bifunctional Enzyme with Glutathione Peroxidase and Phospholipase A2 Activities,” *Antioxid Redox Signal.*, vol. 15, no. 3, pp. 831–844, 2011.

[9] M. H. Park, M. Jo, Y. R. Kim, C. K. Lee, and J. T. Hong, “Roles of peroxiredoxins in cancer, neurodegenerative diseases and inflammatory diseases,” *Pharmacology and Therapeutics*, vol. 163. pp. 1–23, 2016.

[10] B. Knoops, V. Argyropoulou, S. Becker, L. Ferté, and O. Kuznetsova, “Multiple Roles of Peroxiredoxins in Inflammation,” *Mol. Cells*, vol. 39, no. 1, pp. 60–64, 2016.

[11] B. Knoops, J. Goemaere, V. Van Der Eecken, and J.-P. Declercq, “Peroxiredoxin 5: Structure, Mechanism, and Function of the Mammalian Atypical 2-Cys Peroxiredoxin,” *Antioxid. Redox Signal.*, vol. 15, no. 3, pp. 817–829, 2011.

[12] B. Knoops *et al.*, “Cloning and characterization of AOEB166, a novel mammalian antioxidant enzyme of the peroxiredoxin family,” *J. Biol. Chem.*, vol. 274, pp. 30451–30458, 1999.

[13] A. Kropotov *et al.*, “A novel human DNA-binding protein with sequence similarity to a subfamily of redox proteins which is able to repress RNA-polymerase-III-driven transcription of the Alu-family

retroposons in vitro," *Eur J Biochem*, vol. 260, pp. 336–346, 1999.

[14] H. Yamashita *et al.*, "Characterization of Human and Murine PMP20 Peroxisomal Proteins That Exhibit Antioxidant Activity in Vitro," *J. Biol. Chem.*, vol. 274, no. 42, pp. 29897–29904, 1999.

[15] G. Leyens, I. Donnay, and B. Knoops, "Cloning of bovine peroxiredoxins - Gene expression in bovine tissues and amino acid sequence comparison with rat, mouse and primate peroxiredoxins," *Comp. Biochem. Physiol. - B Biochem. Mol. Biol.*, vol. 136, pp. 942–955, 2003.

[16] N. T. Nguyên-nhu *et al.*, "Human peroxiredoxin 5 gene organization, initial characterization of its promoter and identification of alternative forms of mRNA," *Biochim. Biophys. Acta - Gene Struct. Expr.*, vol. 1769, pp. 472–483, 2007.

[17] M. H. Kim *et al.*, "Peroxiredoxin 5 regulates adipogenesis-attenuating oxidative stress in obese mouse models induced by a high-fat diet," *Free Radic. Biol. Med.*, vol. 123, pp. 27–38, 2018.

[18] D. B. Graham *et al.*, "Nitric Oxide Engages an Anti-inflammatory Feedback Loop Mediated by Peroxiredoxin 5 in Phagocytes," *Cell Rep.*, vol. 24, no. 4, pp. 838–850, 2018.

[19] I. Banmeyer, C. Marchand, C. Verhaeghe, B. Vucic, J. F. Rees, and B. Knoops, “Overexpression of human peroxiredoxin 5 in subcellular compartments of Chinese hamster ovary cells: Effects on cytotoxicity and DNA damage caused by peroxides,” *Free Radic. Biol. Med.*, 2004.

[20] I. Banmeyer, C. Marchand, A. Clippe, and B. Knoops, “Human mitochondrial peroxiredoxin 5 protects from mitochondrial DNA damages induced by hydrogen peroxide,” *FEBS Lett.*, vol. 579, pp. 2327–2333, 2005.

[21] S. De Simoni, D. Linard, E. Hermans, B. Knoops, and J. Goemaere, “Mitochondrial peroxiredoxin-5 as potential modulator of mitochondria-ER crosstalk in MPP+-induced cell death,” *J. Neurochem.*, vol. 125, pp. 473–485, 2013.

[22] S. De Simoni, J. Goemaere, and B. Knoops, “Silencing of peroxiredoxin 3 and peroxiredoxin 5 reveals the role of mitochondrial peroxiredoxins in the protection of human neuroblastoma SH-SY5Y cells toward MPP+,” *Neurosci. Lett.*, vol. 433, pp. 219–224, 2008.

[23] G. Walbrecq, B. Wang, S. Becker, A. Hannotiau, M. Fransen, and B. Knoops, “Antioxidant cytoprotection by peroxisomal peroxiredoxin-5,” *Free Radic. Biol. Med.*, vol. 84, pp. 215–226, 2015.

[24] M.-X. Wang *et al.*, “Antioxidant Enzyme Peroxiredoxin 5 Is Upregulated in Degenerative Human Tendon,” *Biochem. Biophys. Res. Commun.*, vol. 284, pp. 667–673, 2001.

[25] J. Yuan, G. A. C. Murrell, A. Trickett, M. Landtmeters, B. Knoops, and M. X. Wang, “Overexpression of antioxidant enzyme peroxiredoxin 5 protects human tendon cells against apoptosis and loss of cellular function during oxidative stress,” *Biochim. Biophys. Acta - Mol. Cell Res.*, vol. 1693, pp. 37–45, 2004.

[26] A.-C. Gérard, M.-C. Many, C. Daumerie, B. Knoops, and I. M. Colin, “Peroxiredoxin 5 Expression in the Human Thyroid Gland,” *THYROID*, vol. 15, no. 3, pp. 205–209, 2005.

[27] H. Y. Yang *et al.*, “Proteomic analysis of protein expression affected by peroxiredoxin v knock-down in hypoxic kidney,” *J. Proteome Res.*, vol. 9, pp. 4003–4015, 2010.

[28] J. Royet, J. M. Reichhart, and J. A. Hoffmann, “Sensing and signaling during infection in Drosophila,” *Curr. Opin. Immunol.*, vol. 17, pp. 11–17, 2005.

[29] S. N. Radyuk *et al.*, “Peroxiredoxin 5 confers protection against oxidative stress and apoptosis and also promotes longevity in Drosophila,” *Biochem. J*, vol. 419, pp. 437–445, 2009.

[30] S. G. Rhee, H. Z. Chae, and K. Kanghwa, “Peroxiredoxins: A historical overview and speculative preview of novel mechanisms and emerging concepts in cell signaling,” *Free Radic. Biol. Med.*, vol. 38, pp. 1543–1552, 2005.

[31] H. A. Woo, S. H. Yim, D. H. Shin, D. Kang, D. Y. Yu, and S. G. Rhee, “Inactivation of Peroxiredoxin I by Phosphorylation Allows Localized H2O2 Accumulation for Cell Signaling,” *Cell*, vol. 140, pp. 517–528, 2010.

[32] H. Sies, “Role of metabolic H2O2 generation: Redox signaling and oxidative stress,” *J. Biol. Chem.*, vol. 289, no. 13, pp. 8735–8741, 2014.

[33] A. Diet *et al.*, “Regulation of peroxiredoxins by nitric oxide in immunostimulated macrophages,” *J. Biol. Chem.*, vol. 282, pp. 36199–36205, 2007.

[34] K. Abbas, J. Breton, C. R. Picot, V. Quesniaux, C. Bouton, and J. C. Drapier, “Signaling events leading to peroxiredoxin 5 up-regulation in immunostimulated macrophages,” *Free Radic. Biol. Med.*, vol. 47, pp. 794–802, 2009.

[35] A. Bast, S. F. Erttmann, R. Walther, and I. Steinmetz, “Influence of iNOS and COX on peroxiredoxin gene expression in primary

macrophages," *Free Radic. Biol. Med.*, 2010.

[36] H. N. Sun *et al.*, "Microglial peroxiredoxin v acts as an inducible anti-inflammatory antioxidant through cooperation with redox signaling cascades," *J. Neurochem.*, vol. 114, pp. 39–50, 2010.

[37] H. I. Choi *et al.*, "Peroxiredoxin v selectively regulates IL-6 production by modulating the Jak2-Stat5 pathway," *Free Radic. Biol. Med.*, vol. 65, pp. 270–279, 2013.

[38] J. Park *et al.*, "Peroxiredoxin 5 (Prx5) decreases LPS-induced microglial activation through regulation of Ca 2 þ / calcineurin-Drp1-dependent mitochondrial fission," *Free Radic. Biol. Med.*, vol. 99, pp. 392–404, 2016.

[39] M. W. Robinson, a. T. Hutchinson, J. P. Dalton, and S. Donnelly, "Peroxiredoxin: A central player in immune modulation," *Parasite Immunol.*, vol. 32, no. 5, pp. 305–313, 2010.

[40] M. W. Robinson, A. T. Hutchinson, S. Donnelly, and J. P. Dalton, "Worm secretory molecules are causing alarm," *Trends Parasitol.*, vol. 26, no. 8, 2010.

[41] T. Shichita *et al.*, "Peroxiredoxin family proteins are key initiators of post-ischemic inflammation in the brain.," *Nat. Med.*, vol. 18, no. 6,

pp. 911–917, 2012.

[42] S. Salzano *et al.*, “Linkage of inflammation and oxidative stress via release of glutathionylated peroxiredoxin-2, which acts as a danger signal,” *PNAS*, vol. 111, no. 33, pp. 12157–12162, 2014.

[43] L. Mullen, E.-M. Hanschmann, C. H. Lillig, L. A. Herzenberg, and P. Ghezzi, “Cysteine Oxidation Targets Peroxiredoxins 1 and 2 for Exosomal Release through a Novel Mechanism of Redox-Dependent Secretion.,” *Mol. Med.*, vol. 21, pp. 98–108, 2015.

[44] B. Knoops *et al.*, “Specific Interactions Measured by AFM on Living Cells between Peroxiredoxin-5 and TLR4 : Relevance for Mechanisms of Innate,” *Cell Chem. Biol.*, vol. 25, pp. 1–10, 2018.

[45] C. A. Neumann *et al.*, “Essential role for the peroxiredoxin Prdx1 in erythrocyte antioxidant defence and tumour suppression,” *Nature*, vol. 424, no. 6948, pp. 561–565, 2003.

[46] K.-K. Lee *et al.*, “Peroxiredoxin II is essential for sustaining life span of erythrocytes in mice,” *Blood*, vol. 101, no. 12, pp. 5033–5038, 2003.

[47] L. Li *et al.*, “Increased susceptibility of MER5 (peroxiredoxin III) knockout mice to LPS-induced oxidative stress,” *Biochem. Biophys.*

Res. Commun., vol. 355, pp. 715–721, 2007.

[48] X. Wang *et al.*, “Mice with Targeted Mutation of Peroxiredoxin 6 Develop Normally but Are Susceptible to Oxidative Stress,” *J. Biol. Chem.*, vol. 278, pp. 25179–25190, 2003.

[49] Y. Wang, S. I. Feinstein, Y. Manevich, Y.-S. Ho, and A. B. Fisher, “Peroxiredoxin 6 gene-targeted mice show increased lung injury with paraquat-induced oxidative stress,” *Antioxid. Redox Signal.*, vol. 8, no. 1&2, pp. 229–237, 2006.

[50] Y. Iuchi *et al.*, “Peroxiredoxin 4 knockout results in elevated spermatogenic cell death via oxidative stress,” *Biochem. J*, vol. 419, pp. 149–158, 2009.

[51] Y. Ji *et al.*, “Peroxiredoxin5 controls vertebrate ciliogenesis by modulating,” *Antioxid. Redox Signal.*, pp. 1–46, 2018.

[52] H. Qin, C. A. Wilson, S. J. Lee, X. Zhao, E. N. Benveniste, and L. Cd, “LPS induces CD40 gene expression through the activation of NF-κB and STAT-1α in macrophages and microglia,” *Blood*, vol. 106, no. 9, pp. 3114–3123, 2005.

[53] J. Uwayama *et al.*, “Tissue Prx I in the protection against Fe-NTA and the reduction of nitroxyl radicals,” *Biochem. Biophys. Res. Commun.*,

vol. 339, pp. 226–231, 2006.

[54] T. H. Kwon *et al.*, “Reactive oxygen species mediated DNA damage is essential for abnormal erythropoiesis in peroxiredoxin II -/- mice,” *Biochem. Biophys. Res. Commun.*, vol. 424, pp. 189–195, 2012.

[55] X. Guo *et al.*, “Overexpression of Peroxiredoxin 4 Attenuates Atherosclerosis in Apolipoprotein E Knockout Mice,” *Antioxid. Redox Signal.*, vol. 17, no. 10, pp. 1362–1375, 2012.

[56] S. U. Kim *et al.*, “Peroxiredoxin II preserves cognitive function against age-linked hippocampal oxidative damage,” *Neurobiol. Aging*, vol. 32, pp. 1054–1068, 2011.

[57] N. Zhang *et al.*, “Serum Amyloid A-Luciferase Transgenic Mice: Response to Sepsis, Acute Arthritis, and Contact Hypersensitivity and the Effects of Proteasome Inhibition,” *J. Immunol.*, vol. 174, pp. 8125–8134, 2018.

[58] T. H. Flo *et al.*, “Lipocalin 2 mediates an innate immune response to bacterial infection by sequestrating iron,” *Nature*, pp. 917–921, 2004.

[59] M. Jo, J. Kim, G. J. Song, M. Seo, X. E. M. Hwang, and X. K. Suk, “Astrocytic Orosomucoid-2 Modulates Microglial Activation and

Neuroinflammation," *J. Neurosci.*, vol. 37, no. 11, pp. 2878–2894, 2017.

[60] T. Hayashi, J. Huang, and S. S. Deeb, "RINX (VSX1), a Novel Homeobox Gene Expressed in the Inner Nuclear Layer of the Adult Retina," *Genomics*, vol. 67, pp. 128–139, 2000.

[61] A. Greenberg *et al.*, "VSX1 : A gene for posterior polymorphous dystrophy and keratoconus," *Hum. Mol. Genet.*, vol. 11, no. 9, pp. 1029–1036, 2002.

[62] M. Oka, K. Shimojima, T. Yamamoto, Y. Hanaoka, S. Sato, and T. Yasuhara, "A novel HYLS1 homozygous mutation in living siblings with Joubert syndrome," *Clin Genet*, no. 1, pp. 739–743, 2016.

[63] H. Jin *et al.*, "The dystrotelin , dystrophin and dystrobrevin superfamily : new paralogues and old isoforms," *BMC Genomics*, vol. 8, no. 19, pp. 1–20, 2007.

[64] J. Goemaere and B. Knoops, "Peroxiredoxin distribution in the mouse brain with emphasis on neuronal populations affected in neurodegenerative disorders," *J. Comp. Neurol.*, vol. 520, pp. 258–280, 2012.

[65] T. M. Penning, "The aldo-keto reductases (AKRs): Overview," *Chem.*

Biol. Interact., vol. 234, no. August 2014, pp. 236–246, 2015.

[66] H. Saito, S. Lund-katz, and M. C. Phillips, “Contributions of domain structure and lipid interaction to the functionality of exchangeable human apolipoproteins,” *Prog. Lipid Res.*, vol. 43, pp. 350–380, 2004.

[67] G. A. Di Lullo, S. M. Sweeney, J. Ko, L. Ala-kokko, and J. D. S. Antonio, “Mapping the Ligand-binding Sites and Disease-associated Mutations on the Most Abundant Protein in the Human, Type I Collagen,” *J. Biol. Chem.*, vol. 277, no. 6, pp. 4223–4231, 2002.

[68] D. W. Nebert, K. Wikvall, and W. L. Miller, “Human cytochromes P450 in health and disease,” *Phil Trans R Soc B*, vol. 368, pp. 1–21, 2013.

[69] C.-S. Yang *et al.*, “Roles of peroxiredoxin II in the regulation of proinfl ammatory responses to LPS and protection against endotoxin-induced lethal shock,” *J. Exp. Med.*, vol. 204, no. 3, pp. 583–594, 2007.

[70] C. Nathan and A. Cunningham-Bussel, “Beyond oxidative stress: an immunologist’s guide to reactive oxygen species,” *Nat Rev Immunol*, vol. 13, no. 5, pp. 349–361, 2013.

[71] M. W. Covert, T. H. Leung, J. E. Gaston, and D. Baltimore, “Achieving Stability of Lipopolysaccharide-Induced NF-kB Activation,” *Science (80-.).*, vol. 309, no. 5742, pp. 1854–1857, 2005.

[72] A.-G. L. Planson *et al.*, “Sulfiredoxin Protects Mice from Lipopolysaccharide-Induced Endotoxic Shock,” *Antioxid. Redox Signal.*, vol. 14, no. 11, pp. 2071–2082, 2011.

[73] R. K. Thimmulappa *et al.*, “Nrf2 is a critical regulator of the innate immune response and survival during experimental sepsis,” *J. Clin. Invest.*, vol. 116, no. 4, pp. 984–995, 2006.

[74] D. Weber, M. J. Davies, and T. Grune, “Determination of protein carbonyls in plasma, cell extracts, tissue homogenates, isolated proteins: Focus on sample preparation and derivatization conditions,” *Redox Biol.*, vol. 5, pp. 367–380, 2015.

[75] K. Grintzalis, D. Zisimopoulos, T. Grune, D. Weber, and C. D. Georgiou, “Method for the simultaneous determination of free/protein malondialdehyde and lipid/protein hydroperoxides,” *Free Radic. Biol. Med.*, vol. 59, pp. 27–35, 2013.

5.10 Supplementary data

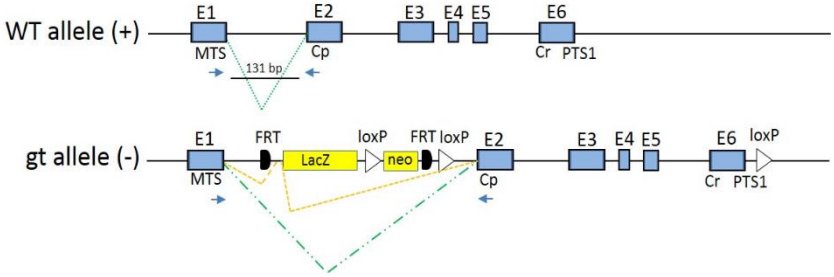

Suppl.Figure 1. Schematic representations of wild type (WT) Prdx5 and the gene-trap (gt) Prdx5 alleles with the three alternative splicing of the gt allele. *The gene-trap knockout construct (gt allele) consists of the lacZ gene as a reporter and the neomycin phosphotransferase gene. Exons (E) 1 to 6, FRT and LoxP recombination sites are depicted. The mRNA splicing sites are indicated in green and yellow.*

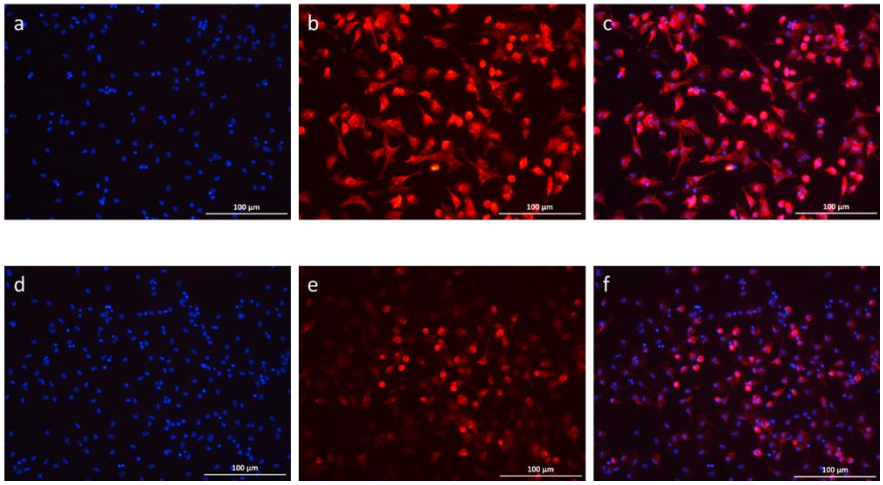

Suppl.Figure 2. Characterization of primary peritoneal cell culture. *The peritoneal cells were fixed with PFA 4% and incubated with CD11b and F4/80 antibodies, using immunofluorescence. (a) DAPI staining, (b) CD11b, (c) merge, (d) DAPI staining, (e) F4/80, (f) merge.*

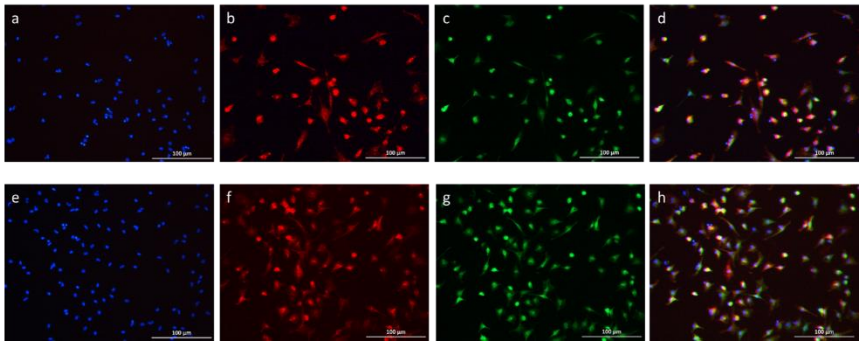

Suppl.Figure 3. Co-expression Prdx5 with CD11b and F4/80 in primary peritoneal cell culture. *Peritoneal cells co-express CD11b or F4/80 with Prdx5. (a) DAPI staining, (b) CD11b, (c) Prdx5, (d) merge, (e) DAPI staining, (f) F4/80, (g) Prdx5, (h) merge.*

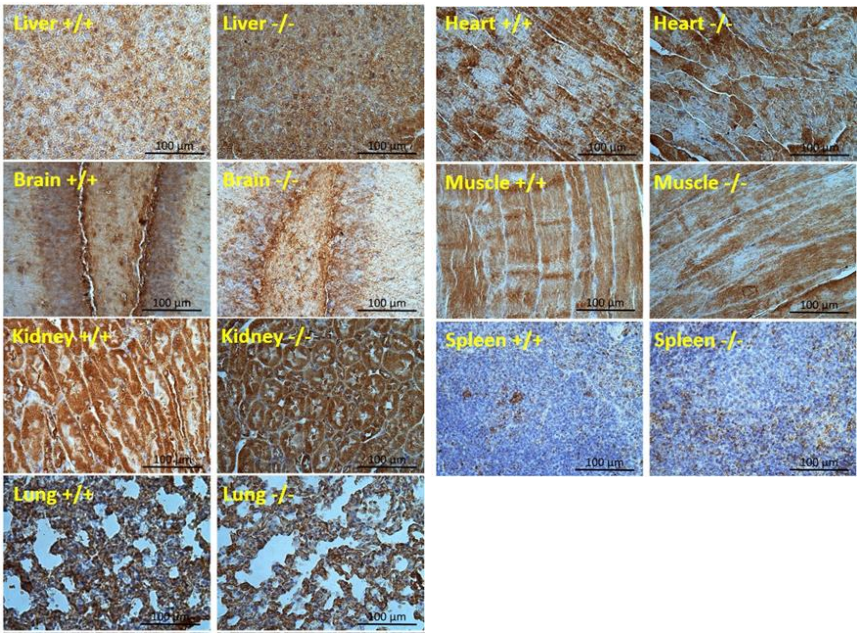

Suppl.Figure 4. Immunodetection of the 4-HNE protein in liver, brain, kidney, lung, heart, muscle, spleen slides of Prdx5$^{+/+}$ and Prdx5$^{-/-}$ mice. *We do not observe any difference between the 2 genotypes.*

Supplementary Table 9. Upregulated genes in *Prdx5*$^{-/-}$ liver. The most affected upregulated genes in liver are listed with the fold change expression, the p values and the Genbank Accesion number.

Upregulated genes in Prdx5 -/- liver				
GeneName	**GeneSymbol**	**Fold Change**	**p-value**	**GenbankAccession**
predicted gene 7969	Gm7969	30,26	0,05	XM_982175
uncharacterized LOC101056219	LOC101056219	20,37	0,00	XM_003945516
membrane metallo endopeptidase	Mme	9,96	0,03	NM_008604
CCR4 carbon catabolite repression 4-like (S. cerevisiae)	Ccrn4l	7,77	0,01	NM_009834
uncharacterized LOC101056207	LOC101056207	6,89	0,01	XM_003945515
cytochrome P450, family 4, subfamily a, polypeptide 32	Cyp4a32	4,92	0,03	NM_001100181
expressed sequence AI835086	AI835086	3,78	0,04	AK043585
homeodomain leucine zipper-encoding gene	Homez	3,57	0,00	NM_001177705
steroid 5 alpha-reductase 1	Srd5a1	3,40	0,05	AK082819
family with sequence similarity 166, member A	Fam166a	3,31	0,01	NM_026624
glutamate receptor interacting protein 1	Grip1	3,22	0,03	NM_028736
solute carrier family 35, member F3	Slc35f3	3,20	0,02	NM_175434
ATPase, Na+/K+ transporting, alpha 3 polypeptide	Atp1a3	3,12	0,02	NM_144921
very low density lipoprotein receptor	Vldlr	3,04	0,00	NM_013703
cytochrome c oxidase subunit VIb polypeptide 2	Cox6b2	3,02	0,04	NM_183405

Supplementary Table 2. **Downregulated genes in *Prdx5*$^{-/-}$ liver.** The most affected downregulated genes in liver are listed with the fold change expression, the p values and the Genbank Accesion number.

Downregulated genes in Prdx5 -/- liver				
GeneName	**GeneSymbol**	**Fold Change**	**p-value**	**GenbankAccession**
peroxiredoxin 5	Prdx5	-72,81	0,03	AK009858
peroxiredoxin 5	Prdx5	-69,10	0,02	NM_012021
serum amyloid A 2	Saa2	-35,01	0,02	NM_011314
serum amyloid A 1	Saa1	-26,14	0,01	NM_009117
sulfotransferase family 1E, member 1	Sult1e1	-9,54	0,01	NM_023135
lipocalin 2	Lcn2	-7,37	0,03	NM_008491
myosin, light polypeptide 1	Myl1	-7,25	0,05	NM_021285
S100 calcium binding protein A9 (calgranulin B)	S100a9	-4,51	0,00	NM_001281852
proteinase 3	Prtn3	-3,87	0,03	NM_011178
orosomucoid 2	Orm2	-3,61	0,04	NM_011016
selenophosphate synthetase 1	Sephs1	-3,49	0,05	NM_175400
5-hydroxytryptamine (serotonin) receptor 6	Htr6	-3,47	0,05	AK134977
midline 1	Mid1	-3,32	0,04	NM_183151
6-phosphofructo-2-kinase/fructose-2,6-biphosphatase 4	Pfkfb4	-3,31	0,01	NM_173019
zinc finger protein 236	Zfp236	-3,10	0,05	NM_177832

Supplementary Table 3. Upregulated genes in *Prdx5*$^{-/-}$ brain. The most affected upregulated genes in brain are listed with the fold change expression, the p values and the Genbank Accesion number. (Continue in the next page)

Upregulated genes in Prdx5 -/- brain				
GeneName	GeneSymbol	Fold Change	p-value	GenbankAccession
sulfotransferase family 3A, member 1	Sult3a1	35,63	0,02	NM_020565
alpha-1-B glycoprotein	A1bg	29,23	0,00	NM_001081067
fatty acid binding protein 1, liver	Fabp1	23,69	0,03	NM_017399
pro-melanin-concentrating hormone	Pmch	22,74	0,02	NM_029971
ATP-binding cassette, sub-family B (MDR/TAP), member 11	Abcb11	12,55	0,05	NM_021022
cytochrome P450, family 2, subfamily c, polypeptide 39	Cyp2c39	12,39	0,00	NM_010003
apolipoprotein A-II	Apoa2	11,79	0,02	NM_013474
oxytocin	Oxt	11,46	0,05	NM_011025
dimethylglycine dehydrogenase precursor	Dmgdh	11,20	0,01	NM_028772
cytochrome P450, family 2, subfamily c, polypeptide 54	Cyp2c54	11,19	0,00	NM_206537
cytochrome P450, family 2. subfamily c, polypeptide 37	Cyp2c37	11,06	0,02	NM_010001
UDP glucuronosyltransferase 2 family, polypeptide B36	Ugt2b36	10,96	0,00	NM_001029867
cytochrome P450, family 2, subfamily f, polypeptide 2	Cyp2f2	10,68	0,01	NM_007817
cerebellin 3 precursor protein	Cbln3	10,56	0,00	NM_019820
group specific component	Gc	9,70	0,03	NM_008096
apolipoprotein C-III	Apoc3	9,70	0,01	NM_023114
complement component 1, r subcomponent A	C1ra	9,59	0,01	NM_023143
cytochrome P450, family 2, subfamily c, polypeptide 54	Cyp2c54	9,44	0,02	NM_206537
UDP glucuronosyltransferase 1 family, polypeptide A6B	Ugt1a6b	9,32	0,04	NM_201410
major urinary protein 3	Mup3	9,04	0,05	NM_001039544
albumin	Alb	9,02	0,00	NM_009654
cytochrome P450, family 2, subfamily c, polypeptide 67	Cyp2c67	8,93	0,02	NM_001024719
apolipoprotein C-I	Apoc1	8,85	0,01	NM_007469
cytochrome P450, family 2, subfamily c, polypeptide 29	Cyp2c29	8,61	0,01	NM_007815
paraoxonase 1	Pon1	8,55	0,03	NM_011134
fructose bisphosphatase 1	Fbp1	8,54	0,04	NM_019395
serine (or cysteine) peptidase inhibitor, clade A, member 1D	Serpina1d	8,50	0,01	NM_009246
cytochrome P450 3A41-like	LOC101056526	8,28	0,03	XM_003946408
major urinary protein 17	Mup17	8,18	0,05	NM_001200006
novel member of the major urinary protein (Mup) gene family	LOC100048884	8,16	0,03	NM_001199333
glutathione S-transferase, alpha 3	Gsta3	7,83	0,01	NM_001077353
alpha-2-HS-glycoprotein	Ahsg	7,81	0,02	NM_013465
serine (or cysteine) peptidase inhibitor, clade A, member 1A	Serpina1a	7,71	0,03	NM_001252569
cytochrome P450, family 8, subfamily b, polypeptide 1	Cyp8b1	7,58	0,02	NM_010012
apolipoprotein H	Apoh	7,58	0,01	NM_013475
serine (or cysteine) peptidase inhibitor, clade A, member 1C	Serpina1c	7,47	0,03	NM_009245
major urinary protein 2	Mup2	7,46	0,02	NM_001045550
serine (or cysteine) peptidase inhibitor, clade A, member 3K	Serpina3k	7,39	0,05	NM_011458
UDP glycosyltransferases 3 family, polypeptide A2	Ugt3a2	7,32	0,05	NM_144845
coagulation factor II	F2	7,32	0,02	NM_010168
aldo-keto reductase family 1, member C12	Akr1c12	7,31	0,01	NM_013777

Supplementary Table 3. Upregulated genes in *Prdx5*$^{-/-}$ brain. The most affected upregulated genes in brain are listed with the fold change expression, the p values and the Genbank Accesion number. (Continue in the next page)

serine (or cysteine) peptidase inhibitor, clade A, member 1A	Serpina1a	7,24	0,04	NM_001252569
fibrinogen gamma chain	Fgg	7,14	0,02	NM_133862
serine (or cysteine) peptidase inhibitor, clade F, member 2	Serpinf2	7,04	0,02	NM_008878
aldolase B, fructose-bisphosphate	Aldob	7,00	0,02	NM_144903
uncharacterized protein C130078N14	C130078N14	6,98	0,00	AK081811
apolipoprotein B	Apob	6,67	0,00	NM_009693
cerebellin 1 precursor protein	Cbln1	6,61	0,02	NM_019626
arginase, liver	Arg1	6,60	0,00	NM_007482
cytochrome P450, family 2, subfamily c, polypeptide 68	Cyp2c68	6,55	0,02	NM_001039555
histocompatibility 2, Q region locus 10	H2-Q10	6,46	0,04	NM_010391
major urinary protein 20	Mup20	6,33	0,05	NM_001012323
major urinary protein 19	Mup19	6,31	0,01	NM_001135127
carboxylesterase 1C	Ces1c	6,27	0,00	NM_007954
kininogen 1	Kng1	6,25	0,01	NM_023125
solute carrier family 27 (fatty acid transporter), member 5	Slc27a5	6,24	0,03	NM_009512
serine (or cysteine) peptidase inhibitor, clade A, member 1D	Serpina1d	6,21	0,02	NM_009246
RIKEN cDNA 1100001G20 gene	1100001G20Rik	6,15	0,01	NM_183249
sulfotransferase family 2A, dehydroepiandrosterone (DHEA)-preferring, member 2	Sult2a2	6,14	0,03	NM_009286
major urinary protein 5	Mup5	6,04	0,05	NM_008649
kininogen 2	Kng2	5,90	0,04	NM_201375
solute carrier family 25, member 47	Slc25a47	5,87	0,01	NM_001012310
fibrinogen alpha chain	Fga	5,86	0,05	NM_010196
alcohol dehydrogenase 1 (class I)	Adh1	5,72	0,00	NM_007409
serine (or cysteine) peptidase inhibitor, clade A, member 1E	Serpina1e	5,70	0,02	NM_009247
alpha-2-glycoprotein 1, zinc	Azgp1	5,64	0,05	NM_013478
insulin-like growth factor binding protein 1	Igfbp1	5,58	0,01	NM_008341
4-hydroxyphenylpyruvic acid dioxygenase	Hpd	5,57	0,01	NM_008277
complement component 9	C9	5,54	0,00	NM_013485
cytochrome P450, family 2, subfamily a, polypeptide 4	Cyp2a4	5,50	0,05	NM_009997
microsomal glutathione S-transferase 1	Mgst1	5,50	0,03	NM_019946
cytochrome P450, family 2, subfamily a, polypeptide 4	Cyp2a4	5,37	0,03	NM_009997
cytochrome P450, family 2, subfamily c, polypeptide 50	Cyp2c50	5,23	0,05	NM_134144
urate oxidase	Uox	5,21	0,02	NM_009474
hypocretin	Hcrt	5,15	0,01	NM_010410
tumor suppressor candidate 5	Tusc5	5,07	0,04	NM_177709
serine (or cysteine) peptidase inhibitor, clade C (antithrombin), member 1	Serpinc1	4,89	0,03	NM_080844
BarH-like 2 (Drosophila)	Barhl2	4,82	0,02	NM_001005477
paired-like homeodomain transcription factor 2	Pitx2	4,81	0,01	NM_001042502
vomeronasal 1 receptor 81	Vmn1r81	4,80	0,00	NM_134210
serine (or cysteine) peptidase inhibitor, clade A, member 6	Serpina6	4,79	0,02	NM_007618
major urinary protein 4	Mup4	4,74	0,01	NM_008648
zinc finger homeobox 2, opposite strand	Zfhx2os	4,73	0,02	NR_004444

Supplementary Table 3. Upregulated genes in *Prdx5*$^{-/-}$ brain. The most affected upregulated genes in brain are listed with the fold change expression, the p values and the Genbank Accesion number.

Upregulated genes in Prdx5 -/- brain				
GeneName	**GeneSymbol**	**Fold Change**	**p-value**	**GenbankAccession**
aldo-keto reductase family 1, member C20	Akr1c20	4,66	0,00	BC021607
BPI fold containing family A, member 1	Bpifa1	4,62	0,04	NM_011126
C-reactive protein, pentraxin-related	Crp	4,62	0,05	NM_007768
apolipoprotein B	Apob	4,58	0,00	NM_009693
UDP glucuronosyltransferase 2 family, polypeptide B5	Ugt2b5	4,54	0,04	NM_009467
3-hydroxy-3-methylglutaryl-Coenzyme A synthase 2	Hmgcs2	4,45	0,04	NM_008256
asialoglycoprotein receptor 1	Asgr1	4,44	0,05	NM_009714
lactamase, beta	Lactb	4,38	0,01	NM_030717
predicted gene 4794	Gm4794	4,38	0,00	NM_001101452
uncharacterized protein 9630017O17	9630017O17	4,37	0,05	AK035916
alpha 1 microglobulin/bikunin	Ambp	4,36	0,01	NM_007443
predicted gene 8541	Gm8541	4,36	0,05	AK136239
BAI1-associated protein 2-like 1	Baiap2l1	4,35	0,01	NM_025833
NIPA-like domain containing 1	Nipal1	4,32	0,02	NM_001081205
sulfotransferase family 2A, dehydroepiandrosterone (DHEA)-preferring, member 6	Sult2a6	4,32	0,05	NM_001081325
inter alpha-trypsin inhibitor, heavy chain 4	Itih4	4,31	0,02	NM_018746
carbonic anhydrase 3	Car3	4,25	0,02	NM_007606
macrophage stimulating 1 (hepatocyte growth factor-like)	Mst1	4,13	0,03	NM_008243
prune homolog 2 (Drosophila)	Prune2	4,07	0,05	NM_181348
delta-like 1 homolog (Drosophila)	Dlk1	4,05	0,05	NM_010052
carboxypeptidase N, polypeptide 1	Cpn1	4,02	0,03	NM_030703
prokineticin 2	Prok2	4,01	0,03	NM_015768
vomeronasal 1 receptor 121	Vmn1r121	4,01	0,05	NM_001166741
carboxylesterase 2A	Ces2a	4,00	0,03	NM_133960
solute carrier family 22, member 28	Slc22a28	3,97	0,01	NM_001013820
serine (or cysteine) peptidase inhibitor, clade D, member 1	Serpind1	3,96	0,03	NM_008223
armadillo repeat containing 3	Armc3	3,91	0,01	NM_001081083

Supplementary Table 3. Upregulated genes in *Prdx5*$^{-/-}$ brain. The most affected upregulated genes in brain are listed with the fold change expression, the p values and the Genbank Accesion number.

cytochrome P450, family 4, subfamily a, polypeptide 10	Cyp4a10	3,83	0,02	NM_010011
cytochrome P450, family 2, subfamily a, polypeptide 12	Cyp2a12	3,79	0,01	NM_133657
aldo-keto reductase family 1, member C6	Akr1c6	3,75	0,02	NM_030611
NADPH oxidase 3	Nox3	3,72	0,03	NM_198958
glutathione S-transferase, alpha 3	Gsta3	3,72	0,00	NM_001077353
regucalcin	Rgn	3,70	0,03	NM_009060
RIKEN cDNA 1300017J02 gene	1300017J02Rik	3,69	0,03	NM_027918
RIKEN cDNA C130046B21 gene	C130046B21Rik	3,67	0,00	XR_168388
RIKEN cDNA A930002I21 gene	A930002I21Rik	3,66	0,00	XR_104815
predicted gene 3942	Gm3942	3,66	0,00	AK036450
insulin-like growth factor 1	Igf1	3,65	0,00	NM_010512
cytochrome P450, family 1, subfamily a, polypeptide 2	Cyp1a2	3,63	0,02	NM_009993
keratin 8	Krt8	3,63	0,01	AK166854
inter alpha-trypsin inhibitor, heavy chain 4	Itih4	3,58	0,00	NM_018746
bile acid-Coenzyme A: amino acid N-acyltransferase	Baat	3,57	0,02	NM_007519
growth hormone	Gh	3,56	0,04	NM_008117
fibrinogen-like protein 1	Fgl1	3,51	0,05	NM_145594
RIKEN cDNA 5730471H19 gene	5730471H19Rik	3,47	0,01	AK133873
cytochrome P450, family 3, subfamily a, polypeptide 44	Cyp3a44	3,44	0,03	NM_177380
carboxylesterase 3A	Ces3a	3,42	0,01	NM_198672
afamin	Afm	3,40	0,00	NM_145146
retinol binding protein 4, plasma	Rbp4	3,39	0,01	NM_001159487
complement component 4 binding protein	C4bp	3,32	0,04	NM_007576
Sumo1 pseudogene	4933411G06Rik	3,29	0,00	NR_045158
ADP-ribosyltransferase 4	Art4	3,23	0,04	NM_026639
delta-like 1 homolog (Drosophila)	Dlk1	3,21	0,03	NM_010052
MAS-related GPR, member X1	Mrgprx1	3,19	0,00	NM_207540
group specific component	Gc	3,15	0,01	NM_008096
ureidopropionase, beta	Upb1	3,09	0,02	NM_133995
collagen, type XVIII, alpha 1	Col18a1	3,07	0,04	NM_001109991
tocopherol (alpha) transfer protein	Ttpa	3,06	0,05	NM_015767
calbindin 2	Calb2	3,04	0,00	NM_007586

Supplementary Table 4. Downregulated genes in *Prdx5*$^{-/-}$ brain. The most affected downregulated genes in brain are listed with the fold change expression, the p values and the Genbank Accesion number.

Downregulated genes in Prdx5 -/- brain				
GeneName	**GeneSymbol**	**Fold Change**	**p-value**	**GenbankAccession**
peroxiredoxin 5	Prdx5	-23,34	0,04	NM_012021
RIKEN cDNA C030010L15 gene	C030010L15Rik	-15,26	0,01	AK021061
predicted gene 3893	Gm3893	-9,15	0,04	NR_033506
glutamate decarboxylase-like 1	Gadl1	-8,45	0,05	NM_028638
RIKEN cDNA 9030404E10 gene	9030404E10Rik	-6,52	0,00	NR_045878
RIKEN cDNA 2410024N13 gene	2410024N13Rik	-6,48	0,00	AK010586
visual system homeobox 1 homolog (zebrafish)	Vsx1	-5,19	0,01	NM_054068
hydrolethalus syndrome 1	Hyls1	-4,73	0,03	NM_029762
dystrotelin	Dytn	-4,59	0,02	NM_001081658
ribosomal protein L18A	Rpl18a	-4,16	0,00	NM_029751
vomeronasal 1 receptor 151	Vmn1r151	-3,93	0,02	NM_001166712
demilune cell and parotid protein 3	Dcpp3	-3,59	0,02	NM_001077633
RIKEN cDNA A330069K06 gene	A330069K06Rik	-3,59	0,02	AK039597
synovial sarcoma, X member A, breakpoint 1	Ssxa1	-3,58	0,01	XM_001481340
glial fibrillary acidic protein	Gfap	-3,44	0,04	NM_001131020
glycerol kinase 5 (putative)	Gk5	-3,40	0,03	NM_177352
predicted gene 4718	Gm4718	-3,29	0,04	XM_003945577
interferon alpha 2	Ifna2	-3,18	0,01	NM_010503
expressed sequence AU015791	AU015791	-3,13	0,03	NR_102381
WAP, follistatin/kazal, immunoglobulin, kunitz and netrin domain containing 2	Wfikkn2	-3,00	0,00	NM_181819
integrin alpha 11	Itga11	-3,00	0,00	NM_176922

Supplementary Table 5. Upregulated proteins in *Prdx5*$^{+/+}$ primary macrophages stressed by LPS compared to PBS. The most affected upregulated proteins in macrophages are listed with the fold change expression, the p values, the Accession number, the peptide counts, the unique peptides and the confidence scores.

Upregulated proteins in Prdx5+/+ cells exposed to LPS compare to Prdx5+/+ without LPS							
Description	Short name	Accession	Max fold change	Anova (p)	Peptide count	Unique peptides	Confidence score
Ybox transcription factor (Fragment)	Ybx1	Q71V06	4,37	0,02	10	2	64,38
CCR4-NOT transcription complex subunit 10	Cnot10	Q8BH15	3,05	0,00	3	2	15,89
Tumor necrosis factor receptor superfamily member 5	Cd40	P27512	3,01	0,00	6	2	33,36
Microtubule-associated protein 4	Map4	P27546	2,53	0,05	14	3	83,04
Small nuclear ribonucleoprotein-associated protein N	Snrpn	P63163	2,50	0,00	12	2	58,25
Uridine phosphorylase 1	Upp1	P52624	2,04	0,02	9	4	75,18
Adenylosuccinate lyase	Adsl	P54822	2,01	0,03	13	3	81,30
Uncharacterized protein	Rubcnl	Q3U2M6	1,99	0,05	5	3	29,95
leucine-rich repeat-containing protein 36	Gm45861	A0A1B0GRY3	1,97	0,05	17	2	95,22
Prostaglandin G/H synthase 2	Ptgs2	Q05769	1,86	0,01	24	10	179,02
Leucine-rich repeat-containing protein 36	Lrrc36	F8WIB5	1,86	0,02	8	1	48,00
MICAL-like protein 2	Mical2	Q3TN34	1,83	0,01	3	2	20,79
Neuroligin 4-like	Nlgn4l	B0F2B4	1,76	0,05	4	2	20,85
Transforming growth factor beta-1	Tgfb1	P04202	1,73	0,01	5	4	27,58
Bcl-2 homologous antagonist/killer	Bak1	Q08734	1,72	0,02	6	2	46,60
Septin-11 OS=Mus musculus GN=Sept11 PE=1 SV=4	sept11	Q8C1B7	1,61	0,01	11	2	56,17
Eukaryotic initiation factor 4A-II	Eif4a2	P10630	1,55	0,02	33	2	215,37
THUMP domain-containing protein 1	Thumpd1	Q9D136	1,54	0,04	7	4	36,10
Uncharacterized protein	Gtf3c1	Q3UHL0	1,51	0,04	8	3	28,59
26S proteasome non-ATPase regulatory subunit 1	Psmd1	Q3TXS7	1,47	0,05	36	11	244,77
H(+)/Cl(-) exchange transporter 7	Clcn7	O70496	1,47	0,02	4	2	33,46
Cis-aconitate decarboxylase	Acod1	P54987	1,44	0,02	33	15	223,37
Irgm1	OTTMUSPWKG00059374	A0A1G5SUJ3	1,42	0,04	4	3	18,91
Peroxiredoxin-5, mitochondrial	Prdx5	P99029	1,41	0,52	16	3	125,32
Vesicular integral-membrane protein VIP36	Lman2	Q9DBH5	1,33	0,04	22	12	143,47
SWI/SNF-related matrix-associated actin-dependent regulator of chromatin subfamily D member 2	Smarcd2	C9J9R8	1,32	0,02	7	2	42,31
MCG126220	Ywhaq	A3KML3	1,30	0,11	44	5	225,95
Adenylosuccinate synthetase isozyme 2	Adss	P46664	1,24	0,01	11	9	88,69
Uncharacterized protein	Pspc1	Q3TEB0	1,24	0,05	10	2	64,13
Peroxisomal multifunctional enzyme type 2	Hsd17b4	P51660	1,21	0,01	5	3	24,98
GATOR complex protein DEPDC5	Depdc5	P61460	1,20	0,01	12	3	72,52
Glycerol-3-phosphate dehydrogenase, mitochondrial	Gpd2	Q64521	1,14	0,02	31	13	212,02

Supplementary Table 6. Downregulated proteins in *Prdx5*$^{+/+}$ primary macrophages stressed by LPS compared to PBS. The most affected upregulated proteins in macrophages are listed with the fold change expression, the p values, the Accession number, the peptide counts, the unique peptides and the confidence scores.

Downregulated proteins in Prdx5+/+ cells exposed to LPS compare to Prdx5+/+ without LPS							
Description	Short name	Accession	Max fold change	Anova (p)	Peptide count	Unique peptides	Confidence score
Signal recognition partide 54 kDa protein	Srp54b	P14576	2,89	0,02	7	2	39,17
Lysozyme	Lyz2	P08905	2,57	0,01	16	6	113,05
UDP-glucose:glycoprotein glucosyltransferase 1	Uggt1	Q6P5E4	2,13	0,04	68	27	509,15
Hydroxymethylglutaryl-CoA lyase, mitochondrial	Hmgcl	P38060	1,99	0,03	6	2	33,95
Neutrophil cytosol factor 2	Ncf2	O70145	1,66	0,03	17	4	116,42
Uncharacterized protein	Cyld	Q3V028	1,63	0,03	11	4	64,23
Uncharacterized protein	Pak7	Q8BVB0	1,62	0,02	8	2	42,43
Zinc finger protein 395	Zfp395	E9Q5N9	1,59	0,01	6	2	21,72
Collagen alpha-1(XXIV) chain	Col24a1	Q30D77	1,58	0,02	18	3	89,57
Bifunctional polynucleotide phosphatase/kinase	Pnkp	G5E8N7	1,56	0,04	11	2	68,29
YLP motif-containing protein 1	Ylpm1	D3YWX2	1,56	0,05	4	2	19,88
Citron Rho-interacting kinase	Cit	P49025	1,54	0,00	15	5	82,14
Plakophilin-4	Pkp4	A2AS45	1,53	0,04	4	2	25,29
DNA topoisomerase 2-beta	Top2b	Q64511	1,50	0,04	38	6	208,64
Protein SEC13 homolog	Sec13	Q9D1M0	1,46	0,02	9	3	57,40
Elongation factor Tu, mitochondrial	Tufm	Q8BFR5	1,46	0,04	25	10	179,64
Aminopeptidase RNPEPL1	Rnpepl1	G5E872	1,46	0,02	6	2	27,12
Rho GTPase-activating protein 17	Arhgap17	E9QAJ9	1,44	0,02	13	3	72,56
Rho guanine nucleotide exchange factor 6	Arhgef6	F6WMJ3	1,41	0,03	9	4	46,99
Uncharacterized protein (Fragment)	Parp8	Q3U1V1	1,40	0,05	3	2	21,16
Uncharacterized protein OS=Mus musculus PE=2 SV=1		Q3U3I6	1,37	0,02	17	5	104,56
Sorting nexin-27	Snx27	Q3UHD6	1,35	0,02	10	6	69,64
NADH dehydrogenase [ubiquinone] iron-sulfur protein 2, mitochondrial	Ndufs2	Q91WD5	1,34	0,01	10	3	69,18
AP-1 complex subunit sigma-3	Ap1s3	Q7TN05	1,32	0,01	3	2	9,01
BTB/POZ domain-containing protein 3	Btbd3	P58545	1,31	0,01	2	2	14,04
Dynein light chain roadblock	Dynlrb1	P62627	1,30	0,00	4	2	30,38
Echinoderm microtubule-associated protein-like 6	Eml6	Q5SQM0	1,30	0,04	28	7	165,78
Retinoid-inducible serine carboxypeptidase	Scpep1	Q920A5	1,29	0,04	15	7	107,74
Uncharacterized protein	Cpsf3	Q3TC91	1,23	0,04	5	4	19,84
Katanin p60 ATPase-containing subunit A-like 2	Katnal2	A0A0E4D014	1,21	0,03	6	2	30,26
Ras GTPase-activating protein 4	Rasa4	Q6PFQ7	1,21	0,00	5	2	37,57
Hepatoma-derived growth factor (Fragment)	Hdgf	P51859	1,19	0,03	4	2	31,82

Supplementary Table 7. Upregulated proteins in *Prdx5*$^{-/-}$ primary macrophages stressed by LPS compared to PBS. The most affected upregulated proteins in macrophages are listed with the fold change expression, the p values, the Accession number, the peptide counts, the unique peptides and the confidence scores. (Continue in the next

Upregulated proteins in Prdx5 -/- cells exposed to LPS compare to Prdx5 -/- without LPS							
Description	Short name	Accession	Max fold change	Anova (p)	Peptide count	Unique peptides	Confidence score
Mitochondrial import inner membrane translocase subunit Tim13	Timm13	P62075	29,75	0,00	7	2	49,06
CCR4-NOT transcription complex subunit 10	Cnot10	Q8BH15	28,76	0,00	3	2	15,89
Uncharacterized protein	Q3THB4	Q3THB4	17,03	0,05	3	2	19,90
Rho GTPase-activating protein 5	Arhgap5	P97393	9,89	0,01	6	2	32,18
E3 ubiquitin-protein ligase Rnf220	Rnf220	Q6PDN6	9,17	0,02	2	2	8,83
Heterogeneous nuclear ribonucleoprotein H2	Hnrnph2	P70333	6,89	0,01	6	2	28,70
Methionine aminopeptidase 2	Metap2	O08663	5,99	0,00	8	4	45,51
ADP-ribosylation factor-like protein 1	Arl1	P61211	5,67	0,02	7	2	57,64
Nitric oxide synthase, inducible	Nos2	P29477	5,55	0,03	12	4	87,39
ESF1 nucleolar pre-rRNA processing protein, homolog (S. cerevisiae)	Esf1	A2APY6	5,34	0,03	2	2	9,99
Protein phosphatase 1G	Ppm1g	Q61074	5,14	0,00	5	2	30,97
4F2 cell-surface antigen heavy chain	Slc3a2	P10852	4,65	0,03	21	2	178,32
Dual-specificity protein phosphatase 3	Dusp3	B1AQF4	4,59	0,00	5	2	33,64
Kinesin family member 23B	Kif23b	E9Q4K7	4,31	0,01	16	2	91,64
Tyrosine-protein kinase JAK1	Jak1	P52332	4,17	0,00	30	2	170,00
Lysophospholipid acyltransferase 7	Mboat7	Q8C4K3	4,16	0,00	7	2	58,33
Receptor-type tyrosine-protein phosphatase S	Ptprs	B0V2N1	4,11	0,02	27	10	150,96
Cohesin subunit SA-1	Stag1	Q9D3E6	3,88	0,00	5	2	24,06
AKNA domain-containing 1	Aknad1	E9Q8N6	3,67	0,00	5	2	31,11
Cytochrome c oxidase assembly factor 7	Coa7	Q921H9	3,57	0,01	7	2	40,60
H2-T23 protein	H2-T23	Q31153	3,44	0,00	14	2	90,22
Neuroligin 4-like	Nlgn4l	B0F2B4	3,33	0,01	4	2	20,85
WASH complex subunit 2	Washc2	Q6PGL7	3,28	0,00	12	2	68,54
Centrosomal protein of 170 kDa	Cep170	Q6A065	3,23	0,01	13	5	68,75
Histone-lysine N-methyltransferase EHMT2	Ehmt2	A2CG76	3,22	0,01	3	2	13,51
Aasdhppt protein	Aasdhppt	Q05C25	3,19	0,00	4	2	19,64
Uncharacterized protein	Rubcnl	Q3U2M6	3,13	0,00	5	3	29,95
Acyl-protein thioesterase 2	Lypla2	Q9WTL7	3,12	0,00	18	9	150,42
Utrophin	Utrn	A0A1W2P7C0	2,85	0,00	2	2	15,11

Supplementary Table 7. Upregulated proteins in *Prdx5*$^{-/-}$ primary macrophages stressed by LPS compared to PBS. The most affected upregulated proteins in macrophages are listed with the fold change expression, the p values, the Accession number, the peptide counts, the unique peptides and the confidence scores. (Continue in the next page)

Moesin	Msn	P26041	2,84	0,02	48	19	330,52
MICAL-like protein 2	Mical2	Q3TN34	2,83	0,03	3	2	20,79
Capping protein (Actin filament), gelsolin-like	Capg	Q99LB4	2,77	0,05	30	15	180,62
ATP synthase subunit d, mitochondrial	Gm10250	G3X9U6	2,76	0,00	7	5	67,69
Tumor necrosis factor receptor superfamily member 5	Cd40	P27512	2,75	0,01	6	2	33,36
Tyrosine-protein kinase CSK	Csk	P41240	2,73	0,00	21	2	150,63
Major histocompatibility complex, class Ib M10.2	H2-M10.1	Q8BGW7	2,72	0,00	6	2	36,54
Tubulin beta-6 chain	Tubb6	Q922F4	2,68	0,03	45	7	251,02
Probable ATP-dependent RNA helicase DDX46	Ddx46	Q569Z6	2,68	0,02	6	3	30,12
BTB (POZ) domain containing 8	A830010M20Rik	A0A1D5RL96	2,66	0,01	27	7	132,48
ATP-dependent 6-phosphofructokinase, muscle type	Pfkm	P47857	2,57	0,02	27	5	147,82
60S acidic ribosomal protein P2	Rplp2	P99027	2,53	0,01	15	5	112,74
Septin-11	Sept11	Q8C1B7	2,49	0,00	11	2	56,17
Translocation protein SEC63 homolog	Sec63	Q8VHE0	2,42	0,01	7	2	42,43
Exosome complex exonuclease RRP44	Dis3	Q9CSH3	2,41	0,04	20	3	120,68
Netrin-G2	Ntng2	Q8R4F1	2,36	0,00	6	3	29,14
Coatomer subunit zeta-1	Copz1	P61924	2,35	0,03	5	4	30,93
Transforming growth factor beta-1	Tgfb1	P04202	2,35	0,00	5	4	27,58
Beta-parvin	Bcarn	Q9JI08	2,32	0,01	4	3	20,92
Glucose-6-phosphate isomerase	Gpi	P06745	2,30	0,00	27	5	206,65
Nephronectin	Npnt	D3Y7X1	2,27	0,00	5	4	26,62
Prostaglandin G/H synthase 2	Ptgs2	Q05769	2,27	0,00	24	10	179,02
Catechol O-methyltransferase	Comt	Q3BS87	2,24	0,02	10	6	89,51
Complement component C8 beta chain	C8b	Q3BH95	2,14	0,00	6	2	28,13
Coiled-coil domain-containing protein 154	Ccdc154	Q6RUT8	2,12	0,05	3	2	15,39
Cationic amino acid transporter 2	Slc7a2	P18581	2,08	0,00	21	7	181,31
Phospholipase A2	Pla2g1b	Q3ZCY2	2,06	0,01	2	2	10,26
60S ribosomal protein L27a	Rpl27a	P14115	2,04	0,04	6	2	43,09
Regulator of G-protein signaling 4	Rgs4	O08899	2,03	0,03	2	2	9,75
Sialidase-1	Neu1	Q3S657	2,02	0,05	3	2	13,92
RuvB-like helicase	Ruvbl2	Q3TXT7	2,01	0,04	6	2	44,05

Supplementary Table 7. Upregulated proteins in *Prdx5*$^{-/-}$ primary macrophages stressed by LPS compared to PBS. The most affected upregulated proteins in macrophages are listed with the fold change expression, the p values, the Accession number, the peptide counts, the unique peptides and the confidence scores. (Continue in the next page)

Upregulated proteins in *Prdx5*-/- cells exposed to LPS compare to *Prdx5*-/- without LPS							
Description	Short name	Accession	Max fold change	Anova (p)	Peptide count	Unique peptides	Confidence score
Fatty acid-binding protein, adipocyte	Fabp4	P04117	2,00	0,01	14	4	96,92
Prostasyclin synthase	Ptgis	O35074	1,99	0,02	30	11	174,70
Eukaryotic translation elongation factor 1 gamma	Eef1g	Q4FZK2	1,98	0,01	31	15	161,26
V-type proton ATPase catalytic subunit A	Atp6v1a	P50516	1,97	0,00	45	17	327,45
Ubiquinol-cytochrome-c reductase complex assembly factor 2	Uqcc2	D3Z4D6	1,96	0,04	2	2	10,58
Uncharacterized protein (Fragment)		Q3BT78	1,95	0,01	4	2	25,14
RIKEN cDNA 1810049P08, isoform CRA_c	Rab43	Q0PD10	1,94	0,02	13	4	83,99
Uncharacterized protein	Zyx	Q3TCR9	1,90	0,03	4	2	24,12
A kinase (PRKA) anchor protein 8	Akap8	Q3SU08	1,90	0,00	6	3	34,83
Plexin-D1	Plxnd1	Q3UH93	1,86	0,00	24	3	130,58
Uncharacterized protein	Surf4	Q3U7E6	1,83	0,00	9	4	54,24
Wbp7 protein (Fragment)	Kmt2b	Q8PHU4	1,82	0,05	7	2	44,01
Receptor-type tyrosine-protein phosphatase F	Ptprf	A2A8L5	1,80	0,03	13	4	78,36
cDNA FLI42424 fis, clone BLADE2004088, moderately similar to Mus musculus PDZ domain actin binding protein Shroom mRNA (Fragment) SV=1		Q6ZVL3	1,79	0,01	2	2	9,51
Actin-related protein 2/3 complex subunit 3	Arpc3	Q9JM76	1,77	0,01	12	4	82,62
Nucleophosmin	Npm1	Q5SQB0	1,74	0,00	18	10	155,05
MHC class III H2-Sip (haplotype a) sex-limited protein mRNA (Fragment)		V5KDD9	1,74	0,00	7	5	41,75
AMP deaminase 3	Ampd3	O08739	1,72	0,01	27	6	168,85
Nucleoporin 205	Nup205	A0A0J9YUD5	1,70	0,05	16	2	112,80
Ubiquitin carboxyl-terminal hydrolase 43	Usp43	A6PWR8	1,70	0,01	9	2	48,33
Glyceraldehyde-3-phosphate dehydrogenase	Gapdh	P16858	1,65	0,04	64	14	280,34
Katanin p60 ATPase-containing subunit A-like 1	Katnal1	Q8K0T4	1,64	0,05	8	2	47,29
Macrophage scavenger receptor types I and II	Msr1	P30204	1,64	0,00	11	2	75,85
Heterogeneous nuclear ribonucleoprotein D-like	Hnrnpdl	Q8C130	1,63	0,01	18	4	135,01
Cis-aconitate decarboxylase	Acod1	P54987	1,62	0,00	33	15	223,37
Ferritin heavy chain	Fth1	P09528	1,61	0,01	13	8	104,90
Nuclear autoantigenic sperm protein	Nasp	Q99MD9	1,61	0,03	12	3	78,99
Dihydrolipoyllysine-residue succinyltransferase component of 2-oxoglutarate dehydrogenase complex, mitochondrial	Dlst	Q9D2G2	1,59	0,05	22	12	125,97

Supplementary Table 7. Upregulated proteins in *Prdx5*$^{-/-}$ primary macrophages stressed by LPS compared to PBS. The most affected upregulated proteins in macrophages are listed with the fold change expression, the p values, the Accession number, the peptide counts, the unique peptides and the confidence scores.

Treslin	Ticrr	Q8BQ33	1,58	0,04	9	2	47,86
Sister chromatid cohesion protein PDS5homolog A	Pds5a	E9QPI5	1,57	0,01	30	12	179,29
Cdc45 protein	Cep95	Q14865	1,56	0,05	14	7	85,26
Proteasome subunit alpha type (Fragment)	Psma4	Q3TI95	1,56	0,02	7	2	60,20
Double-stranded RNA-specific editase 1	Adarb1	Q91Z58	1,50	0,05	7	3	32,27
Proteasome subunit beta type-4	Psmb4	P99026	1,48	0,01	16	7	134,50
Peroxisomal multifunctional enzyme type 2	Hsd17b4	P51660	1,46	0,01	5	3	24,98
Developmentally regulated GTP binding protein 1	Drg1	P32233	1,46	0,04	6	3	35,73
Serine/threonine-protein kinase 10	Stk10	O55098	1,46	0,05	17	9	104,68
Ras-related C3 botulinum toxin substrate 2	Rac2	Q05144	1,45	0,01	17	7	112,79
Uncharacterized protein	Vps39	Q3USY9	1,44	0,02	12	4	61,96
Hyaluronan synthase1	Has1	Q05437	1,44	0,05	4	2	20,57
Glycerol-3-phosphate dehydrogenase, mitochondrial	Gpd2	Q64521	1,44	0,01	31	13	212,02
RIKEN cDNA 4932438A13 gene (Fragment)	9324438A13Rik	A2AB97	1,43	0,01	4	2	24,48
Uncharacterized protein (Fragment)	Cd22	Q3TSF5	1,42	0,05	5	2	27,57
N-glucosaminidase	Naglu	O54753	1,42	0,03	6	2	28,47
Prolyl endopeptidase	Prep	Q54BB9	1,41	0,00	29	12	195,97
Cation-dependent mannose-6-phosphate receptor	M6pr	P24668	1,41	0,03	15	7	99,41
Arf-GAP with Rho-GAP domain, ANK repeat and PH domain-containing protein 1	Arap1	Q4LDD4	1,39	0,00	47	5	351,26
60S ribosomal protein L9	Rpl9	P51410	1,39	0,04	17	4	141,96
Adenylosuccinate synthetase isozyme 2	Adss	P46664	1,37	0,02	11	9	88,69
Coiled-coil domain-containing 141	Ccdc141	A2AST1	1,36	0,04	20	2	101,34
60S ribosomal protein L23	Rpl23	P62830	1,34	0,00	8	3	49,05
Ankyrin repeat and SAM domain-containing protein 6	Ankrd6	A2ANT9	1,31	0,02	2	2	10,41
Sterile alpha motif domain-containing protein 9-like	Samd9l	Q6ZE37	1,30	0,00	27	2	146,47
Adenylosuccinate synthetase isozyme 1	Adss1	P28650	1,28	0,01	11	5	65,43
Annexin A2	Anxa2	P07356	1,28	0,02	51	27	289,65
GATOR complex protein DEPDC5	Depdc5	P61460	1,25	0,00	12	3	72,52
Succinate--CoA ligase [ADP-forming] subunit beta, mitochondrial	Sucla2	Q8CI99	1,24	0,05	24	5	127,88
Transportin 3	Tnpo3	Q6DI95	1,18	0,04	18	6	111,57
Aminoacylase-1	Acy1	Q99JW2	1,10	0,02	20	2	139,09

Supplementary Table 8. Downregulated proteins in *Prdx5*$^{-/-}$ primary macrophages stressed by LPS compared to PBS. The most affected upregulated proteins in macrophages are listed with the fold change expression, the p values, the Accession number, the peptide counts, the unique peptides and the confidence scores. (Continue in the next page)

Downregulated proteins in Prdx5-/- cells exposed to LPS compare to Prdx5-/- without LPS							
Description	Short name	Accession	Max fold change	Anova (p)	Peptide count	Unique peptides	Confidence score
G protein-activated inward rectifier potassium channel 4	Kcnj5	P48545	40,44	0,02	5	2	29,32
CD82 antigen	Cd82	P40237	37,88	0,00	6	2	40,82
Caspase-3	Casp3	P70677	21,32	0,04	2	2	9,25
Uncharacterized protein (Fragment)	Tpr	Q3V1L5	16,89	0,01	15	2	81,19
Cystathionine beta-synthase	Cbs	Q91WT9	11,34	0,00	4	2	20,49
Coiled-coil domain-containing protein 178	Ccdc178	Q8CDV0	11,31	0,01	12	2	64,70
Src kinase-associated phosphoprotein 1	Skap1	Q3UUV5	11,03	0,00	4	2	21,51
BCL-6 corepressor-like protein 1	Bcorl1	A2AQH4	10,97	0,01	4	3	17,76
Sorting nexin-17	Snx17	Q8BVL3	10,81	0,01	4	2	19,17
Plastin-1	Pls1	Q3V0K9	7,70	0,02	26	2	158,34
Plectin (Fragment)	Plec	A0A0R4J218	7,65	0,03	24	2	145,10
Septin-7	sept7	O55131	5,29	0,04	16	1	133,50
Phosphoinositide phospholipase C	Plcd1	G5DD87	5,13	0,02	2	2	9,46
Glutamate receptor 3	Gria3	Q9Z2W9	4,83	0,00	14	3	76,20
MKIAA4151 protein (Fragment)	Golgb1	Q571K1	4,68	0,00	32	11	147,27
Golga1 protein	Golga1	Q66JW2	4,48	0,03	5	2	29,84
Pecanex-like protein 3	Pcnx3	Q8VI59	4,44	0,03	7	2	46,93
Uncharacterized protein	Ctnnb1	Q3UZT7	4,34	0,01	6	2	33,54
Zinc finger CCHC domain-containing protein 4	Zcchc4	Q8BKW4	4,12	0,00	4	2	17,62
Ovostatin homolog	Ovos	Q3UU35	4,00	0,02	6	4	40,87
Telomerase-binding protein EST1A	Smg6	P61406	3,92	0,01	21	2	106,66
N-acetylglucosamine-6-phosphate deacetylase	Amdhd2	Q8JZV7	3,53	0,04	7	3	47,74
Perilipin-3	Plin3	Q9DBG5	3,17	0,05	15	8	101,84
Nuclear receptor subfamily 1, group D, member 2	Nr1d2	Q4VA87	3,05	0,00	2	2	10,25
Myb-binding protein 1A	Mybbp1a	Q7TPV4	3,04	0,00	41	13	258,71
Macrophage-expressed gene 1 protein	Mpeg1	A1L314	3,03	0,00	21	10	160,15
Core histone macro-H2A.1	H2afy	Q9QZQ8	3,03	0,05	4	2	18,29
Annexin A11	Anxa11	P97384	2,97	0,01	17	4	123,82
Rho GTPase-activating protein 18	Arhgap18	Q8K0Q5	2,96	0,00	10	2	48,16
U4/U6 small nuclear ribonucleoprotein Prp31	Prpf31	Q8CCF0	2,91	0,01	7	3	39,40
Sorting nexin-6	Snx6	Q6P8X1	2,90	0,02	6	2	30,89
E3 ubiquitin-protein ligase UBR4 (Fragment)	Ubr4	F6SSP6	2,89	0,00	17	8	98,95
Myristoylated alanine-rich C-kinase substrate	Marcks	P26645	2,89	0,02	12	10	128,59
Interleukin-1 receptor accessory protein-like 1	Il1rapl1	B1ASU0	2,87	0,00	13	4	59,44
Eukaryotic elongation factor 2 kinase	Eef2k	O08796	2,80	0,02	6	3	26,80
Phosphomannomutase	Pmm2	Q545N8	2,72	0,02	11	3	77,65
Glyoxalase domain-containing protein 4	Glod4	Q9CPV4	2,64	0,01	16	6	147,13
Rho-associated protein kinase 1	Rock1	P70335	2,63	0,02	12	2	61,94
Period circadian protein homolog 1	Per1	O35973	2,57	0,02	5	2	27,37
Axonemal dynein light chain domain-containing protein 1 (Fragment)	Axdnd1	J3KMJ8	2,47	0,02	8	2	44,00
Tetratricopeptide repeat protein 34	Ttc34	A0A140LHH0	2,46	0,01	2	2	9,00
Lysozyme	Lyz2	P08905	2,36	0,00	16	6	113,05
Keratin 78	Krt78	E9Q0F0	2,34	0,00	7	4	46,76
PHD finger protein 21B	Phf21b	F8WGM2	2,29	0,03	2	2	15,05
Zinc finger protein castor homolog 1	Casz1	Q9CWL2	2,28	0,02	12	6	56,61
Signal recognition particle 54 kDa protein	Srp54b	P14576	2,28	0,03	7	2	39,17
Kelch repeat and BTB domain-containing protein 3	Kbtbd3	Q8BHI4	2,27	0,02	2	2	8,73
Keratin, type II cytoskeletal 6A	Krt6a	P50446	2,26	0,01	22	2	137,79
Superkiller viralicidic activity 2-like (S. cerevisiae)	Skiv2l	Q6NZR5	2,26	0,03	6	3	27,77
Slit homolog 2 protein	Slit2	A0A140T8T2	2,24	0,04	11	2	46,63
Fanconi anemia, complementation group A	Fanca	B2RWU3	2,20	0,01	8	3	42,75

Supplementary Table 8. Downregulated proteins in *Prdx5*$^{-/-}$ primary macrophages stressed by LPS compared to PBS. The most affected upregulated proteins in macrophages are listed with the fold change expression, the p values, the Accession number, the peptide counts, the unique peptides and the confidence scores. (Continue in the next page)

26S proteasome non-ATPase regulatory subunit 1	Psmd1	Q3TXS7	2,14	0,04	36	11	244,77
Protein FAM208B (Fragment)	Fam208b	A0A1Y7VLA4	2,14	0,04	14	3	61,02
Sugar transporter SWEET1	Slc50a1	D3YXA7	2,13	0,00	2	2	12,64
Rab GTPase-binding effector protein 1	Rabep1	J3QJV7	2,13	0,04	7	2	26,32
THUMP domain-containing protein 1	Thumpd1	Q99J36	2,11	0,00	7	4	36,10
Cytosolic purine 5'-nucleotidase	Nt5c2	E9Q9M1	2,11	0,03	6	4	35,84
Microtubule-associated protein 4	Map4	P27546	2,11	0,02	14	3	83,04
Canalicular multispecific organic anion transporter 2	Abcc3	A0A0R4J015	2,10	0,00	4	2	28,07
Zinc finger E-box-binding homeobox 2	Zeb2	Q9R0G7	2,10	0,03	6	4	26,10
Actin, gamma-enteric smooth muscle	Actg2	P63268	2,10	0,03	73	2	299,40
Zinc finger protein 395	Zfp395	E9Q5N9	2,09	0,00	6	2	21,72
Coiled-coil domain-containing 180	Ccdc180	J3QNE4	2,02	0,00	16	3	77,63
Regulator of G-protein signaling 3	Rgs3	Q9DC04	2,01	0,02	4	2	18,69
Lipase	Lipa	Q3TEL5	2,00	0,00	17	6	114,81
MICOS complex subunit Mic60	Immt	Q8CAQ8	1,97	0,00	28	6	171,67
Serine/threonine-protein phosphatase 2A 55 kDa regulatory subunit B alpha isoform	Ppp2r2a	Q6P1F6	1,97	0,00	21	3	117,33
Uncharacterized protein	Adgre1	Q3U9R0	1,96	0,04	9	3	56,34
Glutathione reductase, mitochondrial	Gsr	P47791	1,96	0,05	20	4	157,67
Peroxiredoxin-5, mitochondrial	Prdx5	P99029	1,95	0,96	16	3	125,32
Ras-related protein Rab-6A	Rab6a	P35279	1,94	0,01	19	3	103,41
Structure-specific endonuclease subunit SLX4 (Fragment)	Slx4	F6XZI3	1,94	0,02	2	2	11,63
Protein diaphanous homolog 1	Diaph1	E9PXV7	1,94	0,00	36	10	229,83
Dolichyl-diphosphooligosaccharide--protein glycosyltransferase subunit STT3B	Stt3b	A0A0R4J0D3	1,94	0,05	13	3	71,84
Mannose-P-dolichol utilization defect 1 protein	Mpdu1	E9PVP3	1,90	0,00	4	2	26,29
Cytochrome P450, family 4, subfamily f, polypeptide 40	Cyp4f40	B2RY43	1,89	0,02	9	5	45,96
CPXV213 protein	CPXV213	A0A1X9T6Y4	1,88	0,05	17	2	74,89
Ephrin type-A receptor 6	Epha6	G1K381	1,87	0,03	16	5	69,00
Kinesin-like protein KIF21B	Kif21b	E9Q0A4	1,86	0,01	12	4	57,25
Tubulin gamma chain	Tubg2	Q6F4J0	1,85	0,00	6	2	35,18
Sodium channel protein	Scn2a	A0A0J9YTW68	1,84	0,00	15	4	75,56
NACHT domain- and WD repeat-containing protein 1	Nwd1	A6H603	1,84	0,01	22	5	132,10
Transmembrane channel-like protein 5	Tmc5	Q32N26	1,82	0,02	20	11	90,29
Keratin, type II cytoskeletal 2 oral	Krt76	Q3UV17	1,82	0,00	20	8	134,14
Protein strawberry notch homolog 1	Sbno1	B2RRI2	1,82	0,02	8	4	58,43
Chromodomain-helicase-DNA-binding protein 1-like	Chd1l	Q9CXF7	1,81	0,00	7	2	41,93
Protein diaphanous homolog 3	Diaph3	F8WI65	1,81	0,03	5	2	24,68
Mitogen-activated protein kinase kinase kinase 5	Map3k5	E9PWG9	1,80	0,02	4	2	21,26
DNA topoisomerase 2-beta	Top2b	Q64511	1,80	0,00	38	6	208,64
Ankyrin repeat containing protein	CPXV AUS1999 867 026	G0XS86	1,79	0,04	6	2	31,39
Neurolysin, mitochondrial	Nln	Q91YP2	1,78	0,00	22	8	158,73
Integrin-associated protein	Cd47	E9Q371	1,77	0,04	7	2	61,62
Dihydrolipoyllysine-residue acetyltransferase component of pyruvate dehydrogenase complex, mitochondrial	Dlat	Q8BMF4	1,75	0,01	17	9	91,76
TP53-binding protein 1	Tp53bp1	F7039	1,75	0,01	12	6	59,64
Probable E3 SUMO-protein ligase RNF212 (Fragment)	Rnf212	A0A062JFM4	1,74	0,01	4	2	10,20
MFLJ00316 protein (Fragment)	Gbp7	Q6KAN1	1,73	0,02	13	6	100,03
Lysophosphatidic acid phosphatase type 6	Acp6	Q8BP40	1,73	0,02	4	2	21,51
Torsin-1A-interacting protein 1	Tor1aip1	Q921T2	1,72	0,01	10	3	67,50
Cytochrome c1, heme protein, mitochondrial	Cyc1	Q9D0M3	1,72	0,03	11	3	67,88
Ubiquitin carboxyl-terminal hydrolase isozyme L5 (Fragment)	Uchl5	A0A087WP81	1,71	0,00	4	2	24,68
WD repeat domain 17	Wdr17	E9Q271	1,68	0,05	5	2	21,61
Receptor-type tyrosine-protein phosphatase kappa	Ptprk	A0A1W2P7Y1	1,68	0,03	6	2	34,88
Uncharacterized protein	Cyld	Q3V028	1,67	0,01	11	4	64,23

Supplementary Table 8. Downregulated proteins in *Prdx5*$^{-/-}$ primary macrophages stressed by LPS compared to PBS. The most affected upregulated proteins in macrophages are listed with the fold change expression, the p values, the Accession number, the peptide counts, the unique peptides and the confidence scores. (Continue in the next page)

Downregulated proteins in Prdx5-/- cells exposed to LPS compare to Prdx5-/- without LPS							
Description	Short name	Accession	Max fold change	Anova (p)	Peptide count	Unique peptides	Confidence score
Collagen alpha-1(XXIV) chain	Col24a1	Q30D77	1,67	0,00	18	3	89,57
Short-chain specific acyl-CoA dehydrogenase, mitochondrial	Acads	Q07417	1,66	0,00	14	2	93,35
14-3-3 protein epsilon	Ywhae	P62259	1,65	0,02	47	17	187,11
Nuclear transcription factor, X-box-binding-like 1	Nfxl1	E9Q8I7	1,65	0,04	2	2	9,03
General vesicular transport factor p115	Uso1	Q9Z1Z0	1,63	0,02	28	9	174,45
Predicted gene 20425	Gm20425	E9Q035	1,63	0,03	25	5	150,90
Ras GTPase-activating protein 4	Rasa4	Q6PFQ7	1,63	0,01	5	2	37,57
Caspase-8	Casp8	O89110	1,62	0,02	19	6	102,55
Tanc1 protein	Tanc1	B9EJ77	1,61	0,04	16	3	96,33
Coatomer subunit epsilon	Cope	O89079	1,61	0,04	15	8	97,58
AHNAK nucleoprotein 2 (Fragment)	Ahnak2	F7CVJ5	1,60	0,00	28	2	214,52
26S proteasome non-ATPase regulatory subunit 2	Psmd2	Q8VDM4	1,60	0,01	36	2	242,94
Importin-4	Ipo4	Q8VI75	1,60	0,02	26	9	164,09
Prosaposin, isoform CRA_e	Psap	Q3UFE8	1,60	0,00	33	2	213,26
Sodium/potassium-transporting ATPase subunit beta-3	Atp1b3	P97370	1,60	0,03	8	2	61,61
CD180 antigen	Cd180	Q62192	1,59	0,02	18	4	124,24
Uncharacterized protein (Fragment)	Lrp1	Q3U434	1,59	0,00	25	7	154,93
Forkhead-associated domain-containing protein 1	Fhad1	A6PWD2	1,59	0,04	13	2	89,01
Testis-specific gene 10 protein	Tsga10	Q6NY15	1,59	0,01	13	5	68,92
NADH dehydrogenase [ubiquinone] 1 beta subcomplex subunit 10 (Fragment)	Ndufb10	D3YUK4	1,58	0,01	8	3	57,44
Fatty acid-binding protein, heart	Fabp3	P11404	1,58	0,05	6	4	37,70
Kinesin heavy chain isoform 5A	Kif5a	P33175	1,57	0,02	10	2	45,24
Carboxypeptidase	Ctsa	P16675	1,57	0,01	12	7	44,87
Serine/threonine-protein kinase N2	Pkn2	Q8BWW9	1,57	0,00	15	2	72,20
Rho-associated protein kinase 2	Rock2	P70336	1,55	0,05	16	2	82,61
Uncharacterized protein	Rab2a	P53994	1,55	0,02	9	3	75,10
Transportin-2	Tnpo2	Q99LG2	1,55	0,03	16	2	86,26
Selection and upkeep of intraepithelial T-cells protein 5	Skint5	A7XUY5	1,54	0,03	44	11	229,53
NADPH oxidase 1	Nox1	Q8CIZ9	1,54	0,00	12	3	75,32
Tyrosine-protein kinase	Hck	0A087WQ0	1,53	0,05	8	4	48,77
Uncharacterized protein	Pak7	Q8BVB0	1,53	0,02	8	2	42,43
Neuropilin-1	Nrp1	P97333	1,53	0,01	4	2	31,03
Maestro heat-like repeat family member 1	Mroh1	E0CZ22	1,53	0,01	6	2	34,40
Isochorismatase domain-containing protein 1	Isoc1	Q91V64	1,53	0,00	9	3	67,32
Aminoacyl tRNA synthase complex-interacting multifunctional protein 1	Aimp1	P31230	1,52	0,05	9	3	57,59
Protein SEC13 homolog	Sec13	Q9D1M0	1,52	0,03	9	3	57,40
Plexin-C1	Plxnc1	Q9QZC2	1,52	0,04	8	2	36,82
Lysophospholipid acyltransferase 5	Lpcat3	Q91V01	1,52	0,02	6	2	47,79
1-phosphatidylinositol 4,5-bisphosphate phosphodiesterase eta-1	Plch1	Q4KWH5	1,52	0,01	32	11	158,06
Estradiol 17-beta-dehydrogenase 11	Hsd17b11	Q9EQ06	1,51	0,04	14	5	129,16
ADP/ATP translocase 1	Slc25a4	P48962	1,51	0,01	22	2	125,79
Guanylate-binding protein 1	Gbp1	Q01514	1,51	0,02	20	7	131,48
Cyp4f15 protein	Cyp4f15	Q8VCA4	1,51	0,01	10	3	64,38
Nebulin (Fragment)	Neb	Q62411	1,51	0,00	7	4	48,92
Cmpt1 protein	Cmpt1	P97427	1,51	0,01	22	9	129,40
Integrin alpha-M	Itgam	Q3U1U4	1,51	0,03	77	3	518,69
Ezrin	Ezr	P26040	1,49	0,04	28	8	198,20
Group XV phospholipase A2	Pla2g15	Q8VEB4	1,49	0,03	8	3	53,77
Exportin-2	Cse1l	Q9ERK4	1,49	0,03	32	13	199,24
Slc2a6 protein	Slc2a6	A2AR26	1,49	0,03	9	4	66,48
MCG140066	700060E02Rik	Q4VA29	1,49	0,02	10	4	77,37

Supplementary Table 8. Downregulated proteins in *Prdx5*$^{-/-}$ primary macrophages stressed by LPS compared to PBS. The most affected upregulated proteins in macrophages are listed with the fold change expression, the p values, the Accession number, the peptide counts, the unique peptides and the confidence scores.

Inositol-3-monophosphate dehydrogenase 1	Impdh1	P50096	1.48	0.00	10	2	62.32
Uncharacterized protein (Fragment)	Pstpip2	Q3UGV1	1.47	0.03	3	2	21.16
Immunity-related GTPase family Q protein	Irgq	Q8VHM9	1.47	0.01	2	2	14.59
Leucine-rich repeat-containing 25	Lrrc25	B9EHD0	1.47	0.01	4	2	12.25
L-lactate dehydrogenase C chain	Ldhc	P00342	1.47	0.05	13	2	84.55
COP9 signalosome subunit associated protein 2	Cops2	Q9WU83	1.47	0.04	7	3	33.35
Heterogeneous nuclear ribonucleoprotein M	Hnrnpm	Q8VDB1	1.46	0.00	30	13	356.13
Keratin, type II cuticular Hb3	Krt83	Q8BZ76	1.45	0.04	10	3	41.75
Exportin-1	Xpo1	Q8K2B3	1.45	0.01	38	15	205.48
Target of Myb protein 1 (Fragment)	Tom1	A0A1D5NL94	1.45	0.03	4	2	27.39
Fumarylacetoacetase	Fah	P35505	1.45	0.02	8	4	51.12
Bifunctional purine nucleotide phosphatase/kinase	Pnkp	Q3TBW7	1.45	0.02	11	2	68.29
TBC1 domain family member 1	Tbc1d1	Q3U479	1.45	0.01	18	5	84.84
Guanine nucleotide-binding protein G(i) subunit alpha-3	Gnai3	P21279	1.44	0.01	6	2	37.85
Proteasome subunit beta type	Psmb3	Q3U4S0	1.44	0.02	21	13	130.93
Oxysterol-binding protein 1	Osbp	Q3TP03	1.43	0.04	5	2	31.52
Ribosomal protein S6 kinase	Rps6ka2	Q3TEC8	1.43	0.03	18	4	110.08
Calmodulin-like protein 3	Calml3	Q8BFZ5	1.42	0.02	201	51	688.48
Serine palmitoyltransferase 2	Sptlc2	P97389	1.41	0.01	17	2	108.79
Dedicator of cytokinesis protein 7	Dock7	Q4VU14	1.40	0.00	19	5	106.16
Xanthine dehydrogenase/oxidase	Xdh	Q00519	1.39	0.00	42	11	338.89
Cytochrome b5	Cyb5a	P56395	1.39	0.05	9	6	79.31
Phosphatidylinositol 4-kinase alpha	Pi4ka	E9Q3L2	1.38	0.03	34	15	158.42
X-ray repair cross-complementing protein 6	Xrcc6	P13466	1.38	0.01	10	2	39.04
Succinyl-CoA:3-ketoacid-coenzyme A transferase 1, mitochondrial	Oxct1	Q3UK81	1.38	0.04	15	4	98.38
Nuclear cap-binding protein subunit 1	Ncbp1	Q3UV19	1.36	0.00	21	11	128.58
Citron Rho-interacting kinase	Cit	P49025	1.36	0.01	15	5	82.14
Calcium-binding mitochondrial carrier protein Scamc-1	Slc25a24	Q3TMC8	1.35	0.04	19	8	148.16
Voltage-dependent anion-selective channel protein 1	Vdac1	Q60932	1.35	0.01	17	6	126.30
Guanylate-binding protein 4	Gbp4	Q4VIQ7	1.35	0.04	36	14	255.66
Mast/stem cell growth factor receptor Kit	Kit	P05532	1.35	0.03	14	3	84.93
Protein LYRIC	Mtdh	Q80WJ7	1.35	0.02	20	7	113.45
Protein SLX4IP	Slx4ip	Q8C7P6	1.35	0.05	4	2	23.59
Neutral cholesterol esterase 1	Nceh1	Q8BLF1	1.34	0.02	15	8	134.97
Mitogen-activated protein kinase 3	Mapk3	Q63844	1.34	0.04	21	6	142.35
Cytochrome b-245 heavy chain	Cybb	Q61093	1.33	0.04	34	11	238.15
Protein PTHB1	Bcas3	Q811G0	1.32	0.05	7	4	39.84
Uncharacterized protein	Tmem173	Q8BVB0	1.32	0.03	3	2	21.36
CTP synthase 2	Ctps2	P70698	1.31	0.03	14	9	105.32
Coiled-coil domain-containing protein 22	Ccdc22	Q8VDF7	1.30	0.02	19	11	105.94
Tyrosine-protein kinase Lyn	Lyn	Q03265	1.30	0.00	16	7	109.84
Complement component 1 Q subcomponent-binding protein, mitochondrial	C1qbp	Q3TLL1	1.30	0.00	13	4	79.80
NADH dehydrogenase [ubiquinone] 1 alpha subcomplex subunit 10, mitochondrial	Ndufa10	Q9DC51	1.29	0.02	9	5	49.01
Cytochrome c oxidase subunit 5B, mitochondrial	Cox5b	P19536	1.29	0.01	5	3	35.31
UDP-N-acetylhexosamine pyrophosphorylase-like protein 1	Uaplg1	Q3TW96	1.28	0.01	39	20	229.16
Fibronectin type 3 and ankyrin repeat domains protein	Fank1	Q3UAM9	1.28	0.01	8	2	54.13
Long-chain specific acyl-CoA dehydrogenase, mitochondrial	Acadl	P51174	1.26	0.04	30	10	186.16
Glycerol-3-phosphate dehydrogenase [NAD(+)]	Gpd1l	B2RS77	1.24	0.03	9	2	45.04
Glyoxylase domain-containing protein 4	Glod4	Q9D4F8	1.24	0.00	11	5	54.11
Intercellular adhesion molecule 2	Icam2	P13630	1.24	0.03	7	3	33.76
Autophagy-related protein 2 homolog B	Atg2b	Q80XX6	1.20	0.00	8	3	43.67

Supplementary Table 9. Upregulated proteins in *Prdx5*$^{-/-}$ primary macrophages compared to *Prdx5*$^{+/+}$ stressed by PBS. The most affected upregulated proteins in macrophages are listed with the fold change expression, the p values, the Accession number, the peptide counts, the unique peptides and the confidence scores. (Continue in the next page)

Upregulated proteins in Prdx5-/- cells compare to Prdx5+/+ cells in PBS							
Description	Short names	Accession	Max fold change	Anova (p)	Peptide count	Unique peptides	Confidence score
G protein-activated inward rectifier potassium channel 4	Kcnj5	P48545	48,03	0,01	5	2	29,32
Phosphoprotein	P/V/C	P14251	28,06	0,00	7	1	39,60
Synemin	Synm	Q70IV5	22,76	0,03	14	1	87,44
Coiled-coil domain-containing protein 178	Ccdc178	Q8CDV0	13,51	0,00	12	2	64,70
Uncharacterized protein (Fragment)	Tpr	Q3V1L5	9,21	0,03	15	2	81,19
Cystathionine beta-synthase	Cbs	Q91WT9	8,56	0,00	4	2	20,49
Plastin-1	Pls1	Q3V0K9	8,00	0,02	26	2	153,34
Sorting nexin-17	Snx17	Q8BVL3	6,93	0,01	4	2	19,17
Perilipin-3	Plin3	Q9DBG5	4,23	0,01	15	8	101,84
Ovostatin homolog	Ovos	Q3UU35	3,99	0,02	6	4	40,87
Uncharacterized protein	Dctn4	Q3TQY2	3,90	0,03	5	1	35,53
MKIAA4151 protein (Fragment)	Golgb1	Q571K1	3,53	0,00	32	11	147,27
Myb-binding protein 1A	Mybbp1a	Q7TPV4	3,28	0,00	41	13	253,71
Phosphomannomutase	Pmm2	Q545N8	3,26	0,00	11	3	77,65
Centaurin beta 2	Acap2	D4AFX6	3,19	0,04	11	1	52,73
Myristoylated alanine-rich C-kinase substrate	Marcks	P26645	2,98	0,01	12	10	128,59
Interleukin-1 receptor accessory protein-like 1	Il1rapl1	P59823	2,67	0,00	13	4	59,44
Annexin A11	Anxa11	P97384	2,67	0,03	17	4	123,82
Squamous cell carcinoma antigen recognized by T-cells 3	Sart3	Q9JLI8	2,66	0,01	6	2	26,95
Microtubule-associated protein 4	Map4	P27546	2,59	0,01	14	3	83,04
Glyoxalase domain-containing protein 4	Glod4	Q9CPV4	2,46	0,02	16	6	147,13
Zinc finger protein castor homolog 1	Casz1	Q9CWL2	2,44	0,01	12	6	56,61
26S proteasome non-ATPase regulatory subunit 1	Psmd1	Q3TXS7	2,31	0,02	36	11	244,77

Supplementary Table 9. Upregulated proteins in *Prdx5*$^{-/-}$ primary macrophages compared to *Prdx5*$^{+/+}$ stressed by PBS. The most affected upregulated proteins in macrophages are listed with the fold change expression, the p values, the Accession number, the peptide counts, the unique peptides and the confidence scores.

Superkiller viralicidic activity 2-like (S. cerevisiae)	Skiv2l	Q6NZR5	2,30	0,03	6	3	27,77
Period circadian protein homolog 1	Per1	O35973	2,17	0,00	5	2	27,37
Kelch repeat and BTB domain-containing protein 3	Kbtbd3	Q8BHI4	2,16	0,03	2	2	8,73
THUMP domain-containing protein 1	Thumpd1	Q99I36	2,10	0,00	7	4	36,10
Protein strawberry notch homolog 1	Sbno1	B2RRI2	2,10	0,00	8	4	53,43
Gamma-aminobutyraldehyde dehydrogenase	Aldh9a1	A7VL18	2,06	0,01	21	8	129,86
Keratin 78	Krt78	E9Q0F0	2,02	0,00	7	4	46,76
Alpha globin 1	Hba-a1	Q91VB8	1,95	0,01	31	2	152,39
Proto-oncogene vav	Vav1	P27870	1,91	0,00	7	2	41,74
Adenylosuccinate lyase	Adsl	P54822	1,87	0,05	13	3	81,30
Predicted gene 20425	Gm20425	E9Q035	1,85	0,02	25	5	150,90
Cytochrome P450, family 4, subfamily f, polypeptide 40	Cyp4f40	B2RY43	1,84	0,03	9	5	45,96
Integrin-associated protein	Cd47	E5Q371	1,84	0,03	7	2	61,62
Zinc finger CCHC domain-containing protein 4	Zcchc4	Q8BKW4	1,78	0,04	4	2	17,62
Metabotropic glutamate receptor subtype 5b	Grm5	B2BH30	1,77	0,04	5	2	22,53
Lipase	Lipa	Q3TEL5	1,73	0,01	17	6	114,81
Bis(5'-adenosyl)-triphosphatase enpp4	Enpp4	Q8BTJ4	1,69	0,03	5	2	26,98
Small nuclear ribonucleoprotein Sm D3	Snrpd3	P62320	1,67	0,05	12	5	83,51
Proteasome subunit beta type	Psmb3	Q545G0	1,66	0,01	21	13	130,53
Protein diaphanous homolog 1	Diaph1	E9PXV7	1,60	0,03	36	10	229,83
Keratin, type II cytoskeletal 2 oral	Krt76	Q3UV17	1,54	0,00	20	8	134,14
Synaptosomal-associated protein 23	Snap23	O09044	1,43	0,00	12	4	81,59
Neurolysin, mitochondrial	Nln	Q91YP2	1,43	0,03	22	8	153,73
Heterogeneous nuclear ribonucleoprotein M	Hnrnpm	Q9D0E1	1,36	0,01	50	13	358,13
Galectin-3-binding protein	Lgals3bp	Q07797	1,32	0,00	19	7	148,66
Long-chain specific acyl-CoA dehydrogenase, mitochondrial	Acadl	P51174	1,24	0,02	30	10	186,36

Supplementary Table 10. Downregulated proteins in *Prdx5*$^{-/-}$ primary macrophages compared to *Prdx5*$^{+/+}$ stressed by PBS. The most affected upregulated proteins in macrophages are listed with the fold change expression, the p values, the Accession number, the peptide counts, the unique peptides and the confidence scores. (Continue in the next page)

Downregulated proteins in Prdx5-/- cells compare to Prdx5+/+ cells in PBS							
Description	Short names	Accession	Max fold change	Anova (p)	Peptide count	Unique peptides	Confidence score
Peroxiredoxin-5, mitochondrial	Prdx5	P99029	157,93	0,00	16	3	125,32
Programmed cell death protein 6	Pdcd6	P12815	17,22	0,00	5	1	28,12
E3 ubiquitin-protein ligase Rnf220	Rnf220	Q6PDX6	9,02	0,04	2	2	8,83
Cilia- and flagella-associated protein 251	Wdr66	E9Q743	8,26	0,00	8	4	40,80
PDZ domain-containing protein 4	Pdzd4	Q8QY39	6,14	0,04	2	1	14,44
Schlafen family member 8	OTTMUSW58G0059301	A0A1G5SJB6	6,08	0,01	11	1	57,95
Centrosomal protein of 170kDa	Cep170	Q8A0B5	5,20	0,03	13	5	68,75
Sjoegren syndrome/scleroderma autoantigen 1 homolog	Ssxa1	P56873	3,84	0,00	3	1	11,03
Eukaryotic translation initiation factor 5A (Fragment)	Eif5a	P63242	3,64	0,01	7	1	48,17
V-type proton ATPase catalytic subunit A	Atp6v1a	P50516	3,56	0,03	45	17	327,45
Homeobox protein TGIF1	Tgif1	P70284	3,50	0,04	2	2	11,13
AKNA domain-containing 1	Akna d1	E9Q8N6	2,96	0,05	5	2	31,11
Receptor-type tyrosine-protein phosphatase S	Ptprs	B0V2N1	2,95	0,03	27	10	150,96
Werner syndrome ATP-dependent helicase homolog	Wrn	O09053	2,74	0,03	6	3	26,88
H2-T23 protein	H2-T23	Q31153	2,66	0,00	14	2	90,22
Histone-lysine N-methyltransferase EHMT2	Ehmt2	A2CG76	2,62	0,03	3	2	13,51
Tyrosine-protein kinase JAK1	Jak1	P52332	2,40	0,03	30	2	170,00
Sentrin-specific protease 7	Senp7	E9Q1L5	2,38	0,00	5	2	29,55
Lysophospholipid acyltransferase 7	Mboat7	Q8CHK3	2,31	0,00	7	2	58,33
Acyl-protein thioesterase 2	Lypla2	Q9WTL7	2,31	0,00	18	9	150,42
E3 ubiquitin-protein ligase listerin	Ltn1	Q6A009	2,24	0,02	4	1	19,09
Nck-associated protein 1-like	Nckap1l	Q8K1X4	2,19	0,03	16	3	103,91
UV excision repair protein RAD23 homolog B	Rad23b	P54728	2,18	0,05	15	3	117,83
UDP-glucose glycoprotein glucosyltransferase 1	Uggt1	Q6P5S4	2,15	0,05	68	27	509,15
Rho GTPase-activating protein 27	Arhgap27	A2AB59	2,14	0,00	8	3	38,53
Glucose-6-phosphate isomerase	Gpi	P06745	2,08	0,01	27	5	206,65
Wbp7 protein (Fragment)	Kmt2b	Q6PHU4	2,06	0,04	7	2	44,01
[Protein ADP-ribosyl]-arginine] hydrolase	Adprh	P54923	2,00	0,04	14	2	87,64
Tyrosine-protein kinase CSK	Csk	P41241	2,00	0,00	21	2	150,63
Moesin	Msn	P26041	1,99	0,01	48	19	320,52

Supplementary Table 10. Downregulated proteins in *Prdx5*$^{-/-}$ primary macrophages compared to *Prdx5*$^{+/+}$ stressed by PBS. The most affected upregulated proteins in macrophages are listed with the fold change expression, the p values, the Accession number, the peptide counts, the unique peptides and the confidence scores. (Continue in the next page)

Ubiquitin carboxyl-terminal hydrolase 43	Usp43	A8FWR8	1,98	0,05	9	2	43,33
Tripartite terminase subunit 1	TRML	Q8JYD4	1,96	0,03	5	2	24,57
Polypyrimidine tract-binding protein 1	Ptbp1	P17225	1,94	0,01	14	1	116,29
Vesicle-fusing ATPase	Nsf	P46460	1,86	0,04	37	10	228,19
Exosome complex exonuclease RRP44	Dis3	Q8CSH3	1,83	0,03	20	3	120,68
Thioredoxin domain-containing protein 17	Txndc17	Q8CQM5	1,82	0,05	13	8	77,96
Capping protein (Actin filament), gelsolin-like	Capg	P24452	1,82	0,01	30	15	180,62
Cystatin-B	Cstb	O62426	1,78	0,04	14	9	54,01
Complement component C8 beta chain	C8b	Q8BH35	1,77	0,03	6	2	28,13
Solute carrier family 25 (Mitochondrial carrier; oxoglutarate carrier), member 11, isoform CRA_b	Slc25a11	Q5SX53	1,76	0,02	13	2	61,95
SUMO-activating enzyme subunit 2	Uba2	Q921F9	1,71	0,05	25	11	173,11
Tropomodulin 2, isoform CRA_c	Tmod2	A0A1L1SU70	1,70	0,02	5	2	13,44
Eukaryotic translation initiation factor 3 subunit C	Eif3c	Q8R1B4	1,69	0,02	30	16	188,09
Beta-actin-like protein 2	Actbl2	Q8BFZ5	1,60	0,01	58	3	300,34
Eukaryotic translation elongation factor 1 gamma	Eef1g	Q4FZK2	1,55	0,01	31	15	161,26
Uncharacterized protein	Rab35	Q3V3B9	1,54	0,04	3	2	14,13
Hypoxia up-regulated protein 1	Hyou1	Q9JKR6	1,54	0,01	48	16	368,73
ATP-dependent Clp protease proteolytic subunit, mitochondrial	Clpp	O88696	1,53	0,02	7	2	39,32
RIKEN cDNA 4932438A13 gene (Fragment)	4932438A13Rik	A2A897	1,52	0,00	4	2	24,48
Uncharacterized protein		C3UBJ6	1,51	0,02	17	5	104,56
ATP-binding cassette, sub-family C (CFTR/MRP), member 8	Abcc8	B2RUS7	1,50	0,04	10	6	38,13
Fatty acid-binding protein, adipocyte	Fabp4	P04117	1,50	0,04	14	4	98,92
N-acetylglucosamine-6-sulfatase	Gns	Q8BFR4	1,47	0,04	20	7	124,27

Supplementary Table 10. Downregulated proteins in *Prdx5*$^{-/-}$ primary macrophages compared to *Prdx5*$^{+/+}$ stressed by PBS. The most affected upregulated proteins in macrophages are listed with the fold change expression, the p values, the Accession number, the peptide counts, the unique peptides and the confidence scores.

Ras-related protein Rab-30	Rab30	Q62359	1,46	0,05	9	3	47,13
Nucleophosmin	Npm1	Q3SQB0	1,45	0,02	18	10	155,05
Ras-related C3 botulinum toxin substrate 2	Rac2	Q05144	1,43	0,03	17	7	112,79
T-lymphocyte surface antigen Ly-9	Ly9	Q01965	1,41	0,02	16	7	101,84
Serine/threonine-protein kinase 10	Stk10	Q55Q98	1,40	0,03	17	9	104,68
Netrin-G2	Ntng2	Q8R4F1	1,39	0,05	6	3	29,14
Ruv8-like helicase	Ruvbl2	Q3TXT7	1,39	0,02	6	2	44,05
Uncharacterized protein	Psmd4	Q3UJG4	1,37	0,01	10	3	63,93
Clustered mitochondria protein homolog	Cluh	Q5SW19	1,36	0,03	7	4	47,24
Stenile alpha motif domain-containing protein 9-like	Samd9l	Q6ZQ37	1,35	0,04	27	2	146,47
Adenylosuccinate synthetase isozyme 2	Adss	P46664	1,35	0,01	11	9	88,69
Alpha-actinin-1	Actn1	Q7TPR4	1,34	0,02	55	7	451,26
Bifunctional polynucleotide phosphatase/kinase	Pnkp	Q3E8N7	1,34	0,00	11	2	68,29
Nuclear receptor coactivator 7	Ncoa7	Q6DFV7	1,33	0,03	7	2	24,74
HBS1-like protein	Hbs1l	Q3TGM7	1,32	0,03	3	2	15,76
AMP deaminase 3	Ampd3	O08739	1,32	0,01	27	6	168,85
Annexin A2	Anxa2	P07356	1,32	0,01	51	27	289,65
Bromodomain and WD repeat domain containing 2, isoform CRA_a	Wdr11	Q3E8J3	1,31	0,04	9	2	51,40
MHC class III H2-Sp (haplotype a) sex-limited protein mRNA (Fragment)		P01029	1,31	0,04	7	5	41,75
Eukaryotic translation initiation factor 3 subunit M	Eif3m	Q9QUK4	1,30	0,05	17	4	114,39
Hyaluronan synthase1	Has1	Q05A37	1,28	0,03	4	2	20,57
Phosphate carrier protein, mitochondrial	Slc25a3	Q8VEM8	1,22	0,03	26	8	175,82
Prolyl endopeptidase	Prep	Q54389	1,18	0,04	29	12	195,97
Probable ATP-dependent RNA helicase DDX17	Ddx17	Q50UI6	1,14	0,04	33	7	238,13

Supplementary Table 11. Upregulated proteins in *Prdx5*$^{-/-}$ primary macrophages compared to Prdx5$^{+/+}$ stressed by LPS. The most affected upregulated proteins in macrophages are listed with the fold change expression, the p values, the Accession number, the peptide counts, the unique peptides and the confidence scores.

Upregulated proteins in Prdx5-/- cells exposed to LPS compare to Prdx5+/+ cells exposed to LPS							
Description	**Short name**	**Accession**	**Max fold change**	**Anova (p)**	**Peptide count**	**Unique peptides**	**Confidence score**
Beta-globin	Hbbt2	A8DV59	2,41	0,02	26	3	160,02
OS=Mus musculus GN=Sash1 PE=1 SV=1	Sash1	F8VQK5	2,26	0,05	11	4	70,22
Heparan-alpha-glucosaminide N-acetyltransferase	Hgsnat	Q3UDW8	1,96	0,02	10	3	59,10
Proteasome subunit beta type-10	Psmb10	O35955	1,90	0,03	5	2	51,62
AW555464 protein	Cep170b	B9EIX2	1,89	0,02	7	2	29,77
Glutathione S-transferase P 1	Gstp1	P19157	1,87	0,01	6	2	43,30
Lysophospholipid acyltransferase 7	Mboat7	Q8CHK3	1,82	0,03	7	2	58,33
Protein phosphatase 1G	Ppm1g	Q61074	1,81	0,04	5	2	30,97
Netrin-G2	Ntng2	Q8R4F1	1,73	0,00	6	3	29,14
Utrophin	Utrn	A0A1W2P7C0	1,71	0,04	2	2	15,11
Uncharacterized protein (Fragment)		Q8BT78	1,57	0,04	4	2	25,14
Septin-11	Sept11	Q8C1B7	1,55	0,02	11	2	56,17
Tyrosine-protein kinase CSK	Csk	P41241	1,53	0,00	21	2	150,63
Plakophilin-4	Pkp4	A2AS45	1,51	0,02	4	2	25,29
Cysteine-rich with EGF-like domain protein 2	Creld2	Q9CYA0	1,47	0,02	2	2	11,31
Macrophage scavenger receptor types I and II	Msr1	P30204	1,35	0,04	11	2	75,85
Uncharacterized protein	Vps39	Q3USV9	1,33	0,04	12	4	61,96
Peroxisomal multifunctional enzyme type 2	Hsd17b4	P51660	1,30	0,03	5	3	24,98
Small nuclear ribonucleoprotein Sm D1	Snrpd1	P62315	1,29	0,03	8	4	47,62
Sister chromatid cohesion protein PDS5 homolog A	Pds5a	E9QPI5	1,26	0,00	30	12	179,29
Uncharacterized protein	Surf4	Q3U7E6	1,24	0,03	9	4	54,24
Period circadian protein homolog 3	Per3	O70361	1,21	0,04	6	2	28,48
Protein ABHD17C	Abhd17c	Q8VCV1	1,17	0,03	3	2	14,99
Adenylosuccinate synthetase isozyme 1	Adssl1	P28650	1,10	0,01	11	5	65,42
MCG16669, isoform CRA_b	Tardbp	Q544R5	1,05	0,03	13	4	78,44

Supplementary Table 12. Downregulated proteins in *Prdx5*$^{-/-}$ primary macrophages compared to Prdx5$^{+/+}$ stressed by LPS. The most affected upregulated proteins in macrophages are listed with the fold change expression, the p values, the Accession number, the peptide counts, the unique peptides and the confidence scores.

Downregulated proteins in Prdx5-/- cells exposed to LPS compare to Prdx5+/+ cells exposed to LPS							
Description	**Short name**	**Accession**	**Max fold change**	**Anova (p)**	**Peptide count**	**Unique peptides**	**Confidence score**
Peroxiredoxin-5, mitochondrial	Prdx5	P99029	419,82	0,00	16	3	125,32
CD82 antigen	Cd82	P40237	11,03	0,05	6	2	40,82
Src kinase-associated phosphoprotein 1	Skap1	Q3UUV5	4,86	0,01	4	2	21,51
Interleukin enhancer-binding factor 3	Ilf3	Q9Z1X4	3,28	0,01	7	2	43,20
Heme-binding protein 1	Hebp1	A0A140T8J4	2,57	0,04	6	2	41,75
Regulator of G-protein signaling 3	Rgs3	Q9DC04	2,09	0,01	4	2	18,69
SUMO-activating enzyme subunit 2	Uba2	Q9Z1F9	1,88	0,02	25	11	173,11
Keratin, type II cytoskeletal 6A	Krt6a	P50446	1,85	0,00	22	2	137,79
CD180 antigen	Cd180	Q62192	1,77	0,02	18	4	124,24
T-lymphocyte surface antigen Ly-9	Ly9	Q01965	1,64	0,02	16	7	101,84
Nuclear receptor subfamily 1, group D, member 2	Nr1d2	Q4VAB7	1,60	0,04	2	2	10,25
Guanylate-binding protein 1	Gbp1	Q01514	1,60	0,02	20	7	131,48
Hypoxia up-regulated protein 1	Hyou1	Q9JKR6	1,57	0,03	48	16	368,73
Axonemal dynein light chain domain-containing protein 1 (Fragment)	Axdnd1	J3KMJ8	1,56	0,04	8	2	44,00
TP53-binding protein 1	Tp53bp1	P70399	1,55	0,00	12	6	59,64
Immunity-related GTPase family Q protein	Irgq	Q8VIM9	1,53	0,01	2	2	14,59
Serine/threonine-protein kinase N2	Pkn2	Q8BWW9	1,52	0,04	15	2	72,20
Bifunctional UDP-N-acetylglucosamine 2-epimerase/N-acetylmannosamine kinase	Gne	Q3UW64	1,52	0,05	6	2	25,98
Cyp4f15 protein	Cyp4f15	Q8VCA4	1,45	0,02	10	3	64,38
Zinc finger protein 395	Zfp395	E9Q5N9	1,43	0,03	6	2	21,72
NADH dehydrogenase [ubiquinone] 1 beta subcomplex subunit 10 (Fragment)	Ndufb10	D3YUK4	1,36	0,05	8	3	57,44
Cyclic AMP-responsive element-binding protein 5	Creb5	A0A0N4SUW5	1,36	0,04	3	3	20,71
Arachidonate 5-lipoxygenase-activating protein	Alox5ap	P30355	1,32	0,02	20	18	85,34
PHD finger protein 21B	Phf21b	F8WGM2	1,30	0,02	2	2	15,05
Adenylosuccinate synthetase isozyme 2	Adss	P46664	1,23	0,05	11	9	88,69
Testis-specific gene 10 protein	Tsga10	Q6NY15	1,22	0,04	13	5	68,92
CTP synthase 2	Ctps2	P70303	1,21	0,01	14	9	102,32

6. Role of peroxiredoxin-5 in tumor suppression: higher occurrence of lymphoma and hepatocarcinoma in *Prdx5* knockout mice

Vasiliki Argyropoulou[1], Charlotte Lefort[1], Morgane Dress[1], Yves Guiot[2], Etienne Marbaix[3], Christine Galant[4], Nicolas Van Baren[5], Bernard Knoops[1]*

Authors affiliation : *[1]Group of Animal Molecular and Cellular Biology, Louvain Institute of Biomolecular Science and Technology (LIBST), Université catholique de Louvain (UCLouvain), 1348, Louvain-la-Neuve, Belgium ; [2]Department of Pathology, Institut de Recherche Expérimentale et Clinique (IREC), Université catholique de Louvain (UCLouvain), Woluwe, Belgium ; [3]Department of Cellular Biology, Institut de Duve, Université catholique de Louvain (UCLouvain), Woluwe, Belgium ; [4]Department of Surgery, Institut de Recherche Expérimentale et Clinique (IREC), Université catholique de Louvain (UCLouvain), Woluwe, Belgium ; [5]Génétique Cellulaire, Institut de Duve, Université catholique de Louvain (UCLouvain), Woluwe, Belgium*

***Correspondence to:** Bernard Knoops, Group of Animal Molecular and Cellular Biology, Louvain Institute of Biomolecular Science and Technology (LIBST), Université catholique de Louvain (UCLouvain), 1348, Louvain-la-

Neuve, Belgium. Phone: +32-10-473760; Fax: +32-10-473515. email: bernard.knoops@uclouvain.be

Running title: Role of peroxiredoxin-5 in tumor suppresion

Keywords: Peroxiredoxin, Prdx5, antioxidant, carcinogenesis, lymphoma, hepatocarcinoma

6.1 Abstract

Peroxiredoxin-5 (Prdx5) is a well-conserved member of peroxiredoxins which is expressed virtually in all tissues of mammals. The main goal of this work was to examine *in vivo* the possible role of Prdx5 as tumor suppressor. *Prdx5* knockout mice (*Prdx5*$^{-/-}$) are viable and fertile but 41% of aging *Prdx5*$^{-/-}$ mice (between 12 and 30 month-old) developed significantly more malignant cancers compared to 16% of aging *Prdx5*$^{+/+}$ animals, suggesting that Prdx5 protein is involved in tumor suppression. Most of the cancers have been histologically analyzed and characterized as lymphoma and hepatocarcinoma. Also, the Akt/PTEN signaling pathway was examined in *Prdx5*$^{-/-}$ mouse embryonic fibroblasts (MEF) by exposing the cells to H_2O_2, LPS, *t*BHP and SIN-1. Our results showed that phosphorylation of Akt is significantly higher in *Prdx5*$^{-/-}$ MEF cells exposed to H_2O_2. Moreover, Western

blotting analyses of Akt/PTEN and MAPK signaling pathways in tumor samples showed that Akt phosphorylation of Akt (Thr308) and p44 was higher in several tumors, while PTEN expression was decreased. These data, but also proteomic observations of the downregulation of proteins related to apoptosis and cell survival in *Prdx5*$^{-/-}$ macrophages, such as the caspase-3, caspase-8 and septin-7, lead us to hypothesize that Prdx5 may play important role in tumor suppression.

6.2 Introduction

Peroxiredoxins (Prdxs or Prxs) are a superfamily of thiol-dependent peroxidases now recognized as major antioxidant enzymes like glutathione peroxidases [1]–[3]. Prdxs reduce hydrogen peroxide, alkyl hydroperoxydes and peroxynitrite in prokaryotic and eukaryotic cells [2], [4], [5]. They are present in all living organisms [3] and more specifically in mammals, the Prdx family is represented by six members (Prdx1-6) [2], [3]. In mammals, Prdxs are localized in different subcellular compartments [6]. Prdxs can be classified in three different subgroups, based mainly on their catalytic mechanism and the number of catalytic cysteines in their molecules [7]. The typical 2-Cys Prdxs (Prdx1-4) have two active cysteines in their molecules and

form an intramolecular disulfide bond upon oxidation. The atypical 2-Cys Prdx (Prdx5) exhibits two active cysteines too but the disulfide bond is intermolecular. Finally the 1-Cys Prdx (Prdx6) has only one catalytic cysteine in its molecule. Prdx5 is the last isoform that has been identified and characterized in mammals. In human and murine cells, Prdx5 can be localized in cytoplasm, nucleus, peroxisomes and mitochondria [7]–[16].

Recently, several studies have revealed different roles for Prdxs in carcinogenesis and tumorigenesis. Indeed, it was reported that Prdxs could inhibit apoptosis and favor cancer cell proliferation but on the other hand it was also shown that Prdxs can act as tumor suppressors [17]. Only a few studies focused on mechanisms implicating Prdxs as tumor suppressors. The most characteristic example is the case of Prdx1, where *Prdx1*$^{-/-}$ mice present hemolytic anaemia and lymphoma [18]. The implication of Prdx1 in the PI3K/Akt/PTEN signaling pathway, a well-studied pathway leading to cell proliferation and tumorigenesis, was investigated. Prdx1 is able to bind to PTEN, a tumor suppressor protein, protecting in this way the PTEN lipid phosphatase activity from inactivation under oxidative stress conditions [19]. When Prdx1 is absent, PTEN is highly oxidized, resulting in Akt high phosphorylation [19]. There are two major sites of phophorylation on Akt that are targeted by two different kinases. Indeed, Pyruvate dehydrogenase kinase 1 (PDK1) phosphorylates Akt on Thr308,while mTOR-Rictor complex

(mTORC2) is responsible for the phosphorylation of Ser473 [37].The phosphorylation of Akt plays a central role in Ras and ErbB-2-induced transformation. Additionally, Prdx1 has been shown to interact with p38 MAPK to promote the mobility and invasion of pancreatic cancer cells [20], while in another study Prdx1 was shown to suppresses the phosphorylation of p38 MAPK and JNK in mouse embryonic fibroblasts (MEFs), acting as anti-apoptotic protein and reducing the oxidative stress damage [21].

A few studies have examined the possible role of Prdx5 in carcinogenesis and tumorigenesis although Prdx5 was shown to be highly expressed in different cancers, such as in colon, gastric, endometrial, breast and lung cancer and also aggressive Hodgkin's lymphomas. These studies suggest that Prdx5 may be involved in cell protection against apoptosis and promote tumorigenesis [22]–[29]. Indeed, it was shown that *Prdx5* transcription mediated by E-twenty-six transcription factor 1 and 2 (Ets1/2) and high-mobility-group protein B1 (HMGB1), is induced in human prostate and epidermoid cancer cells exposed to H_2O_2 or hypoxia, leading to cell resistance against oxidative stress [30]. On the other hand, it has been also proposed that Prdx5 has a tumor suppressor role in adrenocortical carcinoma and in breast cancer [31], [32], since its expression is downregulated in these cancers.

In this study, we report that in aging Prdx5-deficient mice malignant cancers develop significantly more frequently than in aging wild type animals.

Additionally, we investigated the possible implication of Prdx5 in PI3K/Akt/PTEN and MAPK signaling pathways related to tumorigenesis.

6.3 Results

6.3.1 Histological analysis of tissues and tumors

All *Prdx5*$^{-/-}$ and *Prdx5*$^{+/+}$ mice were followed daily in the animal facility. 21 *Prdx5*$^{-/-}$ mice out of 51 (41.18%) presented spontaneously tumors after the age of 12 months, while only 10 *Prdx5*$^{+/+}$ mice out of 62 (16.13%) developed tumors after the age of 12 months (Fig.1A). Tumors in Prdx5$^{-/-}$ mice were present mainly in the abdomen and the neck (Fig.1B). Complete examination

Table 1. *Prdx5*$^{+/+}$ and *Prdx5*$^{-/-}$ mice used for the experiments. Hematoxylin-eosin staining; IHC: Immunohistochemistry; WB: Western Blotting

Prdx5*$^{-/-}$ *Mouse	**Analysis**
281	Hematoxylin-eosin/IHC
483	Hematoxylin-eosin/IHC
323	Hematoxylin-eosin/IHC
498	Hematoxylin-eosin/IHC
573	Hematoxylin-eosin/IHC/WB
601	Hematoxylin-eosin/IHC/WB
591	Hematoxylin-eosin/IHC
423	Hematoxylin-eosin/IHC
615	Hematoxylin-eosin/WB
911	Hematoxylin-eosin/WB
Prdx5*$^{+/+}$ *Mouse	**Analysis**
544	Hematoxylin-eosin/IHC
607	Hematoxylin-eosin/IHC/WB
345	Hematoxylin-eosin/IHC
166 (chimera)	Hematoxylin-eosin/IHC
1027 (control)	Hematoxylin-eosin/WB

of these mice revealed different metastases in other organs, such as lungs, liver, kidneys, stomach, salivary glands and spleen (Fig.1C-F). It is worth to mention that the majority of mice with tumors presented splenomegaly (Fig.1C). The main tumors were formed near organs and they consisted in a solid mass. Tumors were large (2-5 cm) and of red-brown color. It must but noted also that tumors of *Prdx5*$^{+/+}$ mice were mainly present next to the paw, they were smaller (1-2cm) and appeared more white. The number of the mice used for these experiments are summarized in the Table 1.

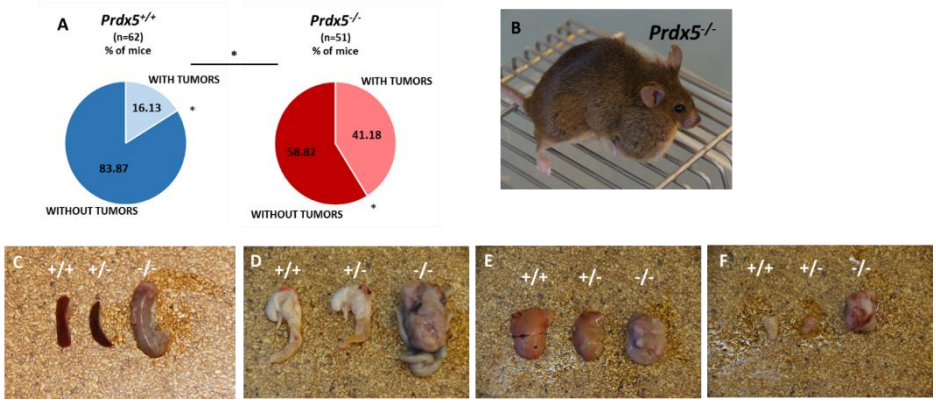

Figure 1. Malignant tumor development in Prdx5$^{-/-}$ and Prdx5$^{+/+}$ mice. *(A) Pie representation of the % of Prdx5$^{-/-}$ and Prdx5$^{+/+}$ mice in which malignant tumors developed. In total 62 Prdx5$^{+/+}$ and 51 Prdx5$^{-/-}$ mice, only the 10 (16.13%) and 21 (41.18%) developed tumors, respectively. Significant is designed by * (p<0.05), ** (p<0.01), *** (p<0.005). (B) Prdx5$^{-/-}$ mouse with tumor in the neck. (C-F) Tumors observed in tissues or organs of Prdx5$^{-/-}$ mice at 15 months of age compared to the same tissue or organ in Prdx5$^{+/-}$ and Prdx5$^{+/+}$ mice of the same littermate. Illustrations of tumors associated to the spleen (C), the stomach (D), the liver (E) or salivary glands (F).*

Sections of all tumors were examined with hemalun-eosine staining (Fig. 2). Some tumors were almost completely composed of small cells, typical lymphocytes, as the two tumors of the 281 *Prdx5*$^{-/-}$ mouse (Fig.2A-B). These tumors appeared to be lymphomas or a type of non-lymphoid hematopoietic tumor. Note that the 281 *Prdx5*$^{-/-}$ mouse presented infiltrations of these cell types in most of its organs except heart and brain. Tumors of 601 *Prdx5*$^{-/-}$ and 607 *Prdx5*$^{+/+}$ mice presented larger cells, similar to hepatocytes, suggesting that these tumors were hepatocarcinomas (Fig.2E-F). The abdominal tumor of 601 Prdx5$^{-/-}$ mouse presented also infiltrated lymphocyte-like cells (Fig.2E).

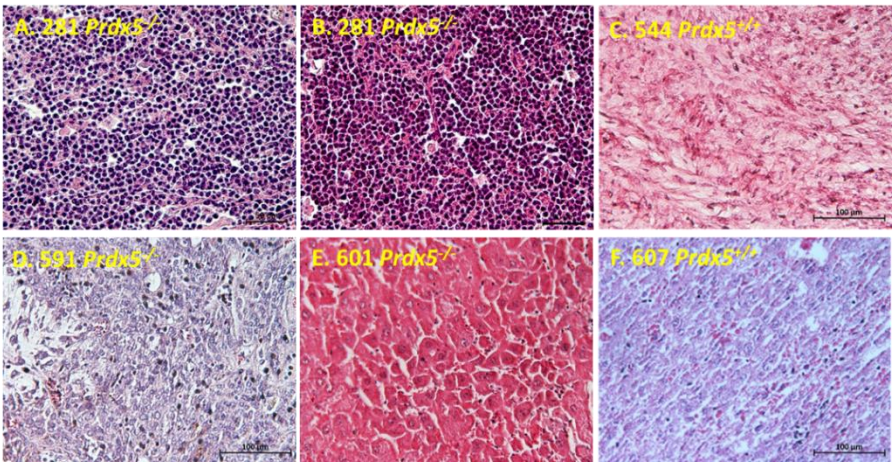

Figure 2. Hematoxylin-eosin-stained sections of different tumors in Prdx5$^{-/-}$ and Prdx5$^{+/+}$ mice. *The 281 Prdx5$^{-/-}$ tumors in the abdomen (A) and in the neck (B) present a large amount of small cells, typical for lymph node. The 544 Prdx5$^{+/+}$ (C) and 591 Prdx5$^{-/-}$ (D) sections are tumors in the paws. The 601 Prdx5$^{-/-}$ (E) and 607 Prdx5$^{+/+}$ (F) sections are presenting tumors from liver.*

At high magnification tumor cells of 281 *Prdx5*$^{-/-}$ mouse (Fig.2A-B) presented round nuclei, with chromatin in small scattered heaps but also small and

multiple nucleoli. These cells appeared to be proliferating but with apoptosis as well. The tumor of 323 and 483 *Prdx5*$^{-/-}$ mice, with similar cells, also showed important proliferation associated with a strong apoptosis (data not shown). Tumor of 483 *Prdx5*$^{-/-}$ mouse was composed of medium to large cells with a round nucleus with one or more nucleoli (data not shown). The tumor of 544 *Prdx5*$^{+/+}$ mouse (Fig.2C) showed connective tissue-like structures with somewhat oblong cells surrounded by fibers. Nucleolus was not visible in the nuclei. The tumor of 498 *Prdx5*$^{-/-}$ mouse showed lymphocyte-like cell infiltrations between glandular cells (data not shown). Cells appeared in mitosis, with the chromatin well separated, the nuclei were more or less round. The tumor of 591 *Prdx5*$^{-/-}$ mouse (Fig.2D) is a heterogeneous tissue, comprising lymphocyte-like cells of medium size, as well as other cell types. Lymphocytes have a more or less round nucleus with one or more nucleoli. The tumor of *423 Prdx5*$^{-/-}$ mouse is particular because it exhibits very few cells (data not shown). A high concentration of red blood cells is observable, and the rest of the tissue is much disorganized, showing a connective tissue structure. The tumor of 345 *Prdx5*$^{+/+}$ mouse showed very few cells that can resemble monocytes or granulocytes, due to the apparent shape of their nucleus (data not shown). Finally, the tumors of the 573 *Prdx5*$^{-/-}$ mouse exhibited medium-sized cells, with somewhat oblong nuclei and chromatin in small scattered heaps (data not shown).

6.3.2 *Prdx5*$^{-/-}$ mice develop different types of lymphoma and hepatocarcinoma

To complete tumor characterization, immunohistochemical analyses of the tumors were performed. Antibodies used were directed to cell markers allowing cell and tumor characterization (Table 2). CD3 is a receptor for T lymphocytes while CD4 and CD8α are specific for some T-cell types. Indeed, CD4 is a glycoprotein found on the surface of T-helper lymphocytes and CD8α is found on the surface of cytotoxic T lymphocytes and Natural Killer cells. CD11, CD31 and CD34 are expressed by neutrophils, myeloid cells, and finally hematopoietic stem cells and megakaryocytes, respectively. F4/80 is also a marker of mouse macrophages. Myeloperoxidase (MPO) is an enzyme highly expressed by neutrophilic granulocytes for the production of halogenated acids that have antimicrobial activity. MPO immunoreactivity allows the

Table 2. Antigens and their target cells or proteins used as markers for tumor immunohistochemistry analysis. The first column presents the antigens recognized by the antibodies. The second column gives the target cell or protein of the antibodies. The source of the antibodies are presenting in the third column and their dilution for the Immunohistochemistry in the fourth column.

Antigen	Target cell/protein	Source	Dilution
CD3	T lymphocytes	Rabbit monoclonal, Abcam, ab16669	1/500
CD4	T-helper lymphocytes	Rabbit monoclonal, Abcam, ab183685	1/1000
CD8α	Cytotoxic T lymphocytes, Natural Killer T cells, Dendritic cells	Rabbit monoclonal, Cell Signaling, 98941	1/400
CD11b	Neutrophils	Rat monoclonal, Iowa-DSHB, M1/70.15.11.5.2	1/500
CD19	B lymphocytes	Rat monoclonal, Abcam, ab25232	1/500
CD31/PECAM-1	Endothelial cells, platelets, macrophages, lymphocytes, myeloid cells	Armenian hamster monoclonal, Iowa-DSHB, 2H8	1/500
CD34	Hematopoietic progenitor stem cells, megakaryocytes	Rabbit monoclonal, Abcam, ab81289	1/1000
F4/80	Macrophages	Rat monoclonal, Bio-Rad, MCA497	1/500
MPO	Myeloperoxidase	Rabbit polyclonal, Abcam, ab9535	1/100
Ki-67	Proliferation marker	Rabbit polyclonal, Abcam, ab15580	1/400
Cytokeratin 8/18	Keratinocytes	Rat monoclonal, Iowa-DSHB, TROMA-I	1/100
Cytokeratin 19	Keratinocytes	Rat monoclonal, Iowa-DSHB, TROMA-III	1/120
p-AKT (Ser473)	phospho-AKT (Ser473)	rabbit monoclonal, Cell Signaling, 4060	1/100
p-AKT (Thr308)	phospho-AKT (Ser473)	rabbit monoclonal, Cell Signaling, 13038	1/1600
AKT (pan)	total AKT	rabbit monoclonal, Cell Signaling, 4691	1/300
PTEN	PTEN	rabbit monoclonal, Cell Signaling, 9188	1/125
β-actin	β-actin (positive control)	Rabbit polyclonal, Sigma, A2066	1/1000

detection of cells originating from the myeloid line, such as basophils, neutrophils, eosinophils, monocytes, macrophages and consequently the detection of leukemia or sarcomas. Ki-67 marker is detectable exclusively in the nuclei of the interphase cells and on the chromosomes in the cells in mitosis. Finally, cytokeratins 8/18 and 19 are part of the family of keratins, components of intermediate filaments, which are specific to particular tissues and organs. Cytokeratin 8/18 is present in significant amounts in hepatocarcinoma and adenocarcinoma type 1 although cytokeratin 19 is present in the adenocarcinomas. All tumors were analyzed in immunohistochemistry using the same antibodies in order to characterize and identify the type of cancer in *Prdx5*$^{-/-}$ and *Prdx5*$^{+/+}$ mice. Table 2 summarizes immunohistochemistry results for each marker used in this study and the type of tumors based on cancer classification in mice [33], [34].

Two representative tumors, one with hepatocyte-like cells derived from 601 *Prdx5*$^{-/-}$ mouse and one with lymphocyte-like cells from the 323 *Prdx5*$^{-/-}$ mouse are presented (Fig.3). Immunostaining control is a β-actin immunodetection and the negative control was achieved by omitting the primary antibody. The tumor of 601 *Prdx5*$^{-/-}$ mouse (Fig.3I-L) was labeled with antibodies against cytokeratins, assuming that cells examined using hemalun-eosin staining were indeed hepatocytes. The significant immunostaining with anti-cytokeratin 8/18 but not with anti-cytokeratin 19 suggests that this tumor is a hepatocarcinoma. The liver of the 607 *Prdx5*$^{+/+}$ mouse, and the liver and abdominal tumor of the 601 *Prdx5*$^{-/-}$ mouse showed the same staining, which classified the cancer as hepatocarcinoma too (Table

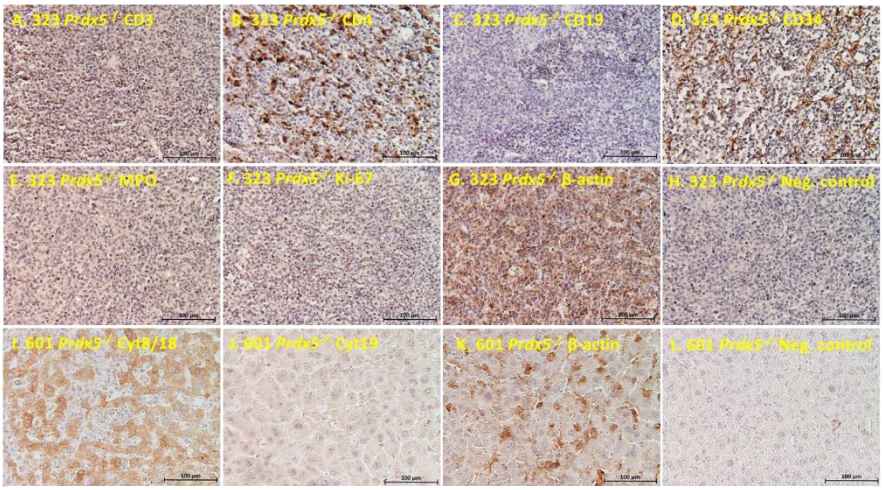

Figure 3. Immunohistochemistry of Prdx5$^{-/-}$ lymphoma and hepatocarcinoma. *Immunostaining was performed with antibodies directed to different markers (see table 1) on sections of lymphoma tumor of 323 Prdx5$^{-/-}$ mouse and hepatocarcinoma tumor of 601 Prdx5$^{-/-}$ mouse. (A) 323 Prdx5$^{-/-}$ CD3, (B) 323 Prdx5$^{-/-}$ CD4, (C) 323 Prdx5$^{-/-}$ CD19, (D) 323 Prdx5$^{-/-}$ CD34, (E) 323 Prdx5$^{-/-}$ MPO, (F) 323 Prdx5$^{-/-}$ Ki-67, (G) 323 Prdx5$^{-/-}$ β-actin (positive control), (H) 323 Prdx5$^{-/-}$ negative control, (I) 601 Prdx5$^{-/-}$ Cyt8/18, (J) 601 Prdx5$^{-/-}$ Cyt19, (K) 601 Prdx5$^{-/-}$ β-actin (positive control), (L) 601 Prdx5$^{-/-}$ negative control.*

3). The tumor of 323 *Prdx5*$^{-/-}$ mouse (Fig.3A-H) was labeled with antibodies directed to hematopoietic tumor-related markers, which were selected after observation of small cells detected with hemalun-eosin staining. This tumor is representative of hematopoietic tumors and is stained for all lymphocyte markers (CD3, CD4, CD19) and other myeloid cell markers (CD34, MPO), as well as the proliferation marker Ki-67. The tumor exhibited a strong staining for CD3 and CD4, indicating the presence of T cells, especially T-helpers (Fig.3A-B).

Table 3. Summary of mice, tissues and markers used to characterize tumors collected from *Prdx5*$^{-/-}$ and *Prdx5*$^{+/+}$ mice. The level of marker immunoreactivity is indicated. (-) non-detectable, (+/-) weak staining (close to background), (+) positive staining in this cell type, (++) stronger positive staining compared to other cell types, (+++) intense staining. The number and the genotype of the mouse are indicated in the first column.

Mouse	Tissue	Markers									Characterization
		positive control	T lymphocytes		B lymphocytes	Myeloid cells		Proliferation	Carcinoma		
		Actin	CD3	CD4	CD19	CD34	MPO	Ki-67	Cyt 8/18	Cyt19	
281 *Prdx5*$^{-/-}$	Tumor - Abdomen	+++	+	-	+++	+	++	+++			Burkitt's lymphoma
	Tumor - Neck	++	+	+	-	++	++	+++			Myeloid sarcoma
483 *Prdx5*$^{-/-}$	Tumor - Neck	++	+	++	-	+	?	++			Precursor T- lymphoblastic lymphoma
323 *Prdx5*$^{-/-}$	Tumor - Abdomen	+++	+++	+++	+	+++	+	+++			Precursor T- lymphoblastic lymphoma
498 *Prdx5*$^{-/-}$	Tumor - Tissue part	+++	+++	+++	++	+++	-	+++			B-cell lymphoma
	Tumor - Fibrus part	+++	+++	++	+++	++	+++	++			B-cell lymphoma
591 *Prdx5*$^{-/-}$	Tumor - Paw	++	++	+++	+	++	++	+++			Anaplastic large cell lymphoma or B-cell lymphoma
423 *Prdx5*$^{-/-}$	Tumor - Abdomen	+++	+++	+++	+++	+++	+++	+++			B-cell lymphoma or Leukemia
601 *Prdx5*$^{-/-}$	Tumor - Abdomen	++	+	++	+	-	-	++	++	-	Hepatocarcinoma
	Liver	++	+	+	-	+	+++	+	+++	-	Hepatocarcinoma
573 *Prdx5*$^{-/-}$	Tumor - Paw	+++	+++	+	+	++	++	+++			Precursor T- lymphoblastic lymphoma
	Tumor - Abdomen	++	-	+	-	++	+++	++			Sarcoma
544 *Prdx5*$^{+/+}$	Tumor - Paw	+	+/-	+/-	-	+	+	+			Lipoma or edema
607 *Prdx5*$^{+/+}$	Liver	+++	++	+/-	+/-	-	-	+	+	-	Hepatocarcinoma
345 *Prdx5*$^{+/+}$	Tumor - Testis	+++	-	++	+/-	-	+++	++			Myeloid leukemia

The CD19 staining was less strong and it can thus be concluded that the tumor is composed mainly of T lymphocytes and not of B lymphocytes (Fig.3C). A strong CD34 staining indicated also the presence of megakaryocytes or hematopoietic stem cells (Fig.3D). Immunodetection of

CD8α, CD11b, CD31 and F4/80 was negative for this tumor. A few cells were labeled for MPO, indicating that the tumor was composed mainly of lymphocytes and not non-lymphoid hematopoietic cells (Fig.3E). The cells were also strongly labeled with anti-Ki-67, indicating that they were under proliferation (Fig.3F). This cancer was thus classified as precursor T-lymphoblastic lymphoma (T-LBL). The cervical tumor of the mouse 483 *Prdx5*$^{-/-}$ was composed of similar cells as the tumor of the 323 *Prdx5*$^{-/-}$ mouse and this cancer was thus also classified as precursor T-LBL (Table 3). The abdominal tumor of the 281 *Prdx5*$^{-/-}$ mouse was composed of B lymphocytes (CD19 positive cells) while the cervical tumor was composed of non-lymphoid hematopoietic cells (CD34, MPO positive cells). Also, the cells were actively dividing as they were Ki-67 positive. The abdominal tumor corresponded to a Burkitt's lymphoma, while the cervical tumor is closer to a myeloid sarcoma due to absence of mature lymphocyte markers. The 544 *Prdx5*$^{+/+}$ mouse had a tumor in the right hind paw. This neoplastic tissue did not appear to be a lymphoma or a non-lymphoid hematopoietic tumor. The loose structure of the tissue suggests a lipoma or edema, thus a benign tumor of the mesenchyme. The cervical tumor of the 498 *Prdx5*$^{-/-}$ mouse was composed of highly proliferating cells but positive for both T (CD3, CD4) and B (CD19) lymphocytes markers. The presence of T and B cell markers made characterization more complicated, assuming that the tumor is B-cell

lymphoma. The abdominal tumor of the 423 *Prdx5*$^{-/-}$ mouse presented the same features. The presence of infiltrated cells in the lungs and spleen, as well as MPO and CD34 labeling, in addition to the large number of erythrocytes could indicate that the cancer corresponded to erythroid leukemia. However, the presence of mature T and B lymphocytes suggested that it could correspond to lymphoma rather than leukemia and complicated the diagnosis. The 591 *Prdx5*$^{-/-}$ mouse presented a tumor in the right front paw, composed of highly proliferative cells with marker for helper T cells and myeloid cells (CD34). Due to the presence of large cells, with low cytoplasm, large and irregular nuclei as well as high proliferation, and the presence of predominantly T cells, the cancer could be classified as anaplastic large cell lymphoma. However, as this type of cancer is rare, its immunohistological phenotype is not known, and the tumor examined here appeared to include other cell types like B lymphocytes, no clear conclusion can be drawn on the characterization of this cancer. The testicular tumor of 345 *Prdx5*$^{+/+}$ mouse was composed of few non-lymphocytic but myeloid and highly proliferative cells. A close-up of the hemalun-eosin stained cells, as well as a more accurate cell observation in the MPO- and Ki-67-labeled sections, showed that the nuclei of these cells are deformed, suggesting the presence of monocytes or granulocytes. This cancer appeared to be a myeloid leukemia. Finally, the 573 *Prdx5*$^{-/-}$ mouse presented a tumor in the paw composed of T

lymphocytes (CD3 positive), poorly differentiated (weak CD4 labeling) and strongly proliferative (Ki-67 positive). This cancer appeared to be precursor T-lymphoblastic lymphoma. On the other hand, the abdominal tumor cells of the same mouse were mostly myeloid (MPO, high CD34, CD3, weak CD19 positive) suggesting that it could correspond to a sarcoma.

6.3.3 Loss of Prdx5 promotes Akt activation by H_2O_2 in MEF cells

Because Akt/PTEN pathway is known to be involved in carcinogenesis and Prdxs have been reported to modulate this pathway [18], [19], we investigated whether Prdx5 may also regulate Akt/PTEN pathway. Treatment of MEFs with H_2O_2 (0-50-100-200µM) for 10 min enhanced Akt phosphorylation of Ser473 (pAkt Ser473) and Thr308 (pAkt Thr308) at a higher levels in *Prdx5*$^{-/-}$ MEF cells compared to *Prdx5*$^{+/+}$ MEF cells (Fig.4A). We do not observe any differences in the phosphorylation of Akt during 100 ng/ml LPS exposure between 0 and 16 hours (Fig.4B). For the MEF cells exposed to 100µM *t*BHP, the phosphorylation level of the Thr308 residue took off and declined gradually over time, for both *Prdx5*$^{+/+}$ and *Prdx5*$^{-/-}$ conditions (Fig.4C). Finally, exposure to 1 mM SIN-1 did not induce Akt phosphorylation in *Prdx5*$^{+/+}$ nor in *Prdx5*$^{-/-}$ MEF cells (Fig.4D). It must be

pointed out here that only exposure of MEF cells to H_2O_2 induced significantly Akt phosphorylation under our experimental conditions.

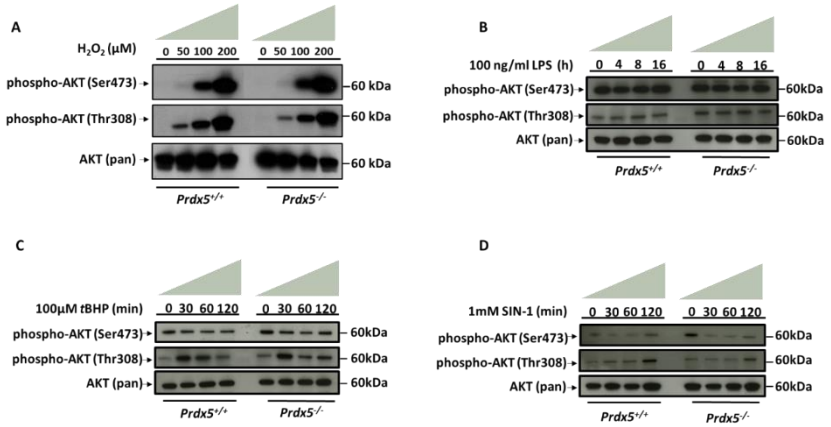

Figure 4. Western blotting analysis of Akt proteins in MEF cells. *(A) Western blotting analysis of MEF cell proteins from Prdx5$^{+/+}$ and Prdx5$^{-/-}$ mice exposed to 0-200μM H_2O_2 for 10 minutes with antibodies anti-phospho-Akt Ser473, anti-phospho-Akt Thr308 and anti-Akt pan. (B) Western blotting analysis of MEF cell proteins from Prdx5$^{+/+}$ and Prdx5$^{-/-}$ mice exposed to 100ng/ml LPS for 0-16 hours labeled with antibodies anti-phospho-Akt Ser473, anti-phospho-Akt Thr308 and anti-Akt pan. (C) Western blotting analysis of MEF cell protein from Prdx5$^{+/+}$ and Prdx5$^{-/-}$ mice exposed to 100μM tBHP for 0-120 minutes with antibodies anti-phospho-Akt Ser473, anti-phospho-Akt Thr308 and anti-Akt pan. (C) Western blotting analysis of MEF cell proteins from Prdx5$^{+/+}$ and Prdx5$^{-/-}$ mice exposed to 1mM SIN-1 for 0-120 minutes with antibodies anti-phospho-Akt Ser473, anti-phospho-Akt Thr308 and anti-Akt pan. (E-F) Quantification by immunoblotting of the phosphorylation of p-Akt (Ser473 and Thr308) expressed as a ratio of the amount of the phosphorylated form on total phosphorylated and non-phosphorylated forms, in MEF cells exposed to 0-200μM H_2O_2. (G-H) Western blotting quantification of the phosphorylation of p-Akt (Ser473 and Thr308) expressed as a ratio of the amount of the phosphorylated form on total of phosphorylated and non-phosphorylated forms, in MEF cells exposed to 100ng/ml LPS. (I-J) Western blotting quantification of the phosphorylation of p-Akt (Ser473 and Thr308) expressed as a ratio of the amount of the phosphorylated form on total phosphorylated and non-phosphorylated forms, in MEF cells exposed to 100μM tBHP. (K-L). Western blottingquantification of the phosphorylation of p-Akt (Ser473 and Thr308) expressed as a ratio of the amount of the phosphorylated form on total phosphorylated and non-phosphorylated forms, in MEF cells exposed to 1mM SIN-1.*

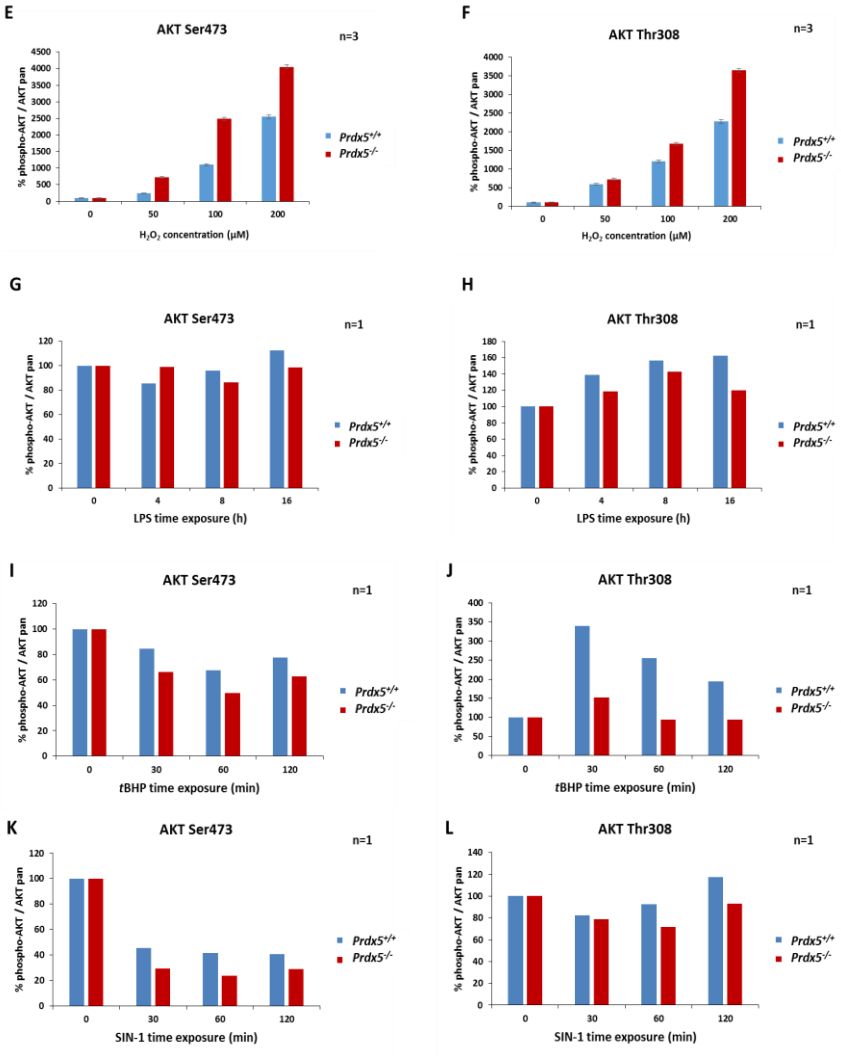
E
AKT Ser473
n=3
% phospho-AKT / AKT pan
H2O2 concentration (μM)
Prdx5+/+
Prdx5-/-
F
AKT Thr308
n=3
% phospho-AKT / AKT pan
H2O2 concentration (μM)
Prdx5+/+
Prdx5-/-
G
AKT Ser473
n=1
% phospho-AKT / AKT pan
LPS time exposure (h)
Prdx5+/+
Prdx5-/-
H
AKT Thr308
n=1
% phospho-AKT / AKT pan
LPS time exposure (h)
Prdx5+/+
Prdx5-/-
I
AKT Ser473
n=1
% phospho-AKT / AKT pan
tBHP time exposure (min)
Prdx5+/+
Prdx5-/-
J
AKT Thr308
n=1
% phospho-AKT / AKT pan
tBHP time exposure (min)
Prdx5+/+
Prdx5-/-
K
AKT Ser473
n=1
% phospho-AKT / AKT pan
SIN-1 time exposure (min)
Prdx5+/+
Prdx5-/-
L
AKT Thr308
n=1
% phospho-AKT / AKT pan
SIN-1 time exposure (min)
Prdx5+/+
Prdx5-/-

6.3.4 Akt/PTEN and MAPK signaling pathways in *Prdx5*$^{-/-}$ tumors

To examine further whether Akt/PTEN but also MAPK signaling pathways were affected in *Prdx5*$^{-/-}$ tumors, Western blotting analyses were carried out to compare tumors and hypertrophied tissues of *Prdx5*$^{+/+}$ and *Prdx5*$^{-/-}$ mice. Expression and phosphorylation level analyses were first performed for Akt and its phosphorylated forms as well as for PTEN in tumors of *Prdx5*$^{-/-}$ mice by immunohistochemistry (Fig.5). Tumor cells were strongly labeled for Akt-pan and PTEN, whereas the labeling for the phosphorylated forms of Akt (Ser473 and Thr308 residues) were much less intense (Fig.5).

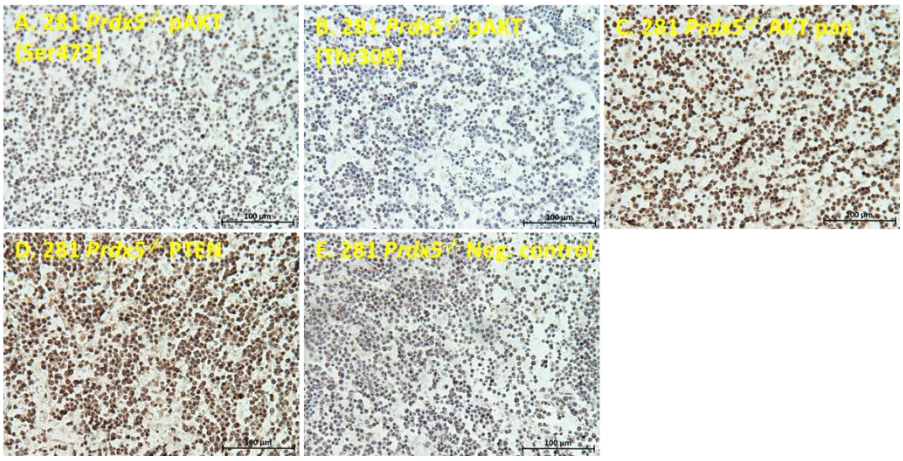

Figure 5. Akt and PTEN immunohistochemistry of Prdx5$^{-/-}$ lymphoma. Immunostaining with antibodies directed to Akt and PTEN in sections of the abdomen tumor of the 281 Prdx5$^{-/-}$ mouse. *(A) p-Akt (Ser473), (B) p-Akt (Thr308), (C) Akt pan, (D) PTEN, (E) negative control.*

Activation of Akt/PTEN pathway in tumors of *Prdx5*$^{-/-}$ mice was also examined by Western blotting (Fig.6A). Western blotting analyses showed that Akt

phosphorylation of Thr308 was higher in certain tumors, such as the tumor in the paw and the abdominal tumor of 573 *Prdx5*$^{-/-}$ mouse, and the liver of 607 *Prdx5*$^{+/+}$ mouse (hepatocarcinoma), in comparison with control tissues. The other tumors that were examined showed quite similar phosphorylation levels to those of control tissues. The Akt and PTEN levels were not quantified for protein samples of seminal glands because proteins of the seminal gland of 607 *Prdx5*$^{+/+}$ and 615 *Prdx5*$^{-/-}$ mice were very weakly detected. Additionally, only the two tumors of the 573 *Prdx5*$^{-/-}$ mouse appeared to show a weakened concentration of PTEN, compared to the control (Fig.6A). On the other hand, all the samples of neoplasms examined exhibited lower PTEN levels than control liver.

Phosphorylation of SAPK/JNK, p44/42 and p38 proteins were examined for MAPK pathway (Fig.6B-D). Phospho-SAPK/JNK was very poorly detected in all tissues examined, even the controls (Fig.6D). The low levels did not allow quantification. Phospho-p38 was less detected in all tumors compared to liver control (Figure 6B). On the other hand, phospho-p38 was undetectable in control spleen and present at low levels in tumors. Phospho-p44/42 was detected but at low levels in most tissues except in 573 *Prdx5*$^{-/-}$ mouse abdominal tumor in which p-p44/42 was even more detected than in the control liver (Fig.6C).

The two tumors of the 573 *Prdx5*$^{-/-}$ mouse showed similar expression levels of the proteins of interest except for the phospho-p44/42, which was more detected in the abdominal tumor. Overall, the levels of the phosphorylated form in Akt (Thr308) was higher in these two tumors, whereas PTEN appeared to be under-expressed (Fig.6A). Phospho-p38 was present at a moderate level, compared to the levels measured in the other samples, while the phospho-SAPK/JNK was almost non-detectable. The two tumors of the 601 *Prdx5*$^{-/-}$ mouse exhibited the same low level for both phospho-Akt with the liver control, while in the abdominal tumor PTEN level was higher. The tumor of 607 *Prdx5*$^{+/+}$ mouse also exhibited low level of phospho-Akt, high PTEN level, an average phospho-p38 level and low level of phospho-p44/42 compared to the levels in other tumors. Finally, the tumor of 911 *Prdx5*$^{-/-}$ mouse showed low levels of phosphorylated forms of Akt, an average level of PTEN and phospho-p38, as well as a slightly low level of phospho-p44/42.

Figure 6. Western blotting analysis of PTEN, Akt, SAPK/JNK, p44/42 and p38 proteins expressed in tumors. *(A) Western blotting analysis of proteins from tumors mice 573 Prdx5*$^{-/-}$*, 911 Prdx5*$^{-/-}$*, 607 Prdx5*$^{+/+}$*, 601 Prdx5*$^{-/-}$*, 615 Prdx5*$^{-/-}$ *was performed with anti-PTEN antibodies, as well as antibodies directed to Akt and its two phosphorylated forms, the phospho-Akt (Thr308) and phospho-Akt (Ser473). Two control tissue samples, from kidney and from liver of Prdx5*$^{+/+}$ *mice were used. Two samples of treated Jurkat cells were used for positive and negative controls of antibodies. Actin immunodetection was used as loading control. (B) Western blotting analysis of proteins from tumors of mice 573 Prdx5*$^{-/-}$*, 911 Prdx5*$^{-/-}$*, 607 Prdx5*$^{+/+}$*, 601 Prdx5*$^{-/-}$*, 615 Prdx5*$^{-/-}$ *labeled with anti-p38 antibodies and its phosphorylated form. The last two lanes have been loaded with proteins of C6 cells treated or not treated with anisomycin which serves as control for antibody specificity. Proteins from two control tissue samples which corresponded to healthy spleen and liver from two Prdx5*$^{+/+}$ *mice, are also labeled. (C) Western blotting analysis of proteins from tumors of mice 573 Prdx5*$^{-/-}$*, 911 Prdx5*$^{-/-}$*, 607 Prdx5*$^{+/+}$*, 601 Prdx5*$^{-/-}$*, 615 Prdx5*$^{-/-}$*, were performed with antibodies anti-p44 / 42 and its phosphorylated form. The last two lanes were loaded with proteins from Jurkat cells and serve as control for antibody specificity.*

(D) Western blotting analysis of proteins of tumors from mice 573 Prdx5$^{-/-}$, 911 Prdx5$^{-/-}$, 607 Prdx5$^{+/+}$, 601 Prdx5$^{-/-}$, 615 Prdx5$^{-/-}$ labeled with anti-SAPK antibodies, anti-JNK and its phosphorylated form. The last two lanes have been loaded with proteins from 293 cells exposed or not to UVs are controls of antibody specificity. (E-F) Western blot densitometry quantification of phosphorylation of Akt, expressed as a ratio of the amount of phosphorylated form on the total of cellular Akt. Ser473 phosphorylated form of is represented by purple bars and Thr308 phosphorylated form by orange bars. (G) Western blot quantification of PTEN, normalized with loading control. (H) Western blot quantification of phosphorylated p38, (I) p44 / 42 and (J) SAPK/JNK expressed as the ratio of the phosphorylated form on total of phosphorylated and non-phosphorylated form.

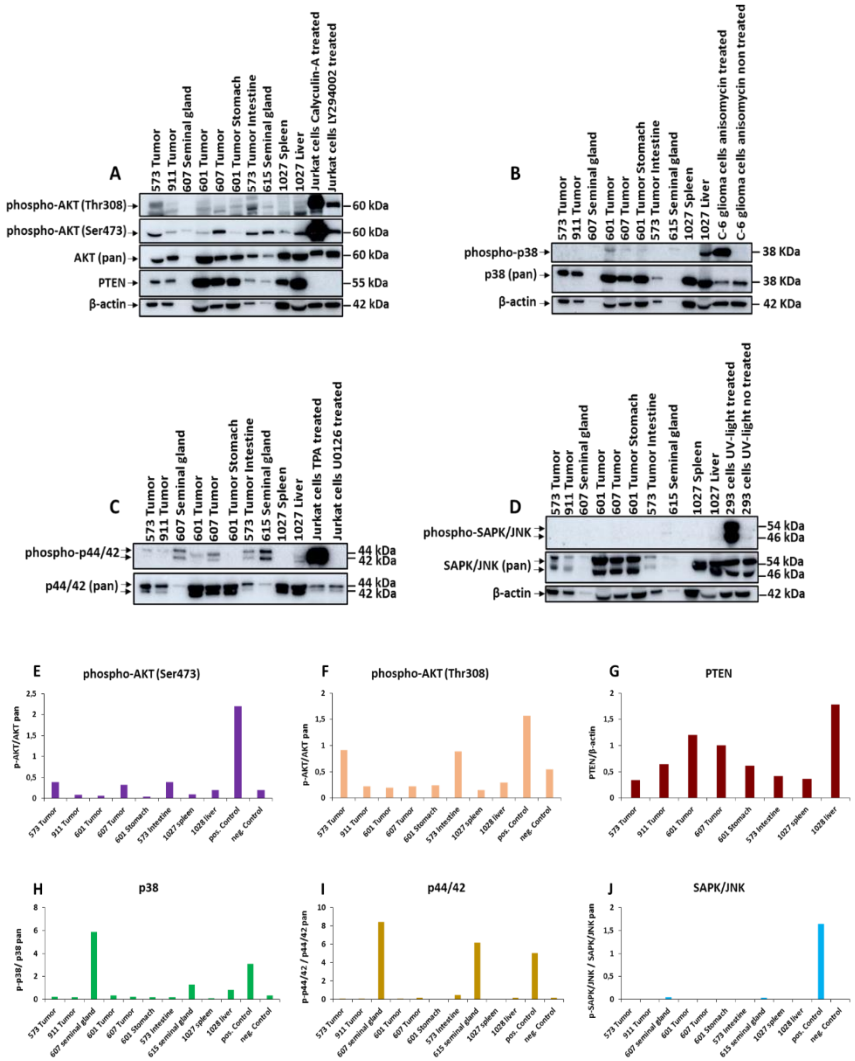

6.4 Discussion

In this study, we report that in aging *Prdx5*$^{-/-}$ mice, the development of several malignant cancers such as lymphomas and hepatocarcinoma occurred significantly more frequently than in wild type animals. Indeed in *Prdx5*$^{+/+}$ mice, tumor developing range was lower (16 %) compared to their *Prdx5*$^{-/-}$ counterpart (41 %). As Prdx5 is virtually expressed in all tissues and cell types in mammals, and considering that Prdx5 has been involved in antioxidant cytoprotective mechanisms, modulation of redox signaling and inflammation, it could be postulated that gene inactivation could be implicated in the development of different malignant cancers. Tumor characterization in this study revealed that most of cancers detected in *Prdx5*$^{-/-}$ mice were lymphomas, divided in sub-categories, such as T-cell lymphoma, B-cell lymphoma, Burkitt's lymphoma and even myeloid leukemia. There are also cases of hepatocarcinoma in *Prdx5*$^{-/-}$ mice. On the other hand, in several *Prdx5*$^{+/+}$ mice the development hepatocarcinoma and myeloid leukemia was also noted. However, carcinogenesis was significantly more frequent in the *Prdx5* deficient mice and lymphomas were the main detected malignant cancer. These findings suggest that Prdx5 could have a tumor suppressor role as other Prdx mammalian members. Indeed, it has been reported that Prdx1 inactivation is associated with the development of

lymphoma in *Prdx1*$^{-/-}$ mice [18]. Other reports are more contradictory about Prdx involvement in lymphoma. For example, Prdx3-5 were shown to be induced in Hodgkin lymphomas [29] while Prdx1-2 are highly expressed in Burkitt's lymphoma [35], suggesting a tumor enhancer role of Prdxs in the development of such lymphoma.

As mentioned previously, *Prdx1*$^{-/-}$ mice were shown to develop hemolytic anemia, lymphoma and several malignant cancers after the age of 9 months [18]. Due to its peroxidase activity, it was postulated that Prdx1 would prevent tumor generation by reducing ROS levels and oxidative DNA damage. But more specifically, it was shown also that Prdx1 binds to tumor suppressor PTEN to protect its lipid phosphatase activity from inactivation under mild oxidative stress [19]. In the case of Prdx1 inactivation, Akt is highly phosphorylated, while Prdx1 inhibits Ras-induced transformation through its peroxidase activity [19]. It is also proposed that activation of PI3K-Akt signaling pathway following loss of PTEN function induces stabilization of c-Myc protein in pancreatic cancer cells [36]. Altogether, these data suggest that Prdx1-deficient mice are more susceptible to transformation through PTEN activity reduction and c-Myc activity enhancement. In accordance with these mechanisms, in the present study, some tumors of Prdx5-deficient mice in which lymphoma was detected, present higher Akt phosphorylation and low levels of PTEN. Our study shows also that in *Prdx5*$^{-/-}$ MEF cells, Akt

phosphorylation is higher for both residues Ser473 and Thr308, while the cells are exposed to H_2O_2. Additionally, we observed higher phosphorylation of Akt only for Thr38 and not for Ser473, after 30 minutes exposure to *t*BHP. Thus, we could hypothesize that *t*BHP is implicated in the PDK1 phosphorylation process. These findings lead us to hypothesize that Prdx5 could protect the tumor suppressor PTEN from oxidation and keep Akt phosphorylation at low levels. Prdx5 can be localized in cytoplasm. It is very likely that cytoplasmic form of Prdx5 interacts in with the PTEN at the membrane and protect it from oxidation as the Prdx1 does [19]. Moreover Prdx1 and Prdx5 are activated by the same Ets transcription factors [30], suggesting that Prdx1 and Prdx5 share common transcription regulation mechanisms. This hypothetic mechanism of Prdx5 should be tested further. Especially, the possible direct interaction between Prdx5 and PTEN, as well as activation of Akt/PTEN downstream targets should be investigated.

It has been shown also that Prdx1 may play a role in the phosphorylation of p38 of the MAPK pathway, involving the formation of a Prdx1-phospho-p38 complex [20]. The suppression of Prdx1, or the decrease of p38 activity, inhibits the formation of cellular protrusions in pancreatic cancer, and thus decreases the mobility and invasion of these cells, showing that Prdx1 promotes pancreatic cancer cell invasion [20]. It was shown earlier that Prdx1 is induced through activation of the ROS/p38 MAPK signal pathway during

LPS exposure and that leads to decrease microglia activation and generation of nitric oxide [38]. In addition, Prdx1 deficiency increased the nuclear translocation of NF-κB mediated-iNOS induction and subsequent NO secretion in LPS-stimulated microglia [38]. In another study, cisplatin treatment enhanced the phosphorylation of p38, MAPK, and JNK, and suppressed the phosphorylation of Erk1/2 in Prdx1-deficient embryonic fibroblasts (MEFs) [21]. Prdx1 modulates apoptosis signal negatively via JNK and positively via ERK, but that p38 MAPK activation may not be modulated by Prdx1 in cisplatin-induced apoptotic signaling. These studies suggest that Prdx1 plays an anti-apoptotic role by reducing cisplatin-induced damage in MEFs [21]. In our study, p38 levels are too low to assume any association between Prdx5 and p38 phosphorylation. Moreover, SAPK/JNK phosphorylation was not detected in tumor samples while p44 phosphorylation was observed only in few tumor samples. These data suggest that there is not a direct link between Prdx5 and the MAPK signaling pathways either because of the very low detection or because the MAPK pathways are not affected in the late stages of carcinogenesis. Therefore, it would be important to examine Prdx5 roles at the different stages of tumorigenesis.

It is known that Prdxs, as antioxidant enzymes, decrease ROS/RNS levels which cause oxidative damages to cells and are involved in different

pathologies, such as cancer. On the other hand, Prdxs may also scavenge H_2O_2, organic peroxides and peroxynitrite in cancer cells, resulting in cancer cell protection against cell death [17], [39]. It has been shown that Prdx5 is upregulated or downregulated in different cancers [22]–[29], [31], [32]. Thus, we can hypothesize that the absence of Prdx5 in our knockout model affects the Akt/PTEN signaling pathway in MEF cells, at embryonic stage, but not at the same level in cancer, when the tumor is already formed. In the same manner, MAPK signaling pathways did not appear to be affected in tumors. How MAPK signaling pathways are affected in *Prdx5*$^{-/-}$ MEF cells should be investigated further by Western blotting, since there are not data for this stage but only for the tumors. Therefore, the role of Prdx5 as a tumor enhancer or suppressor is not completely clear and further mechanistic studies should be performed.

It is worth to mention that in our proteomic analysis of Prdx5-deficient mice, expression of several proteins related to apoptosis were significantly altered compared to wild type animals [40]. For example, caspase-3, a key player in apoptosis, was shown to be downregulated with a fold change of 21.32 in the *Prdx5*$^{-/-}$ phagocytes [40]. Activated caspase-3 catalyzes specific cleavage of many key cellular proteins and is indispensable for apoptotic chromatin condensation and DNA fragmentation [41]. Cells lacking caspase-3 show increased proliferation *in vivo* and hyperproliferation after mitogenic

stimulation *in vitro* [42]. In absence of Prdx5, caspase-3 expression is strongly downregulated. Consequently, cells should not proceed to normal apoptosis and tumor development should be favored. In contrast, in Prdx2-deficient mice, levels of cleaved caspase-3 and other pro-apoptotic proteins are increased, leading to early apoptosis [43]. It appears that interactions between Prdxs and caspase-3 could be different. Additionally, our proteomic analysis revealed also a weaker downregulation of the caspase-8 expression with a fold change of 1.62 in the *Prdx5*$^{-/-}$ phagocytes [40]. Caspase-8 initiates apoptosis directly by cleaving and thereby activating executioner caspases (-3, -6, -7) [44]. We can hypothesize that this weak downregulation of the caspase-8 in the *Prdx5*$^{-/-}$ phagocytes could lead to a stronger downregulation of the caspase-3, which would result in apoptosis inhibition and increase of cell survival. In the same manner, septin-7, a cytoskeletal GTPase that plays essential roles in cell proliferation, cytokinesis and tumorigenesis, is strongly downregulated in *Prdx5*$^{-/-}$ phagocytes with a fold change of 5.29 [40]. It was shown previously that septin-7 inhibits the growth and invasion of glioma and the proliferation in hepatocarcinoma, while its depletion can improve glioblastoma cell migration and invasion [45].

Altogether, these data suggest more complex mechanisms between the pleiotropic antioxidant enzyme Prdx5 and the different signaling pathways related to cell survival, proliferation, apoptosis and carcinogenesis. A deeper

and more detailed investigation should be conducted to clarify the exact and the potential dual role of Prdx5 in the activation or inactivation of these pathways.

6.5 Materials and Methods

6.5.1 Prdx5 knockout mouse generation

Prdx5$^{-/-}$ mice were obtained using a gene-trap strategy, as described previously [40].

6.5.2 Histological analyses of tumors

For histological analyses, tissues and tumors of *Prdx5*$^{+/+}$ and *Prdx5*$^{-/-}$ mice were fixed in 10% buffered neutral formalin. Then, the tissues and tumors were embedded in paraffin and 7µm sections were cut. The sections were mounted on polylysine slides (VWR, 631-0107) and stained with classical hemalun-eosin coloration as following. The sections were deparaffinized in xylol, rehydrated in decreasing ethanol solutions (100-30%), stained with Mayer's hemalun (Carl Roth, Karlsruhe, Germany) for 5 min, washed again,

and stained with 1% eosin (Carl Roth, Karlsruhe, Germany) for 2 minutes. Continuously, the sections were washed in tab water, dehydrated in increasing ethanol solutions (30-100%), treated with xylol, and mounted with Eukitt Quick-hardening mounting medium (Sigma-Aldrich, 03989).

6.5.3 Immunohistochemistry

Immunohistochemistry using different antibodies directed to specific markers was performed to characterize tumors in each mouse. All the sections were deparaffinized in xylol, rehydrated in decreasing ethanol solutions (100-30%) and heated for 20 min in a microwave with 10mM Tris base, 1mM EDTA solution, 0.05% Tween 20 pH 9.0 and blocked with 0.6% H_2O_2 – 50mM TBS for 15 min at RT. Then, they were washed with 50mM TBS – 0.1% TritonX-100 (TTBS) and incubated with TTBS containing 10% non-fat dry milk for 1 hour at RT. The sections were incubated overnight at 4^{o}C with primary antibodies. Incubation with primary antibodies was follwed by washing with TTBS three times for 5 min and incubated with secondary biotinylated antibodies for two hours at RT. Then, sections were washed again three times for 5 min with TBS and incubated for 1 hour with the ABComplex (Complex Avidin-Biotin coupled with peroxidase, Vector, PK-6100). The peroxidase reaction was visualized by incubating sections for 2-

10 min with diaminobenzidine (DAB, Vector, SK-4100) and then stained with hemalun as described previously. The sections were observed with a Polyvar Reichter-Jung microscope. Sections were incubated overnight with the primary antibodies indicated in Table 1. Sections were then incubated with biotinylated anti-rabbit antibody (Vector, BA-1000) 1:500, biotinylated anti-rat antibody (Vector, BA-4001) 1:500 or anti-armenian hamster antibody (Santa Cruz, sc-2789) 1:500 for 2 hours.

6.5.4 Primary culture of mouse embryonic fibroblasts (MEF)

Embryos from *Prdx5*$^{+/+}$ and *Prdx5*$^{-/-}$ mice were collected on 13.5 dpi, as described previously [46]. *Prdx5*$^{+/+}$ and *Prdx5*$^{-/-}$ MEF cells were cultured in 6-well plates for 24 hours in DMEM – GlutaMAX+glucose 4.5g/L (Lonza, 61965-026) with 10% FBS (Lonza, DE14-802F) and 1% streptomycin-penicillin (Gibco, 15140-122). MEF cells were exposed to increasing concentrations of H_2O_2 (0, 50, 100 and 200 µM) for 10 min, to 100ng/ml LPS for 0 to 16 hours, to 100µM *t*BHP for 0 to 120 min and 1mM SIN-1 for 0 to 120 min, at 37°C. After exposure, cells were collected and their proteins were extracted in lysis buffer PBS-Triton X-100 1% containing protease inhibitor cocktail (Roche, 1836170). Protein concentrations were estimated using Pierce BCA protein

assay kit (Thermo-Scientific, 23225) with bovine serum albumin (BSA) as standard.

6.5.5 Western blotting

Protein samples in loading buffer (Tris 45mM pH 6.8, Glycerol 10%, SDS 1%, BPP 0.25%, DTT 0.5M) were subjected to electrophoresis on 12% Mini-Protean SF TGX gels (Bio-rad) using electrophoresis buffer (Tris 50mM, Glycine 150mM, SDS 0.1%) and transferred to nitrocellulose membranes (Amersham Protran 0,45 µM NC GE Healthcare 300mm x 4m, 10.600.002). For blocking, membranes were incubated for 1h at room temperature in blocking solution, 0.1% Tween 20 - TBS buffer (TTBS), containing 5% non-fat dry milk. After blocking, membranes were probed overnight with rabbit anti-phospho-AKT (Ser473) (D9E) monoclonal antibody (Cell Signaling, 4060) 1:2000, rabbit anti-phospho-AKT (Thr473) (D25E6) monoclonal antibody (Cell Signaling, 13038) 1:1000, rabbit anti-AKT (pan) (C67E7) monoclonal antibody (Cell Signaling, 4691) 1:1000, rabbit anti-PTEN (D4.3) monoclonal antibody (Cell Signaling, 9188) 1:1000, rabbit anti-phospho-p38 MAPK (Thr180/Tyr182) polyclonal antibody (Cell Signaling, 9211) 1:1000, rabbit anti-p38 MAPK polyclonal antibody (Cell Signaling, 9212) 1:1000, rabbit anti-phospho-p44/42 MAPK (Erk1/2) (Thr202/Tyr204) polyclonal antibody (Cell

Signaling, 9101) 1:1000, rabbit anti- p44/42 MAPK (Erk1/2) polyclonal antibody (Cell Signaling, 9102) 1:1000, rabbit anti-phospho-SAPK/JNK (Thr183/Tyr185) polyclonal antibody (Cell Signaling, 9251) 1:1000, rabbit anti-SAPK/JNK polyclonal antibody (Cell Signaling, 9252) 1:1000, rabbit anti-Prdx5 polyclonal antibody (Hormonology Laboratory of Marloie, G234) 1:5000, rabbit anti-β-actin polyclonal antibody (Sigma, A2066) 1:1500, followed by horseradish peroxidase-conjugated anti-rabbit secondary antibody (DAKO, p0448) 1:2000 for 1 hour. The reaction was detected by chemiluminescence using ECL Western Lightning Chemiluminescence Reagent Plus (Perkin Elmer Life Sciences, NEL104) and exposed to film (Amersham Hyperfilm™ ECL, 28-9068-37).

6.5.6 Statistical analysis

All statistical analyses were performed with JMP 12.1 by SAS. Statistical comparison of differences between groups was performed using t-test and Fisher's exact test models on the normalized data sets. For all the analyses, a probability value of $p < 0.05$ was considered as statistically significant. Values were expressed as means ± confidence intervals.

6.6 Acknowledgements

Grant sponsor: F.R.S.-FNRS (grant number: PDR T.0090.15) and ARC-Actions de Recherche Concertées. Vasiliki Argyropoulou is a holder of a FRIA fellowship (F.R.S.-FNRS). We thank Pr. René Rezsohazy [(Group of Animal Molecular and Cellular Biology, Louvain Institute of Biomolecular Science and Technology (LIBST), Université catholique de Louvain (UCLouvain)], for the help in the discussion of the results and the advices he provided. We thank Marie Thérèse Ahn for her helpful contribution in the technical procedures. We also acknowledge Catherine Rasse, of the SMCS platform for statistical analyses. We also thank Coralie Piget for her contribution in the well-being of the mice in the animal facility.

6.7 Abbreviations

Akt: Protein kinase B

BCA: Bicinchoninic acid assay

BSA: Bovine serum albumine

DMEM: Dulbecco's Modified Eagle Medium

DTT: Dithiothréitol

EDTA: Ethylene-diamine-tetra-acetic acid

Erk1/2: extracellular signal–regulated kinases 1 and 2

Ets1/2: E-twenty-six transcription factor 1 and 2

FBS: Fetal bovine serum

H_2O_2: Hydrogen peroxide

HMGB1: high–mobility group box 1

iNOS: Nitric oxide synthase

JNK: c-Jun N-terminal kinases

LPS: lipopolysaccharide

MAPK: Mitogen-activated protein kinases

MEF: Mouse embryonic fibroblast

MPO: Myeloperoxidase

Myc: Myelocytomatosis

NF-κB: nuclear factor kappa-light-chain-enhancer of activated B cells

PTEN: Phosphatase and Tensin homolog

Prdx: Peroxiredoxin

p38: p38 mitogen-activated protein kinases

p44/42: p44/42 mitogen-activated protein kinases

RNS: Reactive nitrogen species

ROS: Reactive oxygen species

SAPK: Stress-activated protein kinases

SDS: Sodium dodecyl sulfate

SIN-1: 3-morpholinosydnonimine-N-ethylcarbamide

*t*BHP: tert-Butyl hydroperoxide

TBS: Tris-Buffered saline

6.8 References

[1] S. G. Rhee, "Overview on Peroxiredoxin," *Mol. Cells*, vol. 39, no. 1, pp. 1–5, 2016.

[2] Z. A. Wood, E. Schroder, J. R. Harris, and L. B. Poole, “Structure , mechanism and regulation of peroxiredoxins,” *Trends Biochem. Sci.*, vol. 28, no. 1, pp. 3–8, 2003.

[3] B. Knoops, E. Loumaye, and V. Van Der Eecken, “Evolution of Peroxiredoxins: Taxonomy, homology and characterization,” in *Peroxiredoxin Systems*, 2007, pp. 27–40.

[4] S. G. Rhee and I. S. Kil, “Multiple Functions and Regulation of Mammalian Peroxiredoxins,” *Annu. Rev. Biochem.*, vol. 86, no. 5, pp. 1–27, 2017.

[5] G. Ferrer-Sueta, B. Manta, H. Botti, R. Radi, M. Trujillo, and A. Denicola, “Factors affecting protein thiol reactivity and specificity in peroxide reduction,” *Chem. Res. Toxicol.*, vol. 24, pp. 434–450, 2011.

[6] A. Perkins, K. J. Nelson, D. Parsonage, L. B. Poole, and P. A. Karplus, “Peroxiredoxins: guardians against oxidative stress and modulators of peroxide signaling,” *Trends Biochem. Sci.*, vol. 40, no. 8, pp. 435–445, 2015.

[7] M. S. Seo, S. W. Kang, K. Kim, I. C. Baines, T. H. Lee, and S. G. Rhee, “Identification of a new type of mammalian peroxiredoxin that forms an intramolecular disulfide as a reaction intermediate,” *J. Biol. Chem.*, vol. 275, no. 27, pp. 20346–20354, 2000.

[8] B. Knoops *et al.*, “Cloning and characterization of AOEB166, a novel mammalian antioxidant enzyme of the peroxiredoxin family,” *J. Biol. Chem.*, vol. 274, pp. 30451–30458, 1999.

[9] A. Kropotov *et al.*, “A novel human DNA-binding protein with sequence similarity to a subfamily of redox proteins which is able to repress RNA-polymerase-III-driven transcription of the Alu-family retroposons in vitro,” *Eur J Biochem*, vol. 260, pp. 336–346, 1999.

[10] H. Yamashita *et al.*, “Characterization of Human and Murine PMP20 Peroxisomal Proteins That Exhibit Antioxidant Activity in Vitro,” *J. Biol. Chem.*, vol. 274, no. 42, pp. 29897–29904, 1999.

[11] J.-P. Declercq, C. Evrard, A. Clippe, D. Vander Stricht, A. Bernard, and B. Knoops, “Crystal Structure of Human Peroxiredoxin 5, a Novel Type of Mammalian Peroxiredoxin at 1.5 A Ê Resolution,” *J. Mol. Biol.*, vol. 311, pp. 751–759, 2001.

[12] T. Lee, S. J. Kim, S. W. Kang, K. Lee, S. G. Rhee, and D. Yu, “Molecular Cloning and Characterization of the Mouse Peroxiredoxin V Gene,” *Biochem. Biophys. Res. Commun.*, vol. 362, pp. 356–362, 2000.

[13] N. T. Nguyên-nhu *et al.*, “Human peroxiredoxin 5 gene organization, initial characterization of its promoter and identification of alternative forms of mRNA,” *Biochim. Biophys. Acta - Gene Struct.*

Expr., vol. 1769, pp. 472–483, 2007.

[14] A. Kropotov, N. Usmanova, V. Serikov, B. Zhivotovsky, and N. Tomilin, “Mitochondrial targeting of human peroxiredoxin V protein and regulation of PRDX5 gene expression by nuclear transcription factors controlling biogenesis of mitochondria,” *FEBS J.*, vol. 274, pp. 5804–5814, 2007.

[15] G. Leyens, I. Donnay, and B. Knoops, “Cloning of bovine peroxiredoxins - Gene expression in bovine tissues and amino acid sequence comparison with rat, mouse and primate peroxiredoxins,” *Comp. Biochem. Physiol. - B Biochem. Mol. Biol.*, vol. 136, pp. 942–955, 2003.

[16] G. Leyens, B. Knoops, and I. Donnay, “Expression of peroxiredoxins in bovine oocytes and embryos produced in vitro,” *Mol. Reprod. Dev.*, vol. 69, pp. 243–251, 2004.

[17] C. A. Neumann and Q. Fang, “Are peroxiredoxins tumor suppressors ?,” *Curr. Opin. Pharmacol.*, vol. 7, pp. 375–380, 2007.

[18] C. A. Neumann *et al.*, “Essential role for the peroxiredoxin Prdx1 in erythrocyte antioxidant defence and tumour suppression,” *Nature*, vol. 424, no. 6948, pp. 561–565, 2003.

[19] J. Cao *et al.*, “Prdx1 inhibits tumorigenesis via regulating PTEN/AKT activity,” *EMBO J.*, vol. 28, pp. 1505–1517, 2009.

[20] K. Taniuchi *et al.*, “Peroxiredoxin 1 Promotes Pancreatic Cancer Cell Invasion by Modulating p38 MAPK Activity,” *Pancreas*, vol. 44, no. 2, pp. 331–340, 2015.

[21] D. Ma *et al.*, “Peroxiredoxin I plays a protective role against cisplatin cytotoxicity through mitogen activated kinase signals,” *Oral Oncol.*, vol. 45, no. 12, pp. 1037–1043, 2009.

[22] H. Ahn, J. Yoo, S. Lee, H. Jun, H. Lee, and D. Lee, “Peroxiredoxin 5 promotes the epithelial-mesenchymal transition in colon cancer,” *Biochem. Biophys. Res. Commun.*, vol. 487, no. 3, pp. 580–586, 2017.

[23] B. Kim *et al.*, “Peroxiredoxin 5 overexpression enhances tumorigenicity and correlates with poor prognosis in gastric cancer,” *Int. J. Oncol.*, vol. 51, pp. 298–306, 2017.

[24] J. M. Byun *et al.*, “Overexpression of peroxiredoxin-3 and -5 is a potential biomarker for prognosis in endometrial cancer,” *Oncol. Lett.*, vol. 15, pp. 5111–5118, 2018.

[25] P. Karihtala, A. Mäntyniemi, S. W. Kang, V. L. Kinnula, and Y. Soini, “Peroxiredoxins in Breast Carcinoma,” *Clin. Cancer Res.*, vol. 9, pp.

3418–3424, 2003.

[26] M. J. Seo, X. Liu, M. Chang, and J. H. Park, “GATA-binding protein 1 is a novel transcription regulator of peroxiredoxin 5 in human breast cancer cells,” *Int. J. Oncol.*, vol. 40, pp. 655–664, 2012.

[27] C. Mcdonald, J. Muhlbauer, G. Perlmutter, K. Taparra, and S. A. Phelan, “Peroxiredoxin proteins protect MCF-7 breast cancer cells from doxorubicin-induced toxicity,” *Int. J. Oncol.*, vol. 45, no. 21, pp. 219–226, 2014.

[28] A. Kropotov *et al.*, “Peroxiredoxin V is essential for protection against apoptosis in human lung carcinoma cells,” *Exp. Cell Res.*, vol. 312, pp. 2806–2815, 2006.

[29] H. Bur *et al.*, “Oxidative stress markers and mitochondrial antioxidant enzyme expression are increased in aggressive Hodgkin lymphomas,” *Histopathology*, vol. 0, pp. 319–327, 2014.

[30] M. Shiota *et al.*, “Ets regulates peroxiredoxin1 and 5 expressions through their interaction with the high-mobility group protein B1,” *Cancer Sci*, vol. 99, no. 10, pp. 1950–1959, 2008.

[31] A. Elamin, H. Zhu, A. M. E. L. Hassan, N. Xu, and M. E. Ibrahim, “Peroxiredoxin V : A candidate breast tumor marker of population

specificity," *Mol. Clin. Oncol.*, vol. 1, pp. 541–549, 2013.

[32] G. G. Fernandez-Ranvier *et al.*, "Candidate Diagnostic Markers and Tumor Suppressor Genes for Adrenocortical Carcinoma by Expression Profile of Genes on Chromosome 11q13," *World J Surg*, vol. 32, pp. 873–881, 2008.

[33] H. C. Morse III *et al.*, "Bethesda proposals for classification of lymphoid neoplasms in mice," *Blood*, vol. 100, no. 1, pp. 246–258, 2002.

[34] S. C. Kogan *et al.*, "Bethesda proposals for classification of nonlymphoid hematopoietic neoplasms in mice," *Blood*, vol. 100, no. 1, pp. 238–245, 2002.

[35] A. Trzeciecka *et al.*, "Dimeric peroxiredoxins are druggable targets in human Burkitt lymphoma," *Oncotarget*, vol. 7, no. 2, pp. 1717–1731, 2015.

[36] T. Asano, Y. Yao, J. Zhu, D. Li, J. L. Abbruzzese, and A. G. Reddy, "The PI 3-kinase / Akt signaling pathway is activated due to aberrant Pten expression and targets transcription factors NF-jB and c-Myc in pancreatic cancer cells," *Oncogene*, vol. 23, pp. 8571–8580, 2004.

[37] A. Carnero and J. M. Paramio, "The PTEN/PI3K/AKT pathway in vivo,

cancer mouse models," *Front. Oncol.*, vol. 4, no. 252, pp. 1–10, 2014.

[38] S. U. Kim *et al.*, "Peroxiredoxin I is a ROS/p38 MAPK-dependent inducible antioxidant that regulates NF-κB-mediated iNOS induction and microglial activation," *J. Neuroimmunol.*, 2013.

[39] M. B. Hampton, K. A. Vick, J. J. Skoko, and C. A. Neumann, "Peroxiredoxin involvement in the initiation and progression of human cancer," *Antioxid Redox Signal.*, vol. 28, no. 7, pp. 591–608, 2018.

[40] V. Argyropoulou *et al.*, "Peroxiredoxin-5 protects mice from lipopolysaccharide-induced endotoxic shock," *Antioxid. Redox Signal.*, p. submitted, 2019.

[41] A. G. Porter and R. U. Ja, "Emerging roles of caspase-3 in apoptosis," *Cell Death Differ.*, vol. 6, pp. 99–104, 1999.

[42] M. Woo *et al.*, "Caspase-3 regulates cell cycle in B cells : a consequence of substrate specificity," *Nat Immunol*, vol. 4, no. 10, pp. 1016–1022, 2003.

[43] S. J. Park, J. H. Kim, D. G. Lee, J. M. Kim, and D. S. Lee, "Peroxiredoxin 2 deficiency accelerates age-related ovarian failure through the reactive oxygen species-mediated JNK pathway in mice," *Free Radic.*

Biol. Med., vol. 123, no. February, pp. 96–106, 2018.

[44] D. R. Mcilwain, T. Berger, and T. W. Mak, "Caspase Functions in Cell Death and Disease," *Cold Spring Harb Perspect Biol*, vol. 5, pp. 1–28, 2013.

[45] X. Wang, F. Fei, J. Qu, C. Li, Y. Li, and S. Zhang, "The role of septin 7 in physiology and pathological disease : A systematic review of current status," *J Cell Mol Med.*, vol. 22, pp. 3298–3307, 2018.

[46] M. E. Durkin, X. Qian, N. C. Popescu, and D. R. Lowy, "Isolation of Mouse Embryo Fibroblasts," *Bio Protoc.*, vol. 3, no. 18, pp. 1–5, 2013.

7. What are the consequences of *Peroxiredoxin-5* inactivation in the mouse central nervous system?

Vasiliki Argyropoulou[1], Charlotte Lefort[1], Olivier Schackman[2], Philippe Gailly[2], Bernard Knoops[1]*

[1]Group of Animal Molecular and Cellular Biology, Louvain Institute of Biomolecular Science and Technology (LIBST), Université catholique de Louvain, 1348, Louvain-la-Neuve, Belgium

[2]Group of Cell Physiology, Institute of Neuroscience (IONS), Université catholique de Louvain (UCL), Woluwe, Belgium

Keywords: *Peroxiredoxin, Prdx5, antioxidant, central nervous system, behavioral tests*

[*]***Address correspondence to :*** *Prof. Bernard Knoops, Louvain Institute of Biomolecular Science and Technology (LIBST), Université catholique de Louvain, place Croix du Sud, 4-5 bte L7.07.02, B-1348 Louvain-la-Neuve, Belgium.* ***E-mail :*** *bernard.knoops@uclouvain.be* ***Tel :*** *+32-10-47 37 60 ;* ***Fax :*** *+32-10-47 35 15*

7.1 Abstract

Peroxiredoxins (Prdxs) are a superfamily of thiol-dependent peroxidases expressed in prokaryotes and eukaryotes. In mammals, among the six Prdxs, Prdx5 is expressed in neurons of the central nervous system. In this study, we used transgenic mice in which *Prdx5* gene was inactivated using a gene-trap strategy to examine the consequences of *Prdx5* inactivation in the central nervous system. Our results show that Prdx5 deficiency in mice caused less motor coordination and a tendency of higher anxiety, compared to wild type animals of the same littermates. Moreover, histological analyses suggest that astrocytes and microglia are activated in young *Prdx5*$^{-/-}$ hippocampus area although this activation was not confirmed in aging *Prdx5*$^{-/-}$ mice. These results suggest that Prdx5 could be implicated in motor functions, in behavior and in neuroinflammation in the mouse central nervous system although *Prdx5* inactivation appeared to have weak consequences likely compensated by redundant activities of other Prdxs.

7.2 Introduction

Peroxiredoxins (Prdxs) are a family of thiol-dependent peroxidases [1]–[3], that are able to reduce hydrogen peroxide, peroxynitrite as well as alkyl hydroperoxydes in cells [2], [4], [5]. These enzymes are very well conserved from bacteria to mammals [2], [3]. According to their catalytic mechanism and the number of the active cysteines in their molecules, the mammalian Prdxs are divided in three different subgroups [2], [6]. The first group, called the typical 2-Cys Prdxs, is composed of four members (Prdx1-4). The typical 2-Cys Prdxs exhibit two active cysteines in their molecules and they form an intermolecular disulfide bond upon oxidation [2]. Prdx5 is the only atypical 2-Cys Prdx in mammals. Atypical 2-Cys Prdxs which exhibit also two active cysteines but the disulfide bond is intramolecular, formed in the same molecule [2], [6]. Finally, the Prdx6 is the only 1-Cys Prdx in mammals and it carries only one active cysteine [2]. Prdxs are distributed in almost all subcellular compartments in mammalian cells [7]. Prdx subcellular distribution in human and mouse tissues show different profiles between the six members of the family [8]–[10]. More specifically, the atypical 2-Cys Prdx5 is the last isoform tha has been characterized. In human and murine cells, Prdx5 can be localized in cytoplasm, nucleus, peroxisomes and mitochondria

[6], [11]–[19]. Prdx5 is virtually expressed in all tissues but at different levels depending on the cell type [6], [11], [17].

Because Prdxs may act as cytoprotective antioxidant enzymes against oxidative damage in the brain, several groups have investigated their distribution and expression in healthy mouse brain [9], [10], [20]. Prdx1 is expressedt in Purkinje cells of the cerebellum, in the motoneurons of the spinal cord and in the outer cell layer of the olfactory and respiratory epithelium of the nose [9], [10]. Prdx2 is highly expressed in the meninges, in glial cells of the spinal cord, in neurons of the gray matter in the hippocampus, cerebral cortex, and thalamus [9], [10]. It was shown that Prdx2 is upregulated in the residual motor neurons of amyotrophic lateral sclerosis (ALS) patients [21]. Both Prdx1 and Prdx2 are also upregulated in Alzheimer's disease (AD) brains [22]. Moreover, it was shown that enhanced neuronal expression and activity of Prdx2 protect against ischemic neuronal injury [23]. Prdx3 is detected in glial cells in hippocampus, substantia nigra, cerebral cortex, striatum, white matter of cerebellum and spinal cord [9], [10]. Prdx3 is also present in the ependymal cell layer and the choroid plexus as well as in the basal cell layer of olfactory epithelium. Prdx4 is expressed in the substantia nigra, in the meninges and in the olfactory nerve bundles of the nose [9], [10]. Prdx6 is detected in the ependymal cell layer of the cerebellum, in the corneal epithelium, indifferent layers of the retina, in the

non-pigmented ciliary epithelium and zonular fibers, in the olfactory and respiratory epithelium of the nose, in the olfactory nerve bundles and connective tissue of the nose [9], [10]. Prdx6 is upregulated in astrocytes of G93A mice (animal model of ALS) [24]. Overexpression of Prdx6 accelerates the development of AD through increased amyloidogenesis [25]. Prdxs and Trxs are strongly expressed in embryonic mouse spinal cord and present different patterns in contrast with those observed in the adult mouse spinal cord [26]. Additionally, in a knockout mouse model for the antioxidant enzyme glutathione peroxidase 4 (GPx4), the GPx4 deficiency in dopaminergic neurons present prodromal symptoms of Parkinson's disease like anxiety and decreased locomotion [27].

Even though Prdx5 is mainly expressed in neurons, the enzyme is expressed at low levels in dopaminergic neurons of substantia nigra pars compacta and in a few neurons only [9]. This weak expression could be linked to the fact that these neurons are more vulnerable to oxidative stress and why they undergo degeneration faster in Parkinson's disease [9]. Prdx5 is also highly expressed in choroid plexus, reticular thalamic nucleus, motoneurons of the spinal cord and at lower levels in ependymal layers [10]. It should also be noted that Prdx5 is weakly or not detected by immunohistochemistry in neuroglia (oligodendrocytes, astrocytes and microglia) of mouse healthy brain [9], [10], [20]. Prdx5 shows nuclear staining in the granular cells of the

dentate gyrus of hippocampus and in the molecular layer of the cerebellum, most likely in basket cells [10]. Prdx5 expression is upregulated by amyloid-beta oligomers-induced oxidative stress and it decreases ERK–Drp1-mediated mitochondrial fragmentation and apoptosis of HT-22 neuronal cells [28]. Prdx5 is highly expressed in human SH-SY5Y neuroblastoma cells and its silencing makes these cells more vulnerable to oxidative damages and apoptosis induced by MPP+, a complex I inhibitor which provides an experimental paradigm of Parkinson's disease [29], [30]. Additionally, Prdx5 is upregulated in dorsal root ganglia (DRGs) after sciatic nerve injury [31].

Recently, , an homozygous nonsense mutation (c.361C>T, p.Gln121X) in *Prdx5* gene was found in two children (sisters), suffering from severe motor and mental retardation, cerebral atrophy and epilepsy, suggesting that Prdx5 plays an important role in human central nervous system (personal communication, Drs. Cyril Mignot, Eric Le Guern, Bénédicte Héron and Anne Lombès, La Pitié-Salpêtrière and Cochin Hospital, Paris). Whether such nonsense mutation in human generates a truncated protein or whether the transcript is degraded by the non-sense mediated decay (NMD) is examined in the framework of a collaboration with our group and the French group in Paris. Moreover, the human mutation study is in progress in our lab, using the CRISPR-Cas9 genome engineer system to generate $Prdx5^{Q121X/Q121X}$ and $Prdx5^{-/-}$ cell lines, by Marine Delsaute.

Regarding Prdx5 expression in the CNS and the consequences of gene inactivation *in vitro* but also *in vivo* in the two children, an *in vivo* study of the consequences of Prdx5 inactivation in a mouse model was conducted to examine the functions of the enzyme. In the present study, *Prdx5*$^{-/-}$ and *Prdx5*$^{+/+}$ mice which were generated previously (see chapter 1), were used to perform behavioral, motor, anxiety and memory tests. Moreover, a complete histological analysis of the central nervous system of *Prdx5*$^{-/-}$ mice was performed.

7.3 Results

7.3.1 Neurobehavioral testing

To start this study, a series of behavioral tests were conducted in young adult male *Prdx5*$^{+/+}$ and *Prdx5*$^{-/-}$ mice. Firstly, in the modified SHIRPA test, a series of observations of the mice took place in order to examine spontaneous and provoked behaviors. We did not observe any special behavior in the *Prdx5*$^{-/-}$ mice compared to *Prdx5*$^{+/+}$ mice (data are not shown). Continuously, for the physiocage test, 11 *Prdx5*$^{+/+}$ mice and 10 *Prdx5*$^{-/-}$ mice were examined for their food and water consumption, for their activity in the cages and for the

rearing. *Prdx5*$^{-/-}$ mice appeared to act the same way as control *Prdx5*$^{+/+}$ mice (Fig.1). The rotarod test was performed using 22 *Prdx5*$^{+/+}$ and 17 *Prdx5*$^{-/-}$ mice for 5 days. In the first day of the test, we measured the motor coordination of the mice that was significantly lower in *Prdx5*$^{-/-}$ mice (Fig.2). In the same test, the next 4 days, we measured the learning ability, which was also lower in *Prdx5*$^{-/-}$ mice. In the forced swim test, 22 *Prdx5*$^{+/+}$ and 17 *Prdx5*$^{-/-}$ mice were used to measure the time of swimming and rest during 360s. There was a tendency of *Prdx5*$^{-/-}$ mice for being more anxious but the results were not statistically significant (Fig.3). In the open field test, 14 *Prdx5*$^{+/+}$ and 10 *Prdx5*$^{-/-}$ mice were tested for the ability to discover a new environment. No significant difference was measured for this test (Fig.4). The memory of 14 *Prdx5*$^{+/+}$ and 10 *Prdx5*$^{-/-}$ mice was tested also by Y maze test and no difference was measured between them (Fig.5). In the elevated plus maze test, 22 *Prdx5*$^{+/+}$ and 18 *Prdx5*$^{-/-}$ mice were examined for the time they spent in the close and open arms, to assess their anxiety. The test revealed that there is a tendency of *Prdx5*$^{-/-}$ mice to be more anxious too. However, the difference was not statistically significant (Fig.6). In the grip strength test, the muscle strength of 14 *Prdx5*$^{+/+}$ and 9 *Prdx5*$^{-/-}$ mice was measured but there was no difference between the two genotypes (Fig.7). To assess spatial learning and memory, the water maze test was performed using 14 *Prdx5*$^{+/+}$ and 10 *Prdx5*$^{-/-}$ mice. No significance difference was measured on the escape time of the

mice, neither in the 4 trials with the platform, nor during the probe test without the platform (Fig.8).

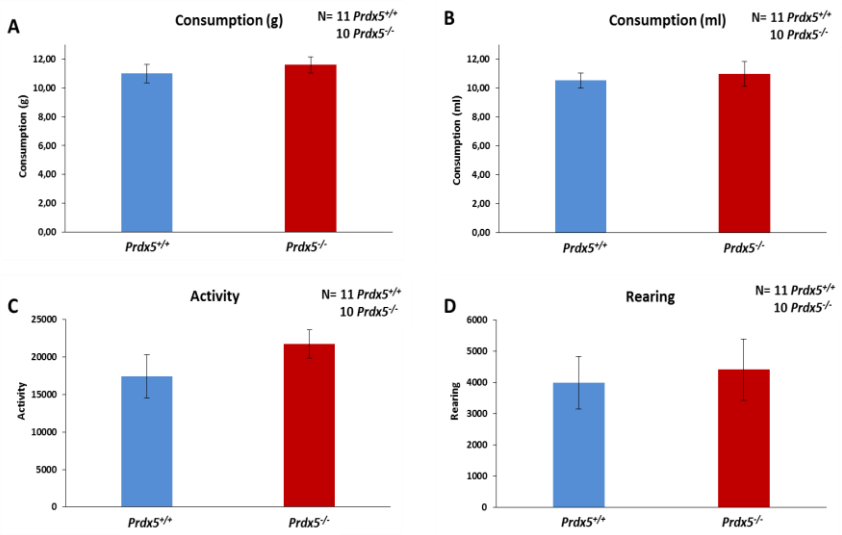

Fig.1. Physiocage test of Prdx5$^{+/+}$ and Prdx5$^{-/-}$ young male mice. *There is no significant difference between the Prdx5$^{-/-}$ and Prdx5$^{+/+}$ mice for the consumption of food (A) and water (B), the activity (C) and the rearing (D).*

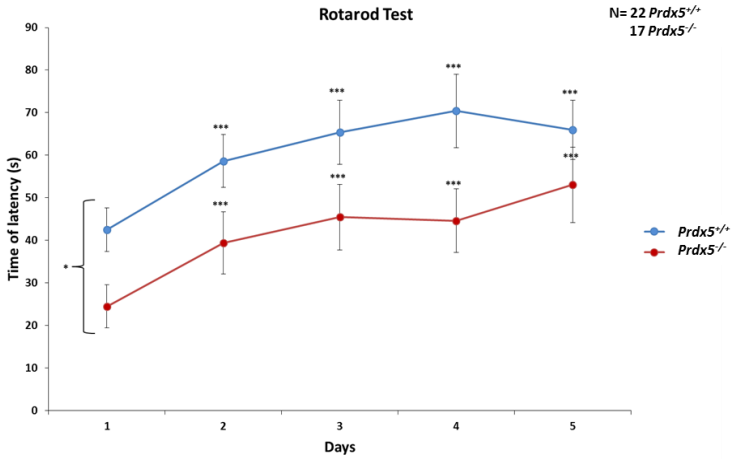

Figure 2. Rotarod test of Prdx5$^{+/+}$ and Prdx5$^{-/-}$ young male mice. *There is significant less coordination in the Prdx5$^{-/-}$ compared to Prdx5$^{+/+}$ mice.*

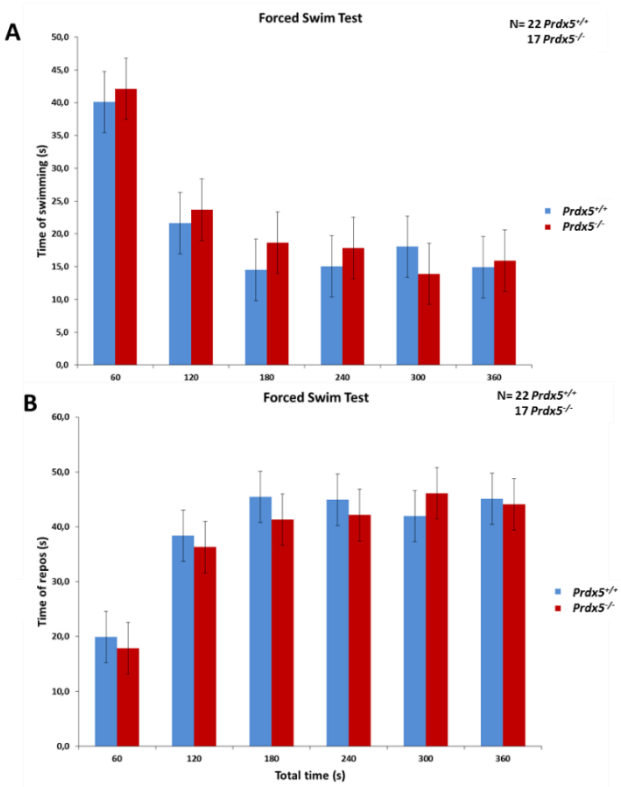

Figure 3. Forced swim test of Prdx5$^{+/+}$ and Prdx5$^{-/-}$ young male mice. *There is no significant difference between the Prdx5$^{-/-}$ and Prdx5$^{+/+}$ mice for the time of swimming (A) and the time of rest (B).*

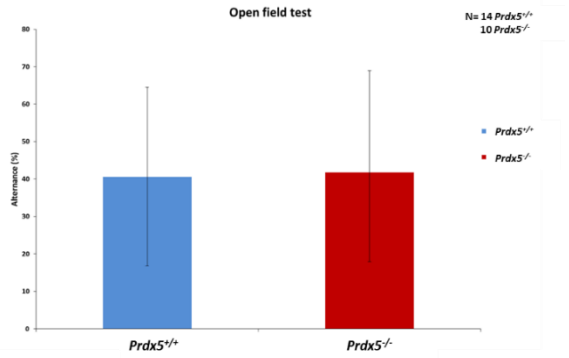

Figure 4. Open field test of Prdx5$^{+/+}$ and Prdx5$^{-/-}$ young male mice. *There is no significant difference between the Prdx5$^{-/-}$ and Prdx5$^{+/+}$ mice for the % alternance.*

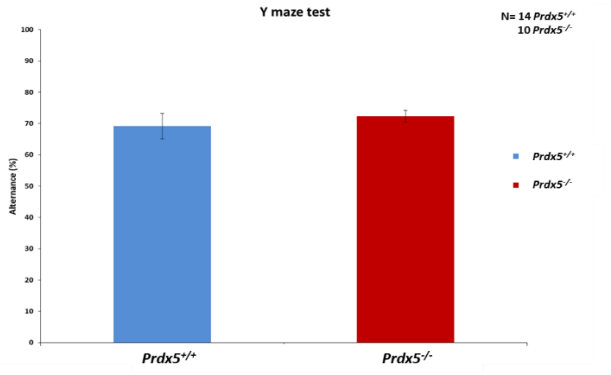

Figure 5. Y maze test of Prdx5$^{+/+}$ and Prdx5$^{-/-}$ young male mice. *There is no significant difference between the Prdx5$^{-/-}$ and Prdx5$^{+/+}$ mice for the % alternance.*

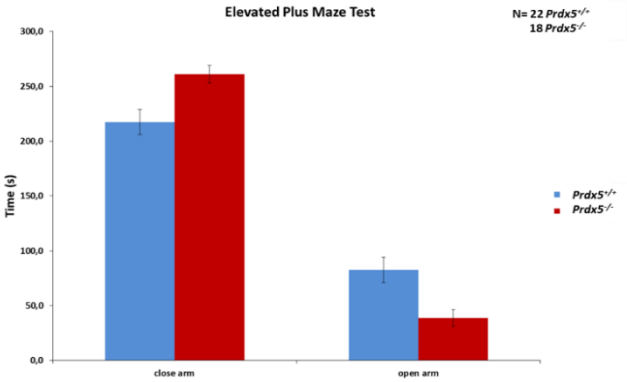

Figure 6. Elevated plus maze test of Prdx5$^{+/+}$ and Prdx5$^{-/-}$ young male mice. *There is no significant difference between the Prdx5$^{-/-}$ and Prdx5$^{+/+}$ mice for the time spent in both open and close arms.*

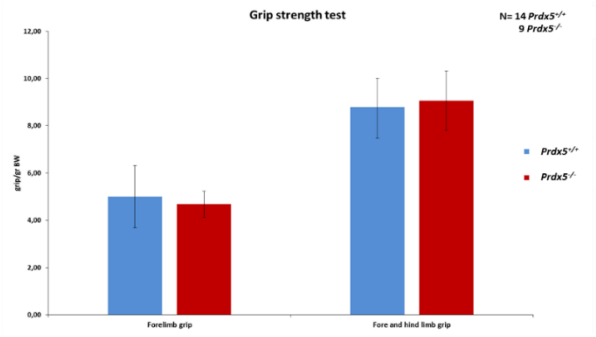

Figure 7. Grip strength test of Prdx5$^{+/+}$ and Prdx5$^{-/-}$ young male mice. *There is no significant difference between the Prdx5$^{-/-}$ and Prdx5$^{+/+}$ mice for the grip/gr of bodyweight for both forelimb and fore and hind limb.*

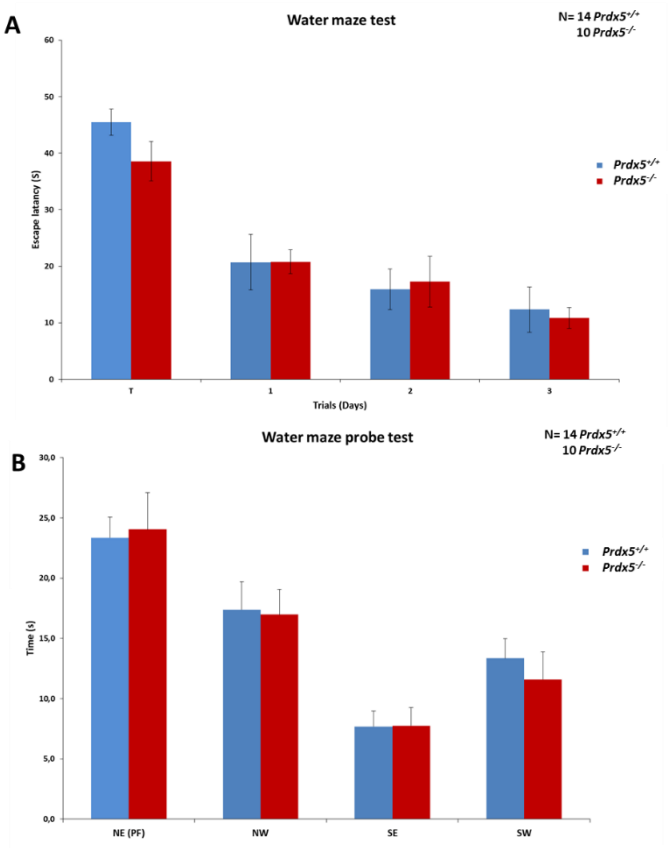

Figure 8. Water maze test of Prdx5$^{+/+}$ and Prdx5$^{-/-}$ young male mice. *There is no significant difference between the Prdx5$^{-/-}$ and Prdx5$^{+/+}$ mice for the escape time (A) and the time to find the orientation of the probe (B).*

7.3.2 Histological analysis

Based on the results from the behavioral tests, different regions of the brain were chosen to be examined more in-depth by immunohistochemistry. The basal ganglia and the cerebellum were selected for the impairment regarding the motor behavior, the hippocampus and the amygdala for the anxiety and the vestibular nuclei for the fear of heights.

To study the neuronal cell populations, a classical Nissl staining was performed on sections of cerebellum, basal ganglia, hippocampus, amygdala and vestibular nuclei from young and old mice. No obvious alterations were detected for the shape, distribution or density of neurons in *Prdx5*$^{-/-}$ mice compared to the *Prdx5*$^{+/+}$ mice (Fig. 9 and 10).

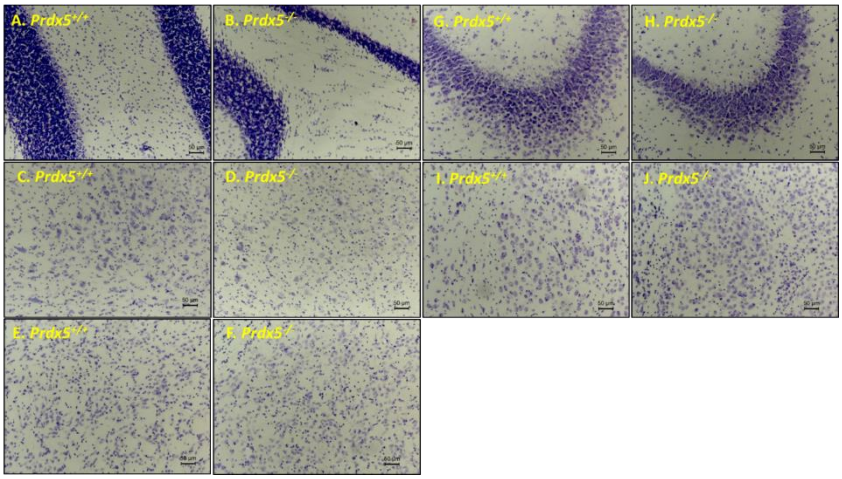

Figure 9. Histological analysis of different brain areas of Prdx5$^{+/+}$ and Prdx5$^{-/-}$ young male mice (Nissl staining). *(A-B) Cerebellum (Layer), (C-D) Cerebellum (Vestibular nuclei), (E-F) Basal ganglia, (G-H) Hippocampus, (I-J) Amygdala*

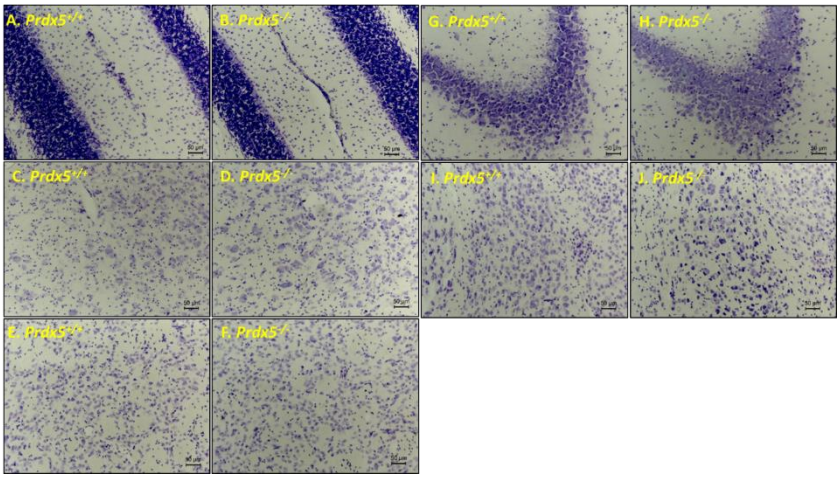

Figure 10. Histological analysis of different brain areas of Prdx5$^{+/+}$ and Prdx5$^{-/-}$ old male mice (Nissl staining). *(A-B) Cerebellum (Layer), (C-D) Cerebellum (Vestibular nuclei), (E-F) Basal ganglia, (G-H) Hippocampus, (I-J) Amygdala*

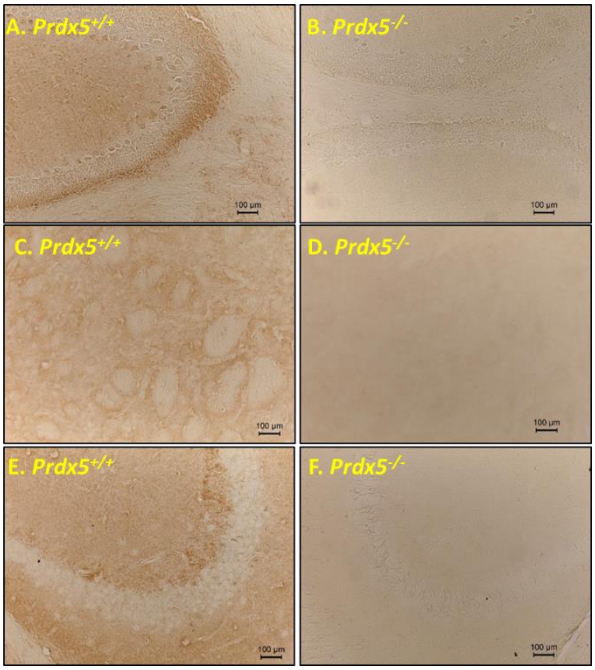

Figure 11. Prdx5 immunostaining of different brain areas of Prdx5$^{+/+}$ and Prdx5$^{-/-}$ young male mice. *(A-B) Cerebellum (Layer), (C-D) Basal ganglia, (E-F) Hippocampus*

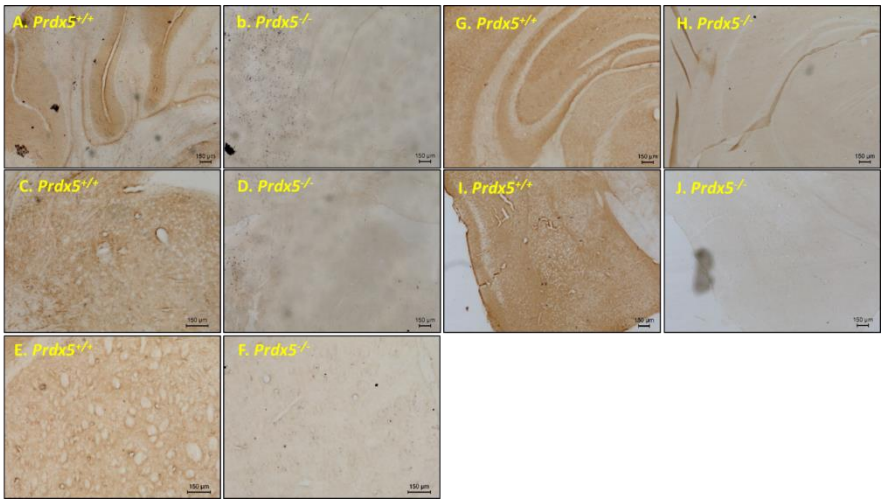

Figure 12. Prdx5 immunostaining of different brain areas of Prdx5$^{+/+}$ and Prdx5$^{-/-}$ old male mice. *(A-B) Cerebellum (Layer), (C-D) Cerebellum (Vestibular nuclei), (E-F) Basal ganglia, (G-H) Hippocampus, (I-J) Amygdala*

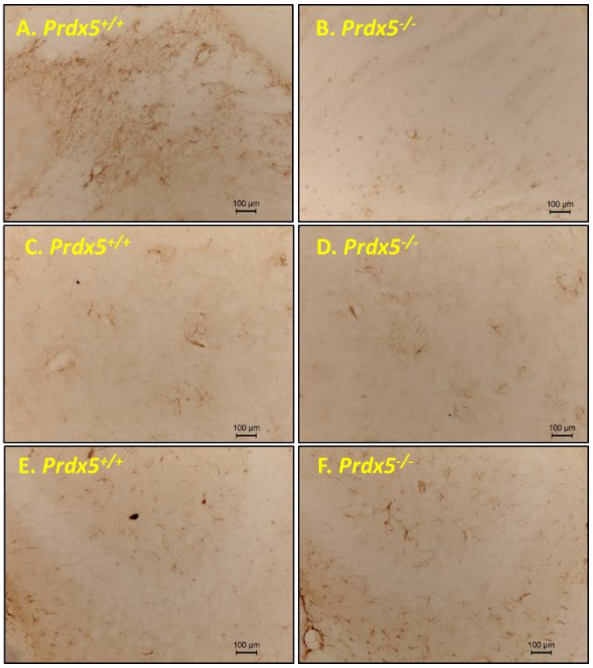

Figure 13. GFAP immunostaining of different brain areas of Prdx5$^{+/+}$ and Prdx5$^{-/-}$ young male mice. *(A-B) Cerebellum (Layer), (C-D) Basal ganglia, (E-F) Hippocampus*

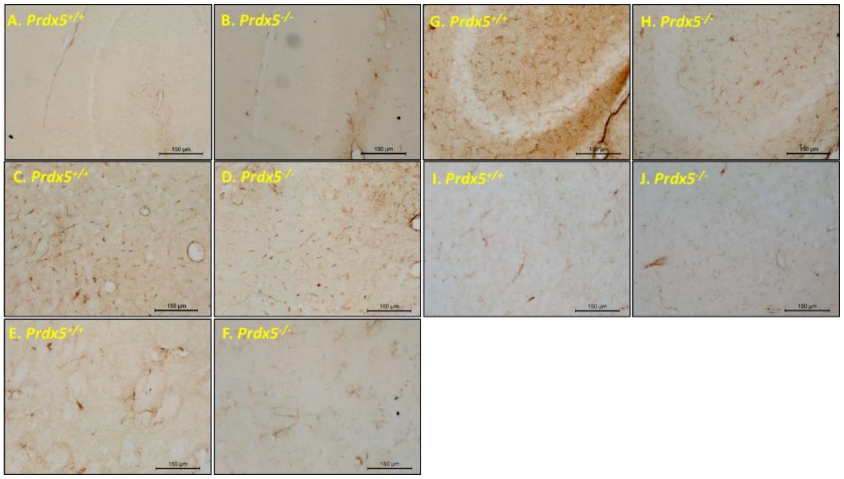

Figure 14. GFAP immunostaining of different brain areas of Prdx5$^{+/+}$ and Prdx5$^{-/-}$ old male mice. *(A-B) Cerebellum (Layer), (C-D) Cerebellum (Vestibular nuclei), (E-F) Basal ganglia, (G-H) Hippocampus, (I-J) Amygdala*

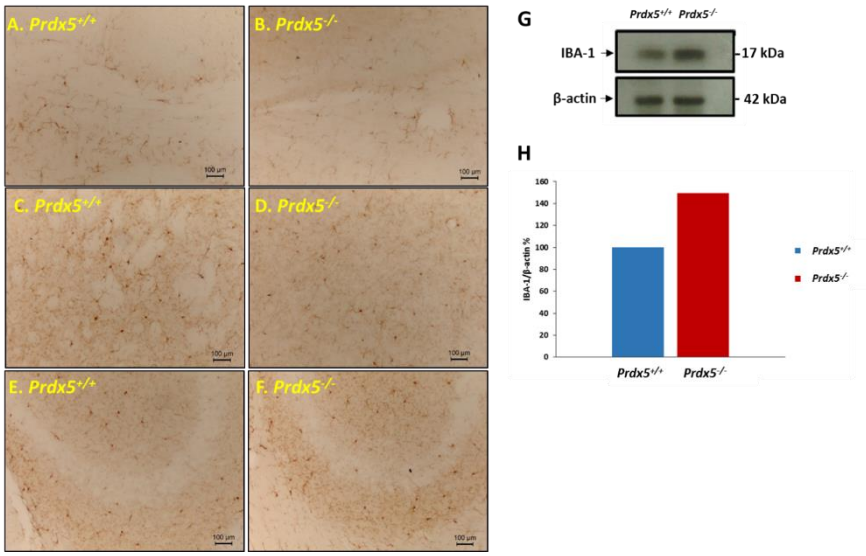

Figure 15. IBA-1 immunostaining of different brain areas of Prdx5$^{+/+}$ and Prdx5$^{-/-}$ young male mice. *(A-B) Cerebellum (Layer), (C-D) Basal ganglia, (E-F) Hippocampus, (G-H) Western blotting analysis and quantification of microglia (IBA-1 marker) in the brain of young adult Prdx5$^{+/+}$ and Prdx5$^{-/-}$ mice.*

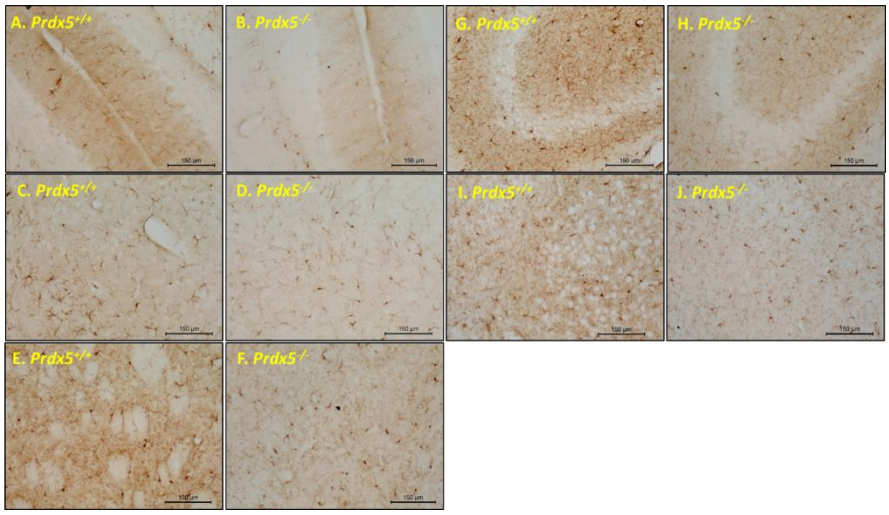

Figure 16. IBA-1 immunostaining of different brain areas of Prdx5$^{+/+}$ and Prdx5$^{-/-}$ old male mice. *(A-B) Cerebellum (Layer), (C-D) Cerebellum (Vestibular nuclei), (E-F) Basal ganglia, (G-H) Hippocampus, (I-J) Amygdala*

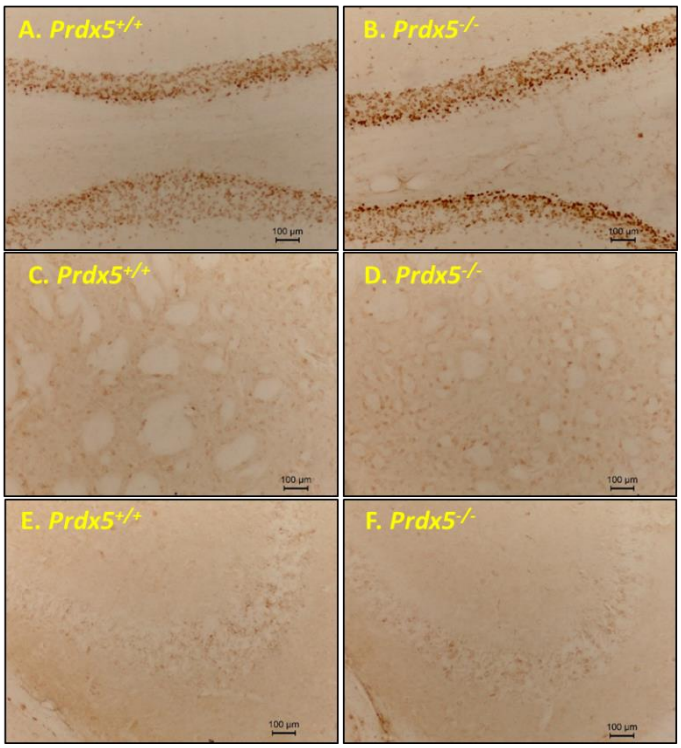

Figure 17. NeuN immunostaining of different brain areas of Prdx5$^{+/+}$ and Prdx5$^{-/-}$ young male mice. *(A-B) Cerebellum (Layer), (C-D) Basal ganglia, (E-F) Hippocampus*

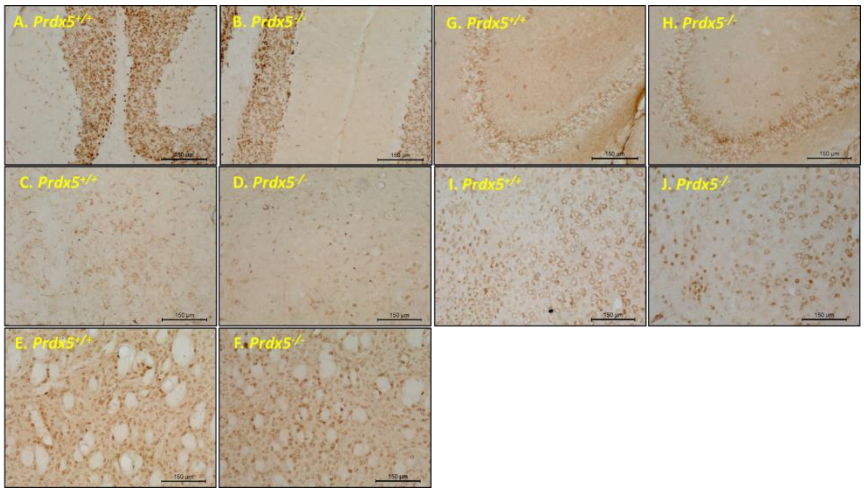

Figure 18. NeuN immunostaining of different brain areas of Prdx5$^{+/+}$ and Prdx5$^{-/-}$ old male mice. *(A-B) Cerebellum (Layer), (C-D) Cerebellum (Vestibular nuclei), (E-F) Basal ganglia, (G-H) Hippocampus, (I-J) Amygdala*

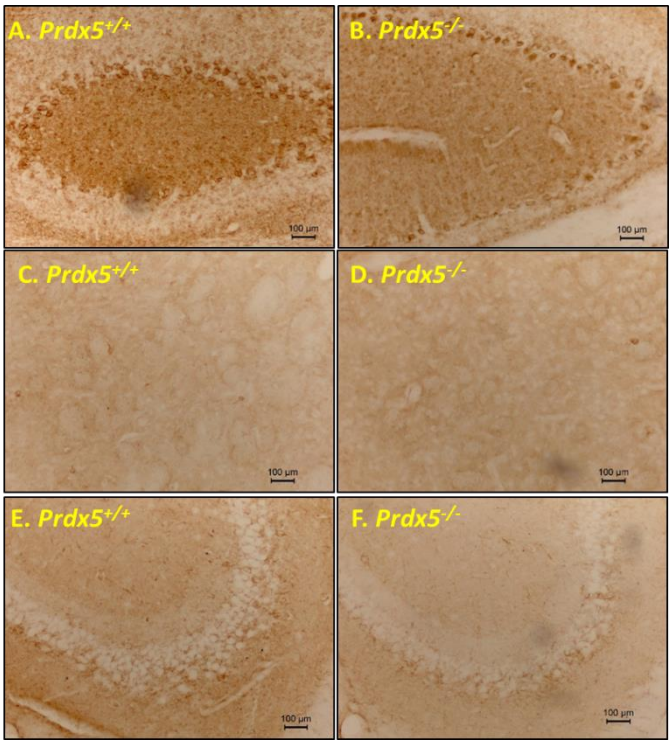

Figure 19. PARV-19 immunostaining of different brain areas of Prdx5$^{+/+}$ and Prdx5$^{-/-}$ young male mice. *(A-B) Cerebellum (Layer), (C-D) Basal ganglia, (E-F) Hippocampus*

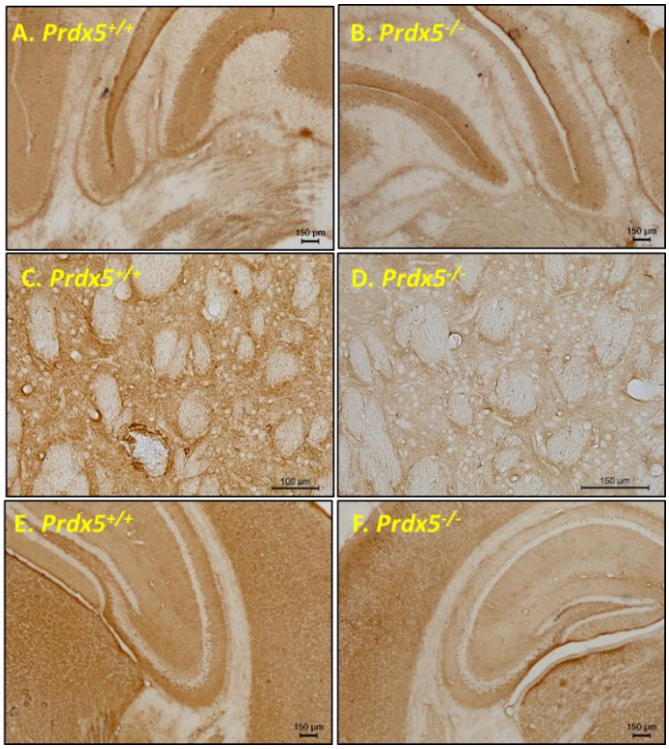

Figure 20. PARV-19 immunostaining of different brain areas of Prdx5$^{+/+}$ and Prdx5$^{-/-}$ old male mice. *(A) Cerebellum (Layer), (B) Basal ganglia, (C) Hippocampus*

Next, to further characterize the different brain cell types, we carried out immunohistochemistry for the same brain regions of young and old *Prdx5$^{+/+}$* and *Prdx5$^{-/-}$* mice. These experiments were performed on three mice per immunodetection, genotype and age.

First, Prdx5 protein was examined in the two genotypes, to confirm that there is no expression of the enzyme in the brain of *Prdx5$^{-/-}$* mice. (Fig.11 and 12). The glial fibrillary acidic protein (GFAP) is expressed by astrocytes in the central nervous system and was used as a marker of activated astrocytes.

Immunostaining of sections suggests that GFAP is decreased in *Prdx5*$^{-/-}$ young mice in cerebellum and increased in hippocampus (Fig.13). On the other hand, in *Prdx5*$^{-/-}$ old mice, GFAP immunostaining appeared to be decreased in hippocampus (Fig.14). However, these differences were mild. IBA-1 immunostaining was used to detect activated microglia in brain sections. In hippocampus of *Prdx5*$^{-/-}$ young mice, IBA-1 immunostaining appeared to be slightly higher compared to the hippocampus of *Prdx5*$^{+/+}$ young mice (Fig.15). This observation was confirmed by Western blotting analysis in brain samples of *Prdx5*$^{-/-}$ and *Prdx5*$^{+/+}$ young mice (Fig. 15G-H). However, in *Prdx5*$^{-/-}$ old mice the IBA-1 staining appeared to be lower in all different brain regions examined (Fig.16). NeuN was used to stain specifically neurons. No difference was observed between *Prdx5*$^{+/+}$ and *Prdx5*$^{-/-}$ mice, as already shown using Nissl staining previously (Fig.17 and 18). Parvalbumin (PARV-19) is a calcium-binding albumin protein, present in GABAergic interneurons in the nervous system, predominantly expressed by chandelier and basket cells in the cortex. In *Prdx5*$^{-/-}$ young mice, expression of PARV-19 was low compared to *Prdx5*$^{+/+}$ animals, especially in the cerebellum (Fig.19). However, no difference was noted in *Prdx5*$^{-/-}$ old mice (Fig.20).

7.4 Discussion

In this study, we examined the functional and histological consequences of *Prdx5* inactivation in the mouse central nervous system. Altogether, our results show that the absence of the functional Prdx5 enzyme in the central nervous system, did not alter dramatically mice behaviors and different markers of central nervous system integrity. However, *Prdx5*$^{-/-}$ mice presented significant less motor coordination and a tendency of higher anxiety as measured using rotarod and elevated plus maze tests, respectively. Although the elevated plus maze test revealed a tendency to anxiety in the *Prdx5*$^{-/-}$ mice, the other tests used to assess the anxiety, like the forced swim and the open field tests did not show a significant difference between *Prdx5*$^{-/-}$ and *Prdx5*$^{+/+}$ mice. It is worth to mention that inactivation of other peroxidases in the central nervous system may affect anxiety in mice. Indeed, it was shown using the open field test that inactivation of *GPx4* in mouse dopaminergic neurons causes higher anxiety and disturbed motor function compared to their wild type littermates [27]. Also, the memory and spatial learning ability of *Prdx5*$^{-/-}$ mice appeared to be unaffected, as measured with Y maze and Water maze tests. However, in a study on Prdx2, it was reported that the 6, 12 and 24 month-old *Prdx2*$^{-/-}$ mice needed more time to find the hidden platform in the Water maze test, suggesting an age-

associated defect in spatial learning [32]. Our behavioral study was conducted with 4-5 month-old *Prdx5*$^{-/-}$ and *Prdx5*$^{+/+}$ mice. It is possible that during aging, spatial learning of *Prdx5*$^{-/-}$ mice could become more affected. A more detailed analysis would be needed, with older mice and with more specific behavioral tests. It must also be noted that in other Prdx study, aged Prdx3 overexpressing mice showed improved cognition that was correlated with reduced brain amyloid beta levels and decreased amyloid beta production, compared to wild type mice [33]. Additionally, in Prdx6 overexpressing mice, it was shown that Prdx6 could accelerate the development of AD through increased amyloidogenesis [25]. On the other hand, none of the Prdx knockout models, except for Prdx2, exhibited a severe phenotype related to defect in the central nervous system [34]–[36], [32], [37]–[39].

Although it was demonstrated that several populations of neurons express high levels of Prdx5 [9] and that humans carrying a nonsense mutation in *Prdx5* gene were suffering from neuronal degeneration as mentioned previously, no significant loss of neurons was detected in brain areas that have been studied in young or aging *Prdx5*$^{-/-}$ mice. We observed some mild differences in the presence of activated astrocytes and microglia in the *Prdx5*$^{-/-}$ mice, more activated astrocytes and microglia in the hippocampus of young *Prdx5*$^{-/-}$ mice and less in old *Prdx5*$^{-/-}$ mice. Light elevation of microglia in the

hippocampus of young *Prdx5*$^{-/-}$ mice was confirmed by Western blot but these results should be confirmed by additional quantifications. Also, the young *Prdx5*$^{-/-}$ mice present lower expression of PARV-19, a marker for interneurons. However, these differences were not dramatic and should be quantified. These findings were thus quite surprising and unexpected. Indeed, as it was mentioned earlier, a recent study suggests that Prdx5 is implicated in the neuroprotection in Alzheimer's disease [28]. This study reports that accumulation of amyloid-beta oligomers led to upregulation of cellular Prdx5 and that overexpression was crucial to prevent neuronal cell death [28]. Taken together, these data, and those mentioned previously, suggest that Prdx5 is an important neuronal cytoprotective enzyme, especially in human.

In order to explain this apparent discrepancy between the function of Prdx5 in mice and humans, we can draw several hypotheses. The first hypothesis is related to the fact that the mutations affecting Prdx5 gene in human (c.361C>T, p.Gln121X) and in our mouse model (*Prdx5*$^{-/-}$) are different and thus affect differently the *Prdx5* gene. The single point mutation (homozygous mutation) in human could lead to a presumably truncated form of Prdx5 protein that would be not functional, whereas in *Prdx5*$^{-/-}$ mice the enzyme is not expressed at all. Nevertheless, if the truncated protein is expressed in human tissues, it how its expression could have an impact on

neuronal cells is still to be elucidated, either by forming aggregates, by affecting signaling cascades among different possible cytotoxic mechanisms, by "fishing" Prdxs, or by inducing oxidative stress due to the loss of the peroxidase activity [40], [41]. For example, it could enhance neuronal cell death by stimulating apoptotic pathway or it could affect the PTEN pathway. As a matter of fact, it has been shown that the loss of a single copy of PTEN leads to mental retardation and epilepsy [42]. Moreover, those symptoms are similar to those depicted for children carrying the *Prdx5* homozygous mutation (Drs. C. Mignot and E. le Guern, personal communication). Further investigations are clearly needed to understand action mechanism of both Prdx5 and its putative truncated form in the brain (PhD project of Marine Delsaute). We could also hypothesize that the severe phenotype can be observed only when the cells lacking Prdx5 expression are stressed or challenged. Indeed, several studies have reported an upregulation of Prdx5 in microglia and macrophages through activation of ROS-sensitive signaling cascade when the cells are exposed to LPS [43], [44]. Using our model of *Prdx5*$^{-/-}$ mice, we have also observed an increased sensitivity of knockout mice under LPS challenge (Chapter 5). Additionally, it was shown that gene expression is dramatically affected between wild type and *Prdx*5 knockdown mice under hypoxia [45]. Finally, upregulation of Prdx5 has been shown in astrocytes of SOD1^{G93A} rat model of ALS (Kuznetsova et al., submitted).

Therefore, we can speculate that under challenging situations related to redox modifications, *Prdx5*$^{-/-}$ mice devoid of Prdx5 would be thus more vulnerable compared to the *Prdx5*$^{+/+}$ mice, highlighting the importance of Prdx5 under oxidative environments.

Strikingly, the mild variation between *Prdx5*$^{-/-}$ and *Prdx5*$^{+/+}$ mice is related to an increase of activated astrocytes and microglia in hippocampus of *Prdx5*$^{-/-}$ young mice. These results could be related to early neuroinflammation. Microglia cells are the major components of the brain immune system [46]. They are morphologically dynamic and exhibit various phenotypes. Under normal conditions, they present their ramified form whereas under oxidative stress they are activated and become enlarged and spherical [46], [47]. Besides, it is well established that microglial cell activation is associated with neuroinflammation and is a hallmark of neurodegenerative events [47], [48].

Why does astrocyte and microglia proliferation/activation take only place in hippocampus and cerebellum? In fact, depending on the brain region, brain cells are differently sensitive to inflammation [49]–[51]. Even though, striatum appears to be more resistant to neuroinflammation compared to other brain regions, it has been reported that hippocampus is a sensitive area [50], [51]. Furthermore, it has been shown that glial cells are not equally distributed within the brain [52]–[54]. Interestingly, in our study, the brain regions that showed an increase in microglia and astrocytes are the regions

known to be the most densely populated by these cell types among the five regions investigated [53], [54]. Therefore our data suggest the elevated number of glial cells appears in regions that are densely populated by those cell types and that are prone to neuroinflammation (at least for the hippocampus). It should also be noted that since we have reported an increase in glial cells in these regions (the elevation was more obvious), it might be possible that we have missed this glial elevation in the other brain regions, leading to a presumably widespread neuroinflammation.

It is then tempting to speculate that glial activation could be modulated by Prdx5. Accordingly, Sun and collaborators [44] have shown that inactivation of *Prdx5* in microglia induced their activation. Furthermore, it has also been reported that Prdx1 is a modulator of microglia activation [55]. Therefore, a novel role of Prdx5 as a regulator of microglial cell activation is still to be determined. It should be pointed out that these data should be interpreted cautiously because these increased concentrations of glial cells were not observed in old mice. Nevertheless we observed these elevations in three independent experiments and we may not completely exclude the possibility that old mice have alleviated the inflammation.

To conclude, *Prdx5*$^{-/-}$ mice tend to be more anxious, they present significant less motor coordination, mild activation of astrocytes and microglia in hippocampus and less signal for a marker of interneurons compared to their

wild type littermates. Although these results should be confirmed by further quantifications, these findings suggest a role of Prdx5 in the central nervous system, implicated mostly in the behavior of the animals under new environments (anxiety), the motor function and probably the response to neuroinflammation. More experiments in behavioral tests and histology are necessary, using mice challenged with inflammatory compounds, such as LPS or virus, to understand better the role of Prdx5 in the central nervous system.

7.5 Materials and Methods

7.5.1 Neurobehavioral testing

Young adult male *Prdx5*$^{-/-}$ and *Prdx5*$^{+/+}$ mice (4-5 month-old) were used for a series of behavioral tests. The transgenic *Prdx5*$^{-/-}$ mice were obtained as described before (see Chapter 5).

7.5.1.1 Modified SHIRPA test

The modified SHIRPA test was used as a simple first-line observational phenotypic test [56]. Briefly, the mice run through a battery of tests consisting in the observation of a variety of spontaneous (viewing jar) and provoked behaviors (arena) such as body position, rearing, locomotor activity, gait, reflexes, and anxiety. A score sheet was used to record the observations.

7.5.1.2 Physiocages test

Physiocages (Panlab-Bioseb, Vitrolles, France) were used to measure individual basal activity [57], [58]. Rearing and locomotor activities were measured during 48 h, after 24 h of habituation.

7.5.1.3 Grip Strength test

Combined forelimb and hindlimb muscle strength was measured by gently lowering a mouse on the top of a grid connected to a sensor (Panlab-Bioseb,

Vitrolles France), so that both front paws and hind paws could grip the grid [59]. Mice were then pulled back steadily down the complete length of the grid until the grip was released. This test consisted of three trials performed with 15 min intervals. Results are means of the two highest values of force recorded, related to body weight.

7.5.1.4 Rotarod test

Mice were tested for their ability to keep their balance and coordination on a rotating rod (Bioseb, Vitrolles, France) [59]. The time (latency) taken to fall off the rod rotating under continuous acceleration (e.g. from 4 to 40 rpm) was measured. Mice performed three trials per day during 5 days. The measured time for each trial was 300s. Animals staying for 300s on the rotating rod, were stopped and recorded as 300s in the test. Results are presented as the mean of the three trials.

7.5.1.5 Open-Field test

This test was used to assess non-forced ambulation in a new environment as mice can move freely without any influence of the examiner [58]. Briefly, mice were placed twice at one-month interval in a square arena (60 x 60 cm) and video-tracked (Ethovision 6.1, Noldus; Wageningen, The Netherlands) for 20 min. The total distance covered by the animals was measured.

7.5.1.6 Elevated Plus Maze test

The elevated plus maze test was used to assess anxiety [58], [60]. Mice were placed in an elevated plus maze consisting of two opposing open arm (exposed place) and two opposing closed arm (safer place). Time spent in each arm and distance covered was recorded by a video tracking system (Ethovision) for 5 min.

7.5.1.7 Y maze test

This test was used to assess working memory [59]. The Y maze was made of 3 identical opaque arms (35 cm length x 5 cm width x 10 cm height) placed at 120° from each other. Mice were placed into a start arm and video-tracked with Ethovision 6.1 for 5 min. Total number of arm entries and arm alternations were recorded. Alternations (taken as an indicator of short-term memory) were determined as successive entries into three different arms.

7.5.1.8 Forced swimming test

The Forced swimming test was carried out according to the literature [61]. Briefly, mice were individually placed in beakers instrumented with a sensor, which records vibrations due to movements, and with a camera recording the displacements in order to quantify activity levels such as swimming periods (mobility) or floating periods (immobility). Raw vibrations data from the sensors were synchronized with the video images from a camera. Automated scoring was performed using the automated FST (Bioseb, Vitrolles, France) for 6 min.

7.5.1.9 Water maze test

The Morris water maze test was used to assess spatial learning and memory [58]–[60]. Water maze was made of a round pool with a diameter of 113 cm, virtually divided into four quadrants (North, South, West and East) and filled with water (26°C). Several visual cues were placed around the pool. Mice were tested on five consecutive days with five consecutive trials per day. During the trials of the first four days, the animals were placed in the pool facing the sidewall and allowed to swim freely to the platform. The latter was placed at the center of the North-West quadrant of the pool and was visible on the training day and submerged 1 cm under the water surface on the three following days. The initial position in which the animal was left in the pool varied among trials. If the animal did not find the platform during a 60 s period, it was gently guided to it, allowed to remain on the platform for 5 s, and removed from the pool before being placed in the next initial starting position in the pool. On the 5th day, the animals were submitted to a probe test, which consisted in allowing the mice to swim freely for 60 s in the pool from which the escape platform had been removed. During all these tests, the mice were video-tracked with Ethovision 6.1. The escape latency time (i.e. the time to reach the platform), the swimming speed, the time spent in each quadrant and the distance from the platform location were registered.

7.5.2 Histological analysis

7.5.2.1 Perfusion and brain extraction

Young (6-7 month-old) and old (18 months-old) *Prdx5*$^{+/+}$ and *Prdx5*$^{-/-}$ mice were perfused with 20ml of 4% paraformaldehyde (PFA) and their brains were collected. The brains were stored in 4% PFA for 48 hours in 4^{o}C and then transferred in 25% sucrose-PBS for 48 hours in 4^{o}C.

7.5.2.2 Fresh-frozen sections

Brains from *Prdx5*$^{+/+}$ and *Prdx5*$^{-/-}$ mice were cut in 25µm sections in microtome and mounted on Superfrost^{+} slides. The slides are dehydrated with increasing ethanol solutions (30-100%), and chloroform/ethanol 100% (1:1) overnight to delipidate them.

7.5.2.3 Nissl staining

The sections were rehydrated in decreasing ethanol solutions (100-30%), stained with 0.1% cresyl violet solution for 10 min, washed with Milli-Q H_2O and dehydrated with increasing ethanol solutions (30-100%) and xylol and mounted with Eukitt Quick-hardening mounting medium (Sigma-Aldrich, 03989). The cresyl violet stains Nissl bodies in the cytoplasm of the neurons in purple-blue.

7.5.2.4 Immunohistochemistry

Immunohistochemistry was performed to examine the expression of specific proteins in different brain areas. Sections of basal ganglia, hippocampus, cerebellum, amygdala and vestibular nuclei were washed with TBS 3 times and endogenous peroxidases were inactivated with 0.6% H_2O_2 – 50mM TBS for 10 min at RT. The sections were washed with TBS 3 times for 5 min and mounted on the Superfrost$^+$ slides. Once the slides were dry, they were washed with 50mM TBS – 0.25% TritonX-100 (TTBS) 2 times for 5 min and incubated with TTBS containing 10% non-fat dry milk for 1 hour at RT. The sections were incubated overnight at 4^{o}C with the primary antibodies,

followed by washing with TTBS 3 times for 5 min and incubated with the secondary biotinylated antibodies for 2 hours at RT. Then, the sections were washed again 3 times for 5 min with TBS and incubated for 1 hour with the ABComplex (Complex Avidin-Biotin coupled with peroxidase, Vector, PK-6100). The peroxidase reaction was visualized by incubating for 2-10 min with diaminobenzidine (DAB, Vector, SK-4100). Finally, the sections were mounted with Eukitt Quick-hardening mounting medium (Sigma-Aldrich, 03989). The slides were observed with a Polyvar Reichter-Jung microscope. Sections were incubated with primary antibodies overnight. Primary antibodies were: rabbit anti-Prdx5 polyclonal antibody (Hormonoly Laboratory-Marloie, G234) 1:2500, mouse anti-NeuN monoclonal antibody (Millipore, MAB377) 1:500, mouse anti-GFAP monoclonal antibody (Sigma-Aldrich, G-3893) 1:200, rabbit anti-IBA1 monoclonal antibody (Wako, 019-19741) 1:500, mouse anti-PARV19 monoclonal antibody (Sigma-Aldrich, P3088) 1:2000. Secondary biotinylated antibodies were incubated for hours with sections. Secondary biolylated antibodies were: biotinylated anti-rabbit antibody (Vector, BA-1000) 1:500, biotinylated anti-mouse antibody (Vector, BA-2000) 1:500.

7.5.2.5 Western blotting

Mouse tissues were homogenized in lysis buffer (Tris 10mM, NaCl 150mM, EDTA 1mM, Triton X-100 1%) containing protease inhibitors cocktail (Roche, 1836170). Protein concentrations were measured using the Pierce BCA protein assay kit (Thermo-Scientific, 23225) and using bovine serum albumin (BSA) as the standard. Protein samples in loading buffer (Tris 45mM pH 6.8, Glycerol 10%, SDS 1%, BPP 0.25%, DTT 0.5M) were subjected to electrophoresis on 12% Mini-Protean SF TGX gels (Bio-Rad) using electrophoresis buffer (Tris 50mM, Glycine 150mM, SDS 0.1%) and transferred to nitrocellulose membranes (Amersham Protran 0.45 µM NC GE Healthcare, 10.600.002). Membranes were first incubated for 1h at room temperature in blocking solution (0.1% Tween 20 - TBS buffer containing 5% non-fat dry milk). After washing with 0.1% Tween 20 - TBS buffer, the membranes were probed with rabbit anti-IBA1 monoclonal antibody (Wako, 019-19741) 1:1000, followed by horseradish peroxidase-conjugated anti-rabbit secondary antibody (DAKO, p0448) 1:2000. The reaction was detected by chemiluminescence using ECL Western Lightning Chemiluminescence Reagent Plus (Perkin Elmer Life Sciences, NEL104) and exposed to film (Amersham Hyperfilm™ ECL, 28-9068-37). The ImageJ software was used for Western blot quantifications.

7.6 References

[1] S. G. Rhee, “Overview on Peroxiredoxin,” *Mol. Cells*, vol. 39, no. 1, pp. 1–5, 2016.

[2] Z. A. Wood, E. Schroder, J. R. Harris, and L. B. Poole, “Structure , mechanism and regulation of peroxiredoxins,” *Trends Biochem. Sci.*, vol. 28, no. 1, pp. 3–8, 2003.

[3] B. Knoops, E. Loumaye, and V. Van Der Eecken, “Evolution of Peroxiredoxins: Taxonomy, homology and characterization,” *Peroxiredoxin Syst.*, pp. 27–40, 2007.

[4] S. G. Rhee and I. S. Kil, “Multiple Functions and Regulation of Mammalian Peroxiredoxins,” *Annu. Rev. Biochem.*, vol. 86, no. 5, pp. 1–27, 2017.

[5] G. Ferrer-Sueta, B. Manta, H. Botti, R. Radi, M. Trujillo, and A. Denicola, “Factors affecting protein thiol reactivity and specificity in peroxide reduction,” *Chem. Res. Toxicol.*, vol. 24, pp. 434–450, 2011.

[6] M. S. Seo, S. W. Kang, K. Kim, I. C. Baines, T. H. Lee, and S. G.

Rhee, “Identification of a new type of mammalian peroxiredoxin that forms an intramolecular disulfide as a reaction intermediate,” *J. Biol. Chem.*, vol. 275, no. 27, pp. 20346–20354, 2000.

[7] A. Perkins, K. J. Nelson, D. Parsonage, L. B. Poole, and P. A. Karplus, “Peroxiredoxins: guardians against oxidative stress and modulators of peroxide signaling,” *Trends Biochem. Sci.*, vol. 40, no. 8, pp. 435–445, 2015.

[8] M. K. Cha, K. H. Suh, and I. H. Kim, “Overexpression of peroxiredoxin i and thioredoxin1 in human breast carcinoma,” *J. Exp. Clin. Cancer Res.*, vol. 28, no. 93, pp. 1–12, 2009.

[9] J. Goemaere and B. Knoops, “Peroxiredoxin distribution in the mouse brain with emphasis on neuronal populations affected in neurodegenerative disorders,” *J. Comp. Neurol.*, vol. 520, pp. 258–280, 2012.

[10] J. R. Godoy *et al.*, “Redox atlas of the mouse. Immunohistochemical detection of glutaredoxin-, peroxiredoxin-, and thioredoxin-family proteins in various

tissues of the laboratory mouse," *Biochim. Biophys. Acta - Gen. Subj.*, vol. 1810, pp. 2–92, 2011.

[11] B. Knoops *et al.*, "Cloning and characterization of AOEB166, a novel mammalian antioxidant enzyme of the peroxiredoxin family," *J. Biol. Chem.*, vol. 274, pp. 30451–30458, 1999.

[12] A. Kropotov *et al.*, "A novel human DNA-binding protein with sequence similarity to a subfamily of redox proteins which is able to repress RNA-polymerase-III-driven transcription of the Alu-family retroposons in vitro," *Eur J Biochem*, vol. 260, pp. 336–346, 1999.

[13] H. Yamashita *et al.*, "Characterization of Human and Murine PMP20 Peroxisomal Proteins That Exhibit Antioxidant Activity in Vitro," *J. Biol. Chem.*, vol. 274, no. 42, pp. 29897–29904, 1999.

[14] J.-P. Declercq, C. Evrard, A. Clippe, D. Vander Stricht, A. Bernard, and B. Knoops, "Crystal Structure of Human Peroxiredoxin 5, a Novel Type of Mammalian Peroxiredoxin at 1.5 A Ê Resolution," *J. Mol. Biol.*, vol. 311, pp. 751–759, 2001.

[15] T. Lee, S. J. Kim, S. W. Kang, K. Lee, S. G. Rhee, and D. Yu, "Molecular Cloning and Characterization of the Mouse Peroxiredoxin V Gene," *Biochem. Biophys. Res. Commun.*, vol. 362, pp. 356–362, 2000.

[16] N. T. Nguyên-nhu *et al.*, "Human peroxiredoxin 5 gene organization, initial characterization of its promoter and identification of alternative forms of mRNA," *Biochim. Biophys. Acta - Gene Struct. Expr.*, vol. 1769, pp. 472–483, 2007.

[17] A. Kropotov, N. Usmanova, V. Serikov, B. Zhivotovsky, and N. Tomilin, "Mitochondrial targeting of human peroxiredoxin V protein and regulation of PRDX5 gene expression by nuclear transcription factors controlling biogenesis of mitochondria," *FEBS J.*, vol. 274, pp. 5804–5814, 2007.

[18] G. Leyens, I. Donnay, and B. Knoops, "Cloning of bovine peroxiredoxins - Gene expression in bovine tissues and amino acid sequence comparison with rat, mouse and primate peroxiredoxins," *Comp. Biochem. Physiol. - B Biochem. Mol. Biol.*, vol. 136, pp. 942–955, 2003.

[19] G. Leyens, B. Knoops, and I. Donnay, “Expression of peroxiredoxins in bovine oocytes and embryos produced in vitro,” *Mol. Reprod. Dev.*, vol. 69, pp. 243–251, 2004.

[20] M. H. Jin *et al.*, “Characterization of neural cell types expressing peroxiredoxins in mouse brain,” *Neurosci. Lett.*, vol. 381, no. 3, pp. 252–257, 2005.

[21] S. Kato *et al.*, “Redox system expression in the motor neurons in amyotrophic lateral sclerosis (ALS): immunohistochemical studies on sporadic ALS, superoxide dismutase 1 (SOD1)-mutated familial ALS, and SOD1-mutated ALS animal models.,” *Acta Neuropathol.*, vol. 110, no. 2, pp. 101–112, 2005.

[22] R. Sultana *et al.*, “Proteomics analysis of the Alzheimer’s disease hippocampal proteome,” *J. Alzheimer’s Dis.*, vol. 11, no. 2, pp. 153–164, 2007.

[23] Y. Gan *et al.*, “Transgenic Overexpression of Peroxiredoxin-2 Attenuates Ischemic Neuronal Injury Via Suppression of a Redox-Sensitive Pro-Death Signaling Pathway,” *Antioxid. Redox Signal.*, vol. 17, no. 5, pp. 719–732, 2012.

[24] C. W. Strey *et al.*, “Dysregulation of stathmin, a microtubule-destabilizing protein, and up-regulation of Hsp25, Hsp27, and the antioxidant peroxiredoxin 6 in a mouse model of familial amyotrophic lateral sclerosis,” *Am. J. Pathol.*, vol. 165, no. 5, pp. 1701–1718, 2004.

[25] H. M. Yun *et al.*, “Acceleration of the development of alzheimer’s disease in amyloid beta-infused peroxiredoxin 6 overexpression transgenic mice,” *Mol. Neurobiol.*, vol. 48, no. 3, pp. 941–951, 2013.

[26] M. Pirson and B. Knoops, “Expression of peroxiredoxins and thioredoxins in the mouse spinal cord during embryonic development,” *J. Comp. Neurol.*, vol. 523, pp. 2599–2617, 2015.

[27] S. C. Schriever *et al.*, “Alterations in neuronal control of body weight and anxiety behavior by glutathione peroxidase 4 deficiency,” *Neuroscience*, vol. 357, pp. 241–254, 2017.

[28] B. Kim, J. Park, K.-T. Chang, and D.-S. Lee, “Peroxiredoxin 5 prevents amyloid-beta oligomer- induced neuronal cell death

by inhibiting ERK– Drp1-mediated mitochondrial fragmentation," *Free Radic. Biol. Med.*, vol. 90, pp. 184–194, 2015.

[29] S. De Simoni, J. Goemaere, and B. Knoops, "Silencing of peroxiredoxin 3 and peroxiredoxin 5 reveals the role of mitochondrial peroxiredoxins in the protection of human neuroblastoma SH-SY5Y cells toward MPP+," *Neurosci. Lett.*, vol. 433, pp. 219–224, 2008.

[30] S. De Simoni, D. Linard, E. Hermans, B. Knoops, and J. Goemaere, "Mitochondrial peroxiredoxin-5 as potential modulator of mitochondria-ER crosstalk in MPP+-induced cell death," *J. Neurochem.*, vol. 125, pp. 473–485, 2013.

[31] L. Valek, M. Kanngieber, A. Haussler, N. Agarwal, C. H. Lillig, and I. Tegeder, "Redoxins in peripheral neurons after sciatic nerve injury," *Free Radic. Biol. Med.*, vol. 89, pp. 581–592, 2015.

[32] S. U. Kim *et al.*, "Peroxiredoxin II preserves cognitive function against age-linked hippocampal oxidative damage," *Neurobiol.*

Aging, vol. 32, pp. 1054–1068, 2011.

[33] L. Chen, R. Na, and Q. Ran, “Enhanced defense against mitochondrial hydrogen peroxide attenuates age-associated cognition decline,” *Neurobiol. Aging*, pp. 1–10, 2014.

[34] Y. Wang, S. I. Feinstein, Y. Manevich, Y.-S. Ho, and A. B. Fisher, “Peroxiredoxin 6 gene-targeted mice show increased lung injury with paraquat-induced oxidative stress,” *Antioxid. Redox Signal.*, vol. 8, no. 1&2, pp. 229–237, 2006.

[35] C. A. Neumann *et al.*, “Essential role for the peroxiredoxin Prdx1 in erythrocyte antioxidant defence and tumour suppression,” *Nature*, vol. 424, no. 6948, pp. 561–565, 2003.

[36] K.-K. Lee *et al.*, “Peroxiredoxin II is essential for sustaining life span of erythrocytes in mice,” *Blood*, vol. 101, no. 12, pp. 5033–5038, 2003.

[37] L. Li *et al.*, “Increased susceptibility of MER5 (peroxiredoxin III) knockout mice to LPS-induced oxidative stress,” *Biochem. Biophys. Res. Commun.*, vol. 355, pp. 715–721, 2007.

[38] Y. Iuchi *et al.*, “Peroxiredoxin 4 knockout results in elevated

spermatogenic cell death via oxidative stress," *Biochem. J*, vol. 419, pp. 149–158, 2009.

[39] X. Wang *et al.*, "Mice with Targeted Mutation of Peroxiredoxin 6 Develop Normally but Are Susceptible to Oxidative Stress," *J. Biol. Chem.*, vol. 278, pp. 25179–25190, 2003.

[40] D. Weber *et al.*, "Proteostasis, oxidative stress and aging," *Redox Biol.*, vol. 13, pp. 550–567, 2017.

[41] T. Grune, "Oxidative stress, aging and the proteasomal system," *Biogerontology*, vol. 1, no. 1, pp. 31–40, 2000.

[42] P. Garcia-Junco-Clemente and P. Golshani, "PTEN: A master regulator of neuronal structure, function, and plasticity," *Commun. Integr. Biol.*, vol. 7, no. 1, p. e28358, 2014.

[43] K. Abbas, J. Breton, C. R. Picot, V. Quesniaux, C. Bouton, and J. C. Drapier, "Signaling events leading to peroxiredoxin 5 up-regulation in immunostimulated macrophages," *Free Radic. Biol. Med.*, vol. 47, pp. 794–802, 2009.

[44] H. N. Sun *et al.*, "Microglial peroxiredoxin v acts as an inducible anti-inflammatory antioxidant through cooperation with redox

signaling cascades," *J. Neurochem.*, vol. 114, pp. 39–50, 2010.

[45] H. Y. Yang *et al.*, "Proteomic analysis of protein expression affected by peroxiredoxin v knock-down in hypoxic kidney," *J. Proteome Res.*, vol. 9, pp. 4003–4015, 2010.

[46] S. Thameem Dheen, C. Kaur, and E.-A. Ling, "Microglial Activation and its Implications in the Brain Diseases," *Curr. Med. Chem.*, 2007.

[47] L. Qin *et al.*, "Systemic LPS causes chronic neuroinflammation and progressive neurodegeneration," *Glia*, 2007.

[48] W. J. Streit, R. E. Mrak, and W. S. T. Griffin, "Microglia and neuroinflammation: A pathological perspective," *J. Neuroinflammation*, 2004.

[49] W. G. Kim, R. P. Mohney, B. Wilson, G. H. Jeohn, B. Liu, and J. S. Hong, "Regional difference in susceptibility to lipopolysaccharide-induced neurotoxicity in the rat brain: role of microglia.," *J. Neurosci.*, 2000.

[50] B. Hauss-Wegrzyniak, M. G. Vannucchi, and G. L. Wenk, "Behavioral and ultrastructural changes induced by chronic

neuroinflammation in young rats," *Brain Res.*, 2000.

[51] S. Liraz-Zaltsman *et al.*, "Regional sensitivity to neuroinflammation: In vivo and in vitro studies," *Synapse*, 2011.

[52] F. Hajós and M. Kálmán, "Distribution of glial fibrillary acidic protein (GFAP)-immunoreactive astrocytes in the rat brain," *Exp. Brain Res.*, vol. 78, pp. 147–163, 1989.

[53] L. J. Lawson, V. H. Perry, P. Dri, and S. Gordon, "Heterogeneity in the distribution and morphology of microglia in the normal adult mouse brain," *Neuroscience*, 1990.

[54] V. L. Savchenko, I. R. Nikonenko, G. G. Skibo, and J. A. McKanna, "Distribution of microglia and astrocytes in different regions of the normal adult rat brain," *Neurophysiology*, 1997.

[55] S. U. Kim *et al.*, "Peroxiredoxin I is a ROS/p38 MAPK-dependent inducible antioxidant that regulates NF-κB-mediated iNOS induction and microglial activation," *J. Neuroimmunol.*, 2013.

[56] D. C. Rogers, E. M. C. Fisher, S. D. M. Brown, J. Peters, A. J.

Hunter, and J. E. Martin, “Behavioral and functional analysis of mouse phenotype: SHIRPA, a proposed protocol for comprehensive phenotype assessment,” *Mamm. Genome*, vol. 8713, pp. 711–713, 1997.

[57] L. Poekes *et al.*, “Defective adaptive thermogenesis contributes to metabolic syndrome and liver steatosis in obese mice,” *Clin. Sci.*, vol. 131, no. 4, pp. 285–296, 2017.

[58] S. Lepannetier *et al.*, “Activation of TRPC1 Channel by Metabotropic Glutamate Receptor mGluR5 Modulates Synaptic Plasticity and Spatial Working Memory.,” *Front. Cell. Neurosci.*, vol. 12, no. September, p. 318, 2018.

[59] R. Rzem *et al.*, “A mouse model of L-2-hydroxyglutaric aciduria, a disorder of metabolite repair,” *PLoS One*, vol. 10, no. 3, 2015.

[60] C. Boucherie *et al.*, “Neural progenitor fate decision defects, cortical hypoplasia and behavioral impairment in Celsr1-deficient mice,” *Mol. Psychiatry*, vol. 23, no. 3, pp. 723–734, 2018.

[61] E. Ahmed, M. K. Tawfik, S. S. Essawy, A. S. Ahmed, and E.

Hermans, “Cysteamine Potentiates the Anti-Depressive Effects of Venlafaxine in Corticosterone-Induced Anxiety/Depression Mouse Model: Effect on Brain-Derived Neurotrophic Factor and Tropomyosin-Related Kinase B,” *Egypt. J. Basic Clin. Pharmacol.*, vol. 8, pp. 1–15, 2018.

PART IV: General discussion, conclusions and perspectives

8. General discussion

The aim of this work was to study Prdx5 *in vivo*, in order to investigate its functions in different physiological and pathological situations. For this purpose, a *Prdx5*$^{-/-}$ mouse model using the gene-trap (gt) strategy was generated by our group in collaboration with Prof. Fadel Tissir (UCLouvain-IoNS). At the time my study started, no *Prdx5*$^{-/-}$ mouse model was described in the literature. Moreover, several attempts to obtain a *Prdx5*$^{-/-}$ mouse model in our lab failed.

Once the first *Prdx5*$^{gt/gt}$ mice were obtained, my research project was focused on the characterization of this mouse model, first by general observations and, secondly, by examining the impact of *Prdx5* inactivation on the central nervous system (CNS). Indeed, the initial goal of my work was to study *Prdx5* functions in the nervous system, based on the observations that Prdx5 is highly expressed in the brain and the spinal cord, but also the discovery by pediatric neurologists at La Pitié-Salpêtrière in Paris of a homozygous mutation in *Prdx5* gene in two children, which were exhibiting mental retardation and epilepsy [291], [305], [312], [313]. In parallel, our interest was also focused on the role of Prdx5 in the immune system and inflammation based on several publications suggesting Prdx5 involvement in pro-inflammatory mechanisms in phagocytes [305], [314], [315]. Moreover, unexpectedly, during the progress of this study, several malignant cancers developed in *Prdx5*$^{-/-}$ mice, suggesting the implication of Prdx5 in carcinogenesis [302], [305], [315]. All these different aspects of my study were divided in the three chapters in this thesis.

8.1 Role of Prdx5 in inflammation

In this study, we showed that *Prdx5*$^{-/-}$ mice are more sensitive to endotoxic shock caused by intraperitoneal injection of LPS. Additionally, a proteomic analysis revealed that different proteins related to the inflammatory response are up- and down-regulated in *Prdx5*$^{-/-}$ peritoneal phagocytes exposed *in vitro* to LPS. Among these proteins, CD82 antigen and the Interleukin enhancer-binding factor 3 (Ilf3) were strongly downregulated. A number of other proteins related to inflammation seem to be downregulated in the *Prdx5*$^{-/-}$ phagocytes, like the CD180 antigen, Ly9 and Irgq. Moreover, the release of the TNF-α from *Prdx5*$^{-/-}$ phagocytes was significantly slightly higher. Interestingly, it was also recently shown that *Prdx5* knockdown in dendritic cells resulted in an increase in inflammatory cytokine and chemokine production [297]. Our main hypothesis for the role of Prdx5 in inflammatory response is based on Prdx5 cytoprotective activity in the cells. It is well known that during inflammation triggered by LPS, the LPS-TLR4 signaling pathway is activated, leading to the production high levels of ROS/RNS and activation of NF-κB [316], [317]. Although macrophages, microglia and neutrophils express high levels of antioxidant enzymes, constitutive expression of these enzymes would not be able to handle the burst of ROS/RNS that are produced during inflammation [318]. Given also the fact that Prdx5 is upregulated in microglia and macrophages during LPS exposure [184], [296], we could hypothesize that inactivation of *Prdx5* gene in our mouse model leads to a greater sensitivity regarding the inflammation process. This sensitivity in LPS has been shown in other knockout models for antioxidant enzymes or for transcription factors which modulate antioxidant enzyme expression. Mice lacking Srx1, Prdx2, Prdx3 or Nrf2 are also more sensitive to LPS-induced endotoxic shock [221], [228], [319], [320]. All of

them cope with oxidative stress within the cell. Therefore, the control of cellular levels of ROS/RNS is crucial to prevent lethality by sepsis and Prdx5 would be an essential scavenger enzyme which affords protection against acute oxidative stress [161], [314].

The second hypothesis relies on the fact that Prdx5 could modulate LPS-TLR4 signaling pathway. It was shown that Prdx5 is involved in the regulation of LPS/TLR4-induced Il-6 production in mouse macrophages, by modulating the jak-stat5 signaling pathway [298]. According to this study, Prdx5 could prevent the phosphorylation of Jak2 by interacting with it through its Cp and hence inhibits partially Il-6 production. In support of this hypothesis, another study has shown that when Prdx5 is upregulated, it inhibits the MAPKs p38 and JNK that are activated by LPS-TLR4 signaling pathway in macrophages [184]. It is tempting to propose that this inhibition is abolished in *Prdx5*$^{-/-}$ mice, leading to the activation of MAPK cascade and triggers an enhancement of inflammatory processes.

We cannot eliminate the possibility that the extracellular form of Prdx5, can act as a DAMP and activates the TLR4 signaling pathway [186], [190]. Indeed, Prdx5, among other Prdxs, has been shown to promote pro-inflammatory cytokines production and release by interacting with TLR4 [186], [188]. The binding and the interaction of the extracellular Prdx5 with TLR4 was recently confirmed by our group in a collaborative project using atomic force microscopy (AFM) [190]. Although these studies suggest that inflammation enhancement by extracellular Prdxs is likely to induce chronic inflammation, the physiological role of the secreted/extracellular Prdx5 is still unknown and remains to be clarified. It could be possible that after Prdx5 is binding to TLR4, other pathways are activated and play a role in the induction of the cytokines. Another possibility is that Prdx5 would be in competition with LPS

for the binding to TLR4 in *Prdx5*$^{+/+}$ macrophages, which could explain the higher sensitivity of the *Prdx5*$^{-/-}$ mice to LPS, when Prdx5 is absent.

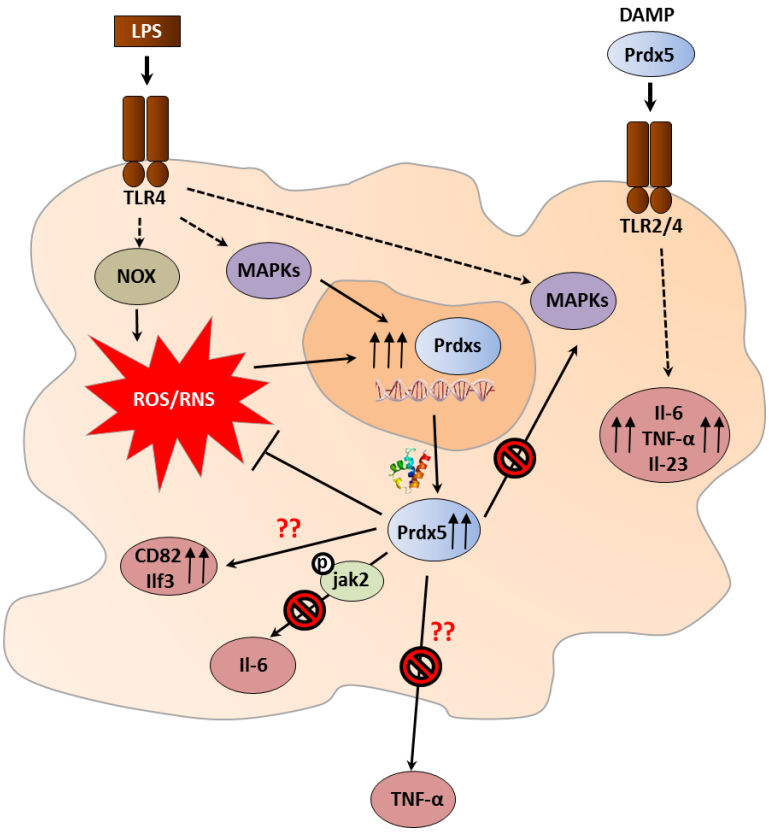

Figure 11. Prdx5 involvement in inflammation in phagocytes. Prdx5 expression is upregulated during inflammation caused by LPS [184], [296]. When LPS/TLR4 pathway is activated, MAPKs can lead to upregulation of Prdx5 expression in cells. Activation of the JNK-dependent NO pathway leads to higher production of ROS/RNS, resulting in upregulation of Prdx5 expression [296]. Prdx5 scavenges the ROS/RNS as a cytoprotective enzyme. Prdx5 inhibits the production of Il-6, by preventing the phosphorylation of jak2, and the MAPKs activated by LPS/TLR4 [184], [298]. Prdx5 can also act as a DAMP, binding to TLR2/4 receptors and increasing the expression and release of Il-6, TNF-α and Il-23 [186], [188], [190]. In the present study, results suggest that Prdx5 would enhances CD82 and Ilf3 expression and would decrease TNF-α release, by still unkown mechanisms.

8.2 Role of Prdx5 in cancer

The role of Prdx5 as a tumor suppressor was investigated, since several aging *Prdx5*$^{-/-}$ mice, representing 41% of the total aging *Prdx5*$^{-/-}$ mice, developed malignant cancers such as lymphomas and hepatocarcinomas. The characterization of the tumors was assessed with the use of specific cell markers of these types of cancer. It is worth to mention that in *Prdx5*$^{+/+}$ mice, malignant cancers were also detected but the range of cancers was significantly lower (16% of the total *Prdx5*$^{+/+}$ mice) and there were different types of cancers (hepatocarcinoma and leukemia, but not lymphoma). Accordingly, in the literature, several papers report the involvement of different Prdxs in lymphomas by suppressing [200] or enhancing [214], [321], [322] their development.

In this study, we attempted to clarify Prdx5 involvement in the signaling pathways leading to carcinogenesis. One of the most common signaling pathway involved in carcinogenesis is the PI3K/Akt/PTEN pathway, which is known for its role in cell cycle regulation and therefore for its implication in cellular quiescence, proliferation, cancer, and longevity [323], [324]. Lymphoma tumors examined in *Prdx5*$^{-/-}$ mice showed higher Akt phosphorylation and low level of PTEN. Additionally, MEF cells of *Prdx5*$^{-/-}$ mice presented higher Akt phosphorylation upon exposure to H_2O_2. In our hypothesis, Prdx5 would protect PTEN from oxidation during oxidative stress conditions, keeping low the levels of phosphorylated Akt. In the absence of Prdx5, PTEN would be overoxidized and subsequently degraded and thus inactivated, leading to higher phosphorylated Akt levels and overactivation of the PI3K/Akt/PTEN pathway, which would lead to cell proliferation and carcinogenesis. This hypothesis is supported by data of the literature showing that when *Prdx1* is silenced, PTEN is also inactivated and Akt

phosphorylation is increased upon oxidative stress [201]. Moreover, it must be emphasized that*Prdx1* and *Prdx5* genes share common transcription regulation mechanisms [196].

The MAPK signaling pathway, which is also linked to carcinogenesis, did not appear to be affected in the tumors analyzed in our mouse model. The phosphorylation of JNK, p38 and p44/42 were kept low or were even absent in *Prdx5*$^{-/-}$ tumors. However, on the contrary, *Prdx1* inactivation decreases the mobility and invasion of pancreatic cancer cells, by forming Prdx1-phospho-p38 complex [203]. On the other hand, in *Prdx1*$^{-/-}$ MEF cells the phosphorylation of p38, MAPK, and JNK was reported to be enhanced while the phosphorylation of Erk1/2 is suppressed, suggesting an anti-apoptotic role of Prdx1 [325].

Prdxs decrease ROS/RNS cellular levels that are thought to contribute to the development of different diseases, such as cancer but Prdxs are also able to scavenge peroxides in cancer cells, potentially protecting cancer cells from lethal oxidative damages [304], [326]. Prdx5 is upregulated or downregulated in different cancers [231], [279], [306], [307], [309]–[311], [321], [327]. Accordingly, the absence of Prdx5 the PI3K/Akt/PTEN signaling pathway is more activated in MEF cells upon hydrogen peroxide exposure, at the embryonic stage, while the pathway is less affected in tumor cells for which carcinogenesis has already occurred. Thus, it is crucial to examine the role of Prdx5 at different stages of carcinogenesis.

Our results suggest that there is a complex mechanism between Prdx5 and the signaling pathways related to cell survival, proliferation, apoptosis and tumorigenesis. A deeper and more detailed investigation should be conducted to clarify the exact and the potential dual role of Prdx5 in

particular and Prdxs in general, in the activation or inactivation of these pathways during carcinogenesis.

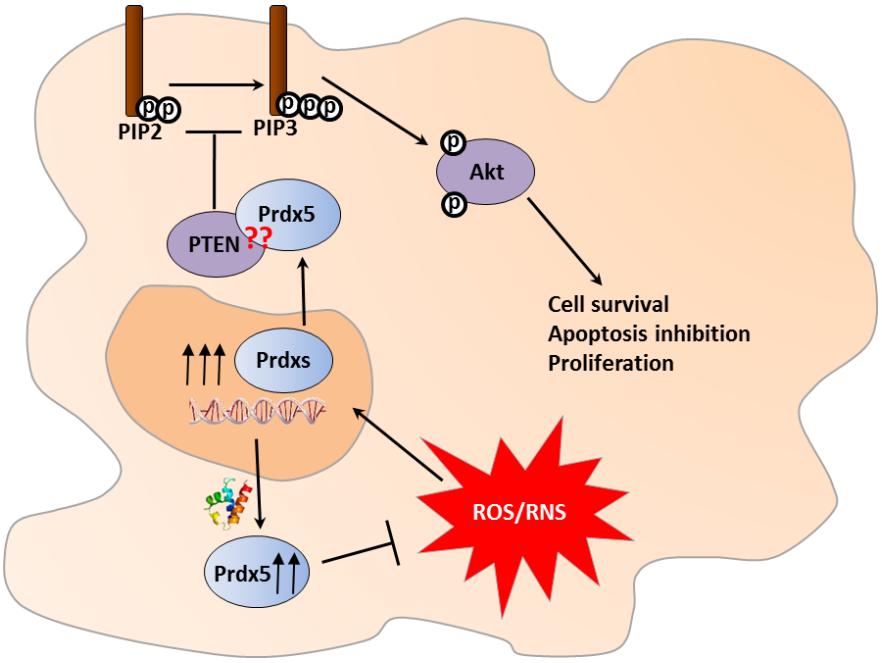

Figure 12. Hypothetical Prdx5 involvement in carcinogenesis. Prdx5 expression is upregulated upon high levels of ROS/RNS or is expressed constitutively at high level, and can act as an antioxidant enzyme to allow cells to cope with ROS/RNS. Prdx5 may protect PTEN from oxidation, thus keeping PTEN active to inhibit the phosphorylation of PIP2 to PIP3. PIP3 recruits Akt, a major protein for activation of pathways related to cell survival, apoptosis inhibition and cell proliferation [323], [324].

8.3 Role of Prdx5 in the central nervous system

In this part of this thesis, which is presented in the last experimental chapter, our goal was to examine the consequences of *Prdx5* inactivation in the CNS. Behavioral tests showed that *Prdx5*$^{-/-}$ mice presented significantly less motor coordination and a tendency of higher anxiety while their memory and

spatial learning ability did not appear to be affected. Accordingly, studies performed on other antioxidant enzyme knockout models, such as the *GPx4*$^{-/-}$ animals, revealed also that mice presented higher anxiety and disturbed motor function [111]. On the contrary, *Prdx2*$^{-/-}$ mice showed age-associated defect in spatial learning [217]. Overall, none of the Prdx knockout mouse models, except *Prdx2*$^{-/-}$ mice, exhibits a severe phenotype linked to CNS defects [179], [200], [212], [217], [228], [238], [261]. Accordingly, no significant loss of neurons was observed in *Prdx5*$^{-/-}$ mice (young and old). However some results suggest that microglia and astrocytes are activated in the hippocampus of young *Prdx5*$^{-/-}$ mice. More consequences of *Prdx5* inactivation was expected in the central nervous system, based its high expression [291] and the severe defects associated to homozygous *Prdx5* mutation in human as mentioned before.

It could be hypothesized that the different phenotype observed for mice and humans is linked to different mutations in the two species as discussed in chapter 7. In human, the non-sense mutation potentially allow the translation of a truncated Prdx5 protein, while in our *Prdx5*$^{-/-}$ mouse model the protein is not expressed at all. If the truncated protein is expressed in human, it could affect neurons either by forming aggregates, by affecting signaling cascades among different possible cytotoxic mechanisms, by "fishing" peroxiredoxins, or by inducing oxidative stress due to the loss of the peroxidase activity [328], [329]. These hypotheses should be tested with further experiments. On the other hand, a severe phenotype could be observed only when the organism is stressed or challenged. This assumption is based on the fact that Prdx5 is upregulated in microglia and macrophages during LPS exposure [184], [296]. or under hypoxia [283]. In our CNS analysis, *Prdx5*$^{-/-}$ mice were not challenged by LPS or hypoxia. Our results suggest that

Prdx5 silencing could activate microglial and astroglial cells in the hippocampus and this could be related to neuroinflammation.

As a conclusion, in our *Prdx5*$^{-/-}$ mouse model, the CNS is not dramatically affected. Our results suggest that some motor functions could be altered as well as the behavior of the animals under new environments (anxiety). Moreover, whether inactivation of *Prdx5* in the CNS affects neuroinflammatory responses is still to be confirmed using challenging conditions.

9. Conclusion and Perspectives

The antioxidant enzyme Prdx5 seems to present multiple roles in different cell procedures. The implication of Prdx5 in inflammation has been demonstrated earlier. In this study, we showed that *Prdx5*$^{-/-}$ mice are more prone to inflammation induced by LPS, as well as many proteins related to inflammation are up- and down-regulated in *Prdx5*$^{-/-}$ phagocytes exposed to LPS. It would be interesting to measure cell apoptosis and possible necrosis in the *Prdx5*$^{-/-}$ mice compared to the *Prdx5*$^{+/+}$. Additionally, the release of inflammatory cytokines should be examined, to determine whether *Prdx5*$^{-/-}$ mice respond differently. The possible Prdx5 role as a DAMP could be tested also in peritoneal *Prdx5*$^{-/-}$ cells, in order to define whether Prdx5 is in competition with LPS for the TLR4 binding on phagocytes.

The absence of Prdx5 didn't affect the number of neurons in the brain and the behavior of the *Prdx5*$^{-/-}$ mice, but it seems to enhance the proliferation of glial cells in hippocampus, a fact that could relate the Prdx5 with the neuroinflammation. Further investigation for the role of Prdx5 in inflammation and also neuroinflammation is necessary, in order to comprehend fully the mechanism through Prdx5 protects the cells. *Prdx5*$^{-/-}$ and *Prdx5*$^{+/+}$ mice could be challenged with paraquat, an organic compound that produces superoxide anions and that is used experimentally to induce Parkinson's disease symptoms in rodents [330]. New behavioral tests and immunohistological analyses could be performed in these animals. Specific behavioral tests linked to neuroinflammation should be performed also in young but also aged animals. Another possibility is to cross *Prdx5*$^{-/-}$ mice with other mice models for neurodegenerative diseases, like for Parkinson's disease, Alzheimer's disease and Amyotrophic lateral sclerosis.

Moreover, in this study we showed an implication of Prdx5 in tumorigenesis. An elevated percentage of *Prdx5*$^{-/-}$ mice present lymphoma and hepatocarcinoma, while *Prdx5*$^{-/-}$ MEF cells are showing higher Akt phosphorylation, a key-protein for the activation of cell survival, proliferation and apoptosis inhibition signaling pathways. On the other hand, in tumor samples the Akt phosphorylation is not elevated strongly, proposing that Prdx5 could have a different role in the activation of the Akt/PTEN signaling pathway during the different stages of development. More mechanistical studies are mandatory to explore the way that Prdx5 is involved in the activation of the pathways leading to tumorigenesis. The tumor samples should be tested for DNA mutations, in order to identify mutated genes related to the tumorigenesis in the mice. *Prdx5*$^{-/-}$ mice could be also crossed with other mouse models more prone to develop cancers, like *Prdx1*$^{-/-}$ mice that present hemolytic anaemia and malignant tumors. Double mutants for Prdx1 and Prdx5 should be examined for their sensitivity to develop cancers. Double mutants *Prdx5*$^{-/-}$ /*PTEN*$^{-/-}$ could be also obtained to study more precisely the role of Prdx5 in the Akt/PTEN signaling pathway.

10. References

[1] B. Halliwell and J. M. C. Gutteridge, *Free Radicals in Biology and Medicine*. 1999.

[2] A. Latifi, M. Ruiz, and C. C. Zhang, “Oxidative stress in cyanobacteria,” *FEMS Microbiol. Rev.*, vol. 33, no. 2, pp. 258–278, 2009.

[3] B. Halliwell, “Reactive Species and Antioxidants. Redox Biology Is a Fundamental Theme of Aerobic Life,” *Plant Physiol.*, vol. 141, no. June, pp. 312–322, 2006.

[4] Y. J. Taverne, D. Merkus, A. J. Bogers, B. Halliwell, D. J. Duncker, and T. W. Lyons, “Reactive Oxygen Species: Radical Factors in the Evolution of Animal Life: A molecular timescale from Earth’s earliest history to the rise of complex life,” *BioEssays*, vol. 40, no. 3, pp. 1–9, 2018.

[5] E. Birben, U. M. Sahiner, C. Sackesen, S. Erzurum, and O. Kalayci, “Oxidative stress and antioxidant defense,” *World Allergy Organ. J.*, vol. 5, no. 1, pp. 9–19, 2012.

[6] C. C. Winterbourn, A. J. Kettle, and M. B. Hampton, “Reactive

Oxygen Species and Neutrophil Function," *Annu. Rev. Biochem.*, vol. 85, no. 1, pp. 765–792, 2016.

[7] C. C. Winterbourn, "Biological Production, Detection, and Fate of Hydrogen Peroxide," *Antioxid. Redox Signal.*, vol. 29, no. 6, pp. 541–551, 2018.

[8] R. Radi, "Peroxynitrite, a stealthy biological oxidant," *J. Biol. Chem.*, vol. 288, no. 37, pp. 26464–26472, 2013.

[9] C. C. Winterbourn, *The biological chemistry of hydrogen peroxide*, 1st ed., vol. 528. Elsevier Inc., 2013.

[10] H. Sies, "Hydrogen peroxide as a central redox signaling molecule in physiological oxidative stress : Oxidative eustress," *Redox Biol.*, vol. 11, pp. 613–619, 2017.

[11] C. Bogdan, "Nitric oxide synthase in innate and adaptive immunity: An update," *Trends Immunol.*, vol. 36, no. 3, pp. 161–178, 2015.

[12] A. Martínez-Ruiz, S. Cadenas, and S. Lamas, "Nitric oxide signaling: Classical, less classical, and nonclassical mechanisms," *Free Radic. Biol. Med.*, vol. 51, no. 1, pp. 17–29, 2011.

[13] C. C. Winterbourn, "Are free radicals involved in thiol-based redox signaling?," *Free Radic. Biol. Med.*, vol. 80, pp. 164–170, 2015.

[14] L. Brunelli, V. Yermilov, and J. S. Beckman, “Modulation of catalase peroxidatic and catalatic activity by nitric oxide,” *Free Radic. Biol. Med.*, vol. 30, no. 7, pp. 709–714, 2001.

[15] S. P. L. Cary, J. A. Winger, E. R. Derbyshire, and M. A. Marletta, “Nitric oxide signaling: no longer simply on or off,” *Trends Biochem. Sci.*, vol. 31, no. 4, pp. 231–239, 2006.

[16] A. Denicola, C. Batthya, E. Lissi, B. A. Freeman, H. Rubbo, and R. Radi, “Diffusion of Nitric Oxide into Low Density Lipoprotein,” *J. Biol. Chem.*, vol. 277, no. 2, pp. 932–936, 2002.

[17] N. Hogg and B. Kalyanaraman, “Nitric oxide and lipid peroxidation,” *Biochim. Biophys. Acta*, vol. 1411, pp. 378–384, 1999.

[18] P. Pacher, J. Beckman, and L. Liaudet, “Nitric Oxide and Peroxynitrite in Health and Disease,” *Physiol. Rev.*, vol. 87, no. 1, pp. 315–424, 2007.

[19] J. M. Souza, G. Peluffo, and R. Radi, “Protein tyrosine nitration-Functional alteration or just a biomarker?,” *Free Radic. Biol. Med.*, vol. 45, no. 4, pp. 357–366, 2008.

[20] M. C. Romero-puertas, M. Laxa, and A. Matte, “S-Nitrosylation of Peroxiredoxin II E Promotes Peroxynitrite-Mediated Tyrosine

Nitration," *Plant Cell*, vol. 19, pp. 4120–4130, 2007.

[21] L. M. Randall *et al.*, "Nitration Transforms a Sensitive Peroxiredoxin 2 into a More Active and Robust Peroxidase," *J. Biol. Chem.*, vol. 289, no. 22, pp. 15536–15543, 2014.

[22] R. De Bont and N. van Larebeke, "Endogenous DNA damage in humans: A review of quantitative data," *Mutagenesis*, vol. 19, no. 3, pp. 169–185, 2004.

[23] K. J. A. Davies, "Oxidative stress, antioxidant defenses, and damage removal, repair, and replacement systems," *IUBMB Life*, vol. 50, no. 4–5, pp. 279–289, 2000.

[24] M. S. Cooke, M. D. Evans, M. Dizdaroglou, and J. Lunec, "Oxidative DNA damage: mechanisms, mutation, and disease," *FASEB J.*, vol. 17, no. 10, pp. 1195–1214, 2003.

[25] S. V. Avery, "Molecular targets of oxidative stress," *Biochem. J.*, vol. 434, no. 2, pp. 201–210, 2011.

[26] B. Halliwell and M. Whiteman, "Measuring reactive species and oxidative damage in vivo and in cell culture: how should you do it and what do the results mean?," *Br. J. Pharmacol.*, vol. 142, pp. 231–255, 2004.

[27] K. Grintzalis, D. Zisimopoulos, T. Grune, D. Weber, and C. D. Georgiou, “Method for the simultaneous determination of free/protein malondialdehyde and lipid/protein hydroperoxides,” *Free Radic. Biol. Med.*, vol. 59, pp. 27–35, 2013.

[28] E. R. Stadtman and R. L. Levine, “Free radical-mediated oxidation of free amino acids and amino acid residues in proteins,” *Amino Acids*, vol. 25, no. 3–4, pp. 207–218, 2003.

[29] M. J. Davies, “Protein oxidation and peroxidation,” *Biochem. J*, vol. 473, pp. 805–825, 2016.

[30] C. D. Georgiou, D. Zisimopoulos, V. Argyropoulou, E. Kalaitzopoulou, G. Salachas, and T. Grune, “Protein and cell wall polysaccharide carbonyl determination by a neutral pH 2,4-dinitrophenylhydrazine-based photometric assay,” *Redox Biol.*, vol. 17, pp. 128–142, 2018.

[31] C. D. Georgiou *et al.*, “Protein carbonyl determination by a rhodamine B hydrazide-based fluorometric assay,” *Redox Biol.*, vol. 17, pp. 236–245, 2018.

[32] M. P. Murphy *et al.*, “Unravelling the Biological Roles of Reactive Oxygen Species,” *Cell Metab*, vol. 13, no. 4, pp. 361–366, 2011.

[33] Y. M. W. Janssen-Heininger *et al.*, “Redox-based regulation of signal

transduction: principles, pitfalls, and promises," *Free Radic. Biol. Med.*, vol. 45, no. 1, pp. 1–17, 2009.

[34] J. J. Tanner, Z. D. Parsons, A. H. Cummings, H. Zhou, and K. S. Gates, "Redox Regulation of Protein Tyrosine Phosphatases: Structural and Chemical Aspects," *Antioxid. Redox Signal.*, vol. 15, no. 1, pp. 77–97, 2011.

[35] H. S. Marinho, C. Real, L. Cyrne, H. Soares, and F. Antunes, "Hydrogen peroxide sensing, signaling and regulation of transcription factors," *Redox Biology*, vol. 2, no. 1. pp. 535–562, 2014.

[36] A. Perkins, K. J. Nelson, D. Parsonage, L. B. Poole, and P. A. Karplus, "Peroxiredoxins: guardians against oxidative stress and modulators of peroxide signaling," *Trends Biochem. Sci.*, vol. 40, no. 8, pp. 435–445, 2015.

[37] S. Iwakami *et al.*, "Concentration-dependent dual effects of hydrogen peroxide on insulin signal transduction in H4IIEC hepatocytes," *PLoS One*, vol. 6, no. 11, pp. 2–11, 2011.

[38] A. Matsuzawa and H. Ichijo, "Redox control of cell fate by MAP kinase: physiological roles of ASK1-MAP kinase pathway in stress signaling," *Biochim. Biophys. Acta - Gen. Subj.*, vol. 1780, no. 11, pp.

1325–1336, 2008.

[39] D. Uberti, E. Yavin, S. Gil, K. R. Ayasola, N. Goldfinger, and V. Rotter, “Hydrogen peroxide induces nuclear translocation of p53 and apoptosis in cells of oligodendroglia origin,” *Mol. Brain Res.*, vol. 65, no. 2, pp. 167–175, 1999.

[40] C. McNeill-Blue, B. A. Wetmore, J. F. Sanchez, W. J. Freed, and B. Alex Merrick, “Apoptosis mediated by p53 in rat neural AF5 cells following treatment with hydrogen peroxide and staurosporine,” *Brain Res.*, vol. 1112, no. 1, pp. 1–15, 2006.

[41] S. Bonello *et al.*, “Reactive oxygen species activate the HIF-1α promoter via a functional NFκB site,” *Arterioscler. Thromb. Vasc. Biol.*, vol. 27, no. 4, pp. 755–761, 2007.

[42] H. Mochizuki, C. J. Murphy, J. D. Brandt, Y. Kiuchi, and P. Russell, “Altered stability of mRNAs associated with glaucoma progression in human trabecular meshwork cells following oxidative stress,” *Investig. Ophthalmol. Vis. Sci.*, vol. 53, no. 4, pp. 1734–1741, 2012.

[43] K. Abdelmohsen *et al.*, “Phosphorylation of HuR by Chk2 Regulates SIRT1 Expression,” *Mol. Cell*, vol. 25, no. 4, pp. 543–557, 2007.

[44] S. H. Yeh *et al.*, “Translational and transcriptional control of Sp1

against ischaemia through a hydrogen peroxide-activated internal ribosomal entry site pathway," *Nucleic Acids Res.*, vol. 39, no. 13, pp. 5412–5423, 2011.

[45] H. Ryu *et al.*, "Sp1 and Sp3 are oxidative stress-inducible, antideath transcription factors in cortical neurons," *J Neurosci*, vol. 23, no. 9, pp. 3597–3606, 2003.

[46] S. E. Purdom-dickinson, E. V Sheveleva, H. Sun, and Q. M. Chen, "Translational control of nrf2 protein in activation of antioxidant response by oxidants," *Mol. Pharmacol.*, vol. 72, no. 4, pp. 1074–1081, 2007.

[47] Q. Zhou *et al.*, "Reactive oxygen species regulate insulin-induced VEGF and HIF-1α expression through the activation of p70S6K1 in human prostate cancer cells," *Carcinogenesis*, vol. 28, no. 1, pp. 28–37, 2007.

[48] W. Li *et al.*, "An internal ribosomal entry site mediates redox-sensitive translation of Nrf2," *Nucleic Acids Res.*, vol. 38, no. 3, pp. 778–788, 2009.

[49] D. D. Zhang, S. Lo, J. V Cross, J. Dennis, M. Hannink, and D. J. Templeton, "Keap1 Is a Redox-Regulated Substrate Adaptor Protein for a Cul3-Dependent Ubiquitin Ligase Complex," *Am. Soc.*

Microbiol., vol. 24, no. 24, pp. 10941–10953, 2004.

[50] A. Kobayashi *et al.*, "Oxidative Stress Sensor Keap1 Functions as an Adaptor for Cul3-Based E3 Ligase To Regulate Proteasomal Degradation of Nrf2 Oxidative Stress Sensor Keap1 Functions as an Adaptor for Cul3-Based E3 Ligase To Regulate Proteasomal Degradation of Nrf2," *Mol. Cell. Biol.*, vol. 24, no. 16, pp. 7130–7139, 2004.

[51] R. Maya *et al.*, "ATM-dependent phosphorylation of Mdm2 on serine 394: role in p53 activation by DNA damage," *Genes Dev.*, vol. 15, pp. 1067–1077, 2001.

[52] Z. Goldberg *et al.*, "Tyrosine phosphorylation of Mdm2 by c-Abl: Implications for p53 regulation," *EMBO J.*, vol. 21, no. 14, pp. 3715–3727, 2002.

[53] H. Zhan, T. Suzuki, K. Aizawa, K. Miyagawa, and R. Nagai, "Ataxia Telangiectasia Mutated (ATM)-mediated DNA damage response in oxidative stress-induced vascular endothelial cell senescence," *J. Biol. Chem.*, vol. 285, no. 38, pp. 29662–29670, 2010.

[54] X. Sun *et al.*, "Activation of the cytoplasmic c-Abl tyrosine kinase by reactive oxygen species," *J. Biol. Chem.*, vol. 275, no. 23, pp. 17237–17240, 2000.

[55] M. Shaw, P. Cohen, and D. R. Alessi, “The activation of protein kinase B by H 2 O 2 or heat shock is mediated by phosphoinositide 3-kinase and not by mitogen-activated protein kinase- activated protein kinase-2,” *Biochem. J*, vol. 336, pp. 241–246, 1998.

[56] A. S. Blair, E. Hajduch, G. J. Litherland, and H. S. Hundal, “Regulation of Glucose Transport and Glycogen Synthesis in L6 Muscle Cells during Oxidative Stress,” *J. Biol. Chem.*, vol. 274, no. 51, pp. 36293–36299, 1999.

[57] A. M. Musti, M. Treier, and D. Bohmann, “Reduced ubiquitin-dependent degradation of c-Jun after phosphorylation by map kinases,” *Science (80-.).*, vol. 275, no. 5298, pp. 400–402, 1997.

[58] J. Guo, Z. Gertsberg, P. Danilo, M. R. Rosen, and S. F. Steinberg, “Reactive Oxygen Species Decrease cAMP Response Element Binding Protein Expression in Cardiomyocytes via a Protein Kinase D1-Dependent Mechanism That Does Not Require Ser 133 Phosphorylation,” *Mol. Pharmacol.*, vol. 76, no. 4, pp. 896–902, 2009.

[59] S. Ahn and D. Thiele, “Redox regulation of mammalian heat shock factor 1 is essential for Hsp gene activation and protection from stress,” *Genes Dev.*, pp. 516–528, 2003.

[60] S. Boisnard *et al.*, “H2O2 activates the nuclear localization of Msn2 and Maf1 through thioredoxins in Saccharomyces cerevisiae,” *Eukaryot. Cell*, vol. 8, no. 9, pp. 1429–1438, 2009.

[61] V. Oliveira-Marques *et al.*, “A quantitative study of the cell-type specific modulation of c-Rel by hydrogen peroxide and TNF-α,” *Redox Biol.*, vol. 1, no. 1, pp. 347–352, 2013.

[62] V. Oliveira-Marques, H. S. Marinho, L. Cyrne, and F. 1 Antunes, “Role of Hydrogen Peroxide in NF- k B Activation : From Inducer to Modulator,” *Antioxid. Redox Signal.*, vol. 11, no. 9, pp. 2223–2243, 2009.

[63] J. Zhu, C. Chen, S. Flavahan, J. Harr, B. Su, and N. A. Flavahan, “Cyclic stretch stimulates vascular smooth muscle cell alignment by redox-dependent activation of Notch3,” *Am J Physiol Hear. Circ Physiol*, vol. 300, pp. 1770–1780, 2011.

[64] N. Coant *et al.*, “NADPH Oxidase 1 Modulates WNT and NOTCH1 Signaling To Control the Fate of Proliferative Progenitor Cells in the Colon,” *Mol. Cell. Biol.*, vol. 30, no. 11, pp. 2636–2650, 2010.

[65] D. Seth, A. Hausladen, Y.-J. Wang, and J. S. Stamler, “Endogenous Protein S-Nitrosylation in E. coli: Regulation by OxyR,” *Science*, vol. 336, no. April, pp. 470–3, 2012.

[66] J. M. Dubbs and S. Mongkolsuk, “Peroxide-Sensing Transcriptional Regulators in Bacteria,” *Stress Environ. Regul. Gene Expr. Adapt. Bact.*, vol. 1, no. 20, pp. 587–602, 2016.

[67] C. Lee *et al.*, “Redox regulation of OxyR requires specific disulfide bond formation involving a rapid kinetic reaction path,” *Nat. Struct. Mol. Biol.*, vol. 11, no. 12, pp. 1179–1185, 2004.

[68] J. M. Hansen, W. H. Watson, and D. P. Jones, “Compartmentation of Nrf-2 redox control: Regulation of cytoplasmic activation by glutathione and DNA binding by thioredoxin-1,” *Toxicol. Sci.*, vol. 82, no. 1, pp. 308–317, 2004.

[69] G. Tell, F. Quadrifoglio, C. Tiribelli, and M. R. Kelley, “The Many Functions of APE1/Ref-1: Not Only a DNA Repair Enzyme,” *Antioxid. Redox Signal.*, vol. 11, no. 3, pp. 601–619, 2009.

[70] M. S. Colman, C. a Afshari, and J. C. Barrett, “Regulation of p53 stability and activity in response to genotoxic stress.,” *Mutat. Res.*, vol. 462, no. 2–3, pp. 179–88, 2000.

[71] J. P. Kruse and W. Gu, “MSL2 promotes Mdm2-independent cytoplasmic localization of p53,” *J. Biol. Chem.*, vol. 284, no. 5, pp. 3250–3263, 2009.

[72] J. P. Kruse and W. Gu, “Modes of p53 Regulation,” *Cell*, vol. 137, no. 4, pp. 609–622, 2009.

[73] H.-D. S. & G.-Q. C. Chuan-Xu Liu, Qian-Qian Yin, Hu-Chen Zhou, Ying-Li Wu, Jian-Xin Pu, Li Xia, Wei Liu, Xin Huang, Tao Jiang, Ming-Xuan Wu, Li-Cai He, Ya-Xue Zhao, Xiao-Lin Wang, Wei-Lie Xiao, Hong-Zhuan Chen, Qian Zhao, Ai-Wu Zhou, Li-Shun Wang, “Adenanthin targets peroxiredoxin I and II to induce differentiation of leukemic cells,” *Nat. Chem. Biol.*, vol. 8, pp. 486–493, 2012.

[74] P. J. Nadeau, S. J. Charette, M. B. Toledano, and J. Landry, “Disulfide Bond-mediated Multimerization of Ask1 and Its Reduction by Thioredoxin-1 Regulate H2O2-induced c-Jun NH2-terminal Kinase Activation and Apoptosis,” *Mol. Biol. Cell*, vol. 18, pp. 3903–3913, 2007.

[75] H. Ichijo *et al.*, “Induction of Apoptosis by ASK1 , a Mammalian MAPKKK That Activates SAPK / JNK and p38 Signaling Pathways,” vol. 90, no. 1997, pp. 1–6, 2014.

[76] C. C. Winterbourn and D. Metodiewa, “Reactivity of biologically important thiol compounds with superoxide and hydrogen peroxide,” *Free Radic. Biol. Med.*, vol. 27, no. 3–4, pp. 322–328, 1999.

[77] S. H. Francis, J. L. Busch, and J. D. Corbin, “cGMP-Dependent Protein Kinases and cGMP Phosphodiesterases in Nitric Oxide and cGMP Action,” *Pharmacol. Rev.*, vol. 62, no. 3, pp. 525–563, 2010.

[78] G. Brown, “Nitric oxide regulates mitochondrial respiration and cell functions by inhibiting cytochrome oxidase,” *FEBS Lett.*, vol. 369, no. 2–3, pp. 136–139, 1995.

[79] E. Aguirre, F. Rodríguez-Juárez, A. Bellelli, E. Gnaiger, and S. Cadenas, “Kinetic model of the inhibition of respiration by endogenous nitric oxide in intact cells,” *Biochim. Biophys. Acta - Bioenerg.*, vol. 1797, no. 5, pp. 557–565, 2010.

[80] D. Mastronicola *et al.*, “Control of respiration by nitric oxide in Keilin-Hartree particles, mitochondria and SH-SY5Y neuroblastoma cells,” *Cell. Mol. Life Sci.*, vol. 60, no. 8, pp. 1752–1759, 2003.

[81] A. Martínez-Ruiz and S. Lamas, “S-nitrosylation: A potential new paradigm in signal transduction,” *Cardiovasc. Res.*, vol. 62, no. 1, pp. 43–52, 2004.

[82] J. R. Lancaster and B. Gaston, “NO and nitrosothiols: spatial confinement and free diffusion.,” *Am. J. Physiol. Lung Cell. Mol. Physiol.*, vol. 287, no. 3, pp. L465-6, 2004.

[83] P. Klatt and S. Lamas, “Regulation of protein function by S-glutathiolation in response to oxidative and nitrosative stress,” *Eur. J. Biochem.*, vol. 267, no. 16, pp. 4928–4944, 2000.

[84] J. J. Mieyal, M. M. Gallogly, S. Qanungo, E. A. Sabens, and M. D. Shelton, “Molecular Mechanisms and Clinical Implications of Reversible Protein *S* -Glutathionylation,” *Antioxid. Redox Signal.*, vol. 10, no. 11, pp. 1941–1988, 2008.

[85] X. Liu and E. C. Theil, “Ferritins: Dynamic management of biological iron and oxygen chemistry,” *Acc. Chem. Res.*, vol. 38, no. 3, pp. 167–175, 2005.

[86] M. Kruszewski, “Labile iron pool: The main determinant of cellular response to oxidative stress,” *Mutat. Res.*, vol. 531, pp. 81–92, 2003.

[87] T. Kurz, A. Leake, T. Von Zglinicki, and U. T. Brunk, “Lysosomal redox-active iron is important for oxidative stress-induced DNA damage,” *Biochem. J.*, vol. 378, pp. 1039–1045, 2004.

[88] D. H. Kang and S. W. Kang, “Targeting Cellular Antioxidant Enzymes for Treating Atherosclerotic Vascular Disease,” *Biomol Ther*, vol. 21, no. 2, pp. 89–96, 2013.

[89] T. Fukai and M. Ushio-fukai, “Superoxide Dismutases: Role in Redox

Signaling, Vascular Function, and Diseases," *Antioxid. Redox Signal.*, vol. 15, no. 6, pp. 1583–1606, 2011.

[90] P. Milani, S. Gagliardi, E. Cova, and C. Cereda, "SOD1 transcriptional and posttranscriptional regulation and its potential implications in ALS," *Neurol. Res. Int.*, pp. 1–9, 2011.

[91] Y. Li *et al.*, "Dilated cardiomyopathy and neonatal lethality in mutant mice lacking manganese superoxide dismutase," *Nat. Genet.*, vol. 11, pp. 376–381, 1995.

[92] H. N. Kirkman, M. Rolfo, A. M. Ferraris, and G. F. Gaetani, "Mechanisms of protection of catalase by NADPH: Kinetics and stoichiometry," *J. Biol. Chem.*, vol. 274, no. 20, pp. 13908–13914, 1999.

[93] J. A. Leopold and J. Loscalzo, "Oxidative Enzymopathies and Vascular Disease," *Arter. Thromb Vasc Biol.*, vol. 25, pp. 1332–1340, 2005.

[94] E. A. Veal, A. M. Day, and B. A. Morgan, "Hydrogen Peroxide Sensing and Signaling," *Mol. Cell*, vol. 26, no. 1, pp. 1–14, 2007.

[95] S. Toppo, L. Flohé, F. Ursini, S. Vanin, and M. Maiorino, "Catalytic mechanisms and specificities of glutathione peroxidases: Variations of a basic scheme," *Biochim. Biophys. Acta*, vol. 1790, no. 11, pp.

1486–1500, 2009.

[96] L. Flohé, “Changing Paradigms in Thiology: From Antioxidant Defense Toward Redox Regulation,” *Methods Enzymol.*, vol. 473, no. 10, pp. 1–39, 2010.

[97] M. Schneider *et al.*, “Mitochondrial glutathione peroxidase 4 disruption causes male infertility,” *FASEB J.*, vol. 23, pp. 3233–3242, 2009.

[98] R. Brigelius-Flohe, “Tissue-specific functions of individual glutathione peroxidases,” *Free Radic. Biol. Med.*, vol. 27, no. 9/10, pp. 951–965, 1999.

[99] R. Brigelius-Flohé and E. S. J. Arnér, “Selenium and selenoproteins in (redox) signaling, diseases, and animal models - 200 year anniversary issue,” *Free Radic. Biol. Med.*, vol. 127, pp. 1–2, 2018.

[100] J. Lu and A. Holmgren, “Selenoproteins,” *J. Biol. Chem.*, vol. 284, no. 2, pp. 723–727, 2009.

[101] Y.-S. Ho *et al.*, “Mice deficient in cellular glutathione peroxidase develop normally and show no increased sensitivity to hyperoxia,” *J. Biol. Chem.*, vol. 272, no. 26, pp. 16644–16651, 1997.

[102] W. Cheng, Y. Ho, B. A. Valentine, D. A. Ross, G. F. Combs, and X. G.

Lei, “Cellular glutathione peroxidase is the mediator of body selenium to protect against paraquat lethality in transgenic mice,” *J Nutr.*, vol. 128, no. 7, pp. 1070–1076, 1998.

[103] J. B. De Haan *et al.*, “Mice with a homozygous null mutation for the most abundant glutathione peroxidase, Gpx1, show increased susceptibility to the oxidative stress- inducing agents paraquat and hydrogen peroxide,” *J. Biol. Chem.*, vol. 273, no. 35, pp. 22528–22536, 1998.

[104] P. Klivenyi *et al.*, “Mice Deficient in Cellular Glutathione Peroxidase Show Increased Vulnerability to Malonate, 3-Nitropropionic Acid, and 1-Methyl-4-Phenyl-1,2,5,6-Tetrahydropyridine,” *J. Neurosci.*, vol. 20, no. 1, pp. 1–7, 2000.

[105] F. F. Chu *et al.*, “Bacteria-Induced Intestinal Cancer in Mice with Disrupted Gpx1 and Gpx2 Genes,” *Cancer Res.*, vol. 64, no. 3, pp. 962–968, 2004.

[106] B. C. An, Y.-D. Choi, I.-J. Oh, J. H. Kim, J.-I. Park, and S. Lee, “GPx3-mediated redox signaling arrests the cell cycle and acts as a tumor suppressor in lung cancer cell lines,” *PLoS One*, vol. 13, no. 9, p. e0204170, 2018.

[107] L. J. Yant *et al.*, “The selenoprotein GPX4 is essential for mouse

development and protects from radiation and oxidative damage insults," *Free Radic. Biol. Med.*, vol. 34, no. 4, pp. 496–502, 2003.

[108] A. Seiler *et al.*, "Glutathione Peroxidase 4 Senses and Translates Oxidative Stress into 12/15-Lipoxygenase Dependent- and AIF-Mediated Cell Death," *Cell Metab.*, vol. 8, pp. 237–248, 2008.

[109] J. Pedro *et al.*, "Inactivation of the ferroptosis regulator Gpx4 triggers acute renal failure in mice," *Nat. Cell Biol.*, vol. 16, no. 12, pp. 1180–1191, 2014.

[110] T. M. Seibt, B. Proneth, and M. Conrad, "Role of GPX4 in ferroptosis and its pharmacological implication," *Free Radic. Biol. Med.*, vol. 133, pp. 144–152, 2019.

[111] S. C. Schriever *et al.*, "Alterations in neuronal control of body weight and anxiety behavior by glutathione peroxidase 4 deficiency," *Neuroscience*, vol. 357, pp. 241–254, 2017.

[112] M. Valko, D. Leibfritz, J. Moncol, M. T. D. Cronin, M. Mazur, and J. Telser, "Free radicals and antioxidants in normal physiological functions and human disease," *Int. J. Biochem. Cell Biol.*, vol. 39, pp. 44–84, 2007.

[113] J. Lu and A. Holmgren, "The thioredoxin antioxidant system," *Free*

Radic. Biol. Med., vol. 66, 2014.

[114] N. Couto, J. Wood, and J. Barber, “The role of glutathione reductase and related enzymes on cellular redox homoeostasis network,” *Free Radic. Biol. Med.*, vol. 95, pp. 27–42, 2016.

[115] M. Deponte, “Glutathione catalysis and the reaction mechanisms of glutathione-dependent enzymes,” *Biochim. Biophys. Acta*, vol. 1830, no. 5, pp. 3217–3266, 2013.

[116] S. E. Welty, D. J. O’Donovan, J. P. Katkin, C. V. Smith, and T. Tamura, “Attenuation of Hyperoxia-Induced Growth Inhibition in H441 Cells by Gene Transfer of Mitochondrially Targeted Glutathione Reductase,” *Am. J. Respir. Cell Mol. Biol.*, vol. 22, no. 6, pp. 732–738, 2000.

[117] K. M. Heyob, L. K. Rogers, and S. E. Welty, “Glutathione reductase targeted to type II cells does not protect mice from hyperoxic lung injury,” *Am. J. Respir. Cell Mol. Biol.*, vol. 39, no. 6, pp. 683–688, 2008.

[118] J. Nordberg and E. S. J. Arnér, “Reactive oxygen species, antioxidants, and the mammalian thioredoxin system,” *Free Radic. Biol. Med.*, vol. 31, no. 11, pp. 1287–1312, 2001.

[119] E.-M. Hanschmann, J. R. Godoy, C. Berndt, C. Hudemann, and C. H. Lillig, “Thioredoxins, glutaredoxins, and peroxiredoxins--molecular mechanisms and health significance: from cofactors to antioxidants to redox signaling.,” *Antioxid. Redox Signal.*, vol. 19, no. 13, pp. 1–200, 2013.

[120] K. Pekkari and A. Holmgren, “Truncated thioredoxin: physiological functions and mechanism,” *Antioxid. Redox Signal.*, vol. 6, no. 1, pp. 53–61, 2004.

[121] G. Spyrou, E. Enmark, A. Miranda-Vizuete, and J. Å. Gustafsson, “Cloning and expression of a novel mammalian thioredoxin,” *J. Biol. Chem.*, vol. 272, no. 5, pp. 2936–2941, 1997.

[122] A. Miranda-Vizuete *et al.*, “Characterization of Sptrx, a Novel Member of the Thioredoxin Family Specifically Expressed in Human Spermatozoa,” *J. Biol. Chem.*, vol. 276, no. 34, pp. 31567–31574, 2001.

[123] L. Nonn, R. R. Williams, R. P. Erickson, and G. Powis, “The absence of mitochondrial thioredoxin 2 causes massive apoptosis, exencephaly, and early embryonic lethality in homozygous mice,” *Mol Cell Biol*, vol. 23, no. 3, pp. 916–922, 2003.

[124] M. Matsui *et al.*, “Early Embryonic Lethality Caused by Targeted

Disruption of the Mouse Thioredoxin Gene," *Dev. Biol.*, vol. 178, no. 208, pp. 179–185, 1996.

[125] E. Holzerova *et al.*, "Human thioredoxin 2 deficiency impairs mitochondrial redox homeostasis and causes early-onset neurodegeneration," *Brain*, pp. 1–9, 2015.

[126] C. H. Lillig, C. Berndt, and A. Holmgren, "Glutaredoxin systems," *Biochim. Biophys. Acta*, vol. 1780, no. 11, pp. 1304–1317, 2008.

[127] S. G. Rhee, W. Jeong, T. S. Chang, and H. A. Woo, "Sulfiredoxin, the cysteine sulfinic acid reductase specific to 2-Cys peroxiredoxin: Its discovery, mechanism of action, and biological significance," *Kidney Int.*, vol. 72, pp. S3–S8, 2007.

[128] A. Hall, K. Nelson, L. B. Poole, and P. A. Karplus, "Structure-based Insights into the Catalytic Power and Conformational Dexterity of Peroxiredoxins," *Antioxid. Redox Signal.*, vol. 15, no. 3, pp. 795–815, 2011.

[129] T. J. Jönsson and W. T. Lowther, "The Peroxiredoxin Repair Proteins," *Subcell Biochem.*, vol. 44, pp. 115–141, 2007.

[130] S. G. Rhee, "Overview on Peroxiredoxin," *Mol. Cells*, vol. 39, no. 1, pp. 1–5, 2016.

[131] Z. A. Wood, E. Schroder, J. R. Harris, and L. B. Poole, “Structure , mechanism and regulation of peroxiredoxins,” *Trends Biochem. Sci.*, vol. 28, no. 1, pp. 3–8, 2003.

[132] B. Knoops, E. Loumaye, and V. Van Der Eecken, “Evolution of Peroxiredoxins: Taxonomy, homology and characterization,” in *Peroxiredoxin Systems*, 2007, pp. 27–40.

[133] S. G. Rhee and I. S. Kil, “Multiple Functions and Regulation of Mammalian Peroxiredoxins,” *Annu. Rev. Biochem.*, vol. 86, no. 5, pp. 1–27, 2017.

[134] G. Ferrer-Sueta, B. Manta, H. Botti, R. Radi, M. Trujillo, and A. Denicola, “Factors affecting protein thiol reactivity and specificity in peroxide reduction,” *Chem. Res. Toxicol.*, vol. 24, pp. 434–450, 2011.

[135] H. Z. Chae, H. J. Kim, S. W. Kang, and S. G. Rhee, “Characterization of three isoforms of mammalian peroxiredoxin that reduce peroxides in the presence of thioredoxin,” *Diabetes Res. Clin. Pr.*, vol. 45, pp. 101–112, 1999.

[136] K. Kim, I. H. Kim, K. Leeo, S. G. Rhee, and E. R. Stadtmann, “The Isolation and Purification of a Specific ‘ Protector ’ Protein Which Inhibits Enzyme Inactivation by a Thiol / Fe (III)/ 02 Mixed-function Oxidation System *,” *J. Biol. Chem.*, vol. 263, no. 10, pp. 4704–4711,

1988.

[137] I. Han Kim, K. Kim, and S. G. Rhee, “Induction of an antioxidant protein of Saccharomyces cerevisiae by 02, Fe3+, or 2-mercaptoethanol,” *Biochemistry*, vol. 86, pp. 6018–6022, 1989.

[138] L. A. Tartaglia, G. Storz, M. H. Brodsky, A. Lai, and B. N. Ames, “Alkyl hydroperoxide reductase from Salmonella typhimurium. Sequence and homology to thioredoxin reductase and other flavoprotein disulfide oxidoreductases,” *J. Biol. Chem.*, vol. 265, no. 18, pp. 10535–10540, 1990.

[139] H. Z. Chae, K. Robinson, L. B. Poole, G. Church, G. Storz, and S. G. Rhee, “Cloning and sequencing of thiol-specific antioxidant from mammalian brain: Alkyl hydroperoxide reductase and thiol-specific antioxidant define a large family of antioxidant enzymes,” *Biochemistry*, vol. 91, pp. 7017–7021, 1994.

[140] V. L. Kinnula *et al.*, “Overexpression of peroxiredoxins I, II, III, V, and VI in malignant mesothelioma,” *J. Pathol.*, vol. 196, pp. 316–323, 2002.

[141] M. S. Seo, S. W. Kang, K. Kim, I. C. Baines, T. H. Lee, and S. G. Rhee, “Identification of a new type of mammalian peroxiredoxin that forms an intramolecular disulfide as a reaction intermediate,” *J. Biol.*

Chem., vol. 275, no. 27, pp. 20346–20354, 2000.

[142] I. Banmeyer, C. Marchand, C. Verhaeghe, B. Vucic, J. F. Rees, and B. Knoops, "Overexpression of human peroxiredoxin 5 in subcellular compartments of Chinese hamster ovary cells: Effects on cytotoxicity and DNA damage caused by peroxides," *Free Radic. Biol. Med.*, vol. 36, no. 1, pp. 65–77, 2004.

[143] A. Kropotov *et al.*, "A novel human DNA-binding protein with sequence similarity to a subfamily of redox proteins which is able to repress RNA-polymerase-III-driven transcription of the Alu-family retroposons in vitro," *Eur J Biochem*, vol. 260, pp. 336–346, 1999.

[144] A.-C. Gérard, M.-C. Many, C. Daumerie, B. Knoops, and I. M. Colin, "Peroxiredoxin 5 Expression in the Human Thyroid Gland," *THYROID*, vol. 15, no. 3, pp. 205–209, 2005.

[145] S. Poncin *et al.*, "Oxidative stress in the thyroid gland: From harmlessness to hazard depending on the iodine content," *Endocrinology*, vol. 149, no. 1, pp. 424–433, 2008.

[146] I. Sasagawa, S. Matsuki, Y. Suzuki, Y. Iuchi, K. Tohya, and M. Kimura, "Possible involvement of the membrane-bound form of peroxiredoxin 4 in acrosome formation during spermiogenesis of rats," *Eur J Biochem*, vol. 3061, pp. 3053–3061, 2001.

[147] S. Watabe, H. Kohno, H. Kouyama, T. Hiroi, and N. Yago, “Purification Mitochondrial and Characterization of a Substrate Protein for Protease in Bovine Adrenal Cortex,” *J. Biochem.*, vol. 654, pp. 648–654, 1994.

[148] B. Knoops *et al.*, “Cloning and characterization of AOEB166, a novel mammalian antioxidant enzyme of the peroxiredoxin family,” *J. Biol. Chem.*, vol. 274, pp. 30451–30458, 1999.

[149] S. Akiba, C. Dodia, X. Chen, and A. B. Fisher, “Characterization of acidic Ca 2 + -independent phospholipase A 2 of bovine lung,” *Comp. Biochem. Physiol. - B*, vol. 120, pp. 393–404, 1998.

[150] S. Portillo-Ledesma *et al.*, “Deconstructing the catalytic efficiency of peroxiredoxin-5 peroxidatic cysteine,” *Biochemistry*, vol. 53, pp. 6113–6125, 2014.

[151] L. Wu and A. B. Reddy, “Rethinking the clockwork: redox cycles and non-transcriptional control of circadian rhythms,” *Biochem. Soc. Trans.*, vol. 42, no. 1, pp. 1–10, 2014.

[152] E. Hanschmann *et al.*, “Both Thioredoxin 2 and Glutaredoxin 2 Contribute to the Reduction of the Mitochondrial 2-Cys Peroxiredoxin Prx3,” *J. Biol. Chem.*, vol. 285, no. 52, pp. 40699–40705, 2010.

[153] B. Hofmann, H. Hecht, and L. Flohé, “Peroxiredoxins,” *Biol. Chem.*, vol. 383, pp. 347–364, 2002.

[154] K. J. Nelson, S. T. Knutson, L. Soito, C. Klomsiri, B. Leslie, and J. S. Fetrow, “Analysis of the peroxiredoxin family: using active site structure and sequence information for global classification and residue analysis,” *Proteins*, vol. 79, no. 3, pp. 947–964, 2011.

[155] L. B. Poole and K. J. Nelson, “Distribution and Features of the Six Classes of Peroxiredoxins,” *Mol. Cells*, vol. 39, no. 1, pp. 53–59, 2016.

[156] Z. A. Wood, L. B. Poole, and P. A. Karplus, “Peroxiredoxin evolution and the regulation of hydrogen peroxide signaling.,” *Science (80-.).*, vol. 300, pp. 650–653, 2003.

[157] H. A. Woo *et al.*, “Reduction of Cysteine Sulfinic Acid by Sulfiredoxin Is Specific to 2-Cys Peroxiredoxins,” *J. Biol. Chem.*, vol. 280, no. 5, pp. 3125–3129, 2005.

[158] J. C. Lim *et al.*, “Irreversible Oxidation of the Active-site Cysteine of Peroxiredoxin to Cysteine Sulfonic Acid for Enhanced Molecular Chaperone Activity,” *J. Biol. Chem.*, vol. 283, no. 43, pp. 28873–28880, 2008.

[159] S. G. Rhee and H. A. Woo, “Multiple Functions of Peroxiredoxins : Peroxidases , Sensors and Regulators of the Intracellular,” *Antioxid. Redox Signal.*, vol. 15, no. 3, pp. 781–794, 2011.

[160] L. E. S. Netto and F. Antunes, “The Roles of Peroxiredoxin and Thioredoxin in Hydrogen Peroxide Sensing and in Signal Transduction,” *Mol. Cells*, vol. 39, no. 1, pp. 65–71, 2016.

[161] B. Knoops, J. Goemaere, V. Van Der Eecken, and J.-P. Declercq, “Peroxiredoxin 5: Structure, Mechanism, and Function of the Mammalian Atypical 2-Cys Peroxiredoxin,” *Antioxid. Redox Signal.*, vol. 15, no. 3, pp. 817–829, 2011.

[162] S. G. Rhee, H. A. Woo, I. S. Kil, and S. H. Bae, “Peroxiredoxin Functions as a Peroxidase and a Regulator and Sensor of Local Peroxides,” *J. Biol. Chem.*, vol. 287, no. 7, pp. 4403–4410, 2012.

[163] T. S. Chang, W. Jeong, S. Y. Choi, S. Yu, S. W. Kang, and S. G. Rhee, “Regulation of peroxiredoxin I activity by Cdc2-mediated phosphorylation,” *J. Biol. Chem.*, vol. 277, no. 28, pp. 25370–25376, 2002.

[164] T. A. Zykova *et al.*, “T-LAK cell-originated protein kinase (TOPK) phosphorylation of Prx1 at Ser-32 prevents UVB-induced apoptosis in RPMI7951 melanoma cells through the regulation of Prx1

peroxidase activity," *J. Biol. Chem.*, vol. 285, no. 38, pp. 29138–29146, 2010.

[165] R. B. Parmigiani *et al.*, "HDAC6 is a specific deacetylase of peroxiredoxins and is involved in redox regulation," *Proc. Natl. Acad. Sci.*, vol. 105, no. 28, pp. 9633–9638, 2008.

[166] J. H. Seo *et al.*, "Novel Protective Mechanism against Irreversible Hyperoxidation of Peroxiredoxin," *J. Biol. Chem.*, vol. 284, no. 20, pp. 13455–13465, 2009.

[167] K. H. Koo *et al.*, "Regulation of thioredoxin peroxidase activity by C-terminal truncation," *Arch. Biochem. Biophys.*, vol. 397, no. 2, pp. 312–318, 2002.

[168] M. Jara, A. P. Vivancos, and E. Hidalgo, "C-terminal truncation of the peroxiredoxin Tpx1 decreases its sensitivity for hydrogen peroxide without compromising its role in signal transduction," *Genes to Cells*, vol. 13, no. 2, pp. 171–179, 2008.

[169] J. Fang, T. Nakamura, D.-H. Cho, Z. Gu, and S. A. Lipton, "S-nitrosylation of peroxiredoxin 2 promotes oxidative stress-induced neuronal cell death in Parkinson's disease," *Proc. Natl. Acad. Sci.*, vol. 104, no. 47, pp. 18742–18747, 2007.

[170] H. Zoon Chae, H. Oubrahim, J. Won Park, S. Goo Rhee, and P. Boon Chock, “Protein Glutathionylation in the Regulation of Peroxiredoxins: A Family of Thiol-Specific Peroxidases That Function As Antioxidants, Molecular Chaperones, and Signal Modulators,” *Antioxid. Redox Signal.*, vol. 16, no. 6, pp. 506–523, 2012.

[171] J. W. Park, J. J. Mieyal, S. G. Rhee, and P. B. Chock, “Deglutathionylation of 2-Cys peroxiredoxin is specifically catalyzed by sulfiredoxin,” *J. Biol. Chem.*, vol. 284, no. 35, pp. 23364–23374, 2009.

[172] J. W. Park, G. Piszczek, S. G. Rhee, and P. B. Chock, “Glutathionylation of peroxiredoxin I induces decamer to dimer dissociation with concomitant loss of chaperone activity,” *Biochemistry*, vol. 50, no. 15, pp. 3204–3210, 2011.

[173] L. Nonn, M. Berggren, and G. Powis, “Increased Expression of Mitochondrial Peroxiredoxin-3 (Thioredoxin Peroxidase-2) Protects Cancer Cells Against Hypoxia and Drug-Induced Hydrogen,” *Mol. Cancer Res.*, vol. 1, no. July, pp. 682–689, 2003.

[174] T. Chang, C. Cho, S. Park, S. Yu, S. W. Kang, and S. G. Rhee, “Peroxiredoxin III , a Mitochondrion-specific Peroxidase , Regulates Apoptotic Signaling by Mitochondria,” *J. Biol. Chem.*, vol. 279, no. 40,

pp. 41975–41984, 2004.

[175] C. Wong *et al.*, “Characterization of Human and Mouse Peroxiredoxin IV: Evidence for Inhibition by Prx-IV of Epidermal Growth Factor- and p53-Induced Reactive Oxygen Species,” *Antioxid. Redox Signal.*, vol. 2, no. 3, pp. 507–518, 2000.

[176] S. Kim *et al.*, “Peroxiredoxin I Is an Indicator of Microglia Activation and Protects against Hydrogen Peroxide-Mediated Microglial Death,” *Biol. Pharm. Bull.*, vol. 31, no. 5, pp. 820–825, 2008.

[177] P. S. Smith-Pearson, M. Kooshki, D. R. Spitz, L. B. Poole, and M. E. Robbins, “Decreasing peroxiredoxin II expression decreases glutathione, alters cell cycle distribution, and sensitizes glioma cells to ionizing radiation and H2 O2,” *Free Radic. Biol. Med.*, vol. 45, no. 8, pp. 1178–1189, 2009.

[178] W. Zhao, G.-C. Fan, Z.-G. Zhang, A. Bandyopadhyay, X. Zhou, and E. G. Kranias, “Protection of peroxiredoxin II on oxidative stress-induced cardiomyocyte death and apoptosis,” *Basic Res Cardiol.*, vol. 104, no. 4, pp. 377–389, 2009.

[179] Y. Wang, S. I. Feinstein, Y. Manevich, Y.-S. Ho, and A. B. Fisher, “Peroxiredoxin 6 gene-targeted mice show increased lung injury with paraquat-induced oxidative stress,” *Antioxid. Redox Signal.*, vol.

8, no. 1&2, pp. 229–237, 2006.

[180] I. Banmeyer, C. Marchand, A. Clippe, and B. Knoops, “Human mitochondrial peroxiredoxin 5 protects from mitochondrial DNA damages induced by hydrogen peroxide,” *FEBS Lett.*, vol. 579, pp. 2327–2333, 2005.

[181] H. A. Woo, S. H. Yim, D. H. Shin, D. Kang, D. Y. Yu, and S. G. Rhee, “Inactivation of Peroxiredoxin I by Phosphorylation Allows Localized H2O2 Accumulation for Cell Signaling,” *Cell*, vol. 140, pp. 517–528, 2010.

[182] S. G. Rhee, H. Z. Chae, and K. Kanghwa, “Peroxiredoxins: A historical overview and speculative preview of novel mechanisms and emerging concepts in cell signaling,” *Free Radic. Biol. Med.*, vol. 38, pp. 1543–1552, 2005.

[183] A. Diet *et al.*, “Regulation of peroxiredoxins by nitric oxide in immunostimulated macrophages,” *J. Biol. Chem.*, vol. 282, pp. 36199–36205, 2007.

[184] K. Abbas, J. Breton, C. R. Picot, V. Quesniaux, C. Bouton, and J. C. Drapier, “Signaling events leading to peroxiredoxin 5 up-regulation in immunostimulated macrophages,” *Free Radic. Biol. Med.*, vol. 47, pp. 794–802, 2009.

[185] A. Bast, S. F. Erttmann, R. Walther, and I. Steinmetz, “Influence of iNOS and COX on peroxiredoxin gene expression in primary macrophages,” *Free Radic. Biol. Med.*, vol. 49, no. 12, pp. 1881–1891, 2010.

[186] T. Shichita *et al.*, “Peroxiredoxin family proteins are key initiators of post-ischemic inflammation in the brain.,” *Nat. Med.*, vol. 18, no. 6, pp. 911–917, 2012.

[187] X. Kuang *et al.*, “Ligustilide ameliorates neuroinflammation and brain injury in focal cerebral ischemia / reperfusion rats : involvement of inhibition of TLR4 / peroxiredoxin 6 signaling,” *Free Radic. Biol. Med.*, vol. 71, pp. 165–175, 2014.

[188] J. R. Riddell, X.-Y. Wang, H. Minderman, and S. O. Gollnick, “Peroxiredoxin 1 Stimulates Secretion of Pro-Inflammatory Cytokines by Binding to Toll-like Receptor 4,” *J Immunol.*, vol. 184, no. 2, pp. 1022–1030, 2010.

[189] J. R. Riddell, P. Maier, S. N. Sass, M. T. Moser, B. A. Foster, and S. O. Gollnick, “Peroxiredoxin 1 Stimulates Endothelial Cell Expression of VEGF via TLR4 Dependent Activation of HIF-1 a,” *PLoS One*, vol. 7, no. 11, pp. 1–13, 2012.

[190] B. Knoops *et al.*, “Specific Interactions Measured by AFM on Living

Cells between Peroxiredoxin-5 and TLR4 : Relevance for Mechanisms of Innate," *Cell Chem. Biol.*, vol. 25, pp. 1–10, 2018.

[191] Y. Lu *et al.*, "Peroxiredoxin 2 activates microglia by interacting with Toll-like receptor 4 after subarachnoid hemorrhage," *J. Neuroinflammation*, vol. 15, no. 87, pp. 1–10, 2018.

[192] S. Salzano *et al.*, "Linkage of inflammation and oxidative stress via release of glutathionylated peroxiredoxin-2, which acts as a danger signal," *PNAS*, vol. 111, no. 33, pp. 12157–12162, 2014.

[193] M. W. Robinson, A. T. Hutchinson, S. Donnelly, and J. P. Dalton, "Worm secretory molecules are causing alarm," *Trends Parasitol.*, vol. 26, no. 8, 2010.

[194] M. W. Robinson, a. T. Hutchinson, J. P. Dalton, and S. Donnelly, "Peroxiredoxin: A central player in immune modulation," *Parasite Immunol.*, vol. 32, no. 5, pp. 305–313, 2010.

[195] C. A. Neumann, J. Cao, and Y. Manevich, "Peroxiredoxin 1 and its role in cell signaling," *Cell Cycle*, vol. 8, no. 24, pp. 4072–4078, 2009.

[196] M. Shiota *et al.*, "Ets regulates peroxiredoxin1 and 5 expressions through their interaction with the high-mobility group protein B1," *Cancer Sci*, vol. 99, no. 10, pp. 1950–1959, 2008.

[197] V. Rani, C. A. Neumann, C. Shao, and J. A. Tischfield, “Prdx1 deficiency in mice promotes tissue specific loss of heterozygosity mediated by deficiency in DNA repair and increased oxidative stress,” *Mutat. Res. - Fundam. Mol. Mech. Mutagen.*, vol. 735, no. 1–2, pp. 39–45, 2012.

[198] E. Aeby *et al.*, “Peroxiredoxin 1 Protects Telomeres from Oxidative Damage and Preserves Telomeric DNA for Extension by Telomerase Report Peroxiredoxin 1 Protects Telomeres from Oxidative Damage and Preserves Telomeric DNA for Extension by Telomerase,” *CellReports*, vol. 17, no. 12, pp. 3107–3114, 2016.

[199] Y. Yan, P. Sabharwal, M. Rao, and S. Sockanathan, “The Antioxidant Enzyme Prdx1 Controls Neuronal Differentiation by Thiol-Redox-Dependent Activation of GDE2,” *Cell*, vol. 138, no. 6, pp. 1209–1221, 2009.

[200] C. A. Neumann *et al.*, “Essential role for the peroxiredoxin Prdx1 in erythrocyte antioxidant defence and tumour suppression,” *Nature*, vol. 424, no. 6948, pp. 561–565, 2003.

[201] J. Cao *et al.*, “Prdx1 inhibits tumorigenesis via regulating PTEN/AKT activity,” *EMBO J.*, vol. 28, pp. 1505–1517, 2009.

[202] B. Turner-Ivey *et al.*, “Role for Prdx1 as a specific sensor in redox-

regulated senescence in breast cancer," *Oncogene*, vol. 32, no. 45, pp. 5302–5314, 2013.

[203] K. Taniuchi *et al.*, "Peroxiredoxin 1 Promotes Pancreatic Cancer Cell Invasion by Modulating p38 MAPK Activity," *Pancreas*, vol. 44, no. 2, pp. 331–340, 2015.

[204] H. Li, X. Sun, S. Yang, Q. Wang, and Z. Wang, "Peroxiredoxin 1 promoted tumor metastasis and angiogenesis in colorectal cancer," *Pathol. - Res. Pract.*, no. 122, pp. 0–1, 2018.

[205] M. Jamaluddin *et al.*, "Role of Peroxiredoxin 1 and Peroxiredoxin 4 in Protection of Respiratory Syncytial Virus-Induced Cysteinyl Oxidation of Nuclear Cytoskeletal Proteins," *J. Virol.*, vol. 84, no. 18, pp. 9533–9545, 2010.

[206] N. Kikuchi *et al.*, "Aggravation of bleomycin-induced pulmonary inflammation and fibrosis in mice lacking peroxiredoxin I," *Am. J. Respir. Cell Mol. Biol.*, vol. 45, pp. 600–609, 2011.

[207] R. A. Egler *et al.*, "Regulation of reactive oxygen species, DNA damage, and c-Myc function by peroxiredoxin 1," *Oncogene*, vol. 24, pp. 8038–8050, 2005.

[208] L. Mullen, E.-M. Hanschmann, C. H. Lillig, L. A. Herzenberg, and P.

Ghezzi, “Cysteine Oxidation Targets Peroxiredoxins 1 and 2 for Exosomal Release through a Novel Mechanism of Redox-Dependent Secretion.,” *Mol. Med.*, vol. 21, pp. 98–108, 2015.

[209] C.-H. Liu *et al.*, “Peroxiredoxin 1 induces inflammatory cytokine response and predicts outcome of cardiogenic shock patients necessitating extracorporeal membrane oxygenation: an observational cohort study and translational approach,” *J. Transl. Med.*, vol. 14, no. 1, p. 114, 2016.

[210] B. Manta, M. Hugo, C. Ortiz, G. Ferrer-sueta, M. Trujillo, and A. Denicola, “The peroxidase and peroxynitrite reductase activity of human erythrocyte peroxiredoxin 2,” *Arch. Biochem. Biophys.*, vol. 484, no. 2, pp. 146–154, 2009.

[211] L. Flohe and R. J. Harris, *Peroxiredoxin Systems*. 2007.

[212] K.-K. Lee *et al.*, “Peroxiredoxin II is essential for sustaining life span of erythrocytes in mice,” *Blood*, vol. 101, no. 12, pp. 5033–5038, 2003.

[213] T. H. Kwon *et al.*, “Reactive oxygen species mediated DNA damage is essential for abnormal erythropoiesis in peroxiredoxin II -/- mice,” *Biochem. Biophys. Res. Commun.*, vol. 424, pp. 189–195, 2012.

[214] A. Trzeciecka *et al.*, “Dimeric peroxiredoxins are druggable targets in human Burkitt lymphoma,” *Oncotarget*, vol. 7, no. 2, pp. 1717–1731, 2015.

[215] W. Luo, I. Chen, Y. Chen, D. Alkam, and Y. Wang, “PRDX2 and PRDX4 are negative regulators of hypoxia-inducible factors under conditions of prolonged hypoxia,” *Oncotarget*, vol. 7, no. 6, pp. 6379–6397, 2016.

[216] Y. Gan *et al.*, “Transgenic Overexpression of Peroxiredoxin-2 Attenuates Ischemic Neuronal Injury Via Suppression of a Redox-Sensitive Pro-Death Signaling Pathway,” *Antioxid. Redox Signal.*, vol. 17, no. 5, pp. 719–732, 2012.

[217] S. U. Kim *et al.*, “Peroxiredoxin II preserves cognitive function against age-linked hippocampal oxidative damage,” *Neurobiol. Aging*, vol. 32, pp. 1054–1068, 2011.

[218] D. Voigt, U. Scheidt, T. Derfuss, W. Brück, and A. Junker, “Expression of the Antioxidative Enzyme Peroxiredoxin 2 in Multiple Sclerosis Lesions in Relation to Inflammation,” *Int. J. Mol. Sci.*, vol. 18, no. 760, pp. 1–10, 2017.

[219] E. Moon *et al.*, “T lymphocytes and dendritic cells are activated by the deletion of peroxiredoxin II (Prx II) gene,” *Immunol. Lett.*, vol.

102, pp. 184–190, 2006.

[220] R. D. Michalek *et al.*, “Peroxiredoxin II Regulates Effector and Secondary Memory CD8+ Cell Responses,” *J. Virol.*, vol. 86, no. 24, pp. 13629–13641, 2012.

[221] C.-S. Yang *et al.*, “Roles of peroxiredoxin II in the regulation of proinfl ammatory responses to LPS and protection against endotoxin-induced lethal shock,” *J. Exp. Med.*, vol. 204, no. 3, pp. 583–594, 2007.

[222] S. W. Kang, T. S. Chang, T. H. Lee, E. S. Kim, D. Y. Yu, and S. G. Rhee, “Cytosolic Peroxiredoxin Attenuates the Activation of JNK and p38 but Potentiates That of ERK in HeLa Cells Stimulated with Tumor Necrosis Factor-α,” *J. Biol. Chem.*, vol. 279, no. 4, pp. 2535–2543, 2004.

[223] H. Y. Won *et al.*, “Ablation of Peroxiredoxin II Attenuates Experimental Colitis by Increasing FoxO1-Induced Foxp3 + Regulatory T Cells,” *J. Immunol.*, vol. 191, pp. 4029–4037, 2013.

[224] C. Biology *et al.*, “Lymphocytes from rheumatoid arthritis patients have elevated levels of intracellular peroxiredoxin 2 , and a greater frequency of cells with exofacial peroxiredoxin 2 , compared with healthy human lymphocytes,” *Int. J. Biochem. Cell Biol.*, vol. 44, no.

8, pp. 1223–1231, 2012.

[225] L. Zhao, J. Du, H. Zhou, D. Liu, M. Gu, and F. Long, “Differences in Proinflammatory Property of Six Subtypes of Peroxiredoxins and Anti- Inflammatory Effect of Ligustilide in Macrophages,” *PLoS One*, vol. 11, no. 10, p. e0164586, 2016.

[226] Z. Cao, D. Bhella, and J. G. Lindsay, “Reconstitution of the Mitochondrial PrxIII Antioxidant Defence Pathway : General Properties and Factors Affecting PrxIII Activity and Oligomeric State,” *J. Mol. Biol.*, vol. 372, pp. 1022–1033, 2007.

[227] Z. Cao, A. W. Roszak, L. J. Gourlay, J. G. Lindsay, and N. W. Isaacs, “Bovine Mitochondrial Peroxiredoxin III Forms a Two-Ring Catenane,” *Structure*, vol. 13, pp. 1661–1664, 2005.

[228] L. Li *et al.*, “Increased susceptibility of MER5 (peroxiredoxin III) knockout mice to LPS-induced oxidative stress,” *Biochem. Biophys. Res. Commun.*, vol. 355, pp. 715–721, 2007.

[229] W. Hu, X. Dang, G. Wang, S. Li, and Y. Zhang, “Peroxiredoxin-3 attenuates traumatic neuronal injury through preservation of mitochondrial function,” *Neurochem. Int.*, vol. 114, pp. 120–126, 2018.

[230] S. De Simoni, J. Goemaere, and B. Knoops, “Silencing of peroxiredoxin 3 and peroxiredoxin 5 reveals the role of mitochondrial peroxiredoxins in the protection of human neuroblastoma SH-SY5Y cells toward MPP+,” *Neurosci. Lett.*, vol. 433, pp. 219–224, 2008.

[231] C. Mcdonald, J. Muhlbauer, G. Perlmutter, K. Taparra, and S. A. Phelan, “Peroxiredoxin proteins protect MCF-7 breast cancer cells from doxorubicin-induced toxicity,” *Int. J. Oncol.*, vol. 45, no. 21, pp. 219–226, 2014.

[232] J. A. Collins *et al.*, “Oxidative Stress Promotes Peroxiredoxin Hyperoxidation and Attenuates Pro-survival Signaling in Aging Chondrocytes,” *J. Biol. Chem.*, vol. 291, no. 13, pp. 6641–6654, 2016.

[233] L. Chen, R. Na, and Q. Ran, “Enhanced defense against mitochondrial hydrogen peroxide attenuates age-associated cognition decline,” *Neurobiol. Aging*, pp. 1–10, 2014.

[234] J. M. Byun *et al.*, “Overexpression of peroxiredoxin-3 and -5 is a potential biomarker for prognosis in endometrial cancer,” *Oncol. Lett.*, vol. 15, pp. 5111–5118, 2018.

[235] R. M. Fereig and Y. Nishikawa, “Peroxiredoxin 3 promotes IL-12 production from macrophages and partially protects mice against

infection with Toxoplasma gondii," *Parasitol. Int.*, vol. 65, no. 6, pp. 741–748, 2016.

[236] J. Fujii, Y. Ikeda, T. Kurahashi, and T. Homma, "Physiological and pathological views of peroxiredoxin 4," *Free Radic. Biol. Med.*, vol. 83, pp. 373–379, 2015.

[237] A. Matsumoto *et al.*, "Cloning of the peroxiredoxin gene family in rats and characterization of the fourth member," *FEBS Lett.*, vol. 443, pp. 246–250, 1999.

[238] Y. Iuchi *et al.*, "Peroxiredoxin 4 knockout results in elevated spermatogenic cell death via oxidative stress," *Biochem. J*, vol. 419, pp. 149–158, 2009.

[239] X. Guo *et al.*, "Overexpression of Peroxiredoxin 4 Attenuates Atherosclerosis in Apolipoprotein E Knockout Mice," *Antioxid. Redox Signal.*, vol. 17, no. 10, pp. 1362–1375, 2012.

[240] D. D. Rowe *et al.*, "Cord blood administration induces oligodendrocyte survival through alterations in gene expression," *Brain Res.*, vol. 1366, pp. 172–188, 2010.

[241] D. D. Rowe, C. C. Leonardo, J. A. Recio, L. A. Collier, A. E. Willing, and K. R. Pennypacker, "Human Umbilical Cord Blood Cells Protect

Oligodendrocytes from Brain Ischemia through Akt Signal Transduction *," *J. Biol. Chem.*, vol. 287, no. 6, pp. 4177–4187, 2012.

[242] L. Valek, M. Kanngieber, A. Haussler, N. Agarwal, C. H. Lillig, and I. Tegeder, "Redoxins in peripheral neurons after sciatic nerve injury," *Free Radic. Biol. Med.*, vol. 89, pp. 581–592, 2015.

[243] S. Yu, Y. Mu, J. Ao, and X. Chen, "Peroxiredoxin IV regulates pro-inflammatory responses in large yellow croaker (pseudosciaena crocea) and protects against bacterial challenge," *J. Proteome Res.*, vol. 9, pp. 1424–1436, 2010.

[244] V. I. Klichko, W. C. Orr, and S. N. Radyuk, "The role of peroxiredoxin 4 in inflammatory response and aging," *Biochim. Biophys. Acta - Mol. Basis Dis.*, vol. 1862, pp. 265–273, 2016.

[245] Q. Wei *et al.*, "Sulfiredoxin–Peroxiredoxin IV axis promotes human lung cancer progression through modulation of specific phosphokinase signaling," *PNAS*, vol. 108, no. 17, pp. 7004–7009, 2011.

[246] J. R. Pedrajas *et al.*, "Glutathione Is the Resolving Thiol for Thioredoxin Peroxidase Activity of 1-Cys Peroxiredoxin Without Being Consumed During the Catalytic Cycle," *Antioxid. Redox Signal.*, vol. 24, no. 3, pp. 115–128, 2016.

[247] A. Smeets, C. Marchand, D. Linard, B. Knoops, and J. P. Declercq, "The crystal structures of oxidized forms of human peroxiredoxin 5 with an intramolecular disulfide bond confirm the proposed enzymatic mechanism for atypical 2-Cys peroxiredoxins," *Arch. Biochem. Biophys.*, vol. 477, pp. 98–104, 2008.

[248] B. Schremmer, Y. Manevich, S. I. Feinstein, and A. B. Fisher, "Chapter 15: Peroxiredoxins in the lung with emphasis on peroxiredoxin VI," in *Peroxiredoxin Systems*, 2007, pp. 317–344.

[249] J. W. Chen, C. Dodia, S. I. Feinstein, M. K. Jain, and A. B. Fisher, "1-Cys peroxiredoxin, a bifunctional enzyme with glutathione peroxidase and phospholipase A2 activities," *J. Biol. Chem.*, vol. 275, no. 37, pp. 28421–28427, 2000.

[250] Y. Manevich and A. B. Fisher, "Peroxiredoxin 6, a 1-Cys peroxiredoxin, functions in antioxidant defense and lung phospholipid metabolism," *Free Radic. Biol. Med.*, vol. 38, no. 11, pp. 1422–1432, 2005.

[251] A. B. Fisher, C. Dodia, S. I. Feinstein, and Y.-S. Ho, "Altered lung phospholipid metabolism in mice with targeted deletion of lysosomal-type phospholipase A 2," *J. Lipid Res.*, vol. 46, pp. 1248–1256, 2005.

[252] I. S. Lee *et al.*, “Transcriptional regulation of the murine 1-cys peroxiredoxin gene by the B cell-specific activator protein, Pax5,” *J. Cell. Biochem.*, 2008.

[253] H.-M. Yun, K.-R. Park, E.-C. Kim, and J. Tae Hong, “PRDX6 controls multiple sclerosis by suppressing inflammation and blood brain barrier disruption,” *Oncotarget*, vol. 6, no. 25, pp. 20875–20884, 2015.

[254] G. Leyens, B. Verhaeghe, M. Landtmeters, J. Marchandise, B. Knoops, and I. Donnay, “Peroxiredoxin 6 Is Upregulated in Bovine Oocytes and Cumulus Cells During In Vitro Maturation: Role of Intercellular Communication 1,” *Biol. Reprod.*, vol. 71, pp. 1646–1651, 2004.

[255] F. M. M. Paula, S. M. Ferreira, A. C. Boschero, and K. L. A. Souza, “Modulation of the peroxiredoxin system by cytokines in insulin-producing RINm5F cells: Down-regulation of PRDX6 increases susceptibility of beta cells to oxidative stress,” *Mol. Cell. Endocrinol.*, vol. 374, pp. 56–64, 2013.

[256] T. Ishii, “Close teamwork between Nrf2 and peroxiredoxins 1 and 6 for the regulation of prostaglandin D2 and E2 production in macrophages in acute inflammation,” *Free Radic. Biol. Med.*, vol. 88,

pp. 189–198, 2015.

[257] H. M. Yun *et al.*, “Acceleration of the development of alzheimer’s disease in amyloid beta-infused peroxiredoxin 6 overexpression transgenic mice,” *Mol. Neurobiol.*, vol. 48, no. 3, pp. 941–951, 2013.

[258] L. Qin *et al.*, “Differentially expressed proteins underlying childhood cortical dysplasia with epilepsy identified by iTRAQ proteomic profiling,” *PLoS One*, vol. 12, no. 2, pp. 1–17, 2017.

[259] J. R. Roede, D. J. Orlicky, A. B. Fisher, and D. R. Petersen, “Overexpression of Peroxiredoxin 6 Does Not Prevent Ethanol-Mediated Oxidative Stress and May Play a Role in Hepatic Lipid Accumulation,” *J. Pharmacol. Exp. Ther.*, vol. 330, no. 1, pp. 79–88, 2009.

[260] J.-N. Ho *et al.*, “Phospholipase A (2) Activity of Peroxiredoxin 6 Promotes Invasion and Metastasis of Lung Cancer Cells,” *Mol. Cancer Ther.*, vol. 9, no. 4, pp. 825–832, 2010.

[261] X. Wang *et al.*, “Mice with Targeted Mutation of Peroxiredoxin 6 Develop Normally but Are Susceptible to Oxidative Stress,” *J. Biol. Chem.*, vol. 278, pp. 25179–25190, 2003.

[262] X. Zha *et al.*, “PRDX6 Protects ARPE-19 Cells from Oxidative Damage

via PI3K/AKT Signaling," *Cell. Physiol. Biochem.*, vol. 36, pp. 2217–2228, 2015.

[263] Y. Wang, S. A. Phelan, Y. Manevich, S. I. Feinstein, and A. B. Fisher, "Transgenic mice overexpressing peroxiredoxin 6 show increased resistance to lung injury in hyperoxia," *Am. J. Respir. Cell Mol. Biol.*, vol. 34, pp. 481–486, 2006.

[264] H. Yamashita *et al.*, "Characterization of Human and Murine PMP20 Peroxisomal Proteins That Exhibit Antioxidant Activity in Vitro," *J. Biol. Chem.*, vol. 274, no. 42, pp. 29897–29904, 1999.

[265] J.-P. Declercq, C. Evrard, A. Clippe, D. Vander Stricht, A. Bernard, and B. Knoops, "Crystal Structure of Human Peroxiredoxin 5, a Novel Type of Mammalian Peroxiredoxin at 1.5 A Ê Resolution," *J. Mol. Biol.*, vol. 311, pp. 751–759, 2001.

[266] T. Lee, S. J. Kim, S. W. Kang, K. Lee, S. G. Rhee, and D. Yu, "Molecular Cloning and Characterization of the Mouse Peroxiredoxin V Gene," *Biochem. Biophys. Res. Commun.*, vol. 362, pp. 356–362, 2000.

[267] M. Dubuisson *et al.*, "Human peroxiredoxin 5 is a peroxynitrite reductase," *FEBS Lett.*, vol. 571, pp. 161–165, 2004.

[268] M. Trujillo *et al.*, "Pre-steady state kinetic characterization of human

peroxiredoxin 5: Taking advantage of Trp84 fluorescence increase upon oxidation," *Arch. Biochem. Biophys.*, vol. 467, pp. 95–106, 2007.

[269] G. Leyens, I. Donnay, and B. Knoops, "Cloning of bovine peroxiredoxins - Gene expression in bovine tissues and amino acid sequence comparison with rat, mouse and primate peroxiredoxins," *Comp. Biochem. Physiol. - B Biochem. Mol. Biol.*, vol. 136, pp. 942–955, 2003.

[270] N. T. Nguyên-nhu *et al.*, "Human peroxiredoxin 5 gene organization, initial characterization of its promoter and identification of alternative forms of mRNA," *Biochim. Biophys. Acta - Gene Struct. Expr.*, vol. 1769, pp. 472–483, 2007.

[271] V. Van der Eecken, A. Clippe, P. P. Van Veldhoven, and B. Knoops, "Mitochondrial targeting of peroxiredoxin 5 is preserved from annelids to mammals but is absent in pig Sus scrofa domesticus," *Mitochondrion*, vol. 11, pp. 973–981, 2011.

[272] V. Van der Eecken *et al.*, "Abolition of peroxiredoxin-5 mitochondrial targeting during canid evolution.," *PLoS One*, vol. 8, no. 9, pp. 12–16, 2013.

[273] M. Pirson, A. Clippe, and B. Knoops, "The curious case of

peroxiredoxin-5 : what its absence in aves can tell us and how it can be used," *BMC Evol. Biol.*, vol. 18, no. 18, pp. 1–11, 2018.

[274] A. Kropotov, N. Usmanova, V. Serikov, B. Zhivotovsky, and N. Tomilin, "Mitochondrial targeting of human peroxiredoxin V protein and regulation of PRDX5 gene expression by nuclear transcription factors controlling biogenesis of mitochondria," *FEBS J.*, vol. 274, pp. 5804–5814, 2007.

[275] G. Leyens, B. Knoops, and I. Donnay, "Expression of peroxiredoxins in bovine oocytes and embryos produced in vitro," *Mol. Reprod. Dev.*, vol. 69, pp. 243–251, 2004.

[276] C. Evrard *et al.*, "Crystal Structure of a Dimeric Oxidized form of Human Peroxiredoxin 5," *J. Mol. Biol.*, vol. 337, pp. 1079–1090, 2004.

[277] C. Evrard, A. Smeets, B. Knoops, and J. P. Declercq, "Crystal structure of the C47S mutant of human peroxiredoxin 5," *J. Chem. Crystallogr.*, vol. 34, no. 8, pp. 553–558, 2004.

[278] M. Fratelli *et al.*, "Identification of proteins undergoing glutathionylation in oxidatively stressed hepatocytes and hepatoma cells," *Proteomics*, vol. 3, no. 7, pp. 1154–1161, 2003.

[279] M. J. Seo, X. Liu, M. Chang, and J. H. Park, “GATA-binding protein 1 is a novel transcription regulator of peroxiredoxin 5 in human breast cancer cells,” *Int. J. Oncol.*, vol. 40, pp. 655–664, 2012.

[280] J. A. Graves, M. Metukuri, D. Scott, K. Rothermund, and E. V. Prochownik, “Regulation of reactive oxygen species homeostasis by peroxiredoxins and c-Myc,” *J. Biol. Chem.*, vol. 284, no. 10, pp. 6520–6529, 2009.

[281] Y. Ji *et al.*, “Peroxiredoxin5 controls vertebrate ciliogenesis by modulating,” *Antioxid. Redox Signal.*, vol. 30, no. 14, pp. 1731–1745, 2018.

[282] M. H. Kim *et al.*, “Peroxiredoxin 5 regulates adipogenesis-attenuating oxidative stress in obese mouse models induced by a high-fat diet,” *Free Radic. Biol. Med.*, vol. 123, pp. 27–38, 2018.

[283] H. Y. Yang *et al.*, “Proteomic analysis of protein expression affected by peroxiredoxin v knock-down in hypoxic kidney,” *J. Proteome Res.*, vol. 9, pp. 4003–4015, 2010.

[284] N. T. Nguyên-Nhu and B. Knoops, “Mitochondrial and cytosolic expression of human peroxiredoxin 5 in Saccharomyces cerevisiae protect yeast cells from oxidative stress induced by paraquat,” *FEBS Lett.*, vol. 544, pp. 148–152, 2003.

[285] G. Walbrecq, B. Wang, S. Becker, A. Hannotiau, M. Fransen, and B. Knoops, “Antioxidant cytoprotection by peroxisomal peroxiredoxin-5,” *Free Radic. Biol. Med.*, vol. 84, pp. 215–226, 2015.

[286] Y. Ma, R. Li, Y. Zhang, L. Zhou, and Y. Dai, “Knockdown of peroxiredoxin 5 inhibits the growth of osteoarthritic chondrocytes via upregulating Wnt/β-catenin signaling,” *Free Radic. Biol. Med.*, vol. 76, pp. 251–260, 2014.

[287] M. X. Wang, A. Wei, J. Yuan, A. Trickett, B. Knoops, and G. A. C. Murrell, “Expression and regulation of peroxiredoxin 5 in human osteoarthritis,” *FEBS Lett.*, vol. 531, pp. 359–362, 2002.

[288] M.-X. Wang *et al.*, “Antioxidant Enzyme Peroxiredoxin 5 Is Upregulated in Degenerative Human Tendon,” *Biochem. Biophys. Res. Commun.*, vol. 284, pp. 667–673, 2001.

[289] J. Yuan, G. A. C. Murrell, A. Trickett, M. Landtmeters, B. Knoops, and M. X. Wang, “Overexpression of antioxidant enzyme peroxiredoxin 5 protects human tendon cells against apoptosis and loss of cellular function during oxidative stress,” *Biochim. Biophys. Acta - Mol. Cell Res.*, vol. 1693, pp. 37–45, 2004.

[290] Y. Zhou *et al.*, “Mouse Peroxiredoxin V Is a Thioredoxin Peroxidase That Inhibits p53-Induced Apoptosis,” *Biochem. Biophys. Res.*

Commun., vol. 927, pp. 921–927, 2000.

[291] J. Goemaere and B. Knoops, “Peroxiredoxin distribution in the mouse brain with emphasis on neuronal populations affected in neurodegenerative disorders,” *J. Comp. Neurol.*, vol. 520, pp. 258–280, 2012.

[292] S. De Simoni, D. Linard, E. Hermans, B. Knoops, and J. Goemaere, “Mitochondrial peroxiredoxin-5 as potential modulator of mitochondria-ER crosstalk in MPP+-induced cell death,” *J. Neurochem.*, vol. 125, pp. 473–485, 2013.

[293] F. Plaisant, A. Clippe, D. Vander Stricht, B. Knoops, and P. Gressens, “Recombinant peroxiredoxin 5 protects against excitotoxic brain lesions in newborn mice,” *Free Radic. Biol. Med.*, vol. 34, no. 7, pp. 862–872, 2003.

[294] J. Park *et al.*, “Peroxiredoxin 5 (Prx5) decreases LPS-induced microglial activation through regulation of Ca 2 þ / calcineurin-Drp1-dependent mitochondrial fission,” *Free Radic. Biol. Med.*, vol. 99, pp. 392–404, 2016.

[295] B. Kim, J. Park, K.-T. Chang, and D.-S. Lee, “Peroxiredoxin 5 prevents amyloid-beta oligomer- induced neuronal cell death by inhibiting ERK– Drp1-mediated mitochondrial fragmentation,” *Free Radic. Biol.*

Med., vol. 90, pp. 184–194, 2015.

[296] H. N. Sun *et al.*, "Microglial peroxiredoxin v acts as an inducible anti-inflammatory antioxidant through cooperation with redox signaling cascades," *J. Neurochem.*, vol. 114, pp. 39–50, 2010.

[297] D. B. Graham *et al.*, "Nitric Oxide Engages an Anti-inflammatory Feedback Loop Mediated by Peroxiredoxin 5 in Phagocytes," *Cell Rep.*, vol. 24, no. 4, pp. 838–850, 2018.

[298] H. I. Choi *et al.*, "Peroxiredoxin v selectively regulates IL-6 production by modulating the Jak2-Stat5 pathway," *Free Radic. Biol. Med.*, vol. 65, pp. 270–279, 2013.

[299] S. N. Radyuk, K. Michalak, V. I. Klichko, J. Benes, and W. C. Orr, "Peroxiredoxin 5 modulates immune response in Drosophila," *Biochim. Biophys. Acta - Gen. Subj.*, vol. 1800, pp. 1153–1163, 2010.

[300] S. N. Radyuk *et al.*, "Peroxiredoxin 5 confers protection against oxidative stress and apoptosis and also promotes longevity in Drosophila," *Biochem. J*, vol. 419, pp. 437–445, 2009.

[301] S. N. Radyuk *et al.*, "Mitochondrial peroxiredoxins are critical for the maintenance of redox state and the survival of adult Drosophila," *Free Radic. Biol. Med.*, vol. 49, pp. 1892–1902, 2010.

[302] A. Nicolussi, S. D. Inzeo, C. Capalbo, G. Giannini, and A. Coppa, “The role of peroxiredoxins in cancer (Review),” *Mol. Clin. Oncol.*, vol. 6, pp. 139–153, 2017.

[303] T. Ishii, E. Warabi, and T. Yanagawa, “Novel roles of peroxiredoxins in inflammation, cancer and innate immunity,” *J. Clin. Biochem. Nutr. JCBN J. Clin. Biochem. Nutr. Soc. Free Radic. Res. Japan Kyoto*, vol. 50, no. 912, pp. 91–105, 2012.

[304] M. B. Hampton, K. A. Vick, J. J. Skoko, and C. A. Neumann, “Peroxiredoxin involvement in the initiation and progression of human cancer,” *Antioxid Redox Signal.*, vol. 28, no. 7, pp. 591–608, 2018.

[305] M. H. Park, M. Jo, Y. R. Kim, C. K. Lee, and J. T. Hong, “Roles of peroxiredoxins in cancer, neurodegenerative diseases and inflammatory diseases,” *Pharmacology and Therapeutics*, vol. 163. pp. 1–23, 2016.

[306] H. Ahn, J. Yoo, S. Lee, H. Jun, H. Lee, and D. Lee, “Peroxiredoxin 5 promotes the epithelial-mesenchymal transition in colon cancer,” *Biochem. Biophys. Res. Commun.*, vol. 487, no. 3, pp. 580–586, 2017.

[307] B. Kim *et al.*, “Peroxiredoxin 5 overexpression enhances tumorigenicity and correlates with poor prognosis in gastric cancer,”

Int. J. Oncol., vol. 51, pp. 298–306, 2017.

[308] J. Liu, X. Feng, Y. Jin, Z. Sun, and H. Meng, "The antitumor activity and preliminary modeling on the potential mechanism of action of human peroxiredoxin-5," *Oncotarget*, vol. 8, no. 16, pp. 27189–27198, 2017.

[309] A. Elamin, H. Zhu, A. M. E. L. Hassan, N. Xu, and M. E. Ibrahim, "Peroxiredoxin V : A candidate breast tumor marker of population specificity," *Mol. Clin. Oncol.*, vol. 1, pp. 541–549, 2013.

[310] P. Karihtala, A. Mäntyniemi, S. W. Kang, V. L. Kinnula, and Y. Soini, "Peroxiredoxins in Breast Carcinoma," *Clin. Cancer Res.*, vol. 9, pp. 3418–3424, 2003.

[311] A. Kropotov *et al.*, "Peroxiredoxin V is essential for protection against apoptosis in human lung carcinoma cells," *Exp. Cell Res.*, vol. 312, pp. 2806–2815, 2006.

[312] J. L. Lu, J.-M. Vallat, J. D. Pollard, B. Knoops, and R. Ouvrier, "Expression of the antioxidant enzyme peroxiredoxin 5 in the human peripheral nervous system," *J. Peripher. Nerv. Syst.*, vol. 11, pp. 318–324, 2006.

[313] M. Pirson and B. Knoops, "Expression of peroxiredoxins and

thioredoxins in the mouse spinal cord during embryonic development," *J. Comp. Neurol.*, vol. 523, pp. 2599–2617, 2015.

[314] B. Knoops, V. Argyropoulou, S. Becker, L. Ferté, and O. Kuznetsova, "Multiple Roles of Peroxiredoxins in Inflammation," *Mol. Cells*, vol. 39, no. 1, pp. 60–64, 2016.

[315] T. Ishii, E. Warabi, and T. Yanagawa, "Novel roles of peroxiredoxins in inflammation, cancer and innate immunity," *J. Clin. Biochem. Nutr.*, vol. 50, no. 2, pp. 91–105, 2012.

[316] C. Nathan and A. Cunningham-Bussel, "Beyond oxidative stress: an immunologist's guide to reactive oxygen species," *Nat Rev Immunol*, vol. 13, no. 5, pp. 349–361, 2013.

[317] M. W. Covert, T. H. Leung, J. E. Gaston, and D. Baltimore, "Achieving Stability of Lipopolysaccharide-Induced NF-kB Activation," *Science (80-.).*, vol. 309, no. 5742, pp. 1854–1857, 2005.

[318] S. Thameem Dheen, C. Kaur, and E.-A. Ling, "Microglial Activation and its Implications in the Brain Diseases," *Curr. Med. Chem.*, 2007.

[319] A.-G. L. Planson *et al.*, "Sulfiredoxin Protects Mice from Lipopolysaccharide-Induced Endotoxic Shock," *Antioxid. Redox Signal.*, vol. 14, no. 11, pp. 2071–2082, 2011.

[320] R. K. Thimmulappa *et al.*, “Nrf2 is a critical regulator of the innate immune response and survival during experimental sepsis,” *J. Clin. Invest.*, vol. 116, no. 4, pp. 984–995, 2006.

[321] H. Bur *et al.*, “Oxidative stress markers and mitochondrial antioxidant enzyme expression are increased in aggressive Hodgkin lymphomas,” *Histopathology*, vol. 0, pp. 319–327, 2014.

[322] P. Peroja, K. Haapasaari, S. Mannisto, and I. Miinalainen, “Total peroxiredoxin expression is associated with survival in patients with follicular lymphoma,” *Virchows Arch.*, vol. 468, pp. 623–630, 2016.

[323] E. C. Lien, C. C. Dibble, and A. Toker, “PI3K signaling in cancer : beyond AKT,” *Curr. Opin. Cell Biol.*, vol. 45, pp. 62–71, 2017.

[324] A. Carnero and J. M. Paramio, “The PTEN/PI3K/AKT pathway in vivo, cancer mouse models,” *Front. Oncol.*, vol. 4, no. 252, pp. 1–10, 2014.

[325] D. Ma *et al.*, “Peroxiredoxin I plays a protective role against cisplatin cytotoxicity through mitogen activated kinase signals,” *Oral Oncol.*, vol. 45, no. 12, pp. 1037–1043, 2009.

[326] C. A. Neumann and Q. Fang, “Are peroxiredoxins tumor suppressors ?,” *Curr. Opin. Pharmacol.*, vol. 7, pp. 375–380, 2007.

[327] G. G. Fernandez-Ranvier *et al.*, “Candidate Diagnostic Markers and

Tumor Suppressor Genes for Adrenocortical Carcinoma by Expression Profile of Genes on Chromosome 11q13," *World J Surg*, vol. 32, pp. 873–881, 2008.

[328] D. Weber *et al.*, "Proteostasis, oxidative stress and aging," *Redox Biol.*, vol. 13, pp. 550–567, 2017.

[329] T. Grune, "Oxidative stress, aging and the proteasomal system," *Biogerontology*, vol. 1, no. 1, pp. 31–40, 2000.

[330] K. Ossowska *et al.*, "Degeneration of dopaminergic mesocortical neurons and activation of compensatory processes induced by a long-term paraquat administration in rats: Implications for Parkinson's disease," *Neuroscience*, vol. 141, no. 4, pp. 2155–2165, 2006.

[331] W. Domej, K. Oettl, and W. Renner, "Oxidative stress and free radicals in COPD – implications and relevance for treatment," *Int. J. COPD*, vol. 9, pp. 1207–1224, 2014.

[332] G. Castello, S. Costantini, and S. Scala, "Targeting the inflammation in HCV-associated hepatocellular carcinoma: A role in the prevention and treatment," *J. Transl. Med.*, vol. 8, no. 109, pp. 1–11, 2010.

[333] C. Klomsiri, P. A. Karplus, and L. B. Poole, "Cysteine-Based Redox

Switches in Enzymes," *Antioxid. Redox Signal.*, vol. 14, no. 6, pp. 1065–1077, 2011.